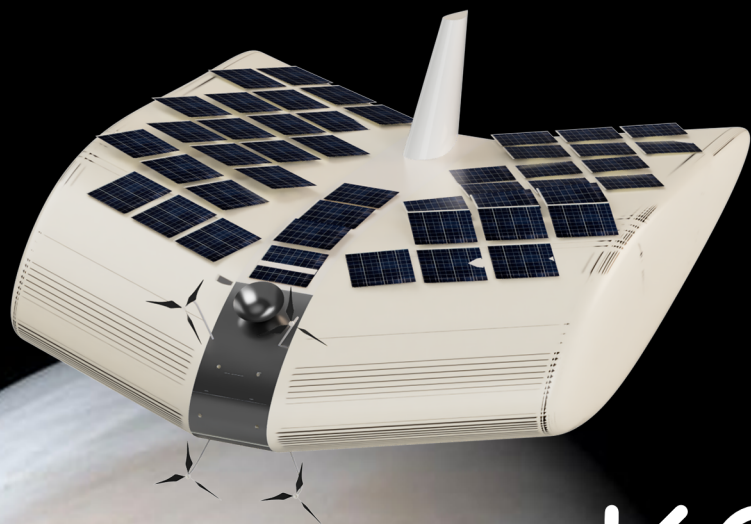


# Kumo: Venus Atmosphere Explorer

Final Report

AE3200: Design Synthesis Exercise

Group 18



This page has been intentionally left blank.

# Kumo: Venus Atmosphere Explorer

## Final Report

Group 18

---

### Student names and numbers

---

Arthur Bronstring	4780744	Irina Dumitrescu	4786262
Paul Eckstein	4860497	Serena Maroquin	4834445
Helena Momoko (Momo) Powis	4534751	Emir Şarlak	4812433
Ishita Sinha	4873165	Michaël Staelens	4796969
Lucas Vieira dos Santos	4833570	Sviatoslav (Sviet) Voloshyn	4774361

---

Version	Date	Comment	Responsible
1.0	22/06/2021	Draft version ready for submission.	All
2.0	29/06/2021	Final version ready for submission.	All

---

Tutor: Dr. ir. Erwin Mooij  
Coaches: MSc. Tara Bründl, MSc. ir. Marie Fayolle  
Teaching Assistant: BSc. Carmen Immerzeel  
Institution: Delft University of Technology  
Place: Faculty of Aerospace Engineering, Delft  
Project Duration: April – July, 2021

Cover image: 3D renders of Kumo's atmospheric probe Tori and orbiter Tsubuyaki over an edited background of a contrast-enhanced false colour view of Venus from Mariner 10, NASA/JPL

# Abstract

This abstract will give an overview of the team’s vision and the Kumo mission objectives. Furthermore, it will address the designs for both the atmospheric probe and the orbiter, where an overview will be given of the most important characteristics.

## Mission

The mission’s primary objective is to detect isotopes and noble gases on Venus to understand the origin and evolution of the planet. The secondary aim is to detect biomarkers that could indicate life signs and detect them. The tertiary aim is the study of the distribution of the currently unknown UV-absorbers present within the Venusian atmosphere. Kumo, named after the Japanese word for “cloud”, is designed to launch from Earth in 2028 on-board a Falcon 9 rocket and enter the Venusian atmosphere to collect data with a preliminary target flight duration of 60 days. This mission could be the first to confirm the presence of specific biomarkers that can indicate potential signs of extraterrestrial life and better understand the composition and evolution of the planet. As the atmospheric probe is inflated and will fly through the Venusian clouds, a satellite will be stationed in an orbit around Venus to relay information to Earth. Both of these mission segments will be discussed below.

## Probe

The atmospheric probe has been designed to fulfil the mission requirements and fit to the constraints set by the launcher and the budget. The selected design concept is a dynastat, a hybrid vehicle combining an airship and an aerodyne flying wing, where the emphasis is put on the latter. This way, the probe can rely on buoyancy for its main source of lift, supported by a fraction of dynamic lift at the upper altitude limit of 65 km. The probe will fly in the Venusian cloud tops between altitudes of 55 km and 65 km, exploring an equatorial band from 0° to 30° north. It will stick to an altitude of 55 km in the nightside, where it will fully rely on buoyancy for lift. On the dayside, a transition will be made to an altitude of 65 km at noon. In the end, the probe is designed to have a central rigid structure, supported by inflatable wings on the side that are to be filled with low-density helium gas upon deployment. Propulsion will be provided by four propellers, logically placed on the structure to improve stability. These will be powered by electric energy provided by the solar arrays, which were designed for the limiting upper altitude of 65 km. To limit the power usage, passive thermal control will be used to provide viable temperature ranges for the instruments contained within the structure. The guidance, navigation and control is limited to the use of laser pointing at night, only using inertial measurement units during the daytime. Finally, telecommunications with the relay satellite will be provided by a high-gain antenna using the X-band frequency. A final concept for the probe is visualised in Fig. 1, while the distribution of mass, power, data rate and cost are in terms of the different subsystems are given in Table 1. The final mass for the probe rounds of at 555 kg, with the total cost for production and testing settling at €377 million.

Table 1: Tori budget

Components	Mass [kg]	Power [W]	Data rate [kbps]	Costs [€M]
Payload	18.5	51.7	107	120
TT&C/C&DH	29	127	-	45
GNC	27.6	51.3	0.06	15
Thermal	23.3	-	0.00105	1.5
Structures	148.1	-	-	12.5
Propulsion	82.6	78260	0.0038	4
Power	225.9	-	0.0011	25
<b>Total</b>	<b>555</b>	<b>78490</b>	<b>107</b>	<b>223</b>

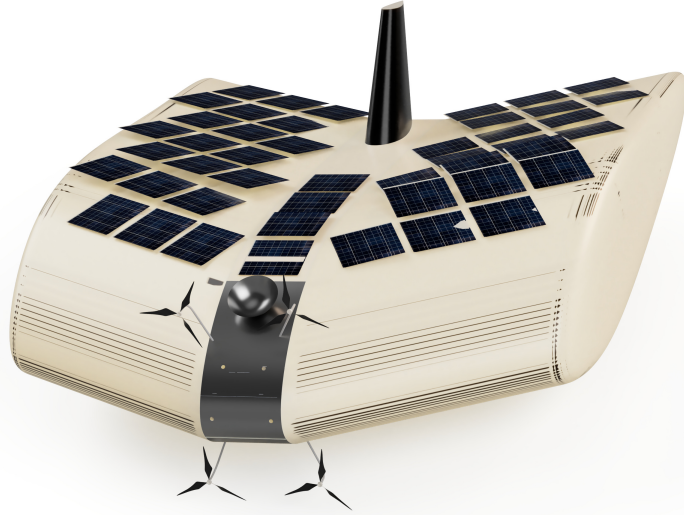
## Orbiter

Next to the probe, an orbiter was designed to relay information to the ground stations on Earth and to perform additional measurements. During the first phase of the mission, it will follow a circular, probe-synchronous relay orbit around Venus at an altitude of 127,000 km. After the probe has collected its first set of measurements, the orbit will be changed to an elliptical science orbit with apocentre at 66,000 km and pericentre at 250 km. Both phases will take up half of the nominal mission time. To provide for orbit insertion and orbit maintenance, the propulsion system was sized, and a bipropellant blowdown was selected, based on NTO/MMH. As the propulsion system power usage is significantly lower for the orbiter than it is for the probe, the solar arrays were sized as such and the on-board systems are protected by means of active thermal control. Finally, the communications system was designed to be similar to the probe, making use of a high gain antenna and the X-band on the deep space network. A final concept for the orbiter is visualised in Fig. 2, while the

**Table 2:** Orbiter budget

Components	Mass [kg]	Power [W]	Data rate [kbps]	Costs [€M]
Payload	33.43	41.2	50	35
TT&C/C&DH	31.43	172.0	-	45
GNC	22.10	22.5	0.001	7
Thermal	20.00	28.0	0.0088	1.5
Structures	212.31	0	0	6
Propulsion	64.70	40.36	0.00375	8
Power	35.62	36.7	0.00124	10
Fuel mass	770.19	0	-	-
<b>Total</b>	<b>1189.78</b>	<b>340.76</b>	<b>50.01479</b>	<b>112.5</b>

distribution of mass, power, data rate and cost are in terms of the different subsystems are given in Table 2. The final mass for the orbiter rounds of at 1116 kg, with the total cost for production and testing settling at €271 million.

**Figure 1:** 3D model of the probe**Figure 2:** 3D model of the orbiter

# Nomenclature

## Abbreviations

Abbreviation	Definition
2D	Two-Dimensional
3D	Three-Dimensional
ADCS	Attitude Determination and Control Subsystem
AIU	AOCS Interface Unit
AM0	Exo atmospheric solar spectrum
AOCS	Attitude Operations and Control
AVL	Athena Vortex Lattice
BCR	Battery charge regulator
BDR	Battery discharge regulator
BOL	Begin of life
BR	Buoyancy Ratio
CD&H	Command and data handling
CDMU	Command & Data Management Unit
CI	Corruption Index
CNES	National Centre for Space Studies
COS	Classes of Supply
COSPAR	Committee on Space Research
CSIS	Center for Strategic and International Studies
DAVINCI	Deep Atmosphere Venus Investigation of Noble gases, Chemistry, and Imaging
DMS	Data Management System
DOD	Depth of discharge
DSE	Design Synthesis Exercise
DSN	Deep Space Network
EEPROM	Electrically Erasable Programmable Read-Only Memory
EOL	End-of-Life
ESA	European Space Agency
ESOC	European Space Operations Centre
Europa-UVS	Europa Ultraviolet Spectrograph
EVE	European Venus Explorer
FBS	Functional Breakdown Structure
FDIR	Failure Detection, Isolation & Recovery
FFBD	Functional Flow Block Diagram
FM	Flight Model
GFRP	Glass Fibre Reinforced Polymer
GII	Gender Inequality Index
GPI	Global Peace Index
GTO	Geo Transfer Orbit
HDI	Human Development Index
HGA	High gain antenna
HPCM	High Power Command Module
HTA	Heavier-Than-Air
IMU	Inertial Measurement Unit
INMS	Ion and Neutral Mass Spectrometer
ISA	International Standard Atmosphere
IST	Innovative sensor technology
JAXA	Japan Aerospace Exploration Agency
KARI	Korea Aerospace Research Institute
KSC	Kenned Space Center
LCP	Liquid Crystal Polymer
LEO	Low Earth Orbit
LIR	Longwave Infrared Camera
LGA	Low gain antenna
LTA	Lighter-Than-Air
LVO	Low Venus Orbit
MASPEX	Mass Spectrometer for Planetary Sciences

Abbreviation	Definition
MIT	Massachusetts Institute of Technology
MLI	Multi-Layer Insulation
MM	Mass Memory
MOMA	Mars Organic Molecule Analyser
MPPT	Maximum power point tracker
MSS	Memory System Supervisor
NASA	National Aeronautics and Space Administration
NEP	Nephelometer
NMS	Neutral Mass and Velocity Spectrometer
NetCDF	Network Common Data Form
OBC	On-board computer
PD&D	Project Design and Development
PE	Polyethylene
PET	Polyethylene Terephthalate
PIC	Processor Interface Controller
PICA	Phenolic Impregnated Carbon Ablator
PL	Payload
PM	Processing Module
PTFE	Polytetrafluorethylene
PVC	Polyvinyl chloride
QM	Qualification Model
RAAN	Right Ascension of the Ascending Node
RAF	Russian Aerospace Federation
RAMS	Reliability, Availability, Maintenance, and Safety
RF	Radio Frequency
RFSA	Russian Federal Space Agency
RM	Reconfiguration Module
ROC	Rate Of Climb
ROI	Return Of Investment
RPM	Rotations Per Minute
RSS	Radio Science Subsystem
RTU	Remote Terminal Unit
SAA	Space Act Agreement
SAM	Sample Analysis at Mars
S/C	Spacecraft
SFG	Safe Guard Memory
SI	Standard International
SNT	System noise temperature
SSMM	Solid State Mass Memory
SSO	Sun-Synchronous Orbit
STP	Standard Temperature and Pressure
TBD	To Be Determined
TFG	Transfer Frame Generator
TPS	Thermal Protection System
TRL	Technology Readiness Level
UIC	User Interface Controller
USAF	United States Air Force
UVI	Ultraviolet Imager
UVIS	Ultraviolet Imaging Spectrograph
VERTIS	Venus Emissivity, Radio Science, InSAR, Topography, and Spectroscopy
VEX	Venus Express
VIMS	Visible and Infrared Mapping Spectrometer
VIRA	Venus international reference atmosphere
VIRTIS	Visible & Infrared Thermal Imaging Spectrometer
VLBI	Very Long Baseline Interferometry
VMC	Venus-Express Monitoring Camera

# Symbols

Symbol	Definition	Unit	Symbol	Definition	Unit
$a$	Acceleration	$\text{m s}^{-2}$	$P_d$	Power dissipated for the probe	W
$a$	Semi-major axis	m	$P_r$	Power required	W
$a_F$	Albedo factor	-	$P_{sol,sp}$	Solar cell power generated per unit area	$\text{W m}^{-2}$
$A$	Wing aspect ratio	-	$p$	Pressure	Pa
$A_{albedo}$	Area subjected to albedo radiation	$\text{m}^2$	$q$	Unit less reflectance factor	-
$A_{cond}$	Conducting area on Tori	$\text{m}^2$	$q_b$	Base shear flow	$\text{N m}^{-2}$
$A_{conv}$	Convective area on Tori	$\text{m}^2$	$q_{b0}$	Base shear flow	$\text{N m}^{-2}$
$A_{IR}$	Area subjected to infrared radiation	$\text{m}^2$	$q_{s0,i}$	Redundant shear flow	$\text{N m}^{-2}$
$A_s$	Sunlit surface area	$\text{m}^2$	$\dot{Q}$	Heat transfer rate	W
$A_{solar}$	Area subjected to solar radiation	$\text{m}^2$	$Q_{absorbed}$	Net heat absorbed into Tori	W
$A_{rad}$	Radiative area on Tori	m	$Q_{cond}$	Heat flow rate due to conduction	W
$au$	Astronomic unit	m	$Q_{conv}$	Heat flow rate due to convection	W
$BR$	Buoyancy ratio	-	$Q_{emitted}$	Net heat emitted by Tori	W
$BER$	Bit error rate	-	$Q_{MLI}$	Heat flow rate through MLI	W
$\frac{b}{fl}$	Span to fuselage length ratio	-	$Q_{net}$	Net heat flow through the probe	W
$C_a$	Chord length	m	$Q_{rad}$	Heat flow rate due to radiation	W
$C_D$	Drag coefficient	-	$R$	Radius	m
$C_{D0}$	Profile drag coefficient	-	$R_v$	Distance from the centre of Venus	m
$C_L$	Lift coefficient	-	$S$	Wing surface area	$\text{m}^2$
$C_{L_{aero}}$	Aerodynamic lift coefficient	-	$S_{SA}$	Solar array surface area	$\text{m}^2$
$c$	Chord length	m	$S_{final}$	Final sustainability score	-
$c_f$	Equivalent skin-friction drag coefficient	-	$SP_1$	Sustainability score for Earth phase	-
$cm$	Centre of mass	m	$SP_2$	Sustainability score for interplanetary phase	-
$cp_s$	Centre of solar radiation pressure	m	$SP_3$	Sustainability score for Venus phase	-
$c_{probe}$	Specific heat capacity of probe body	$\text{J kg}^{-1} \text{K}$	$S_{wet}$	Wet wing surface area	$\text{m}^2$
$c_r$	Root chord length	m	$SNR$	Signal to noise ratio	dB
$c_s$	Speed of light	$\text{m s}^{-1}$	$\frac{S_{encl}}{tc}$	Profile enclosed to bounding box area ratio	-
$D$	Diameter	m	$t_{circ}$	Semi circular part thickness	m
$D_{cylinder}$	Cylindrical body diameter	m	$t_d$	Day time	s
$e$	Oswald efficiency factor	-	$t_e$	Eclipse time	s
$e$	Eccentricity	-	$t_{MLI}$	Thickness of MLI layers	$\mu\text{m}$
$E$	Eccentric anomaly	-	$t_{sk}$	Skin thickness	m
$E_{max}$	Maximum glide ratio	-	$t_{sp}$	Spar thickness	m
$EIRP$	Equivalent isotropic radiated power	dB	$t_{wall}$	Thickness of the conducting wall for Tori	mm
$f$	Mass fraction	-	$T$	Temperature	K
$F_a$	Albedo visibility factor	-	$Th$	Thrust	N
$g$	Gravitational acceleration	$\text{m s}^{-2}$	$T_{in}$	Internal temperature of Tori	K
$g_0$	Standard Earth sea level gravitational acceleration	$\text{m s}^{-2}$	$T_{out}$	External temperature of Tori	K
$G$	Figure of merit for heat pipes	$\text{W m}^{-2}$	$T_D$	Maximum torque	$\text{N m}$
$h$	Altitude	m	$T_{IR}$	Effective black body radiation on Venus	K
$h_a$	Spar length	m	$T_{weq}$	Equivalent wall temperature	K
$h_c$	Convective heat transfer coefficient	-	$\frac{t}{c}$	Thickness to chord ratio	-
$h_{max}$	Maximum stored momentum	$\text{N s}$	$v$	Volume	$\text{m}^3$
$h_{probe}$	Specific altitude of probe m	-	$V$	Velocity	$\text{m s}^{-1}$
$H$	Scale height	m	$V_c$	Circular velocity	$\text{m s}^{-1}$
$i$	Orbit inclination angle	$^\circ$	$V_E$	Atmospheric entry velocity	$\text{m s}^{-1}$
$I_{sp}$	Specific impulse	s	$V_x$	Shear force in x-direction	N
$I_{xx}$	Moment of inertia around x axis	$\text{kg m}^2$	$V_z$	Shear force in z-direction	N
$I_y$	Moment of inertia around y axis	$\text{kg m}^2$	$w_i$	Weights for sustainability per subsystem	-
$I_z$	Moment of inertia around z axis	$\text{kg m}^2$	$t$	thickness	mm
$I_{zz}$	Moment of inertia around z axis	$\text{kg m}^2$	$\bar{x}$	Distance in x to centre of mass	m
$J$	Heat flux intensity	$\text{W m}^{-2}$	$M_{exp}$	Experienced moment	$\text{N m}$
$J_a$	Albedo radiation	$\text{W m}^{-2}$	$M_{max}$	Maximum moment	$\text{N m}$
$J_{IR}$	Planetary radiation flux on Venus	$\text{W m}^{-2}$	$S_{exp}$	Experienced shape factor	m
$J_{sEarth}$	Solar radiation flux on Earth	$\text{W m}^{-2}$	$S_{max}$	Maximum shape factor	m
$J_{sVenus}$	Solar radiation flux on Venus	$\text{W m}^{-2}$	$\alpha$	Absorptivity	-
$k$	Thermal conductivity coefficient	-	$\gamma_E$	Atmospheric entry descent angle	$^\circ$ or rad
$K$	Ballistic parameter	$\text{kg m}^{-2}$	$\Delta$	Step size	-
$k_E$	-	-	$\epsilon$	Emissivity	-
$L$	Lift	N	$\eta$	Efficiency	- or %
$L_{aero}$	Aerodynamic lift	N	$\eta_{antenna}$	Antenna efficiency	-
$L_{buoy}$	Buoyant lift	N	$\theta$	True anomaly (in astrodynamics context)	-
$L_{attenuation}$	Loss due to atmospheric attenuation	dB	$\theta$	Solar time angle (in atmospheric flight context)	$^\circ$
$L_{cable}$	Cable loss	dB	$\theta$	Taper angle of aeroshell back cover	$^\circ$
$L_{space}$	Space propagation loss	dB	$\kappa$	Heat of vaporisation	$\text{J kg}^{-1}$
$l_{sk}$	Length of skin	m	$\lambda$	Wing taper ratio	-
$m$	Mass	kg	$\Lambda_{LE}$	Leading edge sweep angle	rad
$M$	Mean anomaly (in astrodynamics context)	-	$\mu_V$	Standard gravitational parameter of Venus	$\text{m}^3 \text{s}^{-2}$
$M$	Molar mass (in buoyancy context)	$\text{g mol}^{-1}$	$\rho$	Density	$\text{kg m}^{-3}$
$M_{rw}$	Reaction wheel mass	kg	$\sigma$	Stress	Pa
$n_{MLI}$	Number of MLI layers	-	$\sigma_B$	Boltzmann constant	$\text{W m}^{-2} \text{K}^{-4}$
$P$	Orbital period	s	$\tau$	Surface tension	$\text{N m}^{-1}$
$P_a$	Shaft power available	W	$\phi_{sk}$	Skin angle	rad
$P_{fix}$	Fixed subsystem power consumption	W	$\omega$	Angular velocity	rad/s

## Symbol indices

Symbol	Definition
55	Corresponding to conditions at 55 km
65	Corresponding to conditions at 65 km
$\infty$	Corresponding to a galaxy far, far away
a	Albedo
air	Corresponding to the ambient air
apo	Corresponding to the apocentre
cond	Conduction
conv	Convection
cruise	Corresponding to cruise conditions
EV	Entry vehicle
gas	Corresponding to the (expanded) lifting gas
in	Internal / inside
IR	Infra red
max	Maximum
N	Aeroshell nose
opt	Corresponding to optimum conditions
out	External / outside
park	Corresponding to parking orbit
peri	Corresponding to the pericentre
PL	Payload
probe	Probe
rad	Radiative
tank	Corresponding to the pressurised gas tank

# Contents

<b>Abstract</b>	<b>ii</b>
<b>Nomenclature</b>	<b>iii</b>
<b>1 Project overview</b>	<b>1</b>
1.1 Project motivation and objectives . . . . .	1
1.2 Stakeholder requirements . . . . .	1
1.3 Scientific background information . . . . .	2
1.4 Design process . . . . .	2
1.5 Risk evaluation process . . . . .	4
1.6 Sustainability evaluation process . . . . .	4
1.7 Verification and validation process . . . . .	5
<b>2 Mission design</b>	<b>7</b>
2.1 Mission elements . . . . .	7
2.2 Mission operations requirements . . . . .	7
2.3 Market analysis . . . . .	7
2.4 Launch . . . . .	12
2.5 Transfer . . . . .	13
2.6 Orbiter nominal operations . . . . .	14
2.7 Probe atmospheric insertion . . . . .	16
2.8 Probe nominal operations . . . . .	23
2.9 Extended mission operations . . . . .	27
2.10 End-of-life missions . . . . .	27
2.11 Mission design overview . . . . .	28
<b>3 Tori design</b>	<b>36</b>
3.1 Payload . . . . .	36
3.2 Telecommunications and command . . . . .	39
3.3 Guidance, navigation and control . . . . .	48
3.4 Power and propulsion design . . . . .	52
3.5 Thermal control . . . . .	62
3.6 Materials and structures . . . . .	71
3.7 Aerodynamics and stability . . . . .	85
3.8 Design overview . . . . .	92
<b>4 Tsubuyaki design</b>	<b>98</b>
4.1 Payload . . . . .	98
4.2 Telecommunications and command . . . . .	100
4.3 Guidance, navigation and control . . . . .	103
4.4 Power and propulsion . . . . .	106
4.5 Thermal control . . . . .	113
4.6 Materials and structures . . . . .	117
4.7 Design overview . . . . .	121
<b>5 Sensitivity analysis</b>	<b>125</b>
5.1 Tori sensitivity analysis . . . . .	125
5.2 Tamago sensitivity analysis . . . . .	128
5.3 Tsubuyaki sensitivity analysis . . . . .	130
<b>6 Mission risk and sustainability</b>	<b>133</b>
6.1 Mission risk . . . . .	133
6.2 Mission sustainability . . . . .	135
<b>7 Future design and development</b>	<b>138</b>
7.1 Project design and development logic . . . . .	138
7.2 Testing plan . . . . .	141
7.3 Production plan . . . . .	144
7.4 Finances . . . . .	147
<b>8 Conclusion and recommendations</b>	<b>151</b>
<b>References</b>	<b>153</b>
References . . . . .	153

# 1. Project overview

The mission assigned to the team has been set up due to the speculations of phosphine found in the cloud tops of Venus, which could indicate potential life. From this finding, the mission was founded with its own mission objectives. In this chapter, the scientific background will be given along with the mission objectives and mission requirements. Also the general structure for verification & validation, risk and sustainability will be outlined at the end of this chapter.

## 1.1. Project motivation and objectives

In September 2020 an announcement from the Royal Astronomical Society put the planet Venus at the centre of worldwide attention, as it presented papers reporting the apparent presence of phosphine, a potential biomarker, in the cloud decks of the Venusian atmosphere (Greaves et al., 2020). Calculations in (Bains et al., 2020) showed that the levels of phosphine detected would exceed the abundance expected from known abiotic production processes by orders of magnitude. There were two possible explanations: either some unknown abiotic processes are responsible for producing far larger quantities of phosphine, or the extra phosphine might be of biotic origin.

Soon, fellow planetary scientists published papers pointing out flaws in the analysis and interpretation, explaining the absorption line to sulphur dioxide instead (Villanueva et al., 2020), while others re-examined data from the Pioneer Venus mission that seem to support the original paper (Mogul, Limaye, Way, and Cordova, 2021). The discussion on whether there actually was a discovery is still ongoing. However, most papers have similar recommendations for further investigations, calling for ground or space-based observations.

The Kumo mission was born from this very need and aims to provide in-situ measurements in the Venusian atmosphere to contribute new facts to the scientific discussion. Because the opportunity to fly within the Venusian atmosphere is quite unique, it should be leveraged to help answer other questions about our twin planet as well.

In discussion with Dr. Håkan Svedhem, the client, it was found that the measurements of crucial isotope ratios of noble gases for radiometric dating can be used to answer one of the currently most interesting question about the evolution of the planet's atmosphere (Sharpton et al., 2014), thus justifying this becoming the primary mission objective. Furthermore, experts find the recently announced presence of biomarkers in the Venusian atmosphere (Greaves et al., 2020) debatable or unlikely<sup>1</sup>, so in-situ measurements could settle or at least contribute more findings to this debate. Thus the search for the abundance and source of biomarkers, like phosphine and methane, is the secondary mission objective. Lastly, the client suggested equipping the craft with a UV camera to investigate the yet unexplained structure of the atmosphere in the UV spectrum (Pérez-Hoyos et al., 2018).

**Objectives** To help guide the focus of the project, a mission objective statement, a mission need statement and a set of system and performance requirements were established. These statements show the intentions of the project and show what objectives drove the design. They were defined in consultation with Dr. Håkan Svedhem and are as follows.

1. Measure the abundance ratio of noble gas isotopes to investigate atmospheric evolution.
2. Determine abundance and source location of biomarkers like phosphine and methane.
3. Identify the unknown UV-absorber that creates large scale structure in upper atmosphere layers.

**Mission need** Using the above mentioned mission objectives the following need statement was formulated:

“The Kumo mission will investigate the evolution of Venus' atmosphere through in-situ measurements of noble gas isotope ratios, establish the presence of biomarkers and investigate which UV-absorber is appearing in a large scale atmospheric structure.”

**Project objective** The project objective is for ten students to design a mission to Venus, which aims to explore the atmosphere, search for biomarkers, investigate atmospheric evolution and identify UV absorbers within the preliminary target mission duration.

## 1.2. Stakeholder requirements

From the mission objectives and mission statements, stakeholder scientific requirements as well as performance requirement were established, shown in Table 1.1. These stakeholder (STH) requirements are divided into science (SCI), budget (BUD), and performance (PERF) requirements, as well as requirements for safety (SAF), sustainability (SUS), propulsion (PROP), cost (COST), and other requirements (OTH) not belonging to any of the previous overarching requirement topics.

---

<sup>1</sup><https://www.nature.com/articles/d41586-021-00249-y>, retrieved on 26-05-2021

**Table 1.1:** Stakeholder requirements

Identifier	Requirement
KUMO-STH-SCI-04	The mission shall determine the abundance ratio between key isotopes of noble gases at an accuracy sufficient to determine the atmosphere evolution history to 40 Myr.
KUMO-STH-SCI-05	The mission shall determine the abundance and source location of phosphine to an accuracy of 0.2 ppb.
KUMO-STH-SCI-06	The mission shall determine the abundance and source location of methane to an accuracy of 10 ppt.
KUMO-STH-SCI-07	The mission shall investigate the structure of UV-absorbing gases in the atmosphere.
KUMO-STH-BUD-01	Technical requirements shall come from research and negotiations with clients and potential users (scientists). At any time it shall be demonstrated that chosen solutions fulfil the mission requirements and are in line with similar initiatives for missions to Venus (budgets, innovation level, etc.)
KUMO-STH-PERF-02	Five locations of interest, defined by altitude, latitude and local time, shall be covered at least twice for repeat observations with horizontal accuracy of 1 km <TBC>, to confirm deviating/interesting measurements.
KUMO-STH-PERF-03	A band of latitudes 30° north from the equator shall be covered.
KUMO-STH-PERF-04	The lowest altitude to be sampled by the platform shall be lower than 55 km.
KUMO-STH-PERF-05	The highest altitude to be sampled by the platform shall be above 65 km.
KUMO-STH-PERF-06	All science data shall be transmitted to Earth.
KUMO-STH-PERF-07	An extended mission plan shall be defined for the case that the platform will exceed nominal life.
KUMO-STH-PERF-08	Launch date shall be no later than 2028.
KUMO-STH-SAF-01	Any exposure to hazardous materials shall be avoided for all personnel involved.
KUMO-STH-SAF-02	Mission success shall be larger than 95 %, excluding launch failures.
KUMO-STH-SUS-02	The use of radioisotope propulsion systems and/or thermo generators shall be avoided.
KUMO-SUS-PROP-02	The main propellant shall be less toxic than hydrazine.
KUMO-STH-COST-01	The maximum mission cost including launch and operations shall not exceed 1000M euros.
KUMO-STH-OTH-01	A market analysis shall lead to confirmation of primary science objectives.
KUMO-STH-OTH-02	A market analysis shall lead to definition of additional scientific goals and their impact on the nominal mission design.
KUMO-STH-OTH-03	The design shall be presented as a “begin-to-end” design, including launcher selection, interplanetary transfer, in-situ operations, and end of life strategy.
KUMO-STH-OTH-04	Primary focus shall be on platform design, operation, delivery and deployment.
KUMO-STH-OTH-05	Launcher selection shall be based on existing launchers.

### 1.3. Scientific background information

This section briefly outlines the scientific background information and science constants used throughout the design process, primarily pertaining to the Venusian environment.

The gravitational acceleration at a given altitude,  $h$ , is computed using Eq. (1.1).

$$g(h) = g_{surface} \left( \frac{R_V}{R_V + h} \right)^2 \quad (1.1)$$

To simulate the atmospheric density, temperature, and pressure at every altitude  $h$ , the Venus International Reference Atmosphere (VIRA) was used (Kliore, Moroz, Keating, and COSPAR., 1986), providing tabular data of the Venusian atmosphere at discrete altitudes. The values for given altitudes were computed using linear interpolation.

Due to a difference in solar intensity within the Venusian atmosphere, variable over the solar spectrum, no values for the solar flux in relation to the altitude can be found. The solar array power output in relation to the altitude is dependent on the composition of its solar cells, where the efficiency of multi junction solar cells is limited by the efficiency of the different layers in relation to the solar intensity of the targeted sections of the solar solar spectrum. Values of the output power flux for a triple junction GaAs solar cell were found from literature (G. Landis and Haag, 2013). From this, a relation could be found describing the change in power output with altitude over the range of the cloud layer. Finally, an estimate for the power flux could be provided over this range by taking into account the unaltered efficiency for a triple junction GaAs solar cell of 30%. The resulting values for the design conditions of 55 km and 65 km are given in Table 1.2.

The average values for the zonal and meridional winds experienced within the superrotating Venusian atmosphere were found from literature (Sánchez-Lavega et al., 2008; Hueso et al., 2008) and assumed to be constant at a given altitude. Furthermore, it was found that the wind speeds do not vary significantly depending on latitude within the investigated equatorial band (Sánchez-Lavega et al., 2008). The values used are given in the table of constants given in Table 1.2.

### 1.4. Design process

Leading up to this preliminary design report, a conceptual design design was conducted, consisting of a project planning phase, a requirements review phase, and a trade-off phase, which are all defined in the following.

<sup>2</sup> <https://nssdc.gsfc.nasa.gov/planetary/factsheet/venusfact.html>, retrieved on 06-05-2021.

<sup>3</sup> See footnote 2.

<sup>4</sup> [https://pds-atmospheres.nmsu.edu/education\\_and\\_outreach/encyclopedia/gas\\_constant.htm](https://pds-atmospheres.nmsu.edu/education_and_outreach/encyclopedia/gas_constant.htm), retrieved on 06-05-2021.

**Table 1.2:** Science constants used throughout the report.

Parameter	Symbol	Value
<i>General parameters</i>		
Venus radius <sup>2</sup>	$R_V$	6052 km
Surface level gravitational acceleration (Justus and Braun, 2007)	$g_{surface}$	$8.87 \text{ m s}^{-2}$
Average distance of Venus from the Sun <sup>3</sup>	$d$	0.723 AU
Gas constant on Venus <sup>4</sup>	$R$	$188.92 \text{ J kg}^{-1} \text{ K}$
Ratio of specific heats for Venus (Justus and Braun, 2007)	$\frac{C_p}{C_v}$	1.286
<i>Power parameters</i>		
Solar flux at Venus, 55 kilometers altitude	$J_{s_{Venus,55}}$	$1326 \text{ W m}^{-2}$
Solar flux at Venus, 65 kilometers altitude	$J_{s_{Venus,65}}$	$2607 \text{ W m}^{-2}$
Solar flux intensity at Earth (Wertz et al., 2011)	$J_{s_{Earth}}$	$1371 \text{ W m}^{-2}$
Solar flux at Venus, exo-atmospheric	$J_{s_{Venus}}$	$2622 \text{ W m}^{-2}$
Power flux at 55 kilometers	$S_{i_{Venus,55}}$	$404.4 \text{ W m}^{-2}$
Power flux at 65 kilometers	$S_{i_{Venus,65}}$	$752.0 \text{ W m}^{-2}$
<i>Thermal parameters</i>		
Albedo factor of Venus (Wertz et al., 2011)	$a_F$	0.65
Black body effective radiation temperature of Venus	$T_{IR}$	227 K
<i>Atmospheric winds</i>		
Average zonal wind on the day side at $h = 55 \text{ km}$ (Hueso et al., 2008)	$V_{zonal,day,55km}$	$63 \text{ m s}^{-1}$
Average zonal wind on the day side at $h = 60 \text{ km}$ (Hueso et al., 2008)	$V_{zonal,day,60km}$	$90 \text{ m s}^{-1}$
Average zonal wind on the day side at $h = 65 \text{ km}$ (Hueso et al., 2008)	$V_{zonal,day,65km}$	$100 \text{ m s}^{-1}$
Average zonal wind on the night side at $h = 55 \text{ km}$ (Hueso et al., 2008)	$V_{zonal,night,55km}$	$58 \text{ m s}^{-1}$
Average meridional wind at $h = 55 \text{ km}$ (Sánchez-Lavega et al., 2008)	$V_{meridional,55km}$	$0 \text{ m s}^{-1}$
Average meridional wind at $h = 65 \text{ km}$ (Sánchez-Lavega et al., 2008)	$V_{meridional,65km}$	$5 \text{ m s}^{-1}$

**Project planning phase** During the project planning phase, a number of organisational roles necessary for facilitating the smooth flow of the design process were identified. These were then structured into an organogram and assigned to different team members depending on strengths and preferences. Furthermore, five technical departments were established: Power and propulsion, Structures and materials, Mission payload and instrumentation, Flight performance, and Guidance, Telecommunication and navigation. Each technical department was assigned a department head to overlook it. Finally, the technical and organisational roles were connected via the role of the Systems Engineers, overlooking the entire project.

In addition to the division of technical and organisational roles, this phase also consisted of outlining different phases of the design process, identifying relevant tasks in each phase, and drawing up a preliminary project Gantt chart for the duration of the Design Synthesis Exercise (DSE).

**Requirements review phase** In the requirements review phase, stakeholder requirements were extracted from the mission description and from conversations with the customer. A requirements flow-down process was used to identify requirements for individual departments and subsystems; moreover, killer requirements were identified and discarded. In this phase, it was decided to use a relay orbiter for communication between the probe and ground stations. Most importantly, design option trees were created, which led to outlining four possible design concepts, namely a fixed-wing aerodyne, a propelled aerostat, a jellyfish-inspired balloon, and a dynastat relying on both buoyancy and dynamic motion to produce lift. These concepts were singled out to flow down further into the trade-off phase.

**Trade-off phase** Having outlined the four aforementioned design concepts, a trade-off was conducted to assess the likelihood of mission success for each design concept. The winner of this trade-off was the dynastat, since it combines the benefits of the aerodyne and aerostat design options. Another design option tree was drawn up for the dynastat design and based on the scores for the trade-off criteria in the previously conducted trade-off, the final design concept selected was an inflatable flying wing with a non-rigid structure. Furthermore, some preliminary mass and power budget estimations were established for both the probe and the orbiter.

**Preliminary design phase** With the trade-off phase completed, the present preliminary design phase is reached, which is the focus of this report.

## 1.5. Risk evaluation process

The technical risks related to the mission will be addressed throughout the report. These risks may pose a threat to the mission's success as they might involve to partial or even complete subsystem failures. A risk assessment for each major subsystem of both the atmospheric probe and the orbiter can be found in the respective subsystem sections. First, the identified risks will be given a rating with respect to the likelihood of occurrence and the severity of the consequences. A justification will systematically be provided for the assigned ratings. To reduce the identified risks, several mitigation strategies are proposed, after which both the severity and the likelihood are reassessed. Note that a differentiation will be made between actual mitigation strategies and standard procedures. The former will be included in the risk assessment, while some of the latter will be summed up further in this section. Thereafter, a pre- and post-mitigation risk map will be provided for both the probe and the orbiter to visualise the effects of the mitigation strategies as well as to give an overview of the risks that are deemed most prominent to the mission. Finally, an overview will be given of the requirements that flow down from the technical risk assessment and this will help drawing a conclusion on the overall risk level of the Kumo mission.

The risks were ranked based on the severity of their consequences and their likelihood of occurrence. The former is assessed using following categories:

1. **Negligible:** The consequences have no impact on operational efficiency and success of the mission.
2. **Marginal:** The experienced setbacks are not deemed harmful to the project.
3. **Noticeable:** Apparent setback to the mission and reduction in operational efficiency with implications to mission success.
4. **Critical:** The mission success could be jeopardised.
5. **Catastrophic:** Failure of the mission or a major lack of success.

Additionally, the likelihood of occurrence can be classified as very low (<1%), low (1% - 30%), moderate (30-50%), high (50-70%) and very high (>70%).

Finally, some standard procedures that are often put in place next to the actual mitigation strategies are:

- Mechanisms and systems shall be systematically tested.
- Components are inspected or tested for imperfections.
- Calibration of instruments before launch and in flight.
- Elaborate subsystem testing before integration.

Throughout the report, risk assessment will systematically be performed at the end of the designated sections for each subsystems, where a differentiation will be made between risks related to the orbiter and risks related to the atmospheric probe. These risks will be summarised by means of a risk map in Section 6.1, followed by a conclusion on the overall risk assessment for the mission as a whole.

## 1.6. Sustainability evaluation process

Implementing sustainability in space implies that humanity can continue to explore outer space for peaceful purposes as well as for social and economic benefit in the long term. Kumo is a mission that has paid a lot of attention to sustainability aspects at every stage. Hence, to enforce sustainability in the mission, sustainability requirements have been formulated. They will be mentioned in Section 6.2.2. It must be noted that, the overall mission sustainability will be elaborated upon in Section 6.2.

To assess the sustainability of the mission, the contribution of every subsystem to sustainability is quantified. This is done considering the three aspects of environmental, social and economic sustainability. To do this, a value between 0 and 3 is given to grade each subsystem. The explanation of each grade is as follows:

- **Very low (0):** The concept uses components in its design that need to be replaced by more sustainable parts.
- **Low (1):** The concept uses components that are relatively hard to replace with a more sustainable alternative.
- **Reasonable (2):** The concept uses components in its design that are all considered sustainable.
- **High (3):** The concept is completely made up out of the most sustainable components.

The mission is split into three phases to further clarify the contributions. Phase 1 indicates the Earth operations phase, phase 2 refers to the interplanetary phase and phase 3 designates the Venus entry and operations phase. These mission segments will receive a weight as they are not equally important. Phase 1 has a weight of 0.6, phase 2 has a weight of 0.1 and phase 3 has a weight of 0.3. The sustainability quantification per subsystem can be calculated using Eq. (1.2). The scores per subsystem are given as  $SP_1$  for the Earth operations phase,  $SP_2$  for the interplanetary phase and  $SP_3$  for the Venus operations phase. The formula is divided by three to create a value for each subsystem  $i$ , with a sustainability score, ranging between 0 and 1.

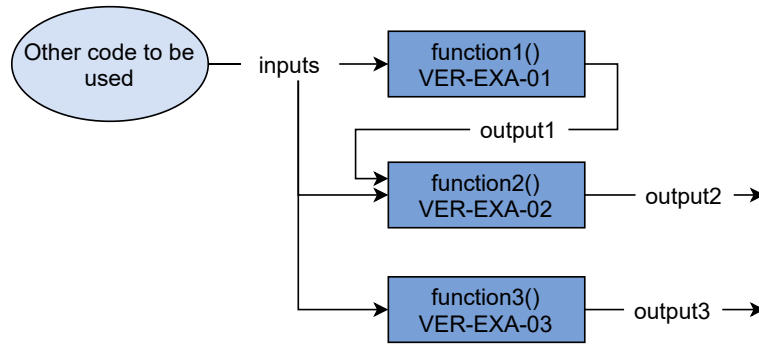


Figure 1.1: Code flow example

$$S_i = \frac{SP_1 \cdot 0.6 + SP_2 \cdot 0.1 + SP_3 \cdot 0.3}{3} \quad (1.2)$$

With the sustainability scores of each subsystem, the final mission sustainability scores for the probe and the orbiter are found. An overview of all scores can be found in Section 6.2. Each individual score per subsystem and the rationale behind these values can be found in their respective subsystem sections.

To account for the different levels of contribution to the sustainability between subsystems, each subsystem received a different weight. The weights that were received per subsystem are described under their individual sustainability sections.

$$S_{final} = \frac{\sum_{i=1}^n w_i S_i}{\sum_{i=1}^n w_i} \quad (1.3)$$

In the end, a final value for the sustainability of the probe and the orbiter is found. This score is rated qualitatively based on the following description :

- **Less than 20%** The mission is unsustainable. The concepts most likely need to be reconsidered in terms of sustainability and most components may need replacement.
- **Between 20% and 50%** The mission has low sustainability. Here, the concepts are more difficult to replace with more sustainable alternatives due to various constraints such as reliability, cost etc. Not all components need replacement, but some revision is needed.
- **Between 50% and 80%** The mission is reasonably sustainable. This means that majority of the components use sustainable alternatives. Here, only the highly weighted subsystems could be reviewed to obtain a better sustainability score.
- **Above 80%** The mission is considered highly sustainable. This is the desired score for Kumo. To obtain this, the components and concepts must be sustainable and efficient. It means all the technical departments have done well in selecting their concepts.

## 1.7. Verification and validation process

The verification procedures for all codes written along the mission were verified using a consistent approach. First, a flow diagram of the code's input, output and functions is given to give a general overview of the flow through the code. An example is seen in Fig. 1.1.

Then, all functions were given an identifier (ID), which is then used to state the specific verification tests performed for each function. A table giving the function's ID as well as the inputs and outputs and the expected function behaviour will be provided. If the function performs as predicted, a check mark is given to the test. The tables will have the format shown in Table 1.3.

Table 1.3: Unit tests for structures

Test	Variables	Expected behaviour	Verified
VER-EXA-01	<b>Input:</b> input <b>Output:</b> output	E.g. doubling input should double output	✓

Several unit tests can be performed, depending on the code. However, some unit tests can be performed in general:

- When checking linear equations with only multiplications or divisions, doubling/halving the input should directly double/halve the output.

- A numerical as well as an analytical model could be made and the outputs can be compared.
- For equations with additions/subtractions, adding an amount to the input should add that same amount to the output.
- Check if the output verification is zero when setting the input to zero, when applicable.
- Check for singularities and prevent the code from crashing.
- Use results from literature to check if the same outputs are given.

Similar tests can be applied for system testing by predicting what the output is when inputs are passed through more than one function and checking if the behaviour is as predicted. Additionally, data from previous resources such as papers and scientific books are used to validate the code itself. Also, all requirements will be verified. If the requirement has been met, a checkmark is placed next to the requirement as seen in Table 1.3. If not, a cross is placed and an explanation of the reason why it has been crossed out will be given as well as the follow up method that should be applied. Furthermore, if no codes were made, verification as well as validation can be executed using either certified off-the-shelf components, certified software or following the testing plan described in Chapter 7.

## 2. Mission design

From the mission objectives and requirements introduced in Chapter 1, the overall mission set up could be made. First, the elements of the mission and their names will be explained. Next, the market analysis will be performed, which will add additional values to the mission. Then, all system levels will be discussed in further detail. Once this has been explained, the extended mission operations as well as the end-of-life will be clarified. After all the steps have been shown, a mission design overview will be demonstrated. This will include the timeline, science operations, functional flow diagrams, and operations and logistics. The chapter will end with a risk analysis and sustainability. Once the general overview is clear, the design can go into more detail for the subsystems which is done in Chapter 3 and Chapter 4.

### 2.1. Mission elements

The Venus atmosphere explorer mission is called Kumo, derived from the Japanese word 雲 (*kumo*) for “cloud”, as the mission serves to investigate the Venusian cloud tops. The mission consists of the following elements:

- **Falcon 9**: The SpaceX Falcon 9 reusable launcher, used to bring the spacecraft into orbit around Earth.
- **Tobu** (飛ぶ, lit. “to fly”): The kick stage designed to propel the spacecraft into an interplanetary transfer orbit to Venus.
- **Tori** (鳥, lit. “bird”): The atmospheric probe collecting *in-situ* data of the Venusian atmosphere.
- **Tamago** (卵, lit. “egg”): The entry vehicle designed to descend into the Venusian atmosphere and deploy the probe within its operational altitude range. This mission element consists of the probe, Tori, and an aeroshell, **Tamago no kara** (卵の殻, lit. “egg shell”), that protects the probe from entry heating and acceleration loads. The entry vehicle also contains the necessary inflating mechanisms for the probe.
- **Tsubuyaki** (つぶやき, lit. “to tweet”): The orbiter designed to relay data and commands between the atmospheric probe and Earth, as well as take science measurements of its own.

Thus, the Kumo mission will be launched by a Falcon, fly to Venus and enter its atmosphere, then hatch from its egg to fly through the clouds and tweet its measurement data back to Earth.

The key parameters relevant for the mission operations planning and design are presented in Table 2.1 for the launcher and the orbiter, and in Table 2.2 for the atmospheric probe.

**Table 2.1:** Key parameters of the launcher and orbiter

Parameter	Value
<i>Falcon 9</i>	
Maximum launch mass	5500 kg
Launcher diameter	4.6 m
<i>Tsubuyaki</i>	
Orbiter dry mass	409 kg
Orbiter wet mass	1116 kg

**Table 2.2:** Key parameters of the atmospheric probe

Parameter	Value
<i>Tori</i>	
Probe mass	555 kg
Buoyant gas volume	706 m <sup>3</sup>
Folded probe dimensions	3 m x 1.5 m x 2.5 m
Buoyant altitude	55 km
Average flight velocity at low altitude during the morning	22 m s <sup>-1</sup>
Average flight velocity at low altitude during the evening	14 m s <sup>-1</sup>
Average flight velocity at high altitude	26 m s <sup>-1</sup>
Latitude change at high altitude	60°

### 2.2. Mission operations requirements

The requirements matrix for the mission operations are presented in Table 2.3. Requirements presented were derived from the user requirements for the mission, and those that were fulfilled are denoted by a checkmark (✓). The fulfilment of requirements KUMO-STH-PERF-02, KUMO-STH-PERF-03, KUMO-STH-PERF-04, KUMO-STH-PERF-05 and KUMO-STH-PERF-06 are documented in Section 2.8. Requirement KUMO-STH-PERF-08 is accomplished in Sections 2.9 and 2.10. Finally, requirement KUMO-STH-PERF-09 is achieved in Section 2.4.

### 2.3. Market analysis

From the mission objective and system requirements, additional value can be added to the mission by studying previous similar deep space missions. By observing their mission objectives as well as their findings and payload they have used, new opportunities and strengths can be added to this mission. To find the strengths and weaknesses from the proposed mission, the mission has to be put into perspective. This perspective is gained by viewing similar missions.

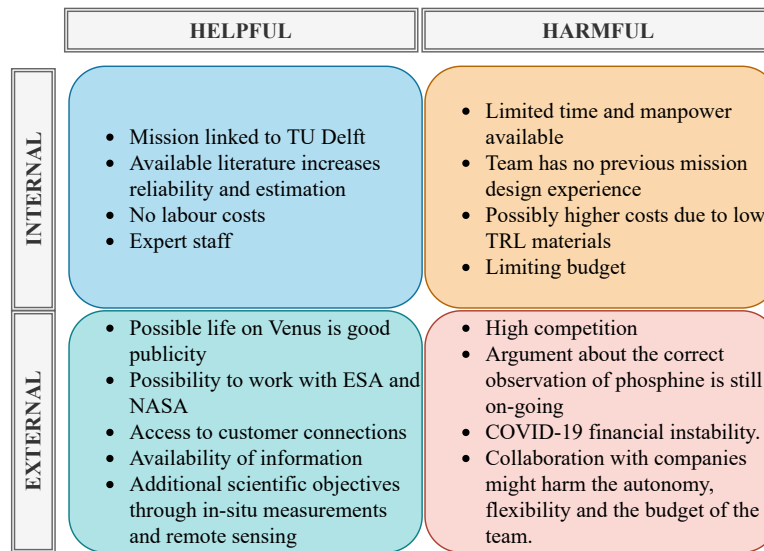


Figure 2.1: SWOT Analysis

First, a SWOT analysis will be carried out to map the strengths, weaknesses, opportunities and threats of the team and the mission. These aspects will be elaborated upon by explaining the factors of each components, such as prospective partners & investors and scientific opportunities. Finally, additional requirements obtained from the additional objectives will be included.

### 2.3.1. SWOT analysis

The market analysis is based on the outline of Fig. 2.1. This chapter will elaborate on the strengths, weaknesses, opportunities and the threats to the mission and the design. In this diagram the technology readiness level is abbreviated to TRL.

#### Strengths

Science data from previous missions to Venus such as, Akatsuki<sup>1</sup>, Venus express<sup>2</sup> and Magellan<sup>3</sup> can be found online for free. This makes validation of the probe and orbiter easier. As the mission is part of a university project, engineers have access to the resources of TU Delft. This gives the Kumo engineers an advantage over engineers in the private sector. Also, the client linked to the Kumo mission provides the team with a vast sum of money and expertise.

#### Weaknesses

Weaknesses are defined as internal factors that could negatively affect both the mission and the team's position in the market. A division is made between team-related and mission related weaknesses. Firstly, the time allocated to this project is around eleven weeks. This in combination with the relatively small size of the team results in constraints that limit the design process. Extensive design analysis that often come with end-to-end mission design of this scale will have to be limited and decisions will have to be made regarding prioritisation of some parts of the design over others. Secondly,

<sup>1</sup><https://darts.isas.jaxa.jp/planet/project/akatsuki/>, retrieved on 30-5-2021

<sup>2</sup><https://www.cosmos.esa.int/web/psa/venus-express>, retrieved on 30-5-2021

<sup>3</sup><https://nssdc.gsfc.nasa.gov/planetary/magellan.html>, retrieved on 30-5-2021

Table 2.3: Requirements matrix for mission operations

Identifier	Requirement	Checked
KUMO-STH-PERF-02	The platform shall fly ten times around Venus.	✓
KUMO-STH-PERF-03	Five locations of interest, defined by altitude, latitude and local time, shall be covered at least twice for repeat observations with latitudinal and longitudinal accuracy of 1 km, to confirm deviating/interesting measurements.	✓
KUMO-STH-PERF-04	A band of latitudes 30° north or south from the equator shall be covered.	✓
KUMO-STH-PERF-05	The lowest altitude to be sampled by the platform shall be higher than 55 km.	✓
KUMO-STH-PERF-06	The highest altitude to be sampled by the platform shall be lower than 65 km.	✓
KUMO-STH-PERF-08	An extended mission plan shall be defined for the case that the platform will exceed nominal life.	✓
KUMO-STH-PERF-09	Launch date shall be no later than 2028.	✓

the team has no prior experience with an end-to-end mission design of this scale. This could potentially slow down the design and increase the probability of erroneous results. Therefore, a search for prospective partners could prove beneficial for the team in case knowledge sharing or transfer is involved. Thirdly, the Kumo mission dares to create a probe that can stay in the atmosphere for approximately 60 days. This has never been done before and thus requires cutting edge technology to make it work. However, to make sure that the mission is successful, the materials chosen must be tested, verified and validated. For this reason, a relatively large external budget must be allocated to the testing, verifying and validating of the materials and components. Finally, the budget for the mission is stated to be at €1 billion. The allocated budget rules out several designs that require more imaginative solutions, which would require extra testing. To ensure that the budget requirement is met, extra science instruments could be added to increase the science data output of the mission. This in turn could increase the potential investors to the project. However, this would effectively increase the complexity of the mission. Else, the mission could opt to use off-the-shelf products to solve its design challenges, which would make the final design lack in innovation.

### Prospective partners and investors

The Kumo mission receives its funding from a client who is linked to ESA. Currently, the collaboration between the team and ESA is very limited. The team could consider strengthening their ties with ESA. In their call for commercial partnerships, they state to be interested in projects concerning robotic exploration of the Moon and Mars or projects related to humans in LEO orbit or beyond<sup>4</sup>. Another path to partnership is to propose a new partnership idea. For this, the team would have to fill in the Commercial Partnership Idea Template. After the submission, an evaluation follows with a subsequent pilot phase in which the best submissions enter into a competition. For this phase, an extensive preparation is required. If the team manages to successfully get through the pilot phase, the partnership is implemented.

NASA is known for subcontracting work to privately owned companies like SpaceX<sup>5</sup> and thus might be an interesting option for the Kumo mission. To do business with NASA, ten steps need to be completed. The steps start from registering your company in North America and end with presenting the product to NASA<sup>6</sup>. A company can then either form a partner agreement or enter a procurement contract with NASA. Since the Kumo mission is not used to directly benefit the US government, the options are limited to a partnership agreement. This partnership agreement would formally be known as a Space Act Agreement (SAA).

The most interesting option would be the Reimbursable SAA. In this case Kumo would pay NASA to be able to use its unique resources. However, as NASA is a governmental agency it is not allowed to compete in the private sector. This means that NASA is not allowed to provide services that are normally available to the private sector.<sup>7</sup> With this SAA option, Kumo will have the least interference from NASA. NASA states to partner up with universities and, as the Kumo mission is linked to the TU Delft, a partnership is applicable. Another option would be for Kumo to separate itself from the university and to set up a company in North America with the risk of losing the current investment of €1 billion. If the team would consider a creating their own company a more complex process would have to be followed.

Working with any of these companies could greatly increase the output of work done for this mission. The team would get access to most advanced workplaces and facilities in the world and could get assistance from experts in the industry. This could, however, come at the cost of the team losing their autonomy, flexibility or even the investment. A potential agreement will also require Kumo to gather a legal team.

Lastly, the nature of this mission is to find signs of life on Venus. The potential abundance of the biomarker, phosphine on Venus caused a stir in both the scientific community and the public. This mission will undoubtedly generate a huge amount of publicity. Publicity is very important in attracting potential investors. It is much easier to find investors if they already know the project exists. This could thus increase the mission budget.

### Scientific opportunities

The main objective of the Kumo mission is to study the planet's evolution with the use of noble gas isotopes. If these are found, further missions to Venus would have to be made to potentially confirm the existence of alien life. In this case, the Kumo team could play a further role in researching Venusian life and help develop further missions to the planet.

The idea of colonising other planets in the solar system has been a popular idea for many years. Frequently, Mars and the Moon are named as prominent candidates. However, a case was also made for Venus. Due to the composition of the Venus atmosphere, breathable air would float to the top of the atmosphere. This gives rise to the idea of humans living in a gigantic balloon like structures floating in the atmosphere of Venus. The atmosphere of Venus has a zone between 50 and 60 km in which the pressure and gravity are similar to that on Earth (Landis, 2020). Important scientific questions that needs to be answered related to this opportunity include, investigating the nature of super-rotation, oceanic history of Venus and geology of the planet. Furthermore, the habitat could be used as a base for asteroid miners to make it economically interesting. Venus has a shorter flight time to the asteroid belt than Earth or Mars (Landis, 2003). To reach these asteroids the colony would have to include a space port. A mission like this could potentially happen but due to

<sup>4</sup>[https://esamultimedia.esa.int/docs/business\\_with\\_esa/ESA\\_CFP\\_Call\\_for\\_Partnerships\\_Dec\\_2019.pdf](https://esamultimedia.esa.int/docs/business_with_esa/ESA_CFP_Call_for_Partnerships_Dec_2019.pdf), retrieved on 28-5-2021

<sup>5</sup><https://www.nytimes.com/2021/04/16/science/spacex-moon-nasa.html>, retrieved on 01-06-2021

<sup>6</sup><https://www.osbp.nasa.gov/business.html>, retrieved on 30-5-2021

<sup>7</sup><https://www.nasa.gov/partnerships/faqs.html>, retrieved on 30-5-2021

the large investments needed and no short term economic gain, it will probably be shelved until a later time. The Kumo mission will pave the way for long duration stay in the Venusian atmosphere and could inspire the idea of a city in the clouds.

Many scientific opportunities have been found to be useful for the Kumo mission, which are based on previous similar deep space missions. The potential opportunities have been listed below:

1. **Material degradation and structural integrity analysis (MO1):** An experiment for the material degradation as well as structural integrity could be carried out. During the flight of the probe, one of the largest problem will be oxidation and material hardening. To monitor this, the thickness of the material can be monitored with the use of ultrasonic sensors. The number of sensors depend on the number of degrees of freedom. As the dynastat inflates, there should be six. Then, the structural integrity can be monitored using fibre optic sensors. There can be two on each side and this can show how the dynastat is behaving during flight as well as checking if it has inflated correctly. These sensors are cheap and light weight.
2. **Aerosol detection (MO2):** Aerosols are a mixture of gas and solid and/or liquid components<sup>8</sup>. These aerosols scatter or absorb light entering the atmosphere, which can determine some aspects of the super-rotation of the atmosphere. Another example that can be done with the detection of aerosols is measuring the amount of sulphur in the solid sulphuric cloud particles, which subsequently can be used to study volcanic activity on Venus. For aerosol detection, instruments called Nephelometers have been used in previous missions. One example is the Nephelometer (NEP) used on the Galileo mission<sup>9</sup> (Meltzer, 2007). Additionally, a study of the cloud structure composition and scattering properties will be performed by the VIRTIS instrument on the orbiter as further explained in Section 4.1. Hence, the data of the NEP and the VIRTIS could be compared to determine the relationship between the aerosols detected within the atmosphere and the light scattering observed outside of the atmosphere.
3. **Measuring lower altitude temperatures (MO3):** More than 75% of the Venusian atmosphere's mass is below 40 km of altitude. The science community still needs an understanding of the thermal structure of this region. The Vega mission was the only one to measure temperature data for those altitudes reliably. However, the data available is not enough to allow an understanding of the characteristics of the atmosphere in this region (Glaze et al., 2018). The probe could have an end-of-life mission that performs an atmospheric descent while measuring the temperatures at altitudes lower than 40 km until it fails. Wireless platinum temperature sensors<sup>10</sup> will be used as platinum is acid resistant<sup>11</sup>. These sensors are lightweight and available at low cost. Also, they can measure temperatures within a wide range of  $-200\text{ }^{\circ}\text{C}$  to  $1000\text{ }^{\circ}\text{C}$ .
4. **Measuring upper atmospheric conditions (MO4):** The atmosphere of Venus has still many unknown features which still need further investigation. One example is measuring the upper atmospheric conditions, such as temperature and pressure. This could be done by the orbiter as its end of life mission when descending into the atmosphere. It is expected that the orbiter will fail soon in the upper cloud layer of the atmosphere. However, any additional data that it can measure while descending could bring additional value to the mission. The same sensors will be used as those mentioned for MO3.
5. **Evolution of cosmic dust (MO5):** Cosmic dust has always been a topic of interest for astronomers, primarily because they pave a way to study the evolution of planets<sup>12</sup>. Recently in 2018, Parker's solar probe reported to have found a dense layer of cosmic dust near the orbit of Venus. This discovery was made by using the Wide-field Imager for Solar Probe (WISPR) instrument on board of the probe<sup>13</sup>. The evolution of this recently found a dust ring and its composition is still a mystery for the scientific community. Hence, this adds to the list of potential additional scientific objectives for Kumo. To carry out this mission objective, additional payload would have to be included on board of the orbiter. However, this would mean that the orbiter should fly in a specific orbit to measure the dust particles, which would over complicate the orbital design. Therefore, the dust analyser has been *discarded* as an option for additional value.
6. **Airglow (MO6):** The Venera-9 and -10 discovered strong airglow in the visible spectrum in the Venus nightside (Slangier, 2001). Mapping the airglow spatial distribution and its temporal variations could contribute to the study of the circulation of the lower thermosphere. Additionally, by doing limb observations at an altitude of 2000 km, the high altitude haze layers can be studied and the atmospheric vertical structure can be determined (Drossart et al., 2004). Measuring the airglow can be done using the VIRTIS instrument on the orbiter as defined in Section 4.1.
7. **Volcanic activity (MO7):** Volcanic activity has previously been determined on Venus. Volcanic activity can be tracked by searching for hot spots which can be detected in the infrared spectrum. Hence, this can be detected with the VIRTIS on board of the orbiter. Thus, additional value can be established without the use of any additional instruments.

<sup>8</sup><https://palas-counts.com/measure/aerosols/>, retrieved on 31-05-2021

<sup>9</sup>[https://pds-atmospheres.nmsu.edu/PDS/data/gp\\_0001/catalog/NEPINST.CAT](https://pds-atmospheres.nmsu.edu/PDS/data/gp_0001/catalog/NEPINST.CAT), retrieved on 31-05-2021

<sup>10</sup><https://www.ist-ag.com/en-us/products-services/temperature-sensors>, retrieved on 02-06-2021

<sup>11</sup><https://nature.berkeley.edu/classes/eps2/wisc/pt.html>, retrieved on 02-06-2021

<sup>12</sup><https://herscheltelescope.org.uk/science/infrared/dust>, retrieved 31-05-2021

<sup>13</sup><https://www.nasa.gov/feature/goddard/2021/nasa-s-parker-solar-probe-sees-venus-orbital-dust-ring-in-first-complete-view>, retrieved 18-06-2021

**Table 2.4:** Table showing opportunities in science data output for the mission

ID	Opportunity	Payload	Cost (M€)	Mass (kg)	Power (kW)
<b>Probe</b>					
MO1	Measure material thickness and structural integrity	Ultrasonic sensors (x6), fibre optic sensors (x2)	0.03	2	0.013
MO2	Measure aerosols from within the atmosphere.	NEP	20	4.8	0.014
MO3	Measure temperatures below 40 km.	Temperature sensors	10E-6	-	-
<b>Orbiter</b>					
MO2	Measuring the cloud structure, composition, and scattering properties	VIRTIS	32	33	36
MO4	Measure upper atmospheric conditions	Temperature sensors	10E-6	-	-
MO6	Measuring airglow/ limb observations	VIRTIS	(32)	33	36
MO7	Measuring volcanic activity	VIRTIS	(32)	33	36

8. **Mapping the gravity field (MO8):** The gravity field is never constant along the entire surface of a planet. This is due to the altitude differences on the surface. These differences causes different gravity forces at different altitudes which can be traced back by the fluctuations an orbiter experiences in its orbit. Such measures are usually carried out by radars or radio science subsystems. An example is given by the Radio Science Subsystem used on the Cassini mission<sup>14</sup>. However, to measure these small fluctuations, the orbiter should be into an orbit relatively close to the surface. This suggests that the orbiter should fly within a specific orbit, which would over complicate the orbit design. Hence, this option has been *discarded*.

All chosen additional values have been stated in Table 2.4 along with their identifier, payload required, mass power required and cost.

### Threats

Bio-markers on Venus are a trending topic. This means that the team can expect be many other mission proposals that have similar objectives. This highly competitive market environment can lead to a more competitive selection process for sponsors. There could even be other proposals from different teams to our customer, which the team should be aware of. Furthermore, the ongoing debate on the correct observation of phosphine as a biomarker means that the mission's goal should not be phosphine-specific.

Another threat would be the financial instability and the market disruptions that the COVID-19 pandemic has caused in the global economy. The pandemic has been budget-constraining for many firms and entrepreneurs, meaning that the availability of financial resources has diminished significantly.

Lastly, should the team decide to collaborate with other companies a legal team should be gathered to deal with creating the contracts. This process will bring risks with it for the team and will cost more money.

### Additional requirements

Based on the opportunities, the Kumo mission has added several additional mission objectives to the mission. These objectives are seen as less important to the primary objectives and will thus receive less priority in design and mission planning. The additional requirements based on the market analysis can be found in Table 2.5.

### 2.3.2. Competitors

Kumo is joint by several other missions in its pursuit to research Venus. These include EVE<sup>15</sup>, Venera-D<sup>16</sup>, VAMP<sup>17</sup>, an unnamed Rocket Lab mission<sup>18</sup>, VERITAS and DAVINCI<sup>19</sup>. The European Venus Explorer (EVE) mission by ESA aims to send and keep a balloon in the atmosphere of Venus for 10 days. In this time, ESA hopes to study the current Venusian climate and investigate the formation and evolution of the planet by measuring the noble gasses and isotopes. The Venus Emissivity, Radio Science, InSAR, Topography, and Spectroscopy mission (VERITAS) by NASA aims to measure the topography of the Venusian surface. The Deep Atmosphere Venus Investigation of Noble gases, Chemistry, and Imaging (DAVINCI) mission by NASA plans to measure the composition of the Venusian atmosphere in a descent

<sup>14</sup><https://solarsystem.nasa.gov/missions/cassini/mission/spacecraft/cassini-orbiter/radio-science-subsystem/>, retrieved on 02-06-2021

<sup>15</sup><https://www.lmd.jussieu.fr/~sllmd/pub/REF/2012ExA...33..305W.pdf>, retrieved on 31-5-2021

<sup>16</sup><https://meduza.io/en/feature/2019/04/03/joint-russia-u-s-project-plans-to-land-a-spacecraft-on-venus-for-the-first-time-since-1985>, retrieved on 31-5-2021

<sup>17</sup><https://www.northropgrumman.com/vamp/>, retrieved on 31-5-2021

<sup>18</sup><https://www.space.com/rocket-lab-venus-life-hunting-mission.html>, retrieved on 31-5-2021

<sup>19</sup><https://www.jpl.nasa.gov/news/nasa-selects-investigations-for-future-key-planetary-mission>, retrieved on 31-5-2021

**Table 2.5:** Requirements based on the market analysis

Identifier	Requirement
KUMO-MA-SCI-MO1	Tori shall expose promising materials to the Venusian atmosphere to measure the material behaviour.
KUMO-MA-SCI-MO2-1	Tori shall measure aerosol particles with a size of at least 1 $\mu$ m at concentrations less than 1 $\text{cm}^3$ (Coradini, 1999).
KUMO-MA-SCI-MO3	Tori shall measure temperatures below 40 km.
KUMO-MA-SCI-MO2-2	Tsubuyaki shall measure the cloud structure, composition and scattering properties with a spectral resolution of 3 nm.
KUMO-MA-SCI-MO4	Tsubuyaki shall measure the temperatures in the upper atmospheric layer.
KUMO-MA-SCI-MO6	Tsubuyaki shall measure airglow with a spectral resolution of 5 nm.
KUMO-MA-SCI-MO7	Tsubuyaki shall measure hot spots with a spectral resolution of 5 nm.

lasting a little over an hour. The Venera-D mission by the Russian Federal Space Agency (RFSA) aims to measure the chemical composition below 20 km of the atmosphere and image the surface of Venus. This is done by landing a craft on the surface and doing measurements for 60 Earth days. The Venus Atmospheric Maneuverable Platform (VAMP) mission, by the Northrop Grumman and L'Garde, intends to fly an inflatable aircraft in the atmosphere of Venus to study the atmosphere of Venus. The unnamed Rocket Lab mission aims to find signs of life on the surface of the planet and study its geographical evolution. The Kumo mission has much overlap with these missions and intends to do most of what the other missions plan to do all by itself. Because of this, even though the competition is fierce, Kumo is the better mission if it can meet all the top level requirements.

## 2.4. Launch

The first phase of the mission is the launch to start the travel to Venus. In the following sections the launcher will be selected together with a suitable launch site.

### 2.4.1. Launcher selection

The selection of the launcher was performed with the general objective of minimising cost. Furthermore, two lower level objectives were considered – risk minimisation and high-standard sustainability insurance. The requirements were primarily those of satisfying the size, mass and performance constraints of the payload to be launched.

The launch payload consists of the probe, the orbiter and the kick stage. The probe and orbiter masses are found to be 1014 kg and 1190 kg in Section 2.7.4 and Section 4.7, respectively. Note that the probe mass includes the entry vehicle and inflation equipment mass, too. The mass of the kick stage was estimated to be 314.1 kg using empirical relations, see Section 2.5.3. Together with the 1795 kg of fuel for the kick-stage, the final wet mass of the launcher's payload was found to be 4323 kg.

With the given requirements, the Falcon 9 reusable launcher from SpaceX was selected, primarily because it is the cheapest commercially available launcher able to transport the required mass to a Geostationary Transfer Orbit (GTO) at \$62 M<sup>20</sup>. The launch to GTO significantly decreases the  $\Delta V$  requirements on the kick stage in comparison with a launch to LEO.

Furthermore, the payload envelope for the fairing of the Falcon 9 launcher has a diameter of 4.6 m and the height of at least 6.7 m after which the cross section is converging up until a maximum height of 11 m<sup>21</sup>. The largest dimension of the payload that has to fit in the fairing is the 4.5 m diameter probe aeroshell heat shield, thus ensuring the compatibility of the launcher.

The risk assessment was performed using the data from past launches. To date, Falcon 9 is by far SpaceX's most commonly used launcher, with 118 out of 126 launches performed by Falcon 9. The significant number of launches sets a low standard deviation to the high 98.31% success rate of launches performed by Falcon 9. Lewis point estimate index, which accounts for small-size estimates when computing success rate, scores Falcon 9 as the most reliable launcher in history as of December 2020<sup>22</sup>.

Sustainability rating of the chosen launch is equally important. It is estimated that Falcon 9 launch produces 425 metric tonnes of CO<sub>2</sub> and 152 metric tonnes of water vapour per launch. These figures rank Falcon 9 fifth and fourth out of eight commercial launchers studied in terms of CO<sub>2</sub> and water vapour, respectively.<sup>23</sup> Furthermore, the reusable nature of the launcher allows for diminishing emissions of the production phase per each launch conducted, which poses a significant advantage among the competitors.

<sup>20</sup><https://www.spacex.com/media/Capabilities&Services.pdf>, retrieved on 22-06-2021

<sup>21</sup>[https://www.spacex.com/media/Falcon\\_Users\\_Guide\\_082020.pdf](https://www.spacex.com/media/Falcon_Users_Guide_082020.pdf), retrieved on 10-06-21

<sup>22</sup><https://www.spacelaunchreport.com/log2020.html>, retrieved on 10-06-21

<sup>23</sup><https://everydayastronaut.com/rocket-pollution/>, retrieved on 10-06-2021

### 2.4.2. Launch site selection

The launch site options of the Falcon 9 launcher are pre-determined by the launch provider. SpaceX utilises four launch sites spread across the United States of America. The most native launch site for Falcon 9 missions is Kennedy Space Center (KSC), Merritt Island, Florida.

Ideally, the launch site shall be located at zero inclination as the interplanetary transfer will be performed in that plane. Any inclination of the launch site above or below zero would require a change of inclination upon launcher separation, thus using the propellant of the kick stage. Since the mass of the kick stage propellant shall be minimised, the inclination of the launch site shall be minimised as well. KSC has the lowest inclination of the four available launch sites at 28° and is thus selected for the mission.

## 2.5. Transfer

Once the platform has been launched, it will need to travel to the desired location, which in this case is Venus. Several assumptions have been made, to facilitate the calculations. With these assumptions, the transfer orbit as well as the  $\Delta V$  and time needed for the transfer can be computed. Furthermore, the kick stage for the interplanetary transfer injection is sized.

### 2.5.1. Assumptions

For the astrodynamics computations, impulsive manoeuvring is assumed (**TF.A.1**). In reality, the execution of the propulsive manoeuvres will not be impulsive, but take a certain burn time. However, with sufficient thrust levels, this burn time can be assumed small compared to the orbital motion. For example, the Venus relay orbit injection burn requires a  $\Delta V$  of 1.93 km s<sup>-1</sup>. The chosen engine (see Section 4.4.5) can provide an average acceleration of

$$a \approx \frac{2T}{m_{begin} + m_{end}} = \frac{2T}{2m_{begin} - m_{prop}} = 0.51 \text{ m s}^{-1} \quad (2.1)$$

Using  $T = 425 \text{ N}$  and  $m_{prop} = 707 \text{ kg}$  from Section 4.4.5 as well as  $m_{begin} = 1190 \text{ kg}$  from Section 4.7.3. Thus the burn would take just 1.1 h out of the 148 h relay orbit period (as can be inferred from Section 2.6.2) rendering the burn time insignificant indeed.

Furthermore, a patched conics approach (**TF.A.2**) was taken for the interplanetary transfer astrodynamics computations. It neglects the gravitational influence of other bodies when inside the sphere of influence of the most attracting body. It simplifies transfer calculations into a series of Kepler orbits and works for straightforward manoeuvres, like the Hohmann transfer. However, it does not allow for computing, e.g., the low energy transfer methods utilising the Lagrange points, as those only appear by the addition of a secondary body. For the mission presented, the Hohmann transfer and thus patched conics approach suffice.

Lastly, the heliocentric orbits of Earth and Venus are assumed circular and without any inclination (**TF.A.3**), to simplify the astrodynamics calculations. In reality none of the planets' orbits are perfectly circular or without any inclination, but in Earth and Venus' case, the eccentricity<sup>24</sup> and inclination<sup>25</sup> with respect to the invariant plane are 0.017, 1.57° and 0.007, 2.19°, respectively.

### 2.5.2. Astrodynamics

The interplanetary transfer from the parking orbit around Earth towards the first orbit around Venus is a Hohmann transfer. It takes 146 Earth days of travel, and presents an insertion window every synodic period of 587 Earth days. The insertion window during the targeted launch year of 2028 is on the 3rd of April, making the spacecraft arrive at Venus on the 27th of July 2028<sup>26</sup>. To make this transfer insertion window, the spacecraft has to be launched on the same day a couple of hours before the burn has to be performed, leaving time for in-orbit checkout and other preparations for the manoeuvre.

The  $\Delta V$  required to enter the transfer trajectory from GTO amounts to 1.80 km s<sup>-1</sup>. This is composed of an inclination correction manoeuvre at apogee and the actual transfer orbit injection at perigee. The former is necessary as the GTO is inclined by 27°<sup>27</sup> and the transfer orbit lies close to the ecliptic plane. The  $\Delta V$  cost of the inclination change is described by

$$\Delta V_{incl} = 2V_{park,apo} \sin(i/2) = 0.746 \text{ km s}^{-1} \quad (2.2)$$

where  $V_{park,apo}$ , the velocity in the GTO parking orbit at apocentre, can be found from the vis-viva equation and  $i$  is the inclination of the GTO. For the transfer burn itself, a certain heliocentric velocity change relative to Earth has to be realised, which translates as a geocentric hyperbolic escape velocity into the  $\Delta V$  required at the pericentre of the GTO in the following way. First, the  $\Delta V$  relative to Earth's circular orbit speed for the Hohmann transfer is computed using

<sup>24</sup><https://www.enchantedlearning.com/subjects/astronomy/glossary/Eccentricity.shtml>, retrieved on 21-06-2021

<sup>25</sup><https://web.archive.org/web/20130501120739/http://home.surewest.net/kheider/astro/MeanPlane.gif>, retrieved on 29-06-2021

<sup>26</sup><http://clowder.net/hop/railroad/EV.htm>, retrieved on 24-06-2021

<sup>27</sup><https://www.spacex.com/media/Capabilities&Services.pdf>, retrieved on 21-06-2021

$$V_{\infty,E} = \sqrt{\frac{\mu_S}{r_E}} - \sqrt{\mu_S \left( \frac{2}{(r_E + r_V)/2} - \frac{1}{r_E} \right)} = 2.50 \text{ km s}^{-1} \quad (2.3)$$

Then, Eq. (2.4) is used to compute the interplanetary transfer injection burn  $\Delta V$  by taking the difference between the velocity required to achieve the hyperbolic escape velocity for the heliocentric transfer and the current velocity in the pericentre of the GTO.

$$\Delta V_{inj} = \sqrt{\mu_E \left( \frac{2}{r_{GTO,p}} + V_{\infty} \right)} = 1.05 \text{ km s}^{-1} \quad (2.4)$$

Alternatives to the Hohmann transfer that were considered include fast transfers, which use more  $\Delta V$  to reach the destination quicker. As there is no need for speeding up the transfer, this option was eliminated. On the other side, low energy transfers allow spending up to 16 % less  $\Delta V$  on the transfer manoeuvres, at the cost of multiplying transfer times by a factor 4 (Topputo et al., 2004). These savings were found to be diminishing returns in the case of this mission, and not strictly necessary as the selected launch vehicle has some performance margin to spare. Thus a Hohmann transfer is chosen for its reasonable transfer time and  $\Delta V$  requirements. By looking at missions like Venus Express (Sanchez Perez and Canabal, 2004) or Magellan<sup>28</sup>, it can be confirmed that (variations on) the Hohmann transfer are a common choice for mission to Venus, thus supporting the choice for this mission.

### 2.5.3. Kick stage sizing

To propel the combination of orbiter and probe from the GTO parking orbit of 200 km by 35,786 km on to a Hohmann transfer orbit from Earth to Venus, a kick stage is used. As it needs to provide a  $\Delta V$  of  $1.80 \text{ km s}^{-1}$  to a combined payload of 2204 kg (1014 kg probe in entry vehicle plus 1190 kg orbiter wet mass), a propellant mass of 1795 kg is found using Tsiolkovsky's rocket equation with a representative upper stage  $I_{sp} = 340 \text{ s}$  (see, for example, the Rutherford engine<sup>29</sup>) and a kick stage dry mass to propellant mass ratio of 17.5 % taken from Zandbergen (2017). This gives a kick stage dry mass of 314.1 kg.

### 2.5.4. Operations

During the transfer, the spacecraft will mostly stay in hibernation, meaning that it only intermittently broadcasts house-keeping data, performs system checks and receives commands or updates to the mission plan and/or software. To enable this, the main orbiter antenna will be facing Earth, and the whole spacecraft will execute a "barbecue roll" around the antenna's axis of symmetry to distribute the solar radiation more evenly and avoid large thermal gradients. This will help the thermal control system in keeping the temperatures in check during the transfer.

Shortly before arrival at Venus, the spacecraft will wake from hibernation, as it is time for the orbiter to separate from the kick stage. The kick stage will ignite one last time to correct the probe's course towards a direct atmospheric entry. The  $\Delta V$  required for this manoeuvre depends on the time of separation, as doing it early in the transfer will cost less  $\Delta V$  than performing the course correction very shortly before Venus. The drawback of early separation is that the probe loses its power and command connection with the orbiter. Further studies should look into the optimal timing and additional design considerations stemming from a choice for a specific separation timing, such as the possibility to include a small antenna on the entry vehicle as well to take over from the orbiter communications link after separation.

## 2.6. Orbiter nominal operations

The mission will make use of two orbits: a relay orbit and a scientific one. The decision was made for optimisation of scientific instruments both on the probe and the orbiter, while sufficient communication is ensured. Although more varied orbits would surely be preferred, the  $\Delta V$  budget drove the maximum difficulty of the orbital change allowed. Higher  $\Delta V$  would theoretically be still possible, though discarded out of sustainability considerations. The current  $\Delta V$  budget drives the orbiter mass close to the payload mass limit of the biggest reusable launcher - Falcon 9. For the aforementioned reasons, the two orbits described in this section have been finalised.

### 2.6.1. Orbit insertion

When arriving at Venus, the orbiter Tsubuyaki will have to exit the hyperbolic venocentric arrival trajectory and insert itself into the relevant orbit. The  $\Delta V$  required for this manoeuvre is given in Eq. (2.6), using the heliocentric velocity difference between the spacecraft and Venus as computed in Eq. (2.5) and a target orbit radius of  $r_{relay} = R_V + h_{relay} = 1.33 \times 10^5 \text{ km}$ . The computation is very similar to the one for the transfer injection burn in Section 2.5.2, but then for Venus and a different target orbit.

<sup>28</sup><https://www2.jpl.nasa.gov/magellan/guide2.html>, retrieved on 21-06-2021

<sup>29</sup><https://www.rocketlabusa.com/about-us/updates/rocket-lab-increases-electron-payload-capacity-enabling-interplanetary-missions-and-reusability/>, retrieved on 10-06-2021

$$V_{\infty,V} = \sqrt{\mu_S \left( \frac{2}{(r_E + r_V)/2} - \frac{1}{r_V} \right)} - \sqrt{\frac{\mu_S}{r_E}} = 2.71 \text{ km s}^{-1} \quad (2.5)$$

$$\Delta V_{insert} = \sqrt{\mu_V \left( \frac{2}{r_{relay}} + V_{\infty,V} \right)} = 1.93 \text{ km s}^{-1} \quad (2.6)$$

The  $\Delta V$  computed for the orbit insertion manoeuvre is used in Section 4.4.5 to find the fuel mass that the orbiter needs to carry.

### 2.6.2. Relay orbit

Upon arrival to Venus, the orbiter will be inserted in the relay-prioritised orbit. The orbit's key objective is to serve as an effective relay unit during the first phase, when the probe will be collecting the raw data. The datalink during this phase is high, which forced an introduction of a probe-stationary orbit. The orbit was designed in a way that the period of one revolution of the probe and the orbiter are equal, thus maximising the possible length of the transfer link per revolution. Designing for the given condition yielded a circular orbit of 133,215 km radius. Furthermore, the orbit will be in the equatorial band, only with a 3.46° inclination.

An issue could arise from the variable velocity of the probe throughout a revolution. The velocity of the probe at night will be 58 m s<sup>-1</sup>, which is twice as low as the 126 m s<sup>-1</sup> during daytime, as presented in Table 2.10. Accounting for the differences in altitudes (55 km and 65 km), the angular velocities are 3.42 × 10<sup>-2</sup> rad h<sup>-1</sup> and 7.41 × 10<sup>-2</sup> rad h<sup>-1</sup>, respectively. In comparison, the angular velocity of the relay orbit is 4.22 × 10<sup>-2</sup> rad h<sup>-1</sup>. Assuming the worst case scenario, when the orbiter and the probe start at dawn, the maximum longitudinal differential between the satellite and the probe will occur when the probe will have traversed 180°, so in 2.05 d. At that time, the satellite will only be 119° away from its starting position. This is the worst case, where the longitudinal difference between the orbiter and the probe will be 61°, which is also the angle that the two bodies make with the centre of Venus. The presented calculation conclusively proves the maximum possible duration for the communications window between the two vehicles to be 100%.

### 2.6.3. Science orbit

In Phase II the probe will re-qualify for collecting repeat observation. The repeat observations are discrete and thus, drive the datalink budget constraints significantly down. At this stage, the orbiter will be relocated into a scientific orbit. The lifted requirements on the data rate will allow the spacecraft to collect its own measurements with the remote sensing equipment. The new orbit will be a highly eccentric one with 300 km pericentre and 66,000 km apocentre altitudes.

The orbit has been inspired by the Venus Express and Akatsuki missions. The apocentre and pericentre altitudes of the Venus Express mission are 250 km and 66,000 km (Hirose et al., 2012), while for the Akatsuki mission the same values amount to 300 km and 80,000 km, respectively<sup>30</sup>. Indeed, this orbit has been proven optimal on multiple occasions for missions with a similar purpose and, more importantly, similar payload. This additionally alleviates some of the requirements on verification and validation of the systemic integration of the payload with the orbital properties. Furthermore, the orbit will keep its inclination of 3.46° to limit the  $\Delta V$  required for orbital changes.

### 2.6.4. Orbit change

Orbital change will be performed using a simple Hohmann transfer. The manoeuvre consists of two phases. First, the thrusters will be pointed backwards in the direction opposite of the initial velocity of the orbiter, hence initiating retrograde motion. Once a  $\Delta V$  of 1.09 km s<sup>-1</sup> will be produced by the thrusters, the circular orbit will transform into an elliptic one with a pericentre at the altitude of interest - at 250 km. In the first phase, the apocentre will remain at 127,163 km<sup>31</sup>.

Subsequently, once the spacecraft will reach the pericentre of the transfer, thrusters will be initiated once more to provide an additional 0.185 km s<sup>-1</sup> of  $\Delta V$  to the prograde motion. This manoeuvre shall lower the apocentre altitude to the required 66,000 km. Together, the two phases require 1.277 km s<sup>-1</sup> of  $\Delta V$ , which drives the sizing of the fuel tanks of the orbiter.

### 2.6.5. Other orbital properties

When performing orbit trade-offs, it is vital to make sure that the selected orbits have a high capacity for power generation. Since the primary power source are the solar arrays, the orbiter needs to be exposed to the sun as often as possible. Because of the high altitudes of both orbits, the orbiter will be relatively well sunlit in both orbits. To quantify the time that the spacecraft remains shadowed by Venus for both orbit, orbital mechanics theory has been used. First, the true anomaly, which is the angle with respect to the pericentre was created as a function of altitude using:

$$\theta = \arccos \left( \frac{\frac{a(1-e^2)}{r} - 1}{e} \right) \quad (2.7)$$

<sup>30</sup>[https://pds.nasa.gov/ds-view/pds/viewMissionProfile.jsp?MISSION\\_NAME=VENUS%20EXPRESS](https://pds.nasa.gov/ds-view/pds/viewMissionProfile.jsp?MISSION_NAME=VENUS%20EXPRESS), retrieved 21-05-2021

<sup>31</sup>Note that this is the altitude of the relay orbit presented in Section 2.6.2

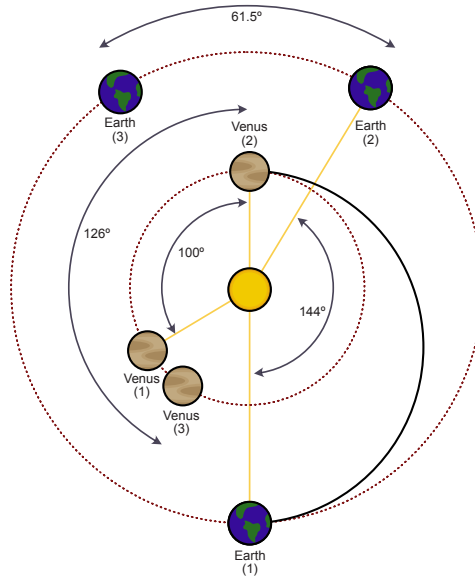


Figure 2.2: Lack of sun obstruction of communications with the Earth during the nominal mission

Afterwards, the true anomalies, corresponding to any two positions on the orbit, were related to the true eccentric anomaly:

$$E = 2 \arctan \left( \sqrt{\frac{1+e}{1-e}} \tan \left( \frac{\theta}{2} \right) \right) \quad (2.8)$$

And, subsequently, to the mean anomaly:

$$M = E - e \sin E \quad (2.9)$$

The time between two points in an orbit was then computed by simply using:

$$t = (M_1 - M_0) \sqrt{\frac{\mu}{a^3}} \quad (2.10)$$

Performing the calculations with the true anomalies at onset and termination of eclipse found using simple geometry, yields an eclipse time of 18.2 min in the best case scenario when the orbiter happens to be at pericentre and 3.88 h when the orbiter is at apocentre if the inclination is ignored. However, since the nominal duration of the second phase is only 30 days, the correct initial apocentre pointing could allow for a maximal 23 min minute eclipse. For a 110 day mission duration, the maximum eclipse time would be 49 min. Afterwards, the remote sensing instruments could be turned off during low-power conditions.

Another important consideration is the ability to communicate with Earth throughout the mission. Fig. 2.2 is a proof that because of the nature of the Hohmann transfer, the Sun will never obstruct communications between the Earth and the orbiter during the nominal mission. Position 1 is the initial position of Earth and Venus at the start of the Hohmann transfer. Position 2 is the relative position of Earth and Venus at the end of the transfer, 146 days later. At this point the Sun is far from being in the way of the line of communications with the ground station. Position 3 is the relative position of Earth and Venus at the end of the nominal mission, 63 days later. Since the angular velocities of the planets are constant, it can be extrapolated that at no point between positions 2 and 3 the Sun will obstruct communications. Furthermore, the worst case will occur at position 3, when the angle that the two planets make with the sun is only  $100^\circ$ , far from the  $180^\circ$  required for obstruction.

## 2.7. Probe atmospheric insertion

Once the probe is decoupled from the orbiter, it will have to enter the Venusian atmosphere. This is a complex process with several phases. First, the general assumptions used for the entry properties are discussed in Section 2.7.1. Then, the entry vehicle design is described in Section 2.7.2 and the entry probe inflation is explained in Section 2.7.3. Following this, the entry profile is analysed in Section 2.7.4 and the probe deployment after entering the atmosphere is analysed in Section 2.7.5. The section concludes with the verification of the entry code in Section 2.7.6.

### 2.7.1. Assumptions and definitions

For the atmospheric entry of the probe, the following assumptions were made:

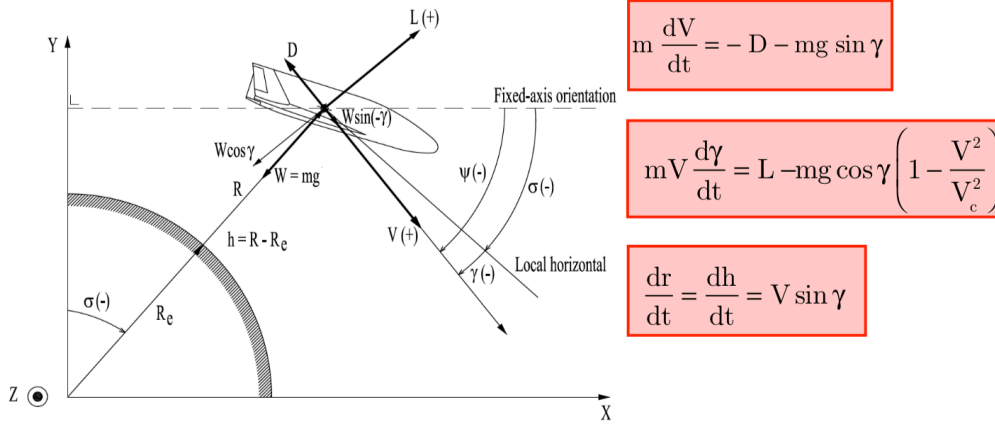


Figure 2.3: Free-body diagram and equations of motion for the entry vehicle (Mooij, 2019)

- **PAI.A.1** Venus is assumed to be spherical and non-rotating. This is an appropriate assumption to make, since the polar and equatorial radii of Venus are equal and the axial rotation is very slow. The atmosphere does rotate significantly faster than the surface, but this is neglected for the time being.
- **PAI.A.2** A ballistic entry was assumed and the effects of lift were neglected.
- **PAI.A.3** For computing the effects of aeroheating, the cold-wall model is used to provide a conservative estimate of the heat flux per unit area experienced by the entry vehicle.
- **PAI.A.4** The heat shield was assumed to be a spherical cap taking up all heat loads. Corner heating and heating of the back cover of the aeroshell were neglected.
- **PAI.A.5** The coefficients used in the Chapman equation are assumed to be the same as on Earth and Mars, since the precise values on Venus are not known. The final value for the heat flux per unit area is multiplied by 1.1 to provide a safety margin of 10%.
- **PAI.A.5** The flow around the entry vehicle is assumed to be linear.
- **PAI.A.6** The specific heat capacity of the heat shield material is assumed to be constant.
- **PAI.A.7** The mass of the entry vehicle during the descent is assumed to be constant.
- **PAI.A.8** The drag coefficient  $C_D$  of the entry vehicle is modelled as follows: From zero velocity up to Mach 20, the drag coefficient is assumed to increase linearly from a value of 1.4 to a value of 1.7, as based on previous atmospheric entry vehicles (Mooij, 2019, Lecture 6). Beyond Mach 20, the drag coefficient is assumed to have a constant value of 1.7.
- **PAI.A.9** The lifting gas for the probe was assumed to be an ideal gas stored in one spherical, thin-walled pressure vessel.
- **PAI.A.10** The circular velocity  $V_c$  was computed for the altitude of the atmospheric entry, set to 150 km, and assumed constant for all computations.

The free-body diagram and corresponding equations of motion for the entry vehicle are illustrated in Fig. 2.3 (Mooij, 2019, Lecture 6). The equations of motion, illustrating change in velocity, flight path angle, and altitude with time, respectively, are the following:

$$\frac{dV}{dt} = -\frac{C_D S}{m} \frac{1}{2} \rho V^2 - g \sin \gamma \quad (2.11)$$

$$\frac{d\gamma}{dt} = -\frac{g}{V} \cos \gamma \left( 1 - \frac{V^2}{V_c^2} \right) \quad (2.12)$$

$$\frac{dr}{dt} = -V \sin \gamma \quad (2.13)$$

The differential equations of motion were integrated using the Runge-Kutta method defined by `scipy.integrate.odeint`.

The heat shield is modelled as a spherical cap and the exposed surface area  $S_N$  of the heat shield is computed using Eq. (2.14), where  $D_N$  is the diameter of the heat shield and  $h_N$  is its height.

$$S_N = \pi \left[ \left( \frac{D_N}{2} \right)^2 + h_N^2 \right] \quad (2.14)$$

The convective heat flux experienced by the entry vehicle can be computed using the empirical Chapman equation, shown in Eq. (2.15) (Mooij, 2019), where  $R_N$  is the nose radius,  $\rho_0$  is the atmospheric density at the target deployment

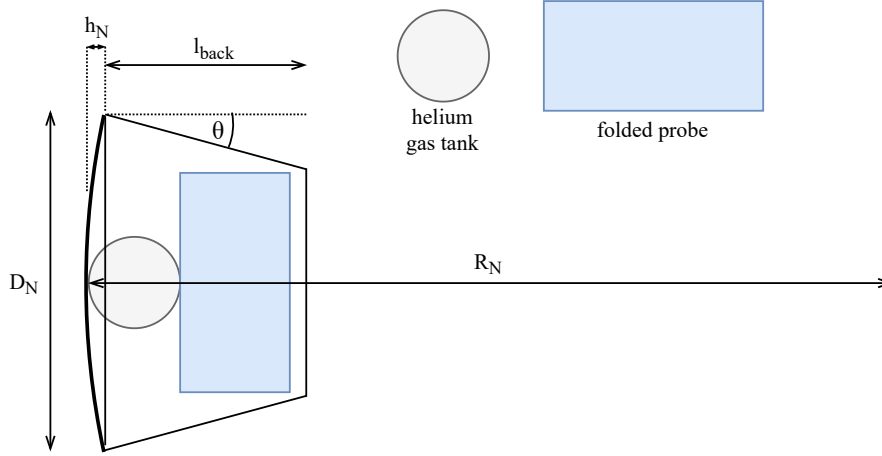


Figure 2.4: Entry vehicle geometry

altitude,  $V_c$  is the circular velocity at the altitude of atmospheric entry,  $c^*$  and  $m$  are empirical constants, and  $n$  is defined by the type of flow present (assumed here to be linear).

$$q_c = c^* \frac{1}{R_N^n} \left( \frac{\rho}{\rho_0} \right)^{1-n} \left( \frac{V}{V_c} \right)^m \quad (2.15)$$

The total heat load  $Q_{tot}$  can be found by integrating the heat flux over the duration of the descent and multiplying the resultant heat flow per unit area with  $S_N$ , as seen in Eq. (2.16). The mass of ablated material can then be computed by dividing the total heat load by the specific heat capacity  $c_{TPS}$  of the Thermal Protection System (TPS) material and the total temperature change  $\Delta T$  found from the temperature ranges computed with Eq. (2.17); this relation is given by Eq. (2.18).

$$Q_{tot} = S_N \int_{t_0}^{t_{end}} q_c dt \quad (2.16)$$

$$T_{w_{eq}} = \sqrt[4]{\frac{q_c}{\sigma_B \epsilon_{TPS}}} \quad (2.17)$$

$$m_{ablated} = \frac{Q_{tot}}{c_{TPS} \Delta T} \quad (2.18)$$

### 2.7.2. Entry vehicle design

The aeroshell for the probe was based on previous atmospheric entry missions, consisting of a heat shield at the front making up the TPS, attached to a back cover taking up compressive stresses and serving as stabilisation of the vehicle. Due to time constraints, the back cover sizing consisted only of a rough mass estimate based on existing aeroshell data, as well as a selection of preliminary dimensions, based on the folded probe size and aeroheating computations. A simple schematic of the entry vehicle geometry is presented in Fig. 2.4.

The front of the aeroshell is a spherical cap; a diameter  $D_{EV}$  of 4.5 m was selected to allow for a more favourable velocity profile and eliminate the need for a parachute, while a nose radius  $R_N$  of 11 m was selected based on a brief sensitivity analysis weighing the reduction in mass of the TPS for a larger nose radius against the change in velocity profile. The back cover of the aeroshell is a truncated cone with length  $l_{back} = 2.8$  m and taper ratio of  $\theta \approx 15^\circ$  selected based on the probe and gas tank to be fit into the entry vehicle.

The material for the TPS was selected to be PICA-X, a version of NASA's Phenolic Impregnated Carbon Ablator (PICA) developed by SpaceX to reduce manufacturing costs<sup>32</sup>.

The back cover for Tamago no kara was based on the one for the Huygens entry capsule (Clausen et al., 1999), which was a stiffened aluminium shell weighing 11.4 kg coated with a 5 kg layer of Prosiol for thermal insulation. Taking into account the larger diameter of Tamago no kara and the overall uncertainty of the back cover dimensions, a fixed back cover mass of 40 kg was selected for conducting entry calculations. A more detailed design of the aeroshell would have to account for shear and buckling stress calculations experienced by the back cover.

The use of a parachute for the entry module was considered at first and later discarded after finding that all necessary deceleration could be provided for by the heat shield alone.

<sup>32</sup><https://core.ac.uk/download/pdf/42731541.pdf>, retrieved 18-06-2021

**Table 2.6:** Parameters for gas tank mass and dimension computations

Parameter	Symbol	Value
Lifting gas	–	He
Specific gas constant <sup>34</sup>	$R_{sp,gas}$	2078.5 J kg <sup>-1</sup> K
Expanded gas volume	$v_{gas}$	706 m <sup>3</sup>
Expanded gas temperature	$T_{gas}$	244 K
Expanded gas pressure	$p_{gas}$	49,765 Pa
Compressed gas pressure	$p_{gas}$	30 MPa
Gas tank material	–	Ti-6Al-4V
Yield strength tank material	$\sigma_{yield}$	880 MPa
Mass density tank material	$\rho_{tank}$	4500 kg m <sup>-3</sup>
Tank volume	$v_{tank}$	1.17 m <sup>3</sup>
Gas tank radius	$R_{tank}$	0.654 m
Gas tank thickness	$t_{tank}$	0.011 m
Lifting gas mass	$m_{gas}$	69 kg
Gas tank mass	$m_{tank}$	269 kg

### 2.7.3. Probe inflating mechanism

The inflating mechanism of the probe consists of a pressurised gas tank attached via a short pipe to the front of the probe. The probe inflation will begin after the back cover of Tamago no kara is blown off at the target deployment altitude and will make use of a blowdown system. The gas tank will be connected to the front of Tamago no kara and will be dropped together with the heat shield once the probe is fully inflated.

The mass of the lifting gas with which the probe is filled, can be derived from the ideal gas law as shown in Eq. (2.19), where  $R_{sp,gas}$  is the specific gas constant of the buoyant chosen buoyant gas,  $p_{gas}$  is the pressure at which the gas is stored, and  $T_{gas}$  is the temperature of the gas. The temperature of the gas was set equal to the atmospheric temperature. The pressure was computed by summing the ambient pressure and the maximum overpressure of the gas; this was given for an altitude of 65 km.

$$p = \rho R_{sp} T = \frac{m}{v} R_{sp} T \Rightarrow m_{gas} = \frac{p_{gas} v_{gas}}{R_{sp,gas} T_{gas}} \quad (2.19)$$

Knowing the expanded volume of the gas to be stored, the volume of the gas tank can be computed from the ideal gas law as derived in Eq. (2.20), which assumes an adiabatic gas expansion during inflation.

$$pv = nRT \Rightarrow \frac{p_{tank} v_{tank}}{p_{gas} v_{gas}} = 1 \Rightarrow v_{tank} = v_{gas} \frac{p_{gas}}{p_{tank}} \quad (2.20)$$

The radius of a spherical gas tank  $R_{tank}$  can then be computed via Eq. (2.21). Knowing this and having selected a tank material, the thickness and mass of the gas tank can then be found using Eq. (2.22) and Eq. (2.23), respectively.

$$v_{tank} = \frac{4}{3} \pi R_{tank}^3 \Rightarrow R_{tank} = \sqrt[3]{\frac{3v_{tank}}{4\pi}} \quad (2.21)$$

$$\sigma_{sphere} = \frac{pR}{2t} \Rightarrow t_{tank} = \frac{p_{tank} R_{tank}}{2\sigma_{yield}} \quad (2.22)$$

$$m_{tank} \approx S_{tank} t_{tank} \rho_{tank} = 4\pi R_{tank}^2 t_{tank} \rho_{tank} \quad (2.23)$$

The parameters and results of the gas tank sizing calculations are presented in Table 2.6. The lifting gas chosen was helium due to its high buoyancy in the Venusian atmosphere and the fact that it is inert and non-toxic. For the gas tanks, the titanium alloy Ti-6Al-4V was selected for its favourable material index for gas tank design, accounting for high yield strength and relatively low mass density. A gas compression pressure of 30 MPa was selected, since this is within the range of pressurisation values commonly seen in industry<sup>33</sup>.

### 2.7.4. Atmospheric entry profile

For Tori's deployment into the atmosphere, a target altitude of 60 km  $\pm$  5 km was set to ensure that the probe would be deployed within its operational altitude range. The maximum deployment velocity was set to Mach 0.7, corresponding to a velocity of 178 m s<sup>-1</sup> (Justus and Braun, 2007), to avoid the potential formation of shock waves along the body of the probe during deployment. Furthermore, as there are no requirements on the exact longitudinal and latitudinal deployment location of the probe, it was decided that the probe would be deployed via a ballistic entry, using an entry descent angle of  $\gamma_E = -6^\circ$ .

<sup>33</sup><https://artes.esa.int/projects/hehvp-helium-highpressure-vessel>, retrieved 21-06-2021

<sup>34</sup>[https://www.ohio.edu/mechanical/thermo/property\\_tables/gas/idealGas.html](https://www.ohio.edu/mechanical/thermo/property_tables/gas/idealGas.html), retrieved 20-06-2021

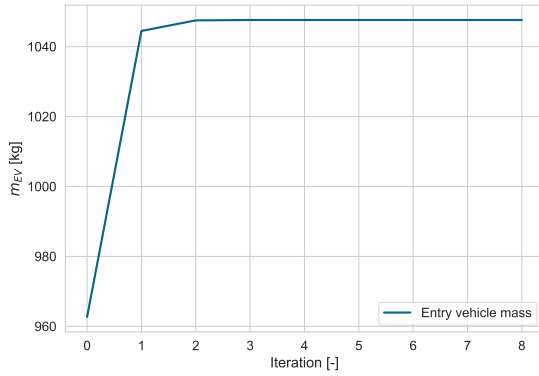


Figure 2.5: Mass iteration for Tamago

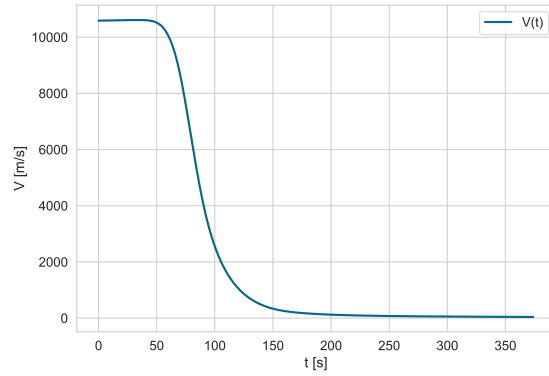


Figure 2.6: Entry vehicle velocity w.r.t. time

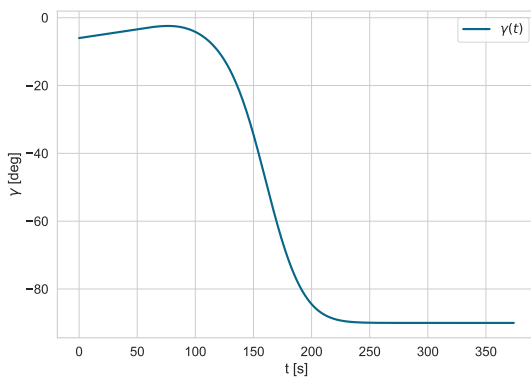


Figure 2.7: Descent angle of the entry vehicle w.r.t. time

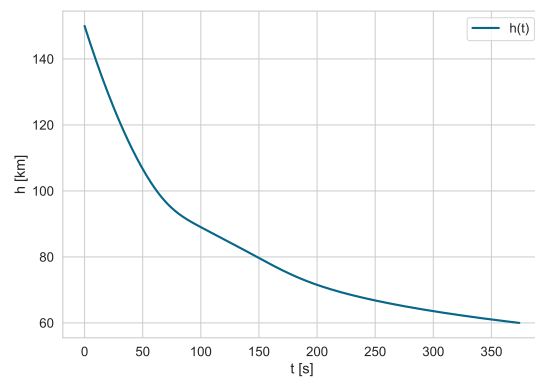


Figure 2.8: Altitude w.r.t. time

The probe deployment allows for separation either before or after orbit insertion of the orbiter. Separation before orbit insertion would mean deploying the probe directly from the interplanetary transfer orbit, giving it an entry velocity  $V_E$  of  $10.588 \text{ km s}^{-1}$ . It is worth noting that all previous Venus missions involving atmospheric entry were deployed directly from their respective interplanetary trajectories, often being fast trajectories with higher resultant entry velocities than the one computed for Kumo. The main benefit of this method, is that the spacecraft brought into orbit around Venus will have a lower mass, thus requiring less fuel to complete orbit insertion. Given the high mass of the probe and lifting gas tank, the additional fuel mass necessary to decelerate the entry module into orbit around Venus was found to be much higher than the heat shield mass increase for an entry from interplanetary trajectory. Thus, it was decided to separate Tamago from Tsubuyaki shortly before arrival at Venus.

The mass of the entry vehicle was found using an iterative process, in which the cumulative mass of the probe, lifting gas, gas tank, back cover and miscellaneous components was kept constant. The necessary heat shield mass was computed for each iteration and then added to the fixed mass to find the starting mass for the next iteration. The results for this mass iteration can be found in Fig. 2.5. As can be observed in the graph, the total mass for Tamago converges to approximately 1048 kg after only a few iterations.

The velocity profiles w.r.t. time and altitude are presented in Figs. 2.6 and 2.9, respectively, with the acceleration w.r.t. time shown in Fig. 2.10. Moreover, the descent angle  $\gamma$  with time is shown in Fig. 2.7. From these, it can be observed that the probe decelerates and the absolute descent angle increasing with time. The entry vehicle decelerates to subsonic velocities without the use of a parachute long before reaching the deployment altitude, reaching a final velocity of  $41.8 \text{ m s}^{-1}$  at 60 km. The maximum deceleration value is of 25.7 g, which indicates that more research and design should be allotted to studying the structural integrity of the aeroshell, particularly the back cover. Due to time constraints, this was left to a future design stage.

The convective heat flux at the stagnation point of the heat shield is presented in Fig. 2.11, with a maximum heat flux per unit area of approximately  $1.3 \text{ W m}^{-2}$ . Furthermore, the temperature at the stagnation point is graphed in Fig. 2.12, indicating a maximum stagnation point temperature of 2242 K, which is well within the operational ranges of PICA (Gökçen, Chen, Skokova, and Milos, 2010). The heat shield thickness obtained from the final entry vehicle iteration is of 2.1 cm, with a corresponding mass of approximately 85 kg. Investigations into the minimum heat shield thickness that can be manufactured is left for a future design stage.

The mass budget for the entry vehicle is presented in Table 2.8. The total entry vehicle mass is constituted of the

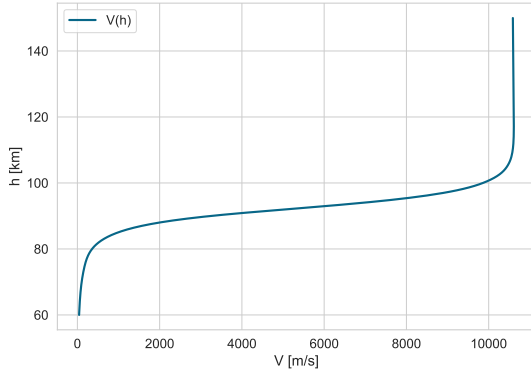


Figure 2.9: Entry vehicle velocity w.r.t. altitude

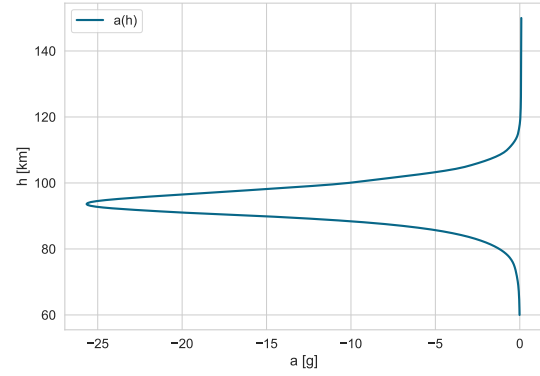


Figure 2.10: Entry vehicle acceleration w.r.t. altitude

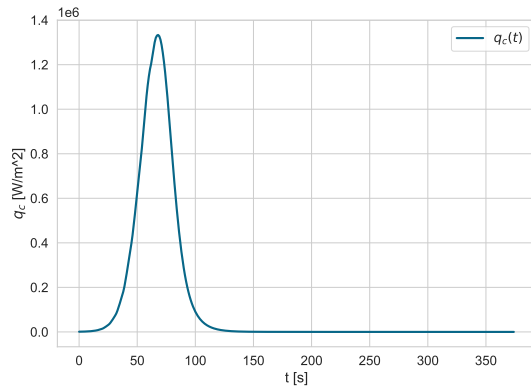


Figure 2.11: Convective heat flux per unit area w.r.t. time

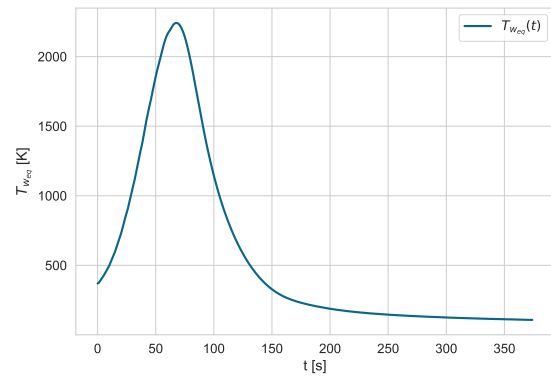


Figure 2.12: Stagnation point temperature w.r.t. time

Table 2.7: Parameters used for computing ballistic entry properties, sorted into constants first and variables second.

Parameter	Symbol	Value
Chapman constants (Mooij, 2019)	$c^*$	$1.1097 \times 10^8 \text{ m}^{-\frac{1}{2}}$
	$n$	0.5
	$m$	3
Entry descent angle	$\gamma_E$	$-10^\circ$
Emissivity (Gökçen et al., 2010)	$\epsilon$	0.931
Back cover length	$l_{back}$	2.8 m
Entry vehicle diameter	$D_N$	4.5 m
Aeroshell nose radius	$R_N$	11 m
Aeroshell nose height	$h_N$	0.4 m
TPS surface area	$S_{TPS}$	16.1 m <sup>2</sup>
TPS material	-	PICA-X
TPS mass density	$\rho_{TPS}$	250 kg m <sup>-3</sup>
TPS specific heat capacity	$c_{TPS}$	$2.177 \times 10^3 \text{ J kg}^{-1} \text{ K}$
Velocity at deployment altitude	$V_{deploy}$	41.8 m s <sup>-1</sup>
Maximum deceleration	$a_{max}$	252 m s <sup>-2</sup> = 25.7 g

probe mass, gas mass, tank mass, back cover mass, and TPS mass, as well as the miscellaneous components mass, which includes the on-board computer, the electrical power subsystem, pressure sensors, and the deployment actuators. Due to time constraints, the mass of the back cover and other components and subsystems of the entry vehicle have only been estimated very preliminarily and their detail design is left for future design stages.

### 2.7.5. Probe deployment and inflation

Probe deployment begins at 60 km altitude, when the probe is unexpanded and free-falling at the initial speed of 41.8 m s<sup>-1</sup>. At that moment, the valve joining the pressurised gas tank attached to the entry capsule and the probe will open, supplying the probe with the Helium gas at an exponentially decreasing rate. For simplicity, the flow rate has been modelled as a

Table 2.8: Tamago mass budget

Component	Symbol	Mass [kg]
Probe	$m_{probe}$	555
Buoyant gas	$m_{gas}$	69
Gas tank	$m_{tank}$	269
Back cover	$m_{shell}$	40
Miscellaneous components	$m_{misc}$	30
TPS	$m_{TPS}$	85
<b>Total</b>	$m_{EV}$	<b>1048</b>

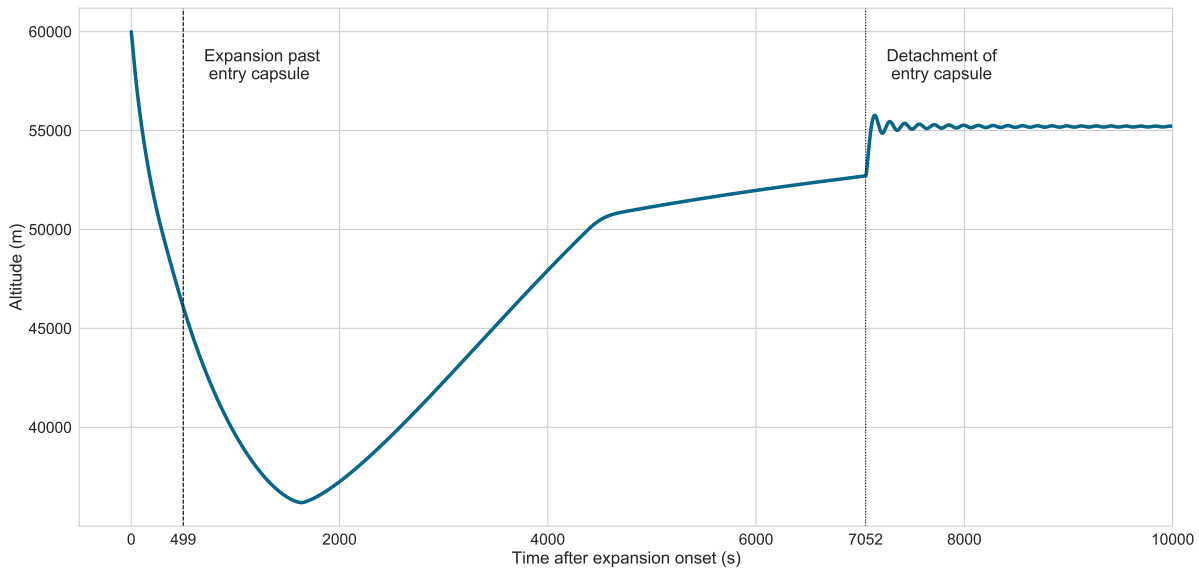


Figure 2.13: Altitude variation with time of the inflation and stabilisation phases

constant ( $100 \text{ dm}^3 \text{ s}^{-1}$  is assumed). At the same time, the backshell of the entry vehicle will detach, lowering the mass of the system to 1008 kg.

Initially, the flow will 'see' the heat shield of the entry probe, as the expansion will first occur in the parallel direction to the flight pass (though opposite direction), due to the region of low pressure created by the entry vehicle. The initial drag coefficient of 0.85 has been assumed, accounting for the absence of the backshell. During the first 500 s, the drag coefficient and the reference surface area stay constant at 0.85 and  $16.074 \text{ m}^2$ , respectively.

Exactly 499 s later, the flying wing has expanded as much as it could without increasing the surface area. At this point, the expansion of the wing will take place sideways. This expansion undoubtedly increases the surface area of the entry capsule. Furthermore, the drag coefficient is assumed to decrease linearly from 0.85 to 0.115, which is a result of a surface area-weighted rule of mixtures applied to the wing and the capsule. The drag coefficient of 0.115 in the expanded state was found by taking an average between the drag coefficient of the expanded probe (0.0084), which covers 86.6% of the area of the total expanded structure and the drag coefficient of the capsule itself (0.85), which covers the remaining 13.5%.

Once the drag coefficient reaches 0.115 and the probe is fully inflated, the entry vehicle is detached together with the gas tank. The drag coefficient becomes equal to that of the probe, which will be found in Section 3.7.2 to be equal to 0.0084. Furthermore, following the detachment, the mass of the system becomes 555 kg.

The described process can be simulated, yielding Figs. 2.13, 2.14 and 2.15. The first dashed vertical line on all three graphs identifies the point at which the probe starts to expand beyond the surface covered by the entry vehicle. The second (dotted) vertical line symbolises the detachment of the entry vehicle as well as the fuel tanks from the probe. Relatively low drag coefficient causes noticeable underdamping as the probe tries to stabilise. The maximum velocity reached during the descent is  $59 \text{ m s}^{-1}$  downwards and  $57 \text{ m s}^{-1}$ . Furthermore, the maximum and minimum accelerations in units of Venusian gravitational constant are 0.51 and 1.75. These values were then used for the sizing of the structural subsystem.

Using the chosen value of the inflation rate of  $0.1 \text{ dm}^3 \text{ s}^{-1}$ , the lowest altitude reached during descent is 36,200 km. More research is required into the feasibility of the chosen inflation rate using current technology. Similar, more research is required into whether both, the ambient and stagnation temperatures at 36,200 km are low enough for the current capacity of the thermal control system of the entry vehicle. If one of the mentioned factors will be proven unfeasible, it can be compensated with the other one. As such, increasing the inflation rate to  $0.5 \text{ dm}^3 \text{ s}^{-1}$  would raise the lowest altitude to 48,000 km. In this case, the loads experienced by the entry vehicle also increase and the time until stabilisation, decreases.

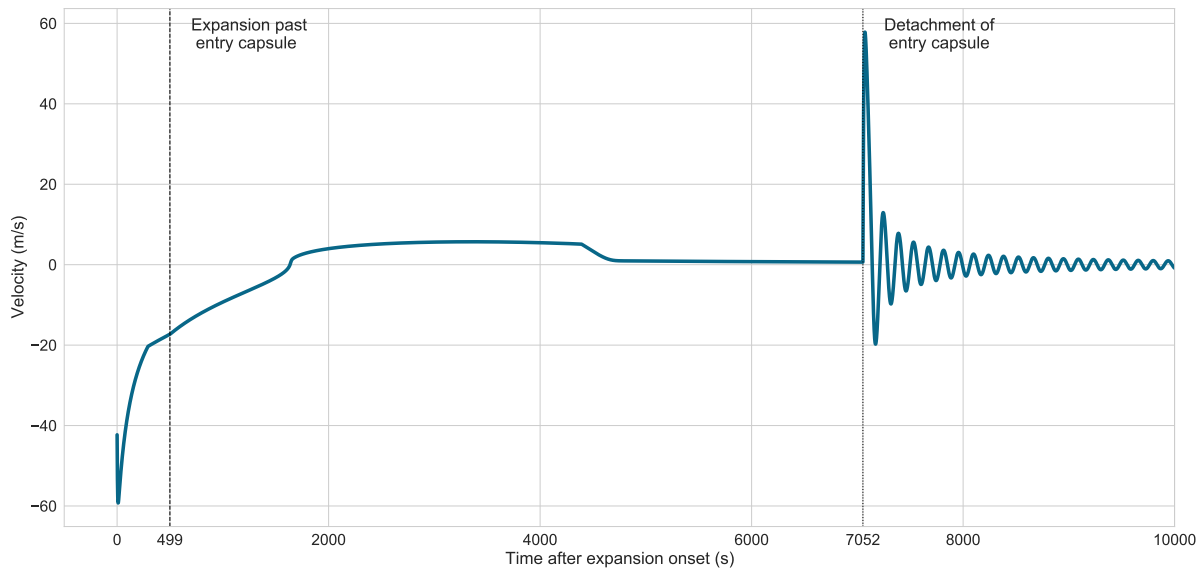


Figure 2.14: Velocity variation with time of the inflation and stabilisation phases

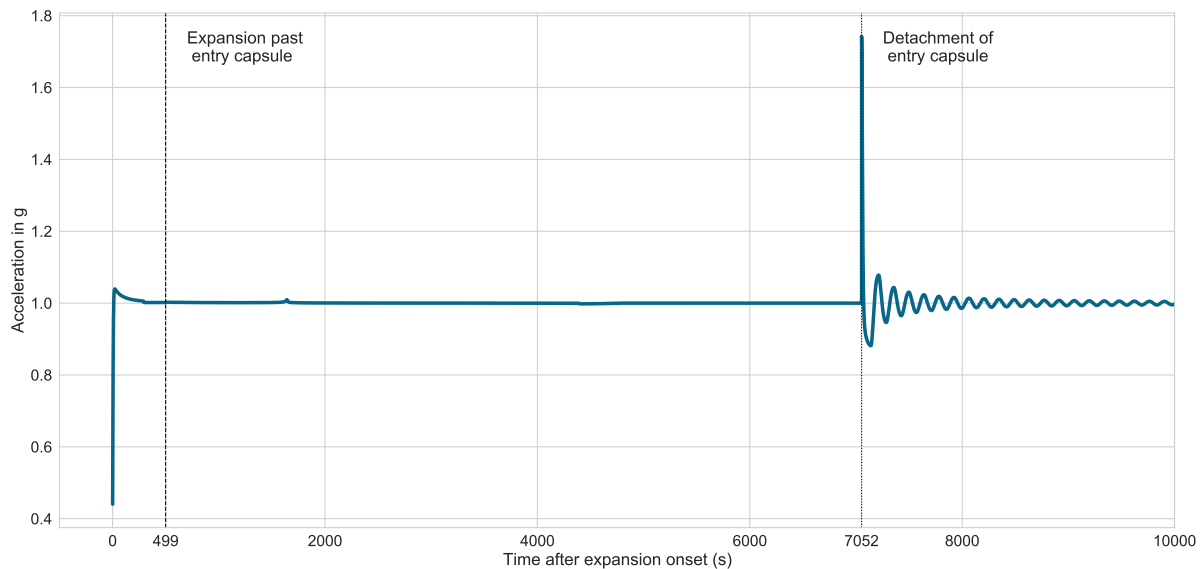


Figure 2.15: Acceleration variation with time of the inflation and stabilisation phases

### 2.7.6. Verification and validation of atmospheric entry code

The code flow for the entry calculations is shown in Fig. 2.16, with the unit tests conducted presented in Table 2.9.

## 2.8. Probe nominal operations

This section outlines the final flight plan for Tori. There are two key requirements that drive the design of the orbiter: KUMO-STH-PERF-02 and KUMO-STH-PERF-04. In particular, the requirements state that the probe shall fly ten revolutions around Venus and that excursions of  $30^\circ$  north or south from the equator shall be allowed.

### 2.8.1. Assumptions

A simplified model of the mission and environment is assumed to get a preliminary estimate of the atmospheric flight duration required to fulfil the science objectives. It uses a simplified representation of the dynamic atmosphere by specifying zonal super-rotation speeds of  $100 \text{ m s}^{-1}$  at the upper 65 km altitude level, as well as  $58 \text{ m s}^{-1}$  and  $63 \text{ m s}^{-1}$  at the lower altitude level of 55 km, for the day and night side, respectively (Sánchez-Lavega et al., 2008). The variation of zonal winds within the operational latitudes ( $\pm 30^\circ$ ) was found to be small (Sánchez-Lavega et al., 2008), hence the previously mentioned constant value is assumed. Furthermore, the worst case poleward flow of  $10 \text{ m s}^{-1}$  (Limaye et al., 1988) is assumed constant over the same range of operational conditions.

For the following analysis, atmospheric flight on a non-rotating planet but inside a superrotating atmosphere is as-

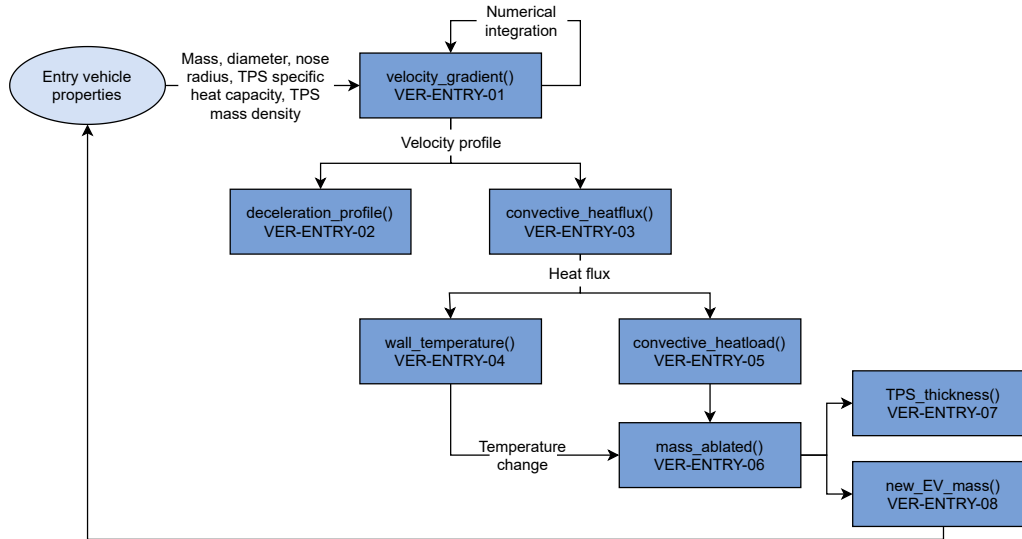


Figure 2.16: Code flow for atmospheric entry

Table 2.9: Unit tests for atmospheric entry code

Test	Variables	Expected outcome	Verified
VER-ENTRY-01	<b>Input:</b> $V, h, K, \gamma_E$ <b>Output:</b> $\frac{dV}{dh}$	The velocity gradient should be negative.	✓
VER-ENTRY-02	<b>Input:</b> $V, h, K, \gamma_E$ <b>Output:</b> $a$	The acceleration should increase with decreasing ballistic parameter.	✓
VER-ENTRY-03	<b>Input:</b> $V, h, R_N$ <b>Output:</b> $q_c$	Convective heat flux should decrease with increasing nose radius.	✓
VER-ENTRY-04	<b>Input:</b> $q_c, \epsilon$ <b>Output:</b> $T_{weq}, \Delta T$	The temperature should decrease with decreasing heat flux and increasing emissivity.	✓
VER-ENTRY-05	<b>Input:</b> $q_c, S_N, V, h, \gamma_E$ <b>Output:</b> $Q_{tot}$	Total heat load increases with increasing heat flux and surface area.	✓
VER-ENTRY-06	<b>Input:</b> $Q_{tot}, c_{TPS}, \Delta T, \gamma_E$ <b>Output:</b> $m_{ablated}$	Mass of ablated material decreases with increasing nose radius.	✓
VER-ENTRY-07	<b>Input:</b> $S_N, m_{ablated}, \rho_{TPS}$ <b>Output:</b> $t_{ablated}$	Thickness of ablated material decreases with decreasing mass of ablated material.	✓
VER-ENTRY-08	<b>Input:</b> $m_{ablated}, m_{fixed}$ <b>Output:</b> $m_{EV,new}$	New entry vehicle mass converges to one value.	✓

sumed. The rotation of Venus can be shown negligible compared to the wind speeds mentioned before, as the surface speed is  $2\pi R_V/T_V = 1.8 \text{ m s}^{-1}$ , with  $R_V = 6052 \text{ km}$  (Seidelmann et al., 2007) and  $T_V = 243$  Earth days (Margot et al., 2021). Furthermore, to show that the atmospheric flight around Venus can be approached similar to flight on a “flat Earth/Venus”, the speed of the probe in the Sun-Venus reference system at 65 km altitude, can be shown to be far below orbital speeds at that same altitude: the probe speed is at most of the order of  $200 \text{ m s}^{-1}$ , while a circular orbit at  $r = 6117 \text{ km}$  yields an orbital speed of  $v_c = \sqrt{\mu_V/r} = 7.3 \text{ km s}^{-1}$  with  $\mu_V = 3.249 \text{ km}^3 \text{ s}^{-2}$  (Konopliv et al., 1999).

To further justify the “flat Venus” assumption, it is shown that the centripetal acceleration required to keep the aircraft flying on a small circle of constant latitude instead of a great circle like an orbit, is negligible compared to the local gravitational acceleration. The worst case centripetal acceleration occurs at the extreme latitude of  $30^\circ$  and at a top ground speed (wind speed plus aircraft speed) estimated to be  $v = 200 \text{ m s}^{-1}$ . The centripetal acceleration equation thus yields  $a_c = v^2/(r \cos 30) = 7.5 \times 10^{-3} \text{ m s}^{-2}$ , which is  $\ll 8.87 \text{ m s}^{-2} = g_V$ <sup>35</sup>. This small acceleration can be easily sustained by aerodynamic lift, as the atmospheric density and pressure at the operational altitudes is non-negligible (Petropoulos, 1988).

Lastly, some terminology used in the following analysis will be defined using Fig. 2.17. With “local time”, the angle  $\theta$  in the invariant plane between the (projection of the) Venus-probe vector and Venus-Sun vector is meant, which is used to replace the ground-referenced longitude coordinate by an atmosphere/Sun-referenced local time. From this, the notion of a “revolution” is defined as the completion of a circle around Venus in the operational band of latitudes ( $0^\circ$  to  $30^\circ$ ). The

<sup>35</sup><https://nssdc.gsfc.nasa.gov/planetary/factsheet/venusfact.html>, retrieved on 28-05-2021

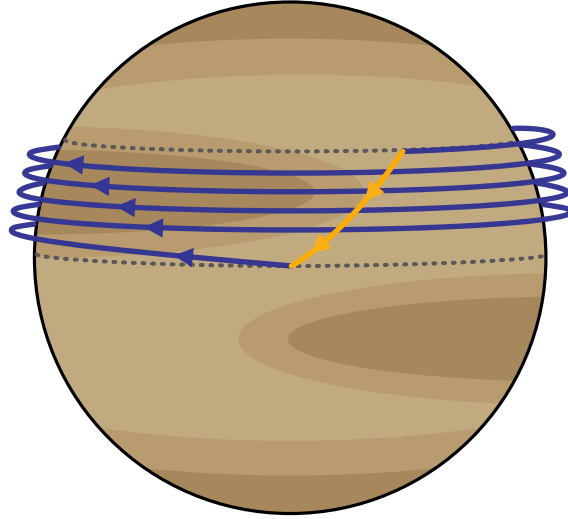


**Figure 2.17:** Simplified flight plan schematic (not to scale). The poleward spiral is depicted in blue, while the travel route back to the equator is shown in orange. The repeat measurements are conducted along the same poleward spiral conducted during the first measurement phase.

atmospheric probe has completed a revolution when it departs from and arrives back at a Sun-referenced point like the subsolar point or terminator. Depending on how long a revolution takes, Venus will have travelled by some angle around the Sun as well, but for the purposes of this preliminary analysis, the orbital motion of Venus is neglected as one revolution takes around 6 Earth days, so Venus will only have moved by  $6.4^\circ$ .

### 2.8.2. Flight plan

A schematic of the nominal flight plan is illustrated in Fig. 2.17. As the wind speeds are only known up to full digits, the actual probe velocity was also rounded to full digits. The flight plan roughly consists of flying a poleward spiral from the equator to the maximum latitude, then returning to the equator to repeat the same flight path. During the night, Tori floats at its minimum altitude. During the day, Tori can fly at the maximum altitude for duration corresponding to a  $60^\circ$  longitude change, while the rest of the day is spent at its lower end altitude to conserve power.

For a first analysis of the flight plan, it was assumed that a solar powered Tori would not produce any forward thrust while travelling on the night side of Venus, thus being carried only by the zonal winds. For an altitude of 55 km on the night side, the wind speed is approximately equal to  $58 \text{ m s}^{-1}$ . Using Eq. (2.24), the night time duration to fly from the sunset terminator to the sunrise terminator was computed to be approximately equal to  $3.308 \times 10^5 \text{ s}$  or 3.8 Earth days. Note that this is equal to the duration of half a revolution at night time conditions.

$$t_{\text{night}} = \frac{\pi(R_V + h_{\text{low}})}{V_{\text{night}}} \quad (2.24)$$

Similarly, the day time duration was computed from the time necessary to traverse half a revolution at daytime conditions. It was computed that Tori will travel with an average forward velocity of  $22 \text{ m s}^{-1}$  at the low altitude during the morning, after which it will climb to the maximum altitude of 65 km and fly with an average cruise speed of  $26 \text{ m s}^{-1}$ . From the power requirements for sustaining flight at 65 km altitude, it was found that Tori can cover a  $60^\circ$  longitude change at high altitude. Finally, the probe will descend and fly with an average velocity of  $14 \text{ m s}^{-1}$  for the remaining daytime. Using Eq. (2.25), a day time duration of  $2.052 \times 10^5 \text{ s}$  or 2.4 Earth days was found.

$$t_{\text{day}} = \frac{90^\circ}{360^\circ} \frac{2\pi(R_V + h_{\text{low}})}{V_{\text{day,low,morn}}} + \frac{60^\circ}{360^\circ} \frac{2\pi(R_V + h_{\text{high}})}{V_{\text{day,high}}} + \frac{90 - 60^\circ}{360^\circ} \frac{2\pi(R_V + h_{\text{low}})}{V_{\text{day,low,eve}}} \quad (2.25)$$

Next, the time available for poleward travel depends on the time necessary for travelling from the maximum latitude back towards the equator. To satisfy the power requirements for this travel, it was decided that the travel should occur on the day side of the planet. Furthermore, the altitude for this transfer was selected to be 55 km, since both the zonal and the meridional wind speeds are lower, thus making it easier for the probe to reach the equator again before it is carried back onto the night side of the planet. The average poleward wind at this altitude is of approximately  $0 \text{ m s}^{-1}$ , while the velocity of the probe is equal to  $22 \text{ m s}^{-1}$ . Using Eq. (2.26), the time necessary for the probe to travel from the maximum latitude of  $30^\circ$  to the equator is approximately equal to  $1.453 \times 10^5 \text{ s}$  or 1.7 Earth days. The daytime duration for this revolution would be equal to  $3.045 \times 10^5 \text{ s}$  or 3.5 Earth days. The travel time to the equator is lower than the daytime duration, meaning that it can be completed within full daylight. The rest of the daytime for that revolution is kept as a buffer for the travel back to the first measurement location.

**Table 2.10:** Summary of flight plan phases for Tori and their respective durations

Tori mission phase	Revolutions	Phase average zonal velocity	Duration
Deployment	< 0.5	90 m s <sup>-1</sup>	< 2.133 × 10 <sup>5</sup> s = 2.5 d
Night time	0.5	58 m s <sup>-1</sup>	3.308 × 10 <sup>5</sup> s = 3.8 d
Daytime	0.5	–	2.052 × 10 <sup>5</sup> s = 2.4 d
Morning at low altitude	0.25	85 m s <sup>-1</sup>	1.129 × 10 <sup>5</sup> s = 1.3 d
Cruise at high altitude	0.17	126 m s <sup>-1</sup>	5.084 × 10 <sup>4</sup> s = 0.6 d
Evening at low altitude	0.18	77 m s <sup>-1</sup>	4.153 × 10 <sup>4</sup> s = 0.5 d
Poleward spiral	4.5	–	2.475 × 10 <sup>6</sup> s = 28.6 d
Daytime during return travel to the equator	0.5	63 m s <sup>-1</sup>	3.045 × 10 <sup>5</sup> s = 3.5 d
Travel from maximum latitude to equator	0.24	63 m s <sup>-1</sup>	1.453 × 10 <sup>5</sup> s = 1.7 d
<b>Total</b>	10	–	5.468 × 10 <sup>6</sup> s = 63.3 d

$$t_{equator} = \frac{30^\circ}{360^\circ} \frac{2\pi(R_V + h_{low})}{V_{max} - V_{pole,low}} \quad (2.26)$$

Furthermore, there is the poleward travel of the probe. The worst case flight plan concept requires retracing the same poleward spiral twice and the travel back to the equator (with buffer) takes approximately half a revolution, it was selected that the travel from the equator to the maximum latitude would be spread out over 4.5 revolutions. Specifically, this would mean conducting four complete revolutions *and* half a revolution on the night side of the planet to account for the travel back to the equator occurring during the daytime, equating to a total duration of  $2.475 \times 10^6$  s or 28.6 Earth days. The lateral distance crossed is approximately equal to 3198 km. This means that the probe needs an average lateral velocity of  $1.3 \text{ m s}^{-1}$  during the poleward spiral. As the meridional winds have an average velocity between  $0 \text{ m s}^{-1}$  and  $5 \text{ m s}^{-1}$ , the probe may need to steer against the poleward flow, particularly at higher altitudes. As the probe will fly mostly at lower altitudes and is designed to have a high enough velocity to oppose the meridional winds, the effects this would have on the flight plan were assumed to be negligible.

Finally, the deployment of Tori in the Venusian atmosphere also has to be accounted for in the flight plan. With nine revolutions reserved for the measurements along the poleward measurements and half a revolution for the return to the equator, approximately half a revolution remains for the atmospheric insertion of the probe. This should occur on the day side of the planet to ensure sufficient power availability during the crucial stage of deployment. Given that the poleward spiral needs to start on the night side of the planet, the deployment does not cause any delay in the flight plan. The maximum duration of this phase is equal to the maximum daytime duration at the deployment altitude of 60 km with an average zonal wind speed of  $90 \text{ m s}^{-1}$ ; this is equal to  $2.133 \times 10^5$  s or 2.5 Earth days, assuming that there is no forward thrust. Most likely, the probe will take less time to reach the night side, depending on the exact location of deployment and the flight conditions, selected to allow for sufficient battery charging before entering the night side of the planet.

The individual mission phases and their durations are presented in Table 2.10.

### 2.8.3. Science operations

The mission will be split up into three phases, each of them with a different scientific purpose.

The first phase consists of the probe flying in the atmosphere and the orbiter being in the circular relay orbit at an altitude of 133,215 km. The probe will measure continuously during day time *only*, for five revolutions around the planet. This is done to save power and, subsequently, save battery mass as the instruments will operate simultaneously. The instruments on the orbiter will remain switched off for this time of period.

Note that the instruments will have to calibrate once reaching the day side again after flying in the night side with the instrumentation off. Also, it will have to re-calibrate when changing its altitude during the day side. This will require at least 30 minutes<sup>36</sup>.

In the second phase, the orbiter will change from the circular relay orbit, to the elliptical scientific orbit with a pericentre of 300 km and an apocentre of 66,000 km. The probe will only measure data in the five repeat points, located in the day side, for a period of 10 minutes for the last five revolutions. This is excluding the time needed to calibrate the instruments. Also, the instruments on the orbiter will be switched on and will start to measure data simultaneously along the entire orbit with the specific time intervals mentioned below:

- at pericentre (300 km) every 300 seconds.
- at 2,000 km every 10 seconds.
- between 10,000 km and 66,000 km every 600 seconds.

<sup>36</sup>[https://www.aiaa.org/docs/default-source/uploadedfiles/education-and-careers/university-students/design-competitions/3rdplace\\_rmit\\_space\\_design.pdf?sfvrsn=4a3eea29\\_0](https://www.aiaa.org/docs/default-source/uploadedfiles/education-and-careers/university-students/design-competitions/3rdplace_rmit_space_design.pdf?sfvrsn=4a3eea29_0), retrieved on 19-06-2021

The pericentre measurements will be done to measure the UV-absorbers from outside of the atmosphere. Additionally, temperature measurements will be performed at this altitude to measure additional value such as hot spots as mentioned in Section 2.3.1.

The measurements at 2,000 km will be carried out to do the limb observations to study the airglow, as is mentioned in Section 2.3.1. Furthermore, the data obtained at an altitude between 10,000-66,000 km will be used to study the global atmospheric dynamics from a distance. This phase will be used to correlate the UV-measurements of the probe with the UV-measurements obtained from the orbiter.

## 2.9. Extended mission operations

After completing their respective nominal missions, both Tori and Tsubuyaki will be tested for their functionalities and then enter their respective extended mission operations. The orbiter extended mission operations are elaborated upon in Section 2.9.1, followed by the probe extended mission operations in Section 2.9.2.

### 2.9.1. Orbiter extended mission operations

The nominal mission of the orbiter ends after the probe has been disposed of and there is no more data to relay between Tori and Earth. A number of diagnostic tests will be run to determine the health of Tsubuyaki's subsystems. The orbiter will then continue to orbit Venus and collect data from the science orbit with the on-board payload and transmitting it to Earth during the available communication windows.

In the future, Tsubuyaki can continue to function as a relay orbiter for potential future Venus missions that may require one. The extended mission operations may last several years, until the inherent degradation of the orbiter subsystems makes continued flight unfeasible.

### 2.9.2. Probe extended mission operations

The nominal mission of the probe ends once it has revisited all the repeat measurement points and conducted the required ten revolutions around Venus. Once the nominal mission has ended, a series of diagnostic tests will assess the health of the probe subsystems and the results will be relayed to the ground stations via the orbiter for data analysis. Given that the functionality of the probe is deemed sufficient to continue flying in the Venusian atmosphere, a new flight plan may be established to visit new measurement locations, which may be located at different altitudes and/or latitudes.

While the diagnostic data from the probe is being processed at the ground station and the extended flight plan is being determined, the probe may continue to fly around Venus at a low altitude to avoid being swept further up north until it receives new commands. The extended mission of the probe should make full use of the probe functionality until degradation due to the acidic atmosphere makes it impossible to continue sustaining flight. The extended flight plan could require travel to altitudes below 55 km, as well as latitudes further north of than 30° or south of the equator. Due to material degradation inside the highly acidic atmosphere, the extended mission operations are unlikely to exceed a duration of a couple months; the precise degradation rate will be measured by the on-board sensors. All diagnostic and measurement data will be relayed to the ground stations for analysis.

## 2.10. End-of-life missions

The End-Of-Life (EOL) missions of the probe and orbiter will be conducted after the nominal mission operations have concluded. In case the extended mission operations are approved after conclusion of the nominal mission operations, then the EOL missions will commence as long as extended mission operations can no longer be sustained. The EOL mission of the orbiter is explained in Section 2.10.1, followed by the one for the probe in Section 2.10.2.

### 2.10.1. Orbiter end-of-life mission

The orbiter EOL mission will consist of continuously lowering the periapsis of the orbiter and doing several passes through the atmosphere before burning up in the atmosphere. This will be a propulsive manoeuvre conducted using the remaining fuel on board and aided by the increasing orbit degradation due to atmospheric drag. Similar to NASA's Magellan orbiter<sup>37</sup> and the main spacecraft of the Pioneer Venus 2 mission<sup>38</sup>, Tsubuyaki will take continuous measurements during its descent into the Venusian atmosphere and relay these back to the ground stations until it is ultimately destroyed. This EOL manoeuvre will provide measurement data at new altitudes while making use of the present spacecraft.

### 2.10.2. Probe end-of-life mission

The probe EOL mission will consist of it slowly releasing its lifting gas to commence a slow descent further into the Venusian atmosphere. During this manoeuvre, the probe will continue to collect measurement data and communicate it to the orbiter. Because of this, the EOL manoeuvre should occur on the dayside of the planet and with the orbiter in full view of the probe, such that the relay of this measurement data is not impeded by power and communication window.

<sup>37</sup><https://solarsystem.nasa.gov/missions/magellan/in-depth/>, retrieved 21-06-2021

<sup>38</sup><https://solarsystem.nasa.gov/missions/pioneer-venus-2/in-depth/>, retrieved 21-06-2021

Furthermore, it should be noted that the release of the lifting gas into the atmosphere will cause a local increase in helium concentration, which will likely pollute noble gas measurements. This issue may be corrected for during data processing on Earth given that the gas release rates are known, so the precise gas flow rate through the release mechanism must be tested before launch. A small pressure sensor could be installed inside the probe to detect potential leakage and relay its measurements to the orbiter, as this data could significantly improve the results of the data processing.

During its EOL descent into the Venusian atmosphere, Tori will likely fail from overheating and accelerated material degradation due to the high temperatures. This, too, will be recorded and relayed back to Earth to serve as data for future studies into material and system resistance to the Venusian atmosphere environment.

## 2.11. Mission design overview

This section gives an overview of the mission design, starting with a functional analysis of the mission, followed by the operations and logistics, and concluding with risk and sustainability of the overall mission operations.

### 2.11.1. Functional analysis

A Functional Flow Block Diagram (FFBD) was created to summarise the entire mission into many individual functions. This diagram helps to get an overview for both the overall missions as well as the functions of each individual subsystem. From the FFBD, a Functional Breakdown Structure (FBS) was made, which elaborated upon the levels from the FFBD. The diagrams were updated continuously throughout the process as the design progressed. The identifiers help to see the different functions that belong together, making it easier to see what each subsystem is supposed to deliver.

The FFBD has been split up into 3 levels. The first level consists of the mission phases from launch to end of life. Each phase contains its own functions, defining the second level. The functions include many sub-functions which, subsequently, construct the third level.

The FBS goes into one, more detailed, level. All these levels create an overview of the interconnections between the subsystems, which are used later to make the hardware diagram as seen in Section 3.8 and Section 4.7.

### 2.11.2. Operations and logistics

This subsection will give an overview of the different mission segments of Kumo and will elaborate on the interconnected nature of each mission element. The operations will be categorised and summarised via an operations flow chart. Additionally, how logistical challenges will be addressed throughout the mission will be elaborated upon.

**Operations** The mission operations of Kumo have been divided into two main segments: Earth operations and Venus operations. Earth operations can be grouped into ground operations and launch operations. Venus operations, on the other hand, are composed of atmospheric operations as well as orbital operations. It is also possible to differentiate within each operation following the mission timeline. This way, atmospheric operations can be expressed in two phases, with the first phase concluding after the successful deployment of the probe. In contrast, the second phase focuses on the in-situ measurements that take place in the atmosphere. The orbital operations can also be divided into two sub-segments as the orbit changes via a propulsive manoeuvre, and each orbit has different purposes. The operations and their connections to each other are summarised in Fig. 2.18, which is an updated version of the operations flow chart from the Midterm Report (Bronstring et al., 2021b).

**Logistics** The logistics of a mission include the contracting and supplying of all essential support services for a space mission, including design and development, purchase, storage, transfer, distribution, maintenance, evacuation, and disposing of mission related materials<sup>39</sup>. For Kumo, a newly formulated, function based Classes of Supply (COS) classification will be introduced. This classification was developed by the Massachusetts Institute of Technology (MIT). This was developed after careful analysis of the COS of many organisations, that carry out substantial logistical operations, including NATO, the United States Military, and NASA. Inspired by the COS classification by MIT, a logistics flow diagram was made in Fig. 2.19. The classes of operations for Kumo are shown by the internal blocks, which are interconnected among each other as well as connected to the external sub classes or equipment of operation.

The main COS blocks for Kumo are:

- **Operations:** This concerns the mission operations that are discussed in the Operations part in paragraph 2.11.2. This involves using different operations equipment and is also interconnected with other COS like sustaining operations, monitoring operations and acquiring data from operations. This also connects to the maintenance and repair COS which involves maintaining an acquired part for the mission for the time until it is integrated into the launcher.
- **Acquisition:** This COS mainly deals with three types of acquisition: data acquisition from operations, infrastructure acquisition and monitoring update acquisition. It involves the use of storage equipment, such that the update of individual parts can be obtained by this COS.

<sup>39</sup>[https://web.archive.org/web/20080705235013/http://spacelogistics.mit.edu/classes20\\_supply.htm](https://web.archive.org/web/20080705235013/http://spacelogistics.mit.edu/classes20_supply.htm), retrieved on 17-06-2021

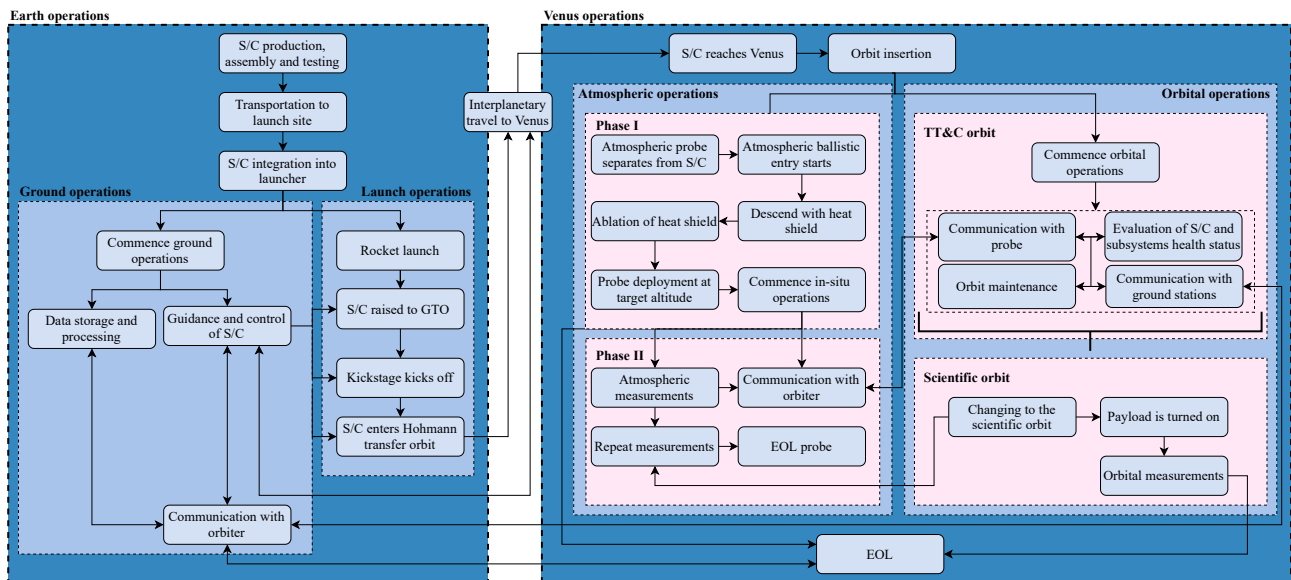


Figure 2.18: Operations flow chart

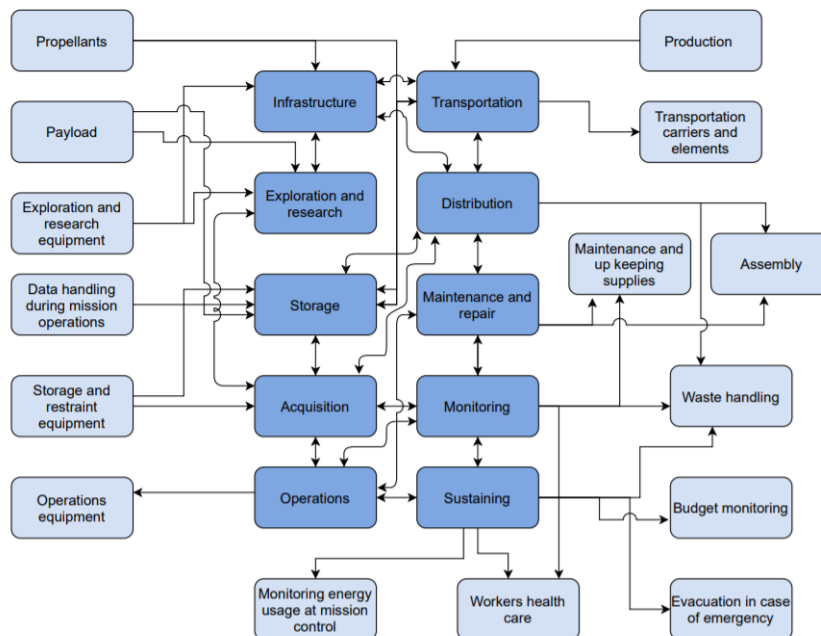


Figure 2.19: Logistics flow chart

- **Storage:** As the name suggests, this COS mainly deals with storage of propellant, payload and data. It is closely connected to transportation, exploration and research, and acquisition. Sometimes, components are stored for a long time, demanding the need of maintenance and repair for the stored items. It is also connected to distribution COS, since, after storage there is a need for distributing the items to various facilities for testing.
- **Exploration and research:** This COS corresponds to the mission objective. Kumo's atmospheric probe is mainly targeted to study the atmosphere of Venus, looking for potential biomarkers, isotopes and UV-absorbers. To achieve this objective, there is need for infrastructure, need for scientific instruments and payload, as well as an exploration and research equipment, to conduct experiments. Since Kumo is a data return mission, the data acquisition also plays a significant role for this COS.
- **Infrastructure:** The infrastructure would include the basic organisational and physical facilities necessary for different operations of Kumo. These encapsulate the facilities of production, storage, transportation, assembly and testing. The payload and propellants need proper infrastructure for storage, from which they can be distributed later. Further, this COS is directly connected to exploration, research, and acquisition.
- **Transportation:** After the individual parts are produced, they are transported to the storage unit. They are then taken for testing to required facilities, and then taken to the launch site for assembly and integration. It is directly

connected to the storage and distribution COS. The propellants need to be transported from storage units, which needs monitoring. It also needs transportation carrier elements, to execute the transportation.

- **Distribution:** Distribution is closely linked to transportation. When the parts are received after production, they need to be distributed to their different testing facilities, which needs transportation. It is also linked to the maintenance and repair COS, which is needed for monitoring any damage done to the parts, while distribution and transportation. It is also linked to storage and acquisition, since the parts and their data come in through the distribution units. After the parts are distributed from the testing facilities, they are sent to the launch site for assembly.
- **Maintenance and repair:** This is an important part of the mission logistics. Maintenance and repair, is directly connected to operations, monitoring, distribution, storage and assembly. To maintain and repair for damages, the supplies must be monitored, and the updated status of repair work must be acquired by the maintenance unit.
- **Monitoring:** For proper maintenance and repair of components, propellant and payload, monitoring is essential. It also connects to the monitoring of waste handling methods from production, monitoring the acquired data and operations at each mission stage. It is also closely linked to the aspect of sustaining, which needs monitoring to keep the mission operations sustainable.
- **Sustaining:** The final, yet important COS of Kumo, is the aspect of sustaining. This entails monitoring the budget, monitoring the health and safety of ground workers involved, and monitoring the energy usage at mission control and operations. This is closely connected to the monitoring COS. Every phase of the mission operations must be checked whether it is sustainable in terms of the aspects previously mentioned, along with efficient waste management techniques.

### 2.11.3. Risk of mission operations

In Table 2.11 both the flight and orbital mechanics as well as system level risks will be discussed, as they are both relevant to the mission design. The numbering from the midterm report (Bronstring et al., 2021b) still applies: 10 for the flight and orbital mechanics department and 11 for the system level risks. Notable is the fact that the most risks in this section stem from the atmospheric entry and the uncertainties surrounding the deployment method for the probe.

**Table 2.11:** Mission risk assessment and mitigation

<p><b>10a-1:</b> <i>Extended night-time traverse.</i></p> <p><b>Assessment L2S3:</b> In case the mission plan involves travelling upstream of the atmosphere, the 'shadowed' portion of the revolution might be higher than expected. The likelihood is low, since the mission plan will determine the flight path in advance with the worst case scenario in mind.</p> <p><b>Mitigation L2S3:</b> The mission plan does not involve any upstream travelling, reducing the likelihood to very low. The severity remains noticeable, as the consequences of a prolonged drift without solar power could push the limits of battery capacity and risk depleting the probes energy reserves entirely. As they can be refilled the next morning, however, this is not a critical risk.</p>
<p><b>10a-2:</b> <i>Higher than expected drag on the orbiter at low altitudes.</i></p> <p><b>Assessment L2S4:</b> Little data on exospheric drag around Venus exists and extrapolation is likely to be inaccurate, but given the success of previous Venus orbiters, the likelihood of the drag being higher than expected is low. Higher than expected decay scores critical on severity, as it is a self-reinforcing process, and could severely shorten the orbiter's lifetime.</p> <p><b>Mitigation L2S2:</b> The first phase relay orbit is far removed from the atmosphere, so the risk of premature decay is negligible. The second phase orbit flies at a 300 km altitude at its periapsis. The likelihood of unexpected drag thus remains low, but the severity can be decreased to marginal because a velocity reduction at periapsis will lower the apoapsis. For the science orbit, the apoapsis, providing ample reserve before the orbit can fully decay due to atmospheric drag.</p>
<p><b>10g-1:</b> <i>Failure to decelerate enough before reaching target altitude.</i></p> <p><b>Assessment L3S4:</b> Failure to decelerate due to the wrongly computed aerodynamic properties will cause the entry vehicle to fall at a higher terminal velocity than expected. Due to buoyant lift and higher densities at lower altitudes, the probe will be pushed up to the correct operating altitude anyway. However, larger velocities pose adverse conditions to the deployment and inflation of the probe, undermining the structural integrity. Hence a critical severity is assigned, with a moderate likelihood.</p> <p><b>Mitigation L2S3:</b> The heat shield is now also designed to function as a shell to deploy from, shielding the inflating probe from the oncoming airflow. This helps reduce the likelihood of failure during deployment from moderate to low, as well as reducing the severity from critical to noticeable.</p>
<p><b>10b-1:</b> <i>Overheating of the entry vehicle.</i></p> <p><b>Assessment L4S4:</b> If the chosen heat dissipation mechanisms are proven ineffective in dealing with the friction-induced temperature de-calibration of scientific equipment may occur. Thus, the severity is deemed critical. The likelihood is high due to the lack of complete knowledge of the atmospheric properties.</p> <p><b>Mitigation L3S3:</b> Margins applied in the heat shield sizing allow for some deviations from the planned entry trajectory, thereby reducing the severity to noticeable. The likelihood can also be reduced by collecting and aggregating more atmospheric data into a high accuracy model.</p>

---

**10c-1: Entry vehicle stability during descent.**

---

**Assessment L3S4:** At the target altitude, the probe may fail to stabilise. The likelihood is medium, due to the unusual deployment methods of the probe. However, there were no failures in the seventeen successful atmospheric entries at Venus.

**Mitigation L3S3:** The severity is reduced by the buoyant nature of the atmospheric probe. It provides a fail-safe mechanics that prevents the probe from crashing despite loss of control or another stabilisation-related failure.

---

**10d-1 Rupture during inflation.**

---

**Assessment L2S5 :** Given a probe inflation rate that is too high for the materials to handle, the probe may rupture. The severity is deemed catastrophic, as the probe would lose buoyancy and dive below the operational altitude. The likelihood for this is deemed low, as the inflation mechanism for the probe will be tested extensively before launch.

**Mitigation L2S5:** For future design, splitting the inflatable part of the probe into separate inflatable cells should be investigated. These cells could be sealed off from each other by valves to avoid excessive leakage of buoyant gas in case of a local rupture. In such a case, the probe could still perform its mission at a lower altitude.

---

**10e-1 Rupture due to turbulence**

---

**Assessment L2S5 :** Once the back cover is released, the turbulence that the probe is subjected to could cause rupture of the probe material. The severity is deemed catastrophic, as the probe would lose buoyancy and dive below the operational altitude. The likelihood for this is deemed low, as extensive simulations and testing will be performed before launch.

**Mitigation L2S5:** For future design, splitting the inflatable part of the probe into different inflatable cells should be investigated.

---

**10f-1 Back cover or heat shield hitting the probe after release**

---

**Assessment L2S5:** Upon release at the target altitude, the back cover or heat shield could be pushed by by the wind because of their specific shapes. The probe could potentially be hit and damaged in the process, leading to catastrophic effects. Due to extensive simulations and testing performed for entry, the likelihood is deemed low.

**Mitigation L2S5:** (1) For future design, a parachute could be considered to be included in the back cover to make sure it does not skip back. (2) For future design, small thrusters could be attached to the heat shield to quickly create distance with the probe.

---

**11a-1: Interruption in measurements due to disturbances.**

---

**Assessment L1S4:** In case a large disturbance, like a cyclone, completely overturns the probe or displaces it significantly from the intended path, the measurements might need to be repeated later, thus extending the mission duration. The likelihood of such a drastic disturbance is very low, as no cyclonic winds have been observed in the equatorial region.

**Mitigation L1S4:** The design is equipped with control surfaces and differential thrust to counter and recover from disturbances introduced by gusts and other turbulences. Larger disturbances cannot be avoided or mitigated that easily, so the severity stays at critical. The likelihood can be reduced to very low by monitoring the winds on Venus and avoiding dangerous regions if detected.

---

**11b-1: Limited power due to insufficient energy reach.**

---

**Assessment L2S4:** Insufficient power available may require the deactivation of near-mission critical systems and instruments. For example, if not enough power is received due to the cloud's opacity, a climbing manoeuvre to an altitude with higher solar flux is needed. This risk is aggravated when the concept is slower, when performing manoeuvres. The dynastat is expected to have a slow response, thus increasing the likelihood.

**Mitigation L2S3:** The severity of insufficient power can be reduced by anticipating a shortage and preventively switching off secondary systems. This can include the propulsion system, as the fail-safe option of a dynastat always is to float at the neutrally buoyant altitude, not requiring any power for staying aloft.

---

**11c-1: Running out of lifting resources.**

---

**Assessment L2S4:** Maintaining the neutrally buoyant altitude requires proper containment of the lifting gas. If depleted before the end of the mission, the probe would crash into the surface, meaning mission failure. The dynastat is only partially dependent on a lighter-than-air gas for its lift, thus reducing the severity.

**Mitigation L1S4:** The severity of a loss of lifting gas cannot be mitigated further, as it is an integral part of the dynastat concept. The likelihood is reduced by including a gas containment layer all around the inside of the lifting gas envelope, preventing the helium from escaping.

---

#### 2.11.4. Sustainability of mission operations

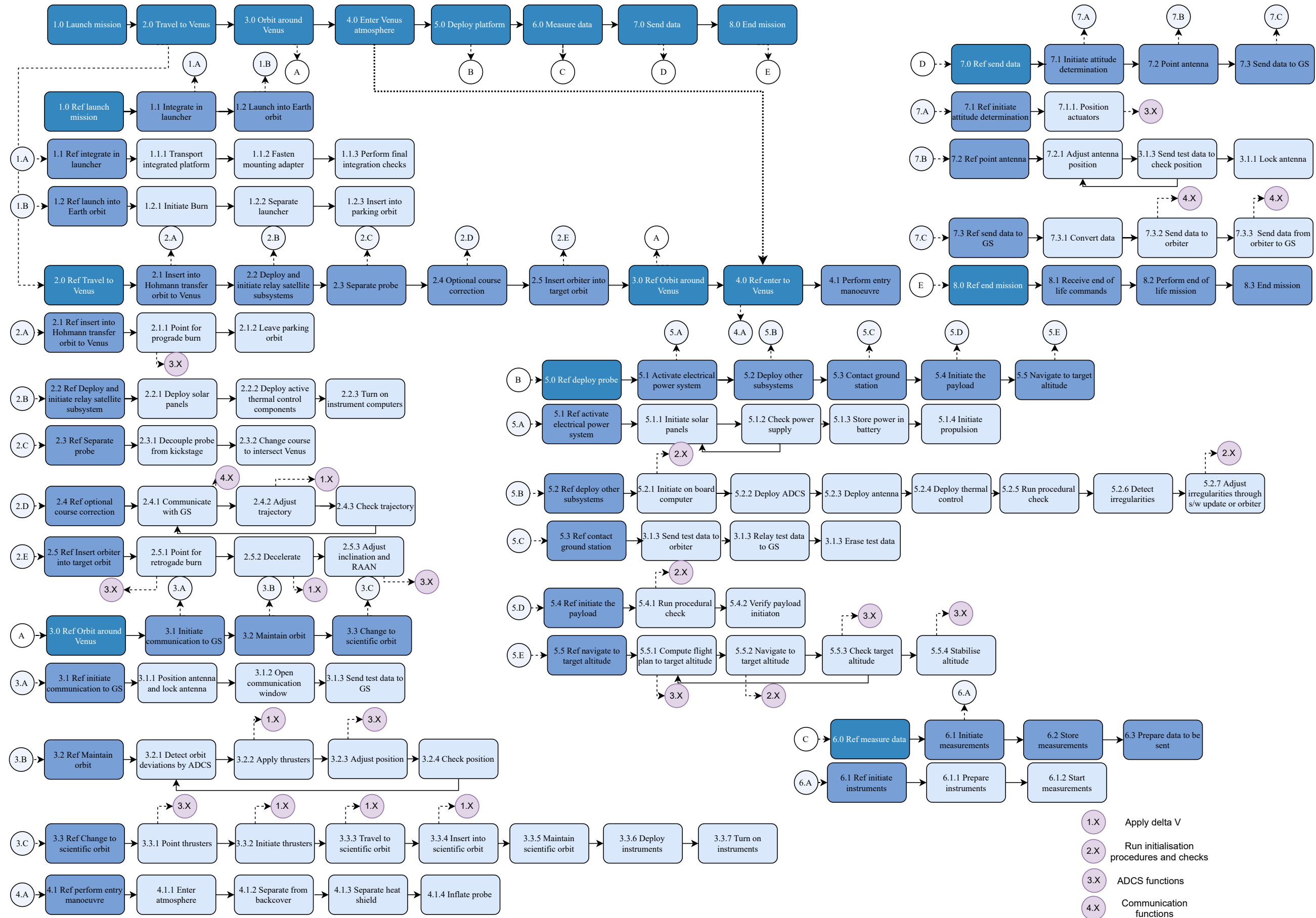
For the Earth segment of the mission, the sustainability of the mission operations was scored “reasonable” (2). This score takes into account the use of a sustainable launcher, as well as the production of the entry vehicle heat shield. The material used for the TPS, PICA-X, is made using phenol, which is a toxic substance that is widely used in the chemical industry for synthesising plastics. This process is dangerous, but common enough to reason that the manufacturing facilities can be equipped to keep staff safety within acceptable bounds. Furthermore, PICA-X was designed to reduce production costs, which is good for economic sustainability. Taking into account the fact that the aeroshell structure is made from aluminium, an easily available material that allows for safe manufacturing of parts, the atmospheric entry was given a “reasonable” (2) grade for sustainability during the Earth segment of the mission.

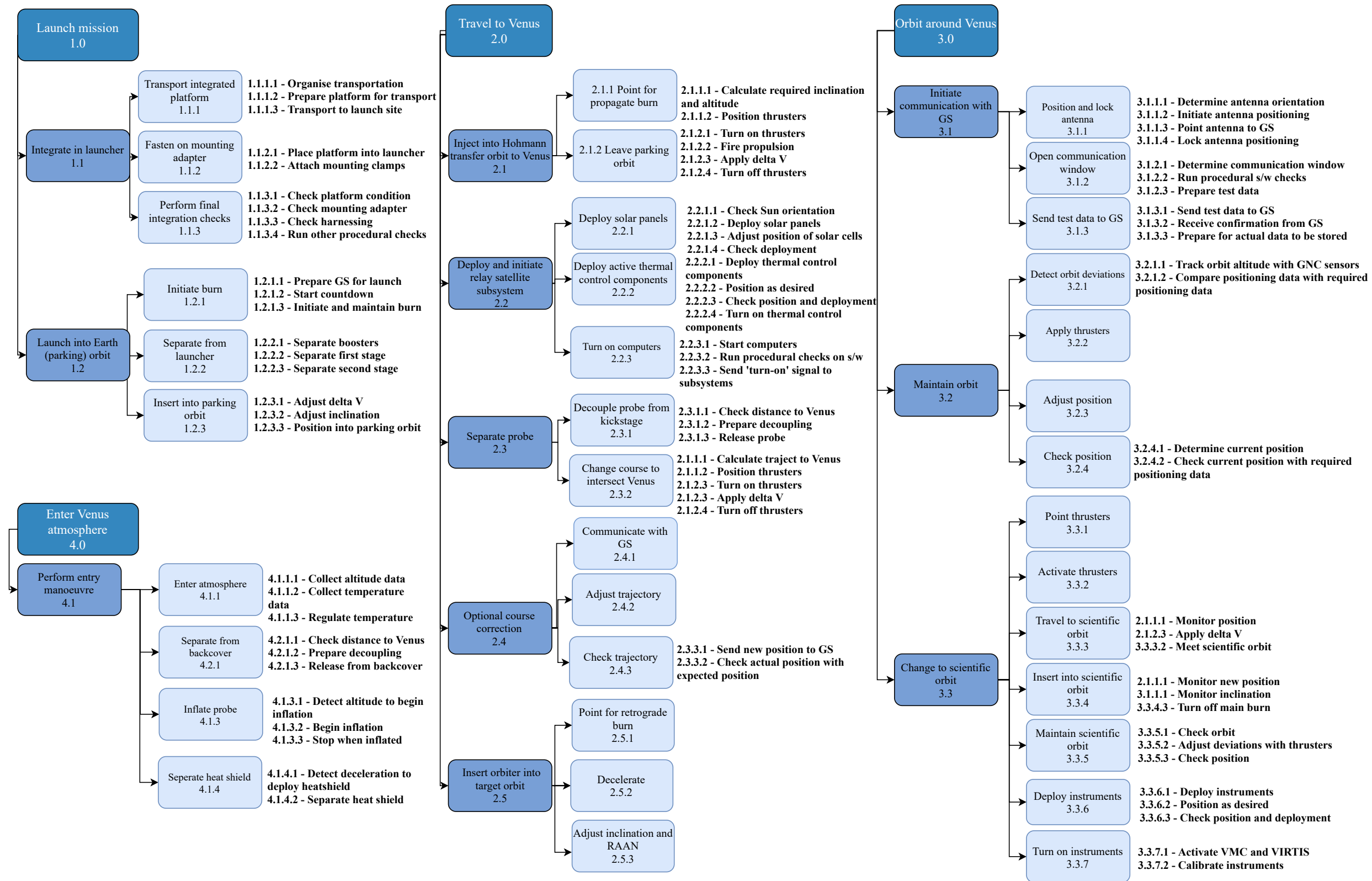
The sustainability of the orbital mechanics for the interplanetary travel phase was scored “reasonable” (2), since the Hohmann transfer orbit selected provides a lower  $\Delta V$  requirement than a fast trajectory would but a higher one than a low energy trajectory using manifolds.

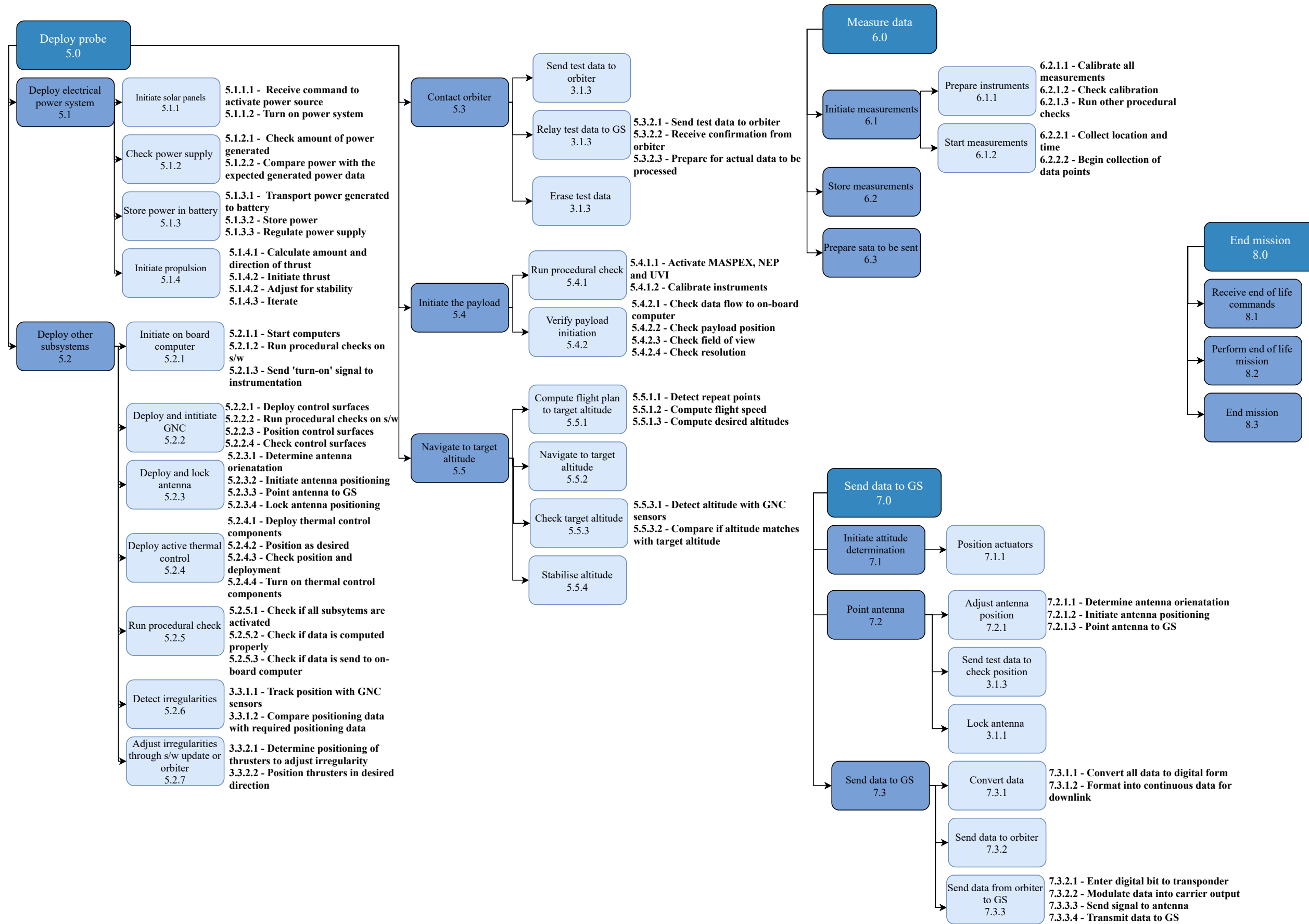
For the Venus segment of the mission, an entry from the interplanetary trajectory was selected, which reduces the total mass of the spacecraft significantly, contributing very positively to environmental and economic sustainability. The aeroshell is released at the target deployment altitude and allowed to crash into the surface, the effect of which is considered negligible due to the low planetary protection level of Venus. The sustainability of the atmospheric entry was thus graded “high” (3) for the Venus segment.

As for the orbiter, the orbit change requires a significant  $\Delta V$  and thus necessitates significant fuel mass to be added to the orbiter. Owing to the contribution to social sustainability of the science data acquired from the new orbit, as well as the possibility to use the orbiter for data relay for future missions, the sustainability of the orbiter during the Venus phase was scored “reasonable” (2).

For both the orbiter and the probe, the potential harm caused by crashing the mission elements into Venus was considered to be alleviated by the contribution the EOL missions have to the overall social sustainability of the mission.







# 3. Tori design

As explained in Chapter 2, the mission contains both a probe (Tori) and an orbiter (Tsubuyaki). The design of Tori will be discussed in detail in this chapter. To start off, the payload will be discussed in Section 3.1 to guarantee all scientific objectives can be fulfilled. Second, to communicate the scientific data, the payload needs a telecommunication and data handling system, which is therefore the next subsystem to be discussed in Section 3.2. Next, GNC will be evaluated in charge of the control and navigation of Tori in Section 3.3. All of these subsystems will need power to function, which then comes to the power subsystem design. The largest part of power consumption comes from the propulsion mechanism, which is needed to perform the manoeuvres given by GNC and C&DH. Hence, the power and propulsion subsystems designs will be explained in Section 3.4. The probe will have to operate between its temperature ranges. Thus, the thermal control subsystem will ensure this and will be discussed as the next topic in Section 3.5. Subsequently, the overall structures of Tori will be designed in Section 3.6, flowing from the size of the subsystems and the support they will need. Finally, the structure will require to be stable, which is then discussed in Section 3.7. The report will end with the budgets for Tori as well as the Tori hardware diagram and its performance in Section 3.8.

## 3.1. Payload

The payload is the main subsystem that will be responsible for carrying out the mission objectives. First, the payload requirements will be stated to relate the chosen instruments to the requirements. Then, an overview of those instruments will be given in Section 3.1.2. Next, the verification and validation will be discussed in Section 3.1.3. Finally, the risks and sustainability strategy will be elaborated upon in Section 3.1.4 and Section 3.1.5, respectively.

### 3.1.1. Requirements

The mission objectives consist of three parts: measuring noble gas isotopes, measuring biomarkers, and measuring UV-absorption levels. The requirements for the payload have been listed in Table 3.1. The requirements with the identity KUMO-STH-SCI flow from the stakeholder requirements and are the main requirements to be fulfilled. Additionally, the requirements starting with KUMO-MA-SCI are the ones derived from the market analysis and are less crucial.

As will be discussed in Section 3.1.2, KUMO-STH-SCI-05 and KUMO-STH-SCI-06 will be easier to fulfill as instruments can be found which simply can measure with this accuracy. KUMO-STH-SCI-04 and KUMO-STH-SCI-07, on the other hand, will be harder to verify, as no specific measurement accuracies are given.

**Table 3.1:** User requirements

Identifier	Requirement	Check
KUMO-STH-SCI-04	The mission shall determine the abundance ratio between key isotopes of noble gases with an accuracy sufficient to determine the atmosphere evolution history to 40 Myr.	n.a.
KUMO-STH-SCI-05	The mission shall determine the abundance and source location of phosphine to an accuracy of 0.2 ppb.	✓
KUMO-STH-SCI-06	The mission shall determine the abundance and source location of methane to an accuracy of 10 ppt.	✓
KUMO-STH-SCI-07	The mission shall investigate the structure of UV-absorbers in the atmosphere.	✓
KUMO-MA-SCI-MO1	Tori shall expose promising materials to the Venusian atmosphere to measure the material behaviour.	✓
KUMO-MA-SCI-MO2-1	Tori shall measure aerosol particles with a size of at least 1 $\mu$ m at concentrations less than 1 $\text{cm}^{-3}$ .	✓
KUMO-MA-SCI-MO3	Tori shall measure temperatures below 40 km.	✓

### 3.1.2. Payload overview

Biomarkers and noble gasses isotopes have been detected using mass spectrometers in previous deep space missions. Therefore, the Mass Spectrometer for Planetary Exploration (MASPEX) will be used to detect both<sup>1 2 3</sup>(Zurbuchen and Martin, 2019; Lewis et al., 2016). This instrument will be used on the Europa Clipper mission and is based on the latest technology available. The MASPEX can measure particles up to 1 ppt, which suffices for the requirements KUMO-STH-SCI-04, KUMO-STH-SCI-05 and KUMO-STH-SCI-06. The MASPEX will take measurements every 0.5 ns.

<sup>1</sup><https://europa.nasa.gov/spacecraft/instruments/maspep/>, retrieved on 02-06-2021

<sup>2</sup>[https://smd-prod.s3.amazonaws.com/science-red/s3fs-public/atoms/files/Europa-PSS\\_Sept\\_2016.pdf](https://smd-prod.s3.amazonaws.com/science-red/s3fs-public/atoms/files/Europa-PSS_Sept_2016.pdf), retrieved on 02-06-2021

<sup>3</sup>[https://www.aiaa.org/docs/default-source/uploadedfiles/education-and-careers/university-students/design-competitions/3rdplace\\_rmit\\_space\\_design.pdf?sfvrsn=4a3eea29\\_0](https://www.aiaa.org/docs/default-source/uploadedfiles/education-and-careers/university-students/design-competitions/3rdplace_rmit_space_design.pdf?sfvrsn=4a3eea29_0), retrieved on 02-06-2021

**Table 3.2:** Probe instruments

Parameter	MASPEX	NEP	UVI	Total
Mass [kg]	8	4.4	4.1	16.5
Power [W]	6.4	11.3	34	51.7
Size [mm]	400x $\varnothing$ 40	Electronics: 165 x $\varnothing$ 188 Sensor assembly: 508x89x127	Electronics unit: 220x220x50 Sensor unit: 199x206x376	$28.66 \times 10^6 \text{ mm}^3$
Data rate [kbps]	57	$10 \times 10^{-3}$	50	107.01
Cost [\$M]	58	20	N/A	N/A
Range	2 – 1000 Da	900 nm, > 1 $\mu$	283 nm and 365 nm	-
Resolution	7,000 – 24,000 $M/\Delta M$	max. 4°	650 LW/PH	-
Sensitivity	1 ppt	$1.1 \times 10^{-8} \text{ m}^{-1} \text{ sr}^{-1} \text{ count}^{-1}$	5 %	-

Since the UV-absorbers detected in the atmosphere are still unknown and all measurements done so far have been performed outside of the atmosphere, an Ultraviolet Imager (UVI) will be placed on board of the probe, which will detect UV-absorbers in its surroundings, within the atmosphere (Yamazaki et al., 2018). This instrument has previously been used for the Akatsuki mission, which measured UV-absorbers in orbit around Venus. However, the instrument is still able to detect UV-absorbers within the atmosphere as its function is to take images of its field of view in the UV-spectrum. Thus, this is independent of the probe being inside or outside of the atmosphere<sup>4</sup>. This instrument focuses on two wavelengths, namely: 283 nm and 365 nm, which are the wavelengths corresponding to sulphur and the unknown UV-absorbers, respectively (Yamazaki et al., 2018). This instrument shall fulfil the requirement KUMO-STH-SCI-07. The UVI will take an image every 11 s.

Finally, aerosols within the atmosphere will be detected using the Nephelometer (NEP), previously used for the Galileo mission. This will be added as additional value as mentioned in Section 2.3.1. The NEP will measure at a wavelength of 900 nm and can measure particles with a size of at least 1  $\mu\text{m}$  (Coradini, 1999), which meets the requirement KUMO-MA-SCI-MO2-1. The NEP will take measurements every 8 seconds.

An overview of the instruments and their characteristics are found in Table 3.2:

Here, the instrument's masses as well as their power consumption, data rates, size, cost, measurement range, resolution and sensitivity are given. It is seen that UVI and VMC do indeed have an overlapping spectral range. Thus, this concludes that the measurements can be compared.

Additionally, ultrasonic sensors will be used to detect corrosion of the material during the probe's nominal mission, but also during its end of life mission. Six sensors will be used, as explained in Section 2.3.1, for all degrees of freedom the dynastat has. Furthermore, temperature sensors will be used to measure the temperature of the atmosphere below altitudes of 40 km during the probe's end of life mission. These sensors, including their wiring system, will weigh no more than 2 kg, consume no more than 13 W and cost no more than \$30,000. These sensors will be required to fulfil requirements KUMO-MA-SCI-MO1 and KUMO-MA-SCI-MO3.

### 3.1.3. Verification and validation

To verify if the MASPEX will be able to detect the noble gasses within the right accuracy, the concentration of the noble gas isotopes to trace back the atmosphere evolution history to 40 Myr should be determined. To do this, the exact isotope ratio should be decided that will help trace back the evolution of Venus. Once, this specific ratio is established, tests using specialised laboratories, such as the Materials and Electrical Components Laboratories at ESA ESTEC, can be done to check whether the instruments chosen are suitable for the objectives. Tests to verify the MASPEX include vacuum tests, where the instrument will be exposed to different noble gasses. Since the noble gas type injected in the environment of the MASPEX is known beforehand, the peak values detected by the MASPEX can be compared to the already verified and validated peak values from previous data. Examples of noble gasses to be tested include Xenon, Krypton and Argon.

The same testing for the MASPEX can be done for interesting biomarkers, such as phosphine and methane.

Furthermore, the UVI needs to be verified as the environments has changed. Previously, it was used to detect UV-absorbers from outside of the Venusian atmosphere. Now, it will be used inside the atmosphere. The UVI can be verified using the same testing facility at ESTEC. However, the instrument will be exposed to UV-radiation instead of ions in a chamber simulating the Venusian atmosphere. Known compounds with their corresponding UV-spectral range will be tested with the UVI such as sulphur and phosphine. The results will again be compared to validated results from previous missions that went to Venus. With these tests, situations such as spectral ranges overlapping each other can be predicted and even avoided if the measurement accuracy is sufficiently high.

<sup>4</sup>suggested by Dr. Stam on 04-06-2021

<sup>4</sup>[http://www.esa.int/Enabling\\_Support/Space\\_Engineering\\_Technology/Materials\\_Electrical\\_Components\\_Laboratory](http://www.esa.int/Enabling_Support/Space_Engineering_Technology/Materials_Electrical_Components_Laboratory), retrieved on 14-06-2021

Finally, the NEP can be tested using the 12 m<sup>3</sup> Dycor® aerosol test chamber offered by TNO<sup>5</sup>. The instrument can be exposed to both chemical and biological materials. The values the Nephelometer detects can be compared to the validated and verified values from previous nephelometers.

Additionally, tests to see the instrument resistance against corrosion and acid can be performed at ESTEC in the Materials and Electrical Components Laboratory<sup>6</sup>.

### 3.1.4. Risk

There are several risks that could occur. In Table 3.3, a list of all possible risks are given along with their likelihood and severity factor and risk mitigation method.

**Table 3.3:** Table showing possible risks, their severity and likelihood

<b>1a-1</b> <i>Failing to measure data.</i>
<b>Assessment L2S5 :</b> Wrongly placed wiring, instrumentation errors or wrongly performed data calculations estimations could lead to failure to measure data and prove catastrophic for the mission.
<b>Mitigation L1S4 :</b> Redundant wiring in case of wire failure will be applied.
<b>1b-1</b> <i>Wrongly calibrated instruments.</i>
<b>Assessment L3S5 :</b> Wrongly calibrated instruments could result in unreliable measurements, which subsequently could lead to serious setbacks. The risk increases especially due to switching the instruments on and off multiple times.
<b>Mitigation L2S4 :</b> (1) Apply safety procedure to access the instruments on Venus from Earth to re-calibrate if necessary. (2) Apply automatic re-calibration system with a specified re-calibration period.
<b>1c-1</b> <i>Instrument damaged due to acidic atmosphere.</i>
<b>Assessment L1S4 :</b> Due to the acidic nature of Venus' atmosphere, instruments could get damaged to a serious extent, with critical consequences.
<b>Mitigation L1S3 :</b> Instruments will be protected by box-like structures that resist the acidic concentrations of the atmosphere. This will function as a protective coating around the structure.
<b>1d-1</b> <i>Instrument damaged during launch or re-entry</i>
<b>Assessment L2S5 :</b> During the re-entry to the Venus atmosphere and the launch from Earth, the payload will be exposed to high temperatures, pressures and loading conditions, which can damage the payload. While the entry vehicle protects against most of these conditions, there is still a low possibility for the payload to get damaged.
<b>Mitigation L1S4 :</b> (1) Protect the instruments with thermal control mechanisms. (2) The instruments will be insulated properly to avoid damage caused by entry conditions.
<b>1e-1</b> <i>Failure in instrument deployment.</i>
<b>Assessment L2S5 :</b> The nephelometer should be properly deployed after entering Venus' atmosphere. Failures in the deployment system of the nephelometer could occur, which consequently influence its performance.
<b>Mitigation L1S4 :</b> Apply a safety mode by adding a redundant deployment mechanism that takes over if the primary deployment mechanism fails (cold redundancy).
<b>1f-1</b> <i>Failing to switch instrument on.</i>
<b>Assessment L2S5 :</b> The payload could fail if the instruments on-board are failing to be turned on properly every time the probe exits the night time. This can be due to an error in the power supply as well as wiring errors.
<b>Mitigation L1S3 :</b> Apply a safety mode by applying a redundant path to the C&DH part that transmits the on/off commands (cold redundancy).

### 3.1.5. Sustainability

The payload on board of Tori is a significant contributor to the social sustainability aspect of Kumo. The study of Venusian atmosphere in search of biomarkers and UV absorbers could sparkle a new discovery in the field of space science altogether. However, sustainability also considers the environmental, political and economical aspects of the mission. Hence, mission payload and instrumentation was considered to be a noticeable contributor to sustainability, and was given a weight of 3. In this subsection, a brief outline of the contribution of payload components, management and transportation, to sustainability will be presented.

First, the individual components on board are reviewed:

- **MASPEX:** As mentioned earlier, this off-the-shelf instrument will be used on the Europa Clipper mission by NASA. The ability to exploit the newest technology, improves the chances of better functionality of MASPEX. The mass and power are also not that high compared to other mass spectrometers like Ion and neutral mass spectrometer

<sup>5</sup>[https://www.tno.nl/media/7701/aerosols\\_flyer.pdf](https://www.tno.nl/media/7701/aerosols_flyer.pdf), retrieved on 14-06-2021

<sup>6</sup>[http://www.esa.int/Enabling\\_Support/Space\\_Engineering\\_Technology/Materials\\_Electrical\\_Components\\_Laboratory](http://www.esa.int/Enabling_Support/Space_Engineering_Technology/Materials_Electrical_Components_Laboratory), retrieved on 14-06-2021

(INMS), which has higher mass and power values, for more or less similar costs. This entails that for an instrument to measure with a high accuracy of 1ppt, the mass, power and costs are highly optimised. Furthermore, the safety of personnel at NASA testing laboratory, during the radiation tests will be actively monitored. Hence, a “high” score of (3) was given to MASPEX.

- **UVI:** This instrument as well is off-the-shelf from JAXA, and was previously used in the Akatsuki mission, successfully. The transportation from Japan to the Netherlands for testing and verification and then to Florida for the launch, would involve additional costs and emissions, which need to be monitored. The costs for UV-radiation tests for UVI, are a bit higher than for other tests, due to its importance to the mission. For this test as well, special attention must be paid to the safety of workers. Hence, a “reasonable” score of (2) was given to UVI.
- **NEP:** This instrument was used previously on the Galileo mission (Ragent et al., 1992), where it operated successfully in measuring aerosols. For Kumo as well, this nephelometer will be responsible to conduct scientific experiments, which will add market value to the mission. This instrument greatly impacts the social sustainability of the mission, apart from environmental and economical aspects and hence, is given a “high” score of (3).

Out of a possible score of 9, the payload instruments on board were scored to have a total of 8. This means that the subsystem sustainability score for this payload components is 88%. However, for the overall sustainability towards mission operations, the three phases, Earth operations  $SP_1$ , interplanetary travel  $SP_2$  and Venus operations  $SP_3$ , have to be scored separately.

A “reasonable” score of (2) for the Earth phase is given for payload. This is considering manufacturing costs and transport emissions from production and testing locations to the launch site. For the interplanetary phase, payload on board Tori will not be used and will not contribute to any space debris and will also not use power. Hence, it is given a “high” score of (3). Finally, for the Venus operations phase, payload on Tori actually starts consuming power and sending the measurement data to Tsubuyaki. The instruments will be tested for optimised operations on Earth. The testing methods used will be non-destructive in nature, like the visual, ultrasonic, radiography and acoustic emission non-destructive methods<sup>7</sup>. This fulfills sustainability requirement KUMO-SUS-PL-01. The payload selection also reviewed the contaminating properties of the concerned instruments, and it was analysed to be less than 30%, which complies with the sustainability requirement<sup>8</sup>. For EOL, the payload on board would just burn up while crashing near the surface, due to high atmospheric temperatures. Hence, a “high” score of (3) was given for this phase.

These scores will be used to further calculate the overall mission sustainability score later.

After analysing the payload, a subsystem is needed to transfer all the data for it to eventually reach Earth. This will be discussed in the next section, called TT&C and C&DH.

## 3.2. Telecommunications and command

The atmospheric probe (Tori) of the Kumo mission will be sending tracking data to the ground station and science, command and telemetry data to the orbiter (Tsubuyaki), which will relay these. Tsubuyaki will have two TT&C functions. First, working as a relay satellite, linking Tori and the ground station and remote sensing satellite. Second, working as a remote sensing satellite, which transmits its science data directly to Earth. This section contains the entire mission telecommunications and data handling operation of the probe. Section 3.2.1 goes over the requirements while Section 3.2.2 explains the telecommunications plan. The operational modes are explained in Section 3.2.3. The communications instruments are picked in Section 3.2.4. With this the Link budgets could be created in Section 3.2.5. In Section 3.2.6 a new architecture for the subsystem is discussed. In Section 3.2.7 the command and data handling of the probe is outlined. An overview of the subsystem can be found in Section 3.2.8. The subsystem is concluded with verification and validation, risk assessment and sustainability in Sections 3.2.9, 3.2.10 and 3.2.11 respectively.

### 3.2.1. Requirements

The requirements of this subsystem can be found in Table 3.4. These requirements are related to the operations of Tori. The requirements related to Tsubuyaki’s operations can be found in Section 4.2.1. It has to be noted that the distance of the requirement KUMO-GNC-02 was rewritten to 158 million km from 261 million km. This is because at the time this was written, the probe was expected to last half a year in the atmosphere instead of 63 days. The distance between Earth and Venus on the 63rd Earth day is 158 million km. It has to be noted that the distance mentioned here is the furthest distance and thus the driving value. The communications will take place during the entire mission and not just at the end. Requirements KUMO-TD-01-1 and KUMO-TD-02-1 are explained in Section 3.2.4. KUMO-TD-03-1 and KUMO-TD-04-1 are explained in Section 3.2.5. The explanation of KUMO-TD-05 can be found in Section 3.2.7. The requirement is not checked off as further testing is required to find its efficacy. The explanation of requirements KUMO-TD-06-1, KUMO-TD-07 and KUMO-TD-08 can also be found in the same section. Requirement KUMO-GNC-02-1 is based on the tracking communication at the furthest away from the ground station.

<sup>7</sup><https://www.flyability.com/ndt>, retrieved 28-06-2021

<sup>8</sup><https://epact2.gsfc.nasa.gov/tycho/STEREOContamControl.htm>, retrieved on 28-06-2021

**Table 3.4:** Requirements for telecommunications and data handling

Identifier	Requirement	Check
KUMO-TD-01-1	Tori shall use a frequency range of between 8.40-8.45 GHz (X-band) and 2.29–2.30 (S-band) GHz for sending messages as downlink.	✓
KUMO-TD-02-1	Tori shall use a frequency range of between 7.145–7.19 GHz (X-band) and 2.11–2.12 GHz (S-band) for for receiving messages as uplink.	✓
KUMO-TD-03-1	Tori shall use a data rate of 256 kbps for sending messages as downlink.	✓
KUMO-TD-04-1	The Tori shall use a data rate of 2 kbps for receiving messages as uplink.	✓
KUMO-TD-05	The system shall be able to detect a communications error with a probability of 0.85 <TBC>.	
KUMO-TD-06-1	Tori shall have a storage capability of 440 GB of data.	✓
KUMO-TD-07	The system shall be able to encode messages to a QPSK Coded Rate 0.8 format.	✓
KUMO-TD-08	The system shall be able to decode messages of a QPSK Coded Rate 0.8 format.	✓
KUMO-GNC-02-1	On-board antenna gain shall be sufficient to communicate at the bandwidth of 1 bps at distances of up to 158 million km.	✓

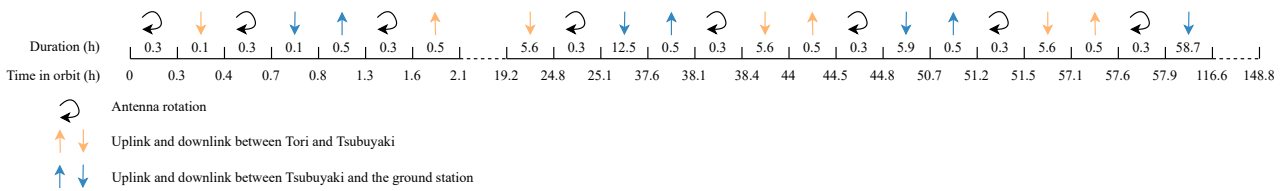


**Figure 3.1:** Overview of communications planning for phase 1

### 3.2.2. Telecommunications overview

To ensure that the science data from Tori reaches Earth, a communications plan was created. This section details the amount of data sent per phase by Tori and Tsubuyaki. The data rates and the modulation method are explained in Section 3.2.5 and Section 3.2.7. As the downlink is the driving factor in the telecommunications, the uplink is neglected in this overview. The data overview is based on the orbits and the payload as stated in Sections 2.6.3, 3.1 and 4.1.

#### Phase 1

In terms of data, Tori produces data from the instruments MASPEX, NEP and UVI, as well as the engineering data from the subsystems. Due to power constraints, the probe will only gather scientific data during the day and engineering data during the entire orbit as described in Section 2.6. As shown in Table 3.2, the total bit rate of the science instruments is 107 kbps, however, due to the time interval of the instruments this data rate has been reduced as described in Section 3.1.2. The data rate is further decreased by compressing the UVI pictures by 4:1. This value is an estimate based on the Clementine mission compressing their UV-images by this rate (Beser, 1994). The science data rate was thus decreased to about 58.1 kbps. The engineering data of the probe is estimated to be 1.42 kbps and engineering data is taken through the entire orbit. Due to the modulation, redundant bits will be added to lower the bit error rate. The data will be multiplied with a factor of 1.25 to create the total data that will be send. With the data rate from Tori to Tsubuyaki being 256 kbps, a time window of about 16.7 h is needed per orbit.

Tsubuyaki will only provide its telemetry data for the first phase, as well as relaying the data from probe. The engineering data of the orbiter was estimated to be 2 kbps. Due to the modulation, the engineering data will be multiplied with the same factor of 1.25. This data will be combined with the probe data to send to the ground station. The data rate of Tsubuyaki to the ground station is 60 kbps. A transfer window of 77.1 h is needed to send the data per orbit.

To ensure that the data can be send to Earth, an overview of the what the orbit should look like in terms of communication was created and can be found in Fig. 3.1. In this figure, the turning of the antenna is denoted to show the importance of this manoeuvre for the subsystem and to show that the orbiter is able to send the large amount of data to Earth. The figure does not include the times when the probe will send its tracking data to Earth. The tracking window will be discussed in Section 3.3.3.

As can be seen in Fig. 3.1, the probe will send its telemetry data to the orbiter, which in turn will send its telemetry data to Earth. This is done to check if the probe and orbiter are operating as they are supposed to be. Right after this, ground station is able to make changes to the operations of, either the probe or the orbiter. It is especially important to plan uplink time as the antenna has to be turned in the right direction to make contact. The ground station is unable to send commands to the orbiter at any time. After the uplinks, the probe and orbiter will start sending large amounts of science data. The duration of the rotation is discussed in Section 4.2.2.

#### Phase 2

In the second phase, Tori will decrease the amount of scientific data output to the five interesting points. The engineering data rate remain unchanged. In the worst case scenario for data rates, the five interesting points would be in the same

probe orbit. The time taken to measure at the interesting points was overestimated to be 10 min. Using the same data rate reductions and the same data rate as in Section 3.2.2 a transfer window of 0.62 h was estimated.

Tsubuyaki changes from only relaying the probe data and sending its own telemetry data to Earth, to also generating scientific data. The data collected by VIRTIS and VMC is outlined in Section 2.8.3. The images taken by Virtis and VMC will also be compressed by a ratio of 4:1, similar to the UVI images. These images are then combined by the engineering data of the orbiter and the probe scientific data. All the collected data is then multiplied by a factor of 1.25 to add redundant bits. To send the data, a transfer window of about 8.8 h, is needed per orbit.

The second phase is harder to plan for than the first place due to the unknown positions of the five repeat measurement points. For this reason, a detailed planning has yet to be made. However, a preliminary strategy was devised. The new orbit of Tsubuyaki makes constant contact between the probe and the orbiter impossible. The new orbit lets Tsubuyaki see the dayside of Venus for 12 h and the nightside of the planet for 12 h.

To make sure that the orbiter will always be able to contact the probe in each orbit, two data transfer windows will be created with twelve hours between them. This ensures that if the orbiter is unable to contact the probe in the first transfer window, it will be able to do so in the second transfer window and vice versa. To avoid these transfer windows, the team should construct a model in which the position of Venus, Earth, Tori and Tsubuyaki are accurately determined relative to each other. However, a preliminary planning is thus already in place to show the data transfer is doable. The orbiter will have little difficulty sending its data as it is almost always in view of Earth as described in Section 2.6.3.

### 3.2.3. Operation modes

Based on Section 3.2.2, three operational modes can be distinguished. These operational modes must ensure that the probe is able to function properly and is able to recover from unforeseen problems that may occur. These operational modes shall give an outline for the desired design of the telecommunications subsystem. These modes are defined so that they can be automated and do not require uplink data from the orbiter.

#### General operations mode

In this mode, Tori has to make scientific measurements as well as sending the data to the orbiter at the same time. Due to the demanding data transfer of the first phase, the probe will need to be able to handle large amount of data at one time. The HGA antenna selected should thus be able to send the science data to the orbiter.

During the collection of data, the probe should also be able to contact the ground station in order track the location of the probe. The probe shall do this with the HGA. However, due to the position of the planets the antenna cannot always point to Earth. This means that the probe should be able to fly without regular positional updates.

#### Safety mode

Due to the nature of the mission, the team should make sure that there is a fail-safe in place. Without a proper safety mode the probe could be lost due to a relatively small mistake.

If the probe and the probe fail to establish contact with the orbiter for a prolonged duration, the probe will enter safety mode. In this mode, the probe will attempt to contact the Tsubuyaki using its LGA antenna. This is due to the idea that the HGA might not be able to be deployed or that because of the narrow bandwidth and a possible problem with the GNC of the probe, Tsubuyaki is impossible to contact. Due to the large coverage of the LGA, less pointing is needed and can this coverage be established. During the safety mode, the probe will turn off the scientific data and only collects engineering data to save power.

#### Power save mode

During the time that the probe is in eclipse, the only source of power is the battery. If the probe were to be using the scientific instruments to make measurements, a lot of power would be needed. This in turn would make the batteries very heavy. To avoid increasing the mass to an unsustainable amount, the probe turns off all its science instruments during the night. The probe will also not send any data during the night for the same reason.

### 3.2.4. Communication instruments

Based on Sections 3.2.2 and 3.2.3 a selection of suitable instruments was made. To create the communication links necessary for the mission success frequency bands, transponders and antennas were selected. They can be found in the following paragraphs.

#### Frequency bands and transponders

For deep-space missions like Kumo there are only three frequency bands available. These are S-band, X-band and Ka band. Of these three, Kumo uses the S-band and the X-band in the deep space bandwidths as defined by NASA (Shin et al., 2014).

The X-band will be used for the science data, control, telemetry and tracking while the S-band will be used in safety mode for safety communications. Based on this Tori and Tsubuyaki will both contain two transponders that can receive and transmit data in the X-band and S-band. The Ka-band would be able to increase the bit rate of the antennas, however this band requires larger antennas and thus increase the weight of the probe and the orbiter.

### Antennas

Following a similar approach as previous missions, like Venus Express (Sivac and Schirmann, 2007) and Cassini (Taylor et al., 2002), the low transmission rate will be done through omnidirectional low gain antennas (LGA) and the high data rates through high gain antennas (HGA). Therefore, Tori and Tsubuyaki will contain an HGA and an LGA for the communication link between the two vehicles and the ground station. As mentioned in the reasoning for the transponder configurations, the frequency band used in the architecture is related to the type of data it is transmitting.

The HGA of Tori was used in the Mars Odyssey mission. As for specifics, the HGA will have a diameter of 1.3 m with a gain of 38.3 dB and 36.6 dB for transmitting (downlink) and receiving (uplink) respectively. The HGA will be used to transmit data in the X-band frequency range. (Makovsky et al., 2002). To point the antenna, a gimbal will be placed to point the antenna. The selected gimbal is the Type 22 Antenna Pointing Assembly which has an accuracy of  $0.02^\circ$ <sup>9</sup>.

Tsubuyaki will have the same HGA as the Mars Express mission. This antenna has a diameter of 1.6 m and an efficiency of 0.7<sup>10</sup>. The antenna will be used to transmit science data in the X-band frequency range. To point the antenna, the same gimbal will be used as for the antenna of Tori.

The selected LGA for both the probe and the orbiter was used in the Venus Express mission. It is an hemispherical quadrifilar S-band omnidirectional antenna with a coverage angle of  $95^\circ$  (Sivac and Schirmann, 2007). As this antenna will be used only in emergencies and tracking data it will only be used sparingly. For its tracking purpose, as described in Section 3.3.3, the LGA will send a signal from the Venusian atmosphere to Earth.

The ground station used in the mission will be the Deep Space Network (DSN). In particular the 34 meter antennas of the DSN will be utilised. These antennas have a gain of 68.3 dB when receiving the signal at the X-band frequency. Other less expensive options were considered, however, due to the large transfer window needed, as described in Section 3.2.2, the DSN was the deemed to be the best option.

### 3.2.5. Link budget

To ensure that the bit error rate (BER) is  $10^{-5}$ , a modulation of QPSK, with a coded rate of 0.80 was implemented. This means that redundant bits will be included into the every transmission. As the coded rate is 0.80 the amount of bits will have to be multiplied by a factor of 1.25. This modulation method will create a link margin of 3.4 dB (Wertz et al., 2011). This margin will be used in uplinks and downlinks. The system shall thus be able to encode and decode in the QPSK format with a coded rate of 0.80.

The system noise temperature (SNT) was estimated using the values from the Venus Flagship mission and the DSN documentation (Hall et al., 2009; Imbriale, 2002). The SNT of Tori and Tsubuyaki are 28.6 dB – K and 30.5 dB – K respectively. As these values are heavily dependent on the exact type instrumentation used, it has to be noted that these values are a rough estimate. The system noise temperature of the 34 m DSN network antennas were determined to be 26.6 dB – K using NASA documentation (Imbriale, 2002).

The transmitter powers of the probe HGA, orbiter HGA, LGA and the ground station are 15 W, 60 W, 10 W and 20 kW, respectively (Makovsky et al., 2002; Sivac and Schirmann, 2007; Cornish et al., 2014)<sup>11</sup>.

The distances between Tori, Tsubuyaki and the Ground station are based on the orbits as described in Section 2.6. In phase 1, the maximum distance between Tori and Tsubuyaki will be about 130.000 km, due to the inclination of 30 deg that Tori will have. In phase 2 Tsubuyaki will change to an elliptical orbit with an apocentre of 66.000 km. The maximum distance between Tsubuyaki and Tori is about 71.400 km due to the inclination of Tori. The maximum distance between the Tsubuyaki and the ground station will be 0.99 au in phase 1 and 1.06 au in phase 2.

The atmospheric loss of Venus is very small and barely absorbs the signal. For the X-band frequencies, this would be 0.02 dB at an altitude of 65 km and 0.06 dB at an altitude of 55 km. For the S-band frequencies it would be negligible (Hall et al., 2009; Häusler et al., 2007). The attenuation of Earth's atmosphere was estimated to be 0.17 dB for the X-band and 0.04 dB for the S-band (Hall et al., 2009; Wertz et al., 2011).

The pointing loss of the probe antenna is based on the gimbal accuracy, and the change in gain per angle of boresight change as denoted in Odyssey Telecommunications (Makovsky et al., 2002). As both Tori and Tsubuyaki use the same gimbal as described in Section 3.2.4, and a similar parabolic antenna a pointing loss of 0.1 dB was estimated for both. The pointing loss of the ground station was estimated to be 0.1 dB as denoted in the same Mars Odyssey telecommunications report.

The line loss of the signal is based on the cables used in the probe and the orbiter. To estimate the loss, first the length of the cable between the computer and the antenna was estimated. For the probe, this was around 1 m and for the orbiter it was around 0.5 m. Based on the length of the cable and the frequency of the signal through them, a rough estimate of the line loss could be made. The line loss of the probe was estimated to be 1.4 dB and the line loss of the orbiter was estimated to be 1.2 dB<sup>12</sup>. The line loss of the omnidirectional antenna was determined to be 0.65 dB and was found in a similar

<sup>9</sup>[https://www.moog.com/content/dam/moog/literature/Space\\_Defense/spaceliterature/spacecraft\\_mechanisms/moog-type-22-apm-datasheet.pdf](https://www.moog.com/content/dam/moog/literature/Space_Defense/spaceliterature/spacecraft_mechanisms/moog-type-22-apm-datasheet.pdf), retrieved on 13-6-2021

<sup>10</sup>[https://pds.nasa.gov/ds-view/pds/viewInstrumentProfile.jsp?INSTRUMENT\\_ID=MRS&INSTRUMENT\\_HOST\\_ID=MEX](https://pds.nasa.gov/ds-view/pds/viewInstrumentProfile.jsp?INSTRUMENT_ID=MRS&INSTRUMENT_HOST_ID=MEX), retrieved on 20-6-2020

<sup>11</sup>[https://pds.nasa.gov/ds-view/pds/viewInstrumentProfile.jsp?INSTRUMENT\\_ID=MRS&INSTRUMENT\\_HOST\\_ID=MEX](https://pds.nasa.gov/ds-view/pds/viewInstrumentProfile.jsp?INSTRUMENT_ID=MRS&INSTRUMENT_HOST_ID=MEX), retrieved on 20-6-2020

<sup>12</sup><https://www.minicircuits.com/WebStore/Cables.html>, retrieved on 14-6

**Table 3.5:** Mission link budgets between Tori and Tsubuyaki

Parameter	Unit	Downlink Phase 1	Uplink Phase 1	Downlink Phase 2	Tracking Phase 2
Antenna gain	dBi	38.3	40.0	38.3	38.3
Satellite TX power	dBW	11.8	17.8	11.8	11.8
Line loss	dB	-1.4	-1.2	-2.4	-1.4
EIRP	dBW	48.6	56.5	48.6	48.6
Propagation range	km	130,000	130,000	71,400	$158 \cdot 10^6$
Space loss	dB	-213.4	-212.0	-208.0	-275.0
Atmospheric losses	dB	-0.02	-0.02	-0.02	-0.04
Gain	dBi	41.4	36.6	41.4	68.3
Line loss	dB	-1.2	-1.4	-1.2	-0.5
C	dB	-124.6	-119.9	-119.2	-158.6
System noise temperature	dB-K	30.5	28.6	30.5	26.6
G/T	dB/K	11.0	8.3	11.0	41.7
Receiver C/N	dB-Hz	73.6	80.1	78.9	43.4
Data rate per user	dB-Hz	54.1	33.0	54.1	0
Available Eb/N	dB	19.5	47.1	24.8	43.4

fashion as the previous line losses. The line loss of the ground station was estimated to be 0.5 dB using SMAD (Wertz et al., 2011).

For the probe a data rate of 256 kbps was selected for the downlink as this was the maximum data rate as indicated in the Odyssey mission specifics (Makovsky et al., 2002). The downlink data rate from Tsubuyaki to the ground station was determined to be 60 kbps as this would be the largest value to still close the link budget as can be seen in Table 3.5. The uplink data rate for the link between the probe and the orbiter was estimated to be 2 kbps as based on SMAD. This is because the probe does not need data from the orbiter, however the data rate from the ground station is about 2 kbps and thus this value was used in the link budget (Wertz et al., 2011). The data rate of the emergency link between the probe and the orbiter was determined to be 10 bps as is common (Shambayati et al., 2011). The emergency link between the orbiter and the ground station as well as the GNC link between the probe and the ground station were determined to be 1 bps to pass the link margin. As the GNC link is used for tracking a large data rate is not required.

As can be seen in Table 3.5, all the link budgets close and show that the probe is able to send the data to Tsubuyaki and Earth. The links between the orbiter and Earth can be found in Section 4.2.4. The link budgets not included in the table that have also been checked to close, are the phase-2 uplink of the probe to orbiter, the phase-1 and phase-2 emergency downlink between the probe and the orbiter and the phase-1 GNC downlink of the probe. These link budgets, however, are not design driving.

### 3.2.6. New proposal for telecommunications architecture

During the detailed design phase, a different telecommunications architecture was conceived. This architecture aims to erase the difficulties of the tracking procedure. Due to the large amount of data needed to be sent, a large antenna was needed. To make sure the probe and the orbiter do not lose each other, the antennas could be constantly pointing at each other. This would mean that the antennas are “locked-on” to each other. To facilitate this, the orbiter would have to be able to either send all its data after the probe dies or the orbiter would need a second antenna. This way the orbiter can have one antenna continuously pointing to the probe and have another antenna continuously pointing the Earth.

#### Advantages

With the orbiter having two antennas, the orbiter would not need to rotate to relay the information. The orbiter thus would not need to carry extra propulsion to facilitate the rotations. However, as explained in Section 4.2.2, the mass induced by the rotation is negligible. If the antennas are locked on to each other, tracking with Earth would not be possible. This procedure should thus make sure that tracking in this manner is not necessary. Due to this procedure the antennas will be continuously facing each other. This means that the antennas will do the pointing through out the orbit. Large amounts of data will thus be guaranteed to be able to be sent. As tracking is hard in the atmosphere of Venus, using the lock-on would alleviate the issues with tracking.

#### Disadvantages

A second antenna will mean a large addition of mass to the orbiter. Based on Table 4.6, the extra mass will be 21.73 kg. This value is without the CD&H unit, as a second one is not necessary. This is a significant increase of the mass and will lead to a large increase of the total mass of the orbiter. Due to the new design architecture a large amount of power will be necessary. To make sure the lock-on effect works the probe antenna will have to be switched on during the entire rotation. This includes the time it spends in the eclipse. This would therefore greatly increase the mass of the probe as a

172 W subsystem will have to be on the entire mission duration. The battery will increase the mass with 90 kg which in turn will increase the structure weight. After the first phase of the mission, the orbiter will enter the elliptical orbit. This means that the orbiter and the probe are not near each other anymore meaning that the lock on process is not possible. After the second phase, the probe will reach EOL. Thus, after the first phase the antenna pointing to Venus will be useless in terms of mission operation. The extra antenna is therefore only useful in the first 30 days. Missions like Akatsuki and Venus Express have lasted nine years or longer which makes the extra antenna useless for almost 99.9% of the mission time<sup>13</sup>.

The team considered switching the telecommunications design to the new architecture for its reliability in tracking, however due to the increase of the mass it does not seem favourable to switch. It was also considered to have a lock-on after each rotation. However, this would mean that the orbiter will have to find the probe in the atmosphere. If finding the position of the probe becomes an issue, the LGA will be used to point the relay satellite to its location. As this is already part of the design, there is no use in changing the approach. Thus, the team will stick to the current design.

### 3.2.7. Command and data handling

The command and data handling unit will be based on the same components and configuration used as for the Venus Express (Sivac and Schirmann, 2007). Each component with their corresponding subcomponents will be explained.

#### Command and Data Unit

Two command and data units (CDMU) will be used for redundancy. They control ground command, reception and execution, onboard housekeeping and science data telemetry storage and formatting for transmission as well as onboard data management, control-law processing and execution of onboard control procedures. Each CDMU contains two processing modules (PM). One will process the Data Management System (DMS) software and one will process the Attitude Operations and Control System (AOCS) software. To process the software, each PM contains a random-access memory (RAM), an Electrically Erasable Programmable Read-Only Memory (EEPROM) and a microprocessor.

Furthermore, each CDMU contains two Reconfiguration Modules (RM) which incorporates a built-in failure system that ensures system-level fault detection and isolation integrity with the Failure Detection, Isolation & Recovery (FDIR) and autonomously reconfigures the PMs. They have a clock function to maintain onboard timing and a watchdog function that, when triggered, sends a reconfiguration. Then, a reconfiguration function is included that perform an autonomous reconfiguration of the CDMU when it receives a minimum two of the four reconfiguration requests from the four RMs request to the High Power Command Module (HPCM).

The HPCM is a decoder that processes the telecommands transmitted by the transponders. When telecommands are accepted, they are passed to the PMs.

Next, a transfer frame generator (TFG) is included that includes 3 channels: one for realtime telemetry, one for telemetry stored in the Solid-State Mass Memory (SSMM), and one for idle frames.

Finally, the CDMU contains a Centralised Memory Module (CMM) that consists of PROM cassette. The PROM cassette holds the default software explained in Section 3.2.7. Also, a Safe Guard Memory (SGM) which itself includes a RAM and an EEPROM is comprised.

The processor within the CDMU is the RAD750 computer is able to process the scientific data and send the data away at the same time. This is determined by the information in Section 3.2.2. Phase 1 has the largest data rate for measuring data and sending data in the entire mission. During phase 1 the RAD750 should be able to send 256 kbps as well as make measurements of 58.1 kbps for science measurements and 1.42 kbps for engineering data. These values are explained in Section 3.2.2. The data rates would combine to a value of 315.52 kbps. Since the RAD750 is able to process 100 Mbps, no problems concerning the computer processing are expected (Brown, Agle, Martinez, and Napier, 2011). For contingency a second RAD750 is added as a back-up in case the first RAD750 dies.

#### Interfaces

A recognised interface unit, previously used for the Mars and Venus Express, will be used that will group all data-handling interface functions with non-standard equipment into two units.

First, the Remote Terminal Unit (RTM) will be used to manage the interfaces between the instruments and all platform equipment except Attitude Operations and Control (AOC).

Second, the AOCS Interface Unit (AIU) will only focus on the interfaces with all the AOCS functions. By implementing the signals received from the sensors, the actuators can be controlled.

#### Solid-State Mass Memory

The SSMM will be used to store all scientific data and housekeeping telemetry. It contains two Memory Masses (MMs) of 440 GBit<sup>14</sup> for redundancy. Also, two redundant controller paths are used with each a Memory System Supervisor (MSS) and a Processor module Interface Controller (PIC). The MSS controls the SSMM and to monitors tasks and the PIC receives

<sup>12</sup><https://solarsystem.nasa.gov/missions/akatsuki/in-depth/>, retrieved on 28-6-2021

<sup>13</sup><https://solarsystem.nasa.gov/missions/venus-express/in-depth/>, retrieved on 28-6-2021

<sup>14</sup>[https://www.mrcy.com/legacy\\_assets/siteassets/product-datasheets/rfm/5008.21e\\_trrust-stor-vpx-srio\\_ssd-argon2.pdf](https://www.mrcy.com/legacy_assets/siteassets/product-datasheets/rfm/5008.21e_trrust-stor-vpx-srio_ssd-argon2.pdf), retrieved on 18-06-2021

the packets (housekeeping and science) from the DMS processors and it sends the events and the housekeeping data and any other packets requested by ground back.

Furthermore, it consists of a User Interface Controller (UIC) that provides two interfaces to the payloads with high data rate (VIRTIS and VMC), two interfaces with the TFGs of the CDMU and the interfaces to the memory modules.

Then, a file and packet controller controls and manages access to the MMs and also performs the file-management functions.

Last, a DC/DC converter provides the necessary voltages to the SSMM internal electronics.

### Error detection, encoding and decoding

Encoding and decoding the commands and telemetry data is done for two reasons. The first reason is to make sure that no unauthorised person can send commands to Tori or Tsubuyaki and influence their operations. The second reason is to add redundancies to the data rate to make sure that the data reaches Earth without any mistakes.

Redundancies are added by encoding the bits into the QPSK coded Rate 0.80 format. This adds an extra redundant bit to every four bits. Using this format the BER will be reduced to  $10^{-5}$  (Wertz et al., 2011). To put this into perspective, in phase 1 the probe has to send about 15 Mbit per orbit. With this BER, 150 bit out of the 15 Mbit will be corrupted. These corrupted bits can be restored by using interpolation due to most other bits not being corrupted. Decreasing the BER would mean increasing the amount of redundant bits that need to be sent which is not ideal as the transfer times are already quite demanding. Increasing the BER would mean accepting a larger amount of corrupted data which is also not ideal as accurate scientific data is needed to answer the research questions. In the end this data format was chosen due to its low link margin and the low BER.

The RM is supposed to catch any mistakes that are made in the data. Determining the exact probability depends on the chosen RM unit. According to literature a properly implemented watchdog unit has a probability of catching mistakes for 85% (Beningo, 2010). Further testing should confirm whether the RM unit can hold this standard or do even better.

To make the data accessible to the general public the telemetry data will be formatted into Network Common Data Form (NetCDF). This format is used by NASA's Jet Propulsion Laboratory<sup>15</sup>. This data can then easily be interpreted and used in the creation of models.

A final lay out of the data flow within all C&DH components is depicted in Fig. 3.2. This diagram shows the central role of the CDMU. It also shows the workings of the AIU, RTU and the SSMM in relation to the CDMU and each other.

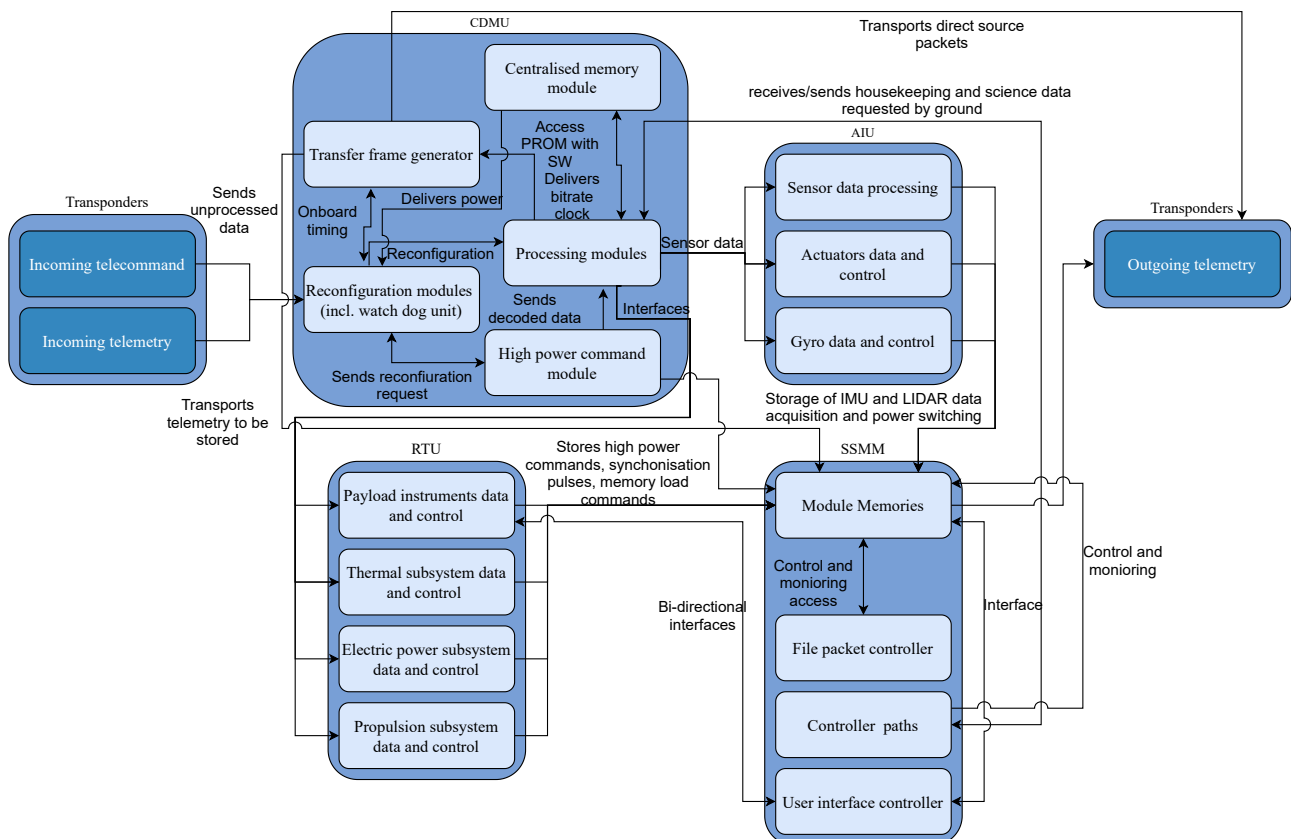


Figure 3.2: Data handling block diagram

<sup>15</sup><https://www.unidata.ucar.edu/software/netcdf/usage.html>, retrieved on 9-6-2021

## Software

Two pieces of software will be used, which includes the DMS and AOCS software. The DMS software is used for the following applications (Sivac and Schirmann, 2007):

- Management of mission timeline and Failure detection, isolation, and recovery (FDIR)
- Management of SSMM
- Management of payload
- Management of remote PMs

The AOCS software is used for the following purposes:

- Management of resources
- Process of sensor outputs and actuator inputs
- Algorithm management of AOCS
- Management of platform
- Management of gyro software
- The ephemerides propagator, which provides the AOCS modes with the spacecraft inertial directions to the Sun.
- Management of the AOCS mode, which manages the transitions between the various AOCS modes.
- Management of the AOCS algorithm, which performs attitude estimation and control, and the flight/trajectory control in each mode.
- Management of the AOCS FDIR, which manages the FDIR at AOCS equipment and AOCS functional levels

Additionally, a Kalman filter was added that makes estimations in an uncertain situation<sup>16</sup>. An example of its application would be for data noise reduction (Leśniak et al., 2009).

An estimation of the amount of software code lines has been made. According to ADSEE, an average of 15K lines are included for the AOCS or GNC is incorporated. Also, the Cassini mission had a total of 32K lines (Zandbergen, 2017). This mission also contained a probe and an orbiter, which is similar to the Kumo mission. Thus, a base of 15K lines has been taken as a base for the AOCS software as well as being the maximum code lines assigned to each section of the software.

A diagram of the software layout is given in Fig. 3.3. Here, the software functions are given in the boxes. Subsequently, these are interconnected with arrows explaining the input and outputs that goes into each function. Additionally, a dotted line stating the amount of approximated software lines is given to approximate the final amount of software lines. This amount is estimated to be 47.5 K lines in total.

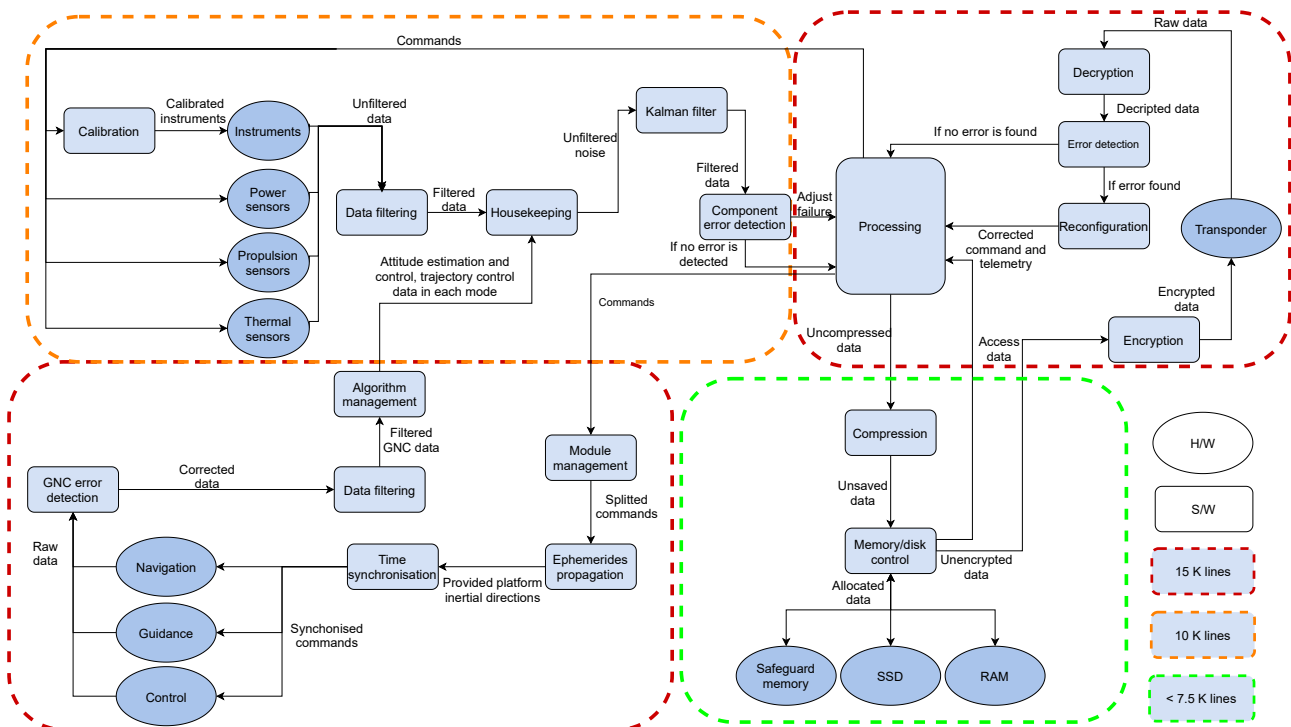
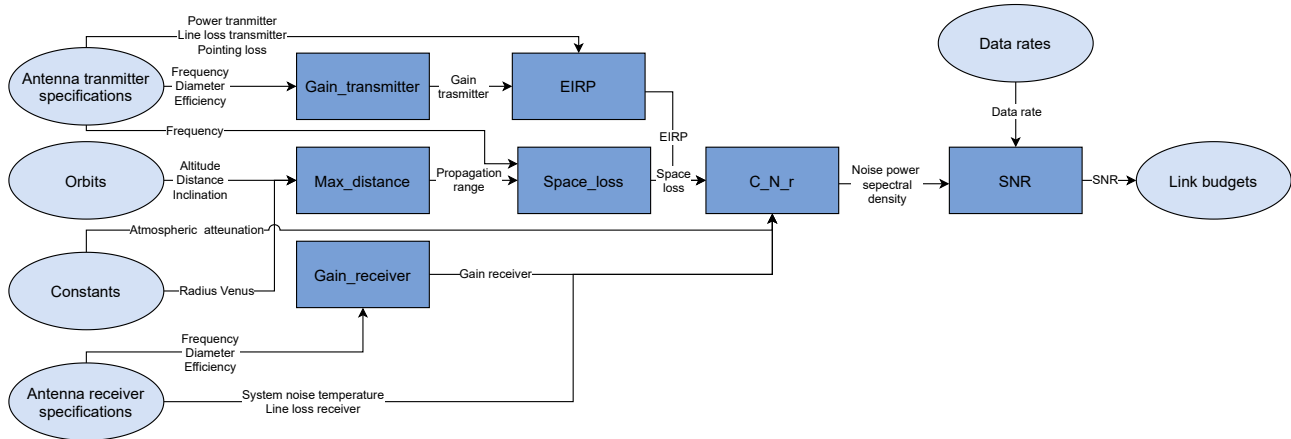


Figure 3.3: Software Diagram

<sup>16</sup><https://www.bzarg.com/p/how-a-kalman-filter-works-in-pictures/>, retrieved on 18-06-2021

**Table 3.6:** Mass and power budget of the telecommunication and command subsystem of the probe

Component	Mass [kg]	Power [W]
HGA	3.15	15
LGA	0.04	10
Transponder	5.4	38
Cables	3	-
Gimbal	7.5	30
C&DH unit	10	34
<b>Total</b>	<b>28.88</b>	<b>127</b>

**Figure 3.4:** Overview of the link budget program

### 3.2.8. Subsystem overview

In this section the individual components of the subsystem are listed with the mass and power budgets. Table 3.6 shows the overview. The mass and the power of the HGA, LGA, Transponders, cables can be found in (Makovsky et al., 2002; Sivac and Schirmann, 2007; Wertz et al., 2011). The gimbal mass and power is provided on the data sheet<sup>17</sup>. To estimate the C&DH unit a similar unit from the Magellan mission was used<sup>18</sup>.

### 3.2.9. Verification and validation

#### Model verification and validation

To create the link budgets a Python program was used. The first iteration of this program was based on an example of SMAD (Wertz et al., 2011). To verify the initial model, it was made sure that it gave the same outcome as the ones denoted in SMAD. The code was then specified for each individual mission link budget. The unit tests can be found in Table 3.7. An overview of the link budget code can be found in Fig. 3.4.

#### Overall subsystem verification and validation

The subsystem uses a lot of off-the-shelf products. This means that the individual objects have already been proven to work under certain desired conditions. However, this does mean that special tests considering the entire system should be devised. These tests should determine how well the subsystem can handle the amount of data needed for the mission. The C&DH unit and the software should be rigorously tested to make sure that it will not fail during the mission.

Other test that should be performed include the antenna deployment test, radiation test to check if the CD&H unit does not get corrupted and a test to check the Resistance of the HGA and the LGA of the probe in the Venusian atmosphere.

### 3.2.10. Risk assessment

This section contains the final risk assessment of the detailed design of Tori's TT&C subsystem. In Table 3.8, the principal risks of the subsystem can be found. The most critical risk was found to be 3a-2, covering the loss in communication between Tori and Tsubuyaki due to equipment failure.

### 3.2.11. Sustainability

The TT&C subsystem mostly uses off-the-shelf products which will decrease the necessity for design and development of the component. However for risk mitigation the subsystem added more components. However, this adds weight to the

<sup>17</sup>[https://www.moog.com/content/dam/moog/literature/Space\\_Defense/spaceliterature/spacecraft\\_mechanisms/moog-type-22-apm-datasheet.pdf](https://www.moog.com/content/dam/moog/literature/Space_Defense/spaceliterature/spacecraft_mechanisms/moog-type-22-apm-datasheet.pdf), retrieved on 22-6-2021

<sup>18</sup><https://magellan.aero/wp-content/uploads/C&DH.pdf>, retrieved on 22-6-2021

**Table 3.7:** Unit tests for the link budgets code

Test	Variables	Expected outcome	Y/I/N
VER-TD-011	<b>Input:</b> $L_{cable}$ <b>Outputs:</b> SNR	Increasing the cable loss of each antenna should decrease the signal to noise ratio of each budget by the twice the amount.	Y
VER-TD-012	<b>Input:</b> $Diameter$ <b>Outputs:</b> Gain, EIRP, SNR	Increasing the diameter of the HGA antennas increases the gain, EIRP and SNR.	Y
VER-TD-013	<b>Input:</b> $Coverage$ <b>Outputs:</b> Gain, EIRP, SNR	Lowering the coverage angle of the LGA antenna will increase the gain, EIRP and SNR.	Y
VER-TD-014	<b>Inputs:</b> $Transmitterpower$ <b>Output:</b> EIRP, SNR	Multiplying the transmitter power of all antennas by ten increases the EIRP and the SNR by 10 dB	Y
VER-TD-015	<b>Inputs:</b> $L_{pointing}$ <b>Output:</b> EIRP, SNR	Increasing the pointing loss of all antenans should decrease the EIRP, SNR	Y
VER-TD-016	<b>Inputs:</b> $\eta_{antenna}$ <b>Output:</b> Gain	Decreasing the efficiency of all HGAs should decrease the antenna gain and thus decrease the SNR.	Y
VER-TD-017	<b>Inputs:</b> $Range$ <b>Output:</b> $L_{space}$	Decreasing the range between the orbit and probe and between the orbiter and Earth should decrease the space loss and increase the SNR.	Y
VER-TD-018	<b>Inputs:</b> $L_{attenuation}$ <b>Output:</b> $SNR$	Increasing the atmospheric attenuation of Earth and Venus will decrease the SNR	Y
VER-TD-019	<b>Inputs:</b> $SNT$ <b>Output:</b> $SNR$	Increasing the system noise temperature of Tori, Tsubuyaki and the GS will decrease the SNR	Y

respective systems.

Sending data at night, would imply more components would have to be operative, needing power. This would increase the battery weight. The antenna and communications are powered by solar energy. The renewable energy source and the reduced mass makes it very sustainable.

The CD&H unit of the subsystem for both the probe and the orbiter will have to be on during the entire mission to ensure that the mission goes according to schedule. This means the unit use a significant amount of power during the mission.

The CD&H unit and the antenna of the orbiter will be on during the interplanetary segment as well as the science segment to send telemetry data back to Earth. However, since the solar panels will be deployed in the interplanetary phase, the components will be operating on solar power completely.

Due to large tracking necessity, the DSN will be used. The DSN antennas are placed in the following countries: Australia, Spain and the United States. These countries have good ratings in the Corruption Index, Human Development Index, Global inequality index and global peace index.

The probe TT&C subsystem is given a “high” (3) score for the launch and interplanetary segments, a “reasonable” (2) score for the Venus operations phase as the components will operate on solar energy. Since the CD&H unit would have to be operative during the eclipse, a large amount of power would be needed. The probe TT&C subsystem will receive a weight of 2, as the telecommunication subsystem will be operative for a large amount of time but will not have a large effect on the sustainability.

To orient Tori and navigate it properly, a GNC subsystem is needed. This subsystem will require tracking which is interrelated with telecommunications. Therefore, this will be the next topic to be discussed below.

### 3.3. Guidance, navigation and control

This section comprises the detailed design of Tori’s GNC subsystem. In Section 3.3.1, the proposed requirements to the subsystem can be found. After that, Section 3.3.2 describes the design process of the attitude determination sensors and Section 3.3.3 shows the design of the tracking system. In the end, the risks and sustainability aspects of the subsystems are discussed in sections 3.3.4 and 3.3.5, respectively.

#### 3.3.1. GNC requirements

During the design, requirements have been created for all elements of the Kumo mission, including for the GNC subsystem. This section presents in Table 3.9 the final requirements for Tori’s GNC subsystem including their status. In this report, the phrasing of the requirements has been tailored to the current architecture of the mission, as it was not known from the beginning of the project that two vehicles, Tori and Tsubuyaki, would be used.

**Table 3.8:** Risk assessment and mitigation

<p><b>3a-1:</b> <i>Loss in communication between Tori and Tsubuyaki due to equipment failure.</i></p> <p><b>Assessment L2S5:</b> With an antenna failure, the transmission of science and telemetry data between Tori and Tsubuyaki would be halted. This is a catastrophic event with a moderate chance of happening.</p> <p><b>Mitigation L2S4:</b> The communication link between the vehicles contains two antennas, a LGA and a HGA (cold redundancy). In case of a single antenna failure, telemetry and science could be still transmitted. Depending on the type of failure, science data may not be entirely retrieved (e.g., if the HGA fails, the budget to send science and telemetry data will not allow complete retrieval of science data).</p>
<p><b>3b-1:</b> <i>Loss in communication between Tori and Tsubuyaki due to software failure.</i></p> <p><b>Assessment L2S4:</b> The telecommunication software could wrongly handle the received and sent data. For example, if the software cannot convert measurements to a digital signal, no science data can be returned to Earth. This type of failure, even though critical, is not very common.</p> <p><b>Mitigation L2S3:</b> In case of software failures, the ground station can contact the mission segments to send fixes for the software.</p>
<p><b>3c-1:</b> <i>The data might be converted wrongly.</i></p> <p><b>Assessment L2S4:</b> The software responsible for data conversion might operate unexpectedly. For example, the software could wrongly convert the measurements to a digital signal. As this would mainly be caused by a software flaw, it has a low likelihood.</p> <p><b>Mitigation L1S4:</b> Because of the low likelihood, extensive verification and validation are enough to guarantee no conversion errors.</p>
<p><b>3d-1:</b> <i>The data storage might erase the data too soon.</i></p> <p><b>Assessment L2S4:</b> If the on-board software deletes the measured data before sending it to the ground station, the mission is brought to a critical position. This type of error is software related, which has a low likelihood.</p> <p><b>Mitigation L1S4:</b> Because of the low likelihood, extensive verification and validation are enough to guarantee data will only be deleted after the system is certain the data has been sent.</p>
<p><b>3e-1:</b> <i>Data may be lost during transmission.</i></p> <p><b>Assessment L2S3:</b> Part of the data could be lost during transmission, leading to critical failure. However, because modern software is robust in correcting data lost during transmissions, this risk has a low likelihood.</p> <p><b>Mitigation L1S3:</b> Because of the low likelihood, extensive verification and validation are enough to guarantee the ground station can interpret the data even with transmission losses.</p>
<p><b>3f-1:</b> <i>Lack of tracking due to obstruction of probe from Earth.</i></p> <p><b>Assessment L3S4:</b> If the probe cannot be tracked, the vehicle might get lost in the Atmosphere. In this situation, no communication between probe and orbiter will be possible, and no data gathered by the probe will be retrieved. The mission, however, would still be able to retrieve the science data of the orbiter. Because of that, instead of catastrophic, this risk is critical to the mission.</p> <p><b>Mitigation L2S3:</b> (1) Two tracking methods are used, where in case of obstruction of probe from Earth the ranging and Doppler method is used. (2) An LGA is in place, which has a high coverage as it can send data in multiple directions.</p>

### 3.3.2. Attitude determination

Tori will be the first controllable aerial vehicle in Venus atmosphere. It will collect science data throughout the ten revolutions around the planet. Therefore, its orientation is needed for proper instruments pointing and flight heading. This section elaborates on the challenges of attitude determination in Venus' atmosphere and on the design of Tori's GNC subsystem.

Inside the Venusian clouds, not all conventional attitude sensors can operate. The cloud's opacity limits the use of optical sensors. Stars will not be visible from the altitudes Tori will be flying; therefore, star trackers are not feasible. The VEGA mission balloons have used sun sensors in the clouds (Quadrelli et al., 2015). However, research is still needed to confirm that this sensor can operate from all altitudes Tori will fly. Magnetometers are also not possible to work on the planet, which lacks a magnetic field. On top of that, the harsh atmosphere environment and the extended mission duration impose a challenge for the components' survival. Because of that, the selection of intrusive and environment exposed components was avoided.

The selection of Tori's sensors covered the GNC requirements, the flight environment constraints and the solutions found by past and proposed missions. Two modern sensing techniques have been considered for relative flight attitude determination: flush air data and laser air data sensing. For both methods, testing is needed to validate the use of those systems in Venus. Flush air data is an intrusive sensing technique, making it more challenging to function in the atmosphere. Therefore, laser data sensing will be used. On top of that, Tori will also contain four Sun sensors and two inertial measurement units (IMUs). Table 3.10 shows, for each sensor, the quantity, mass and power.

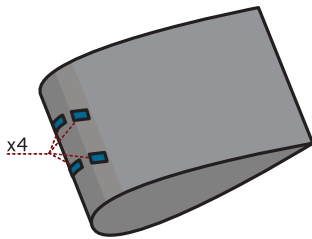
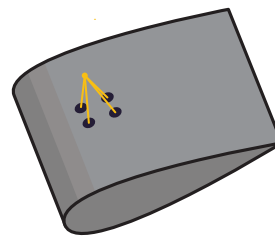
Due to the requirement KUMO-AD-05, the GNC subsystem should be single-failure tolerant. Therefore, the number of components and their positioning is made to guarantee redundancy. Tori will contain four Sun sensors. Technically, two perpendicular sensors could determine the vector pointing from the vehicle to the Sun. However, extra two sensors are added to comply with the redundancy requirement. The configuration of the Sun sensors can be seen in Fig. 3.5. To also include redundancy for the IMU, two units will be used.

**Table 3.9:** Requirements for the GNC subsystem

Identifier	Requirement	Check
KUMO-AD-01	The attitude determination system shall determine the vehicle orientation with a minimum of 5 deg accuracy.	✓
KUMO-AD-05	The attitude control system shall be able to operate with a maximum of 1 actuator failure.	✓
KUMO-GNC-05	Collisions shall be avoided with objects larger than 1 cm <TBC>.	✗
KUMO-GNC-06	Guidance communications shall be prioritised in the downlink and uplink.	✓
KUMO-GNC-10	The ground segment shall be able to override any other instructions to the actuator thrusters throughout the mission.	✓
KUMO-GNC-14	Functional redundancy shall be implemented for the control subsystem.	✓

**Table 3.10:** Tori's attitude and position determination sensors

Component	Quantity [-]	Mass [kg]	Power [W]
IMU	2	4.08	34
Sun sensors	4	0.38	0.25
Laser sensor	4	4.5	17
Pressure sensor	3	0.23	-

**Figure 3.5:** Tori's Sun sensors location**Figure 3.6:** Tori's lasers location

The laser air data sensing is inspired by the National Aerospace Laboratory (NLR) system, successfully tested in flight on Earth. The system contains four lasers focused on a point in the atmosphere. The energy of the laser is backscattered by particles in the air. The Doppler shift in the signal is measured to determine the airspeed vector. NLR has demonstrated the system in various flight conditions, including within clouds (Verbeek and Jentink, 2012). However, as mentioned earlier, testing will be needed to verify and validate the system's operation in Venus. The four lasers will be positioned inside the payload bay, pointing to the same location through a window. The lasers configuration can be seen in Fig. 3.6.

The disadvantage of laser air data sensing is that it does not provide readings of the atmospheric pressure. Therefore, diaphragm pressure sensors will be equipped in Tori's structure. Those sensors are inspired by the ones used by the Pioneer Venus' probes (Seiff, Juergens, and Lepetich, 1980). One could argue that the selection of sensors exposed to the atmosphere conflicts with the argument used to select laser instead of air data sensing. However, in the pressure sensors case, the Pioneer Venus mission has demonstrated the in-situ feasibility.

Two critical conditions were considered when making the strategy for the operation of the sensors. (1) The Sun sensors might be obstructed by the opacity of the clouds during the flight at 55 km. (2) The Sun sensors will not work during 98.2 h of flight in the planet's shadow. In those flight conditions, the IMU will be without one of its sources to correct the bias. The second critical condition was used for the IMU design as it is the longer the probe would fly without the data from Sun sensors. Requirement KUMO-AD-01 establishes that the vehicle's attitude shall be determined with a maximum of 5° accuracy. Together, the maximum accuracy error and the flight duration in shadow imply that an IMU with a minimum  $0.05^\circ \text{ h}^{-1}$  bias stability is required. Based on the required bias stability, an off-the-shelf IMU was selected.

The attitude determination strategy for Tori's will be done as follows. Sun sensors, laser air data, and IMU will operate during the entire flight in daylight. In case of Sun sensor obstruction during the flight at 55 km, the vehicle will be guided by the IMU and the laser air data. When back to 65 km altitude, the Sun sensors will be able again to contribute to the drift correction of the IMU. Furthermore, during the entire flight in the shadow, the IMU and laser air data will be responsible for the vehicle's attitude sensing.

### 3.3.3. Tracking

Several space missions have successfully achieved spacecraft tracking. For the Kumo mission, Tori and Tsubuyaki will be able to be tracked using two techniques. First, the vehicles will be tracked using two-way ranging and doppler measurements. Second, Very long Baseline Interferometry (VLBI) tracking will be used. This section explains how both techniques will be used in the mission.

VLBI is a technique that has been shown feasible by missions in Venus, Saturn and Titan. In Venus, the tracking of the VEGA atmosphere balloons (Quadrelli et al., 2015) and the ESA's Venus Express (VEX) (Duev, D. A. et al., 2012) can be mentioned. The same tracking technique was applied to Cassini while it was orbiting Saturn (Jones et al., 2014) and to the Huygens probe in the atmosphere of Titan (Pogrebenko et al., 2004). Furthermore, NASA has proposed this tracking technique to its Flagship mission concept, which is similar to Kumo as both have an atmospheric probe and orbiter that need to be tracked.

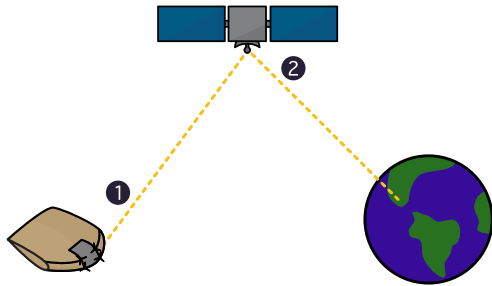


Figure 3.7: Range and doppler tracking

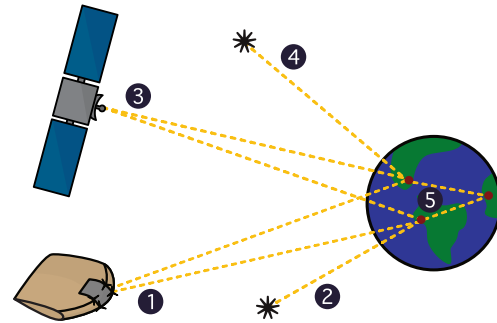


Figure 3.8: VLBI tracking

Ranging measurements will be determined by the time of the round-travel of a range signal. Those measurements will allow the determination of the position between Tsubuyaki-GS and Tori-Tsubuyaki. With the position of the objects determined, doppler tracking is used to obtain the range rate between the vehicles. While ranging is measured by the duration of the signal travel, the doppler shift is measured by the frequency shift due to the vehicle's relative speed (Thornton and Border, 2005a). In Fig. 3.7 the two-way ranging and doppler measurements architecture can be seen. Those measurements will be performed for paths (1) and (2), where Tori sends a signal to Tsubuyaki that sends a signal to Earth. For each of the two paths, the ranging and doppler measurements will be made.

VLBI is a second method that will also track the vehicles by directly measuring reference angles and angle rates. The method will measure the arriving signal of each vehicle and a known source, called a phase-reference calibrator, by a number of ground stations. The phase-reference calibrator has not yet been decided on at this stage of the mission design; however, it is known that a source with a few degrees from each vehicle will allow more accurate measurements. The difference in arrival time of the signal on each different ground stations will determine the angular component of the source of the signal (Thornton and Border, 2005b). In summary, Fig. 3.8 shows how the VLBI tracking of the vehicles will occur. (1) Tori sends a signal to several ground stations on Earth. (2) Tori's phase-reference calibrator is observed by the ground stations. (3) Tsubuyaki sends a signal to several ground stations on Earth. (4) Tsubuyaki's phase-reference calibrator is observed by the ground stations. (5) The signal received by various telescopes - twenty were used for Huygens - are sent to a processing network. For Kumo, the European VLBI network will be used. This network is the same used by VEX and Huygens. Algorithms at the network will use the VLBI, ranging, and Doppler data to determine the probe's position.

A recommendation for a further stage of the mission design is to study the possibility of an additional mission achievement through a VLBI experiment. The experiment involves performing in-beam VLBI observations where a signal from Tori and Tsubuyaki is received by multiple ground stations and used to determine the angle between the two vehicles. This experiment, if successful, aggregates a remarkable achievement to Kumo.

Concerning the accuracy of the measurements, Iess et al. provides a typical accuracy that can be expected from the measurements of the two tracking techniques. The values of expected measurement accuracy can be found in Table 3.11. For the accuracy of the estimated vehicle's position, it is expected that a one-kilometre accuracy can be achieved. This value was determined from the values achieved by the Huygens mission.<sup>19</sup>

Table 3.11: Expected accuracy of tracking measurements

Measurement	Expected accuracy
Doppler	0.1 mm
Range	2 m
VLBI	1 nrad

### 3.3.4. Risk assessment

With the detailed design of Tori's GNC subsystem, a reassessment of the risks is needed. This section elaborates on risks considered in previous reports of the mission. That included removing the risks that are not relevant to the final subsystem configuration, updating the ones that needed more description, and considering the risks introduced by new components

<sup>19</sup>[http://www.esa.int/Science\\_Exploration/Space\\_Science/Cassini-Huygens/Tracking\\_Huygens\\_during\\_its\\_descent](http://www.esa.int/Science_Exploration/Space_Science/Cassini-Huygens/Tracking_Huygens_during_its_descent), retrieved on 15-6-2021

in the design. The final list with the main risks of the subsystem can be seen in Table 3.12, where risk 2b-1, covering the obstruction of optical sensors by cloud opacity, is found to be most critical post-mitigation.

**Table 3.12:** Risk assessment and mitigation

<p><b>2a-1:</b> <i>Failure of attitude determination sensors.</i></p> <p><b>Assessment L4S4:</b> The failure would result in a wrong reading of Tori's attitude, causing undesirable control commands and leading to a critical mission failure.</p> <p><b>Mitigation L2S3:</b> Cold redundancy was added to the subsystem. For example, four Sun sensors are used, allowing single-failure of components. The same principle was used for the configuration design of all sensors.</p>
<p><b>2b-1:</b> <i>Optical sensors obstructed by cloud opacity.</i></p> <p><b>Assessment L3S4:</b> Without the optical sensors, the probe will not be able to correct the IMU drift.</p> <p><b>Mitigation L2S4:</b> (1) The IMU was designed to allow for drift considering worst-case scenario's. (2) When flying at 65 km altitude, the probe will be in an area with lower cloud opacity, which will allow it to use the optical sensors. (3) The advantage of laser data sensor is that it was demonstrated on Earth clouds, which indicates it would be able to function during all flight altitudes. However, the system needs to be validated for the worst cloud opacity the probe will experience at Venus.</p>
<p><b>2c-1:</b> <i>Optical sensors damaged during flight.</i></p> <p><b>Assessment L2S3:</b> Particles may damage the optical sensors of the spacecraft during entry and atmosphere flight. The damage could lead to the inability of bias correction and attitude determination. Even though this event would be severe to the mission, the likelihood of happening is low.</p> <p><b>Mitigation L1S3:</b> Laser air sensing will be positioned inside Tori's structure. They will observe the atmosphere through windows placed in the structure.</p>
<p><b>2d-1:</b> <i>Autonomous navigation system software failure.</i></p> <p><b>Assessment L2S4:</b> Software bugs can occur for distant spacecraft with a limited power budget, certainly given the duration of the mission and the Venusian environment. This risk, however, has a low chance of occurring as on-board software are sufficiently verified and validated.</p> <p><b>Mitigation L2S3:</b> The ground station can send control to remove bugs in the software. However, because communication is not always possible and takes a long time, it has only a slight reduction in risk severity.</p>
<p><b>4a-1:</b> <i>Noise and interference from other sources may reduce guidance accuracy.</i></p> <p><b>Assessment L2S2:</b> The guidance system may be affected by noise from other spacecraft using similar frequencies. The severity is marginal as guidance does not need to be frequent, and the likelihood is low because of the newly developed filtering methods and state-of-art antennae, as well as the quality of research in the field.</p> <p><b>Mitigation L1S2:</b> Tori will have a Kalman filter.</p>

### 3.3.5. Sustainability

The sustainability score of the GNC subsystem is mostly driven by the redundancy of the components needed and the fact that it needs to be turned on most of the mission. Other considerations go into re-use of components from previous missions.

The ensure that the subsystem does not fail, redundant components are added. This however increases the weight of the subsystem, which will negatively affect the sustainability. GNC needs to be turned on most of the time to determine the position of the probe. As this will require a lot of power the system will be less sustainable.

The subsystem uses a lot of off-the-self products meaning that the individual components will not have to be designed and developed which will safes time and resources. The data rate of the subsystem will be small and therefore will not put a strain on the data rate.

In the Earth and interplanetary segment the GNC subsystem will not be used. Meaning that it received a score of "High" (3). The GNC subsystem was marked with a score of "reasonable" (2) for the last segment as the components all work on solar energy but are not perfectly sustainable. The weight of the subsystem compared to the other probe subsystems was deemed to be a 1 as the subsystem only affects the sustainability very little.

GNC as well as many other subsystems will require power. Also, a propulsion system is necessary to perform the necessary manoeuvres that GNC might need to orient and control the aircraft. This will be the next subsystem to be defined.

## 3.4. Power and propulsion design

As will become evident in this section, the designs of the power and propulsion subsystems for the atmospheric probe are coupled. Which is why the subsystems are discussed in the same section. The requirements for both subsystems will be discussed in Section 3.4.1 and Section 3.4.5, after which first the assumptions used are stated in Section 3.4.2 and the design process for the power subsystem and later the design for the propulsion system will be laid out in Section 3.4.3 and Section 3.4.6, respectively. Finally, the verification and validation processes for each of the subsystems are discussed in

Section 3.4.4 and Section 3.4.7, followed by a risk in Section 3.4.8 and sustainability assessment in Section 3.4.9 for both power and propulsion.

### 3.4.1. Power subsystem requirements

The requirements for the power subsystem are given in Table 3.13. They can be categorised under two main categories, these being the performance and endurance of the system. They include requirements for different components of the system, these being distribution, power source and storage unit.

**Table 3.13:** Power subsystem requirements

Identifier	Requirement	Check
KUMO-PW-01	The power system shall be operational for the duration of the mission.	✓
KUMO-PW-02	The primary power source shall generate a nominal power of 78.2 kW at EOL conditions.	✓
KUMO-PW-03	The power system shall be able to provide a peak power of 78.3 kW at EOL conditions.	✓
KUMO-PW-04	The power storage unit shall have a capacity of 4526 J at EOL conditions.	✓
KUMO-PW-05	The power storage unit shall have a specific energy of 15 Wh/kg at EOL conditions.	✓
KUMO-PW-06	The power storage unit shall have an energy density of 7370 Wh/m <sup>3</sup> at EOL conditions.	✓
KUMO-PW-07	The power storage unit shall have a cycle life of at least 8 cycles.	✓
KUMO-PW-08	The power distribution system shall provide continuous power distribution.	✓
KUMO-PW-09	The power distribution cables shall be shielded from temperature differences and the corresponding stresses.	✓
KUMO-PW-10	The power distribution system shall be able to supply power with an efficiency of 90 %.	✓

- KUMO-PW-02 - This value was found based on what the subsystems need in terms of power and with an assumed yearly degradation coefficient of 0.1.
- KUMO-PW-03 - This value was found based on what the subsystems need in terms of power, with telecommunications providing most of the deviation with nominal power, and with an assumed yearly degradation coefficient of 0.1.
- KUMO-PW-04 - This value was found based on the total amount of energy needed to provide the selected subsystems with power at night time.
- KUMO-PW-05 - This value was applied in accordance with the sensitivity analysis as to avoid the total probe mass exceeding 1000 kg .
- KUMO-PW-06 - This value was found based on the total amount of energy needed to provide the selected subsystems with power at night time and an estimation for the size of the battery compartment in the probe.
- KUMO-PW-07 - This value was found based on the times the battery will have to be charged/discharged, with a margin of 50%. These cycles are directly related to amount of eclipse periods and thus the amount of revolutions around the planet.
- KUMO-PW-09 - This value was argued based on need to maximise efficiency to avoid divergence of solar array mass upon iteration as well as to minimise heat generated by energy losses.

### 3.4.2. Power assumptions

Three main assumptions were made for the power subsystem:

- **PW.A.1:** Power usage during daytime is uniform, such that the nominal power is considered to be the same as the peak power.
- **PW.A.2:** The power distribution unit (PDU) does not cause any additional power losses.
- **PW.A.3:** The power flux and solar flux remains constant for a certain altitude.

### 3.4.3. Power design process

To design a power subsystem fitting for the design and mission concept, several potential candidates were proposed, after which a qualitative trade-off was performed to select the most feasible idea. The design options can be categorised under external, internal and hybrid systems, referring to the energy sources used. Mounted and integrated solar arrays, batteries and fuel cells will be discussed. Thermo-electric cells were not considered for a trade-off due to the low TRL of three (National Research Council, 2012). If deemed optimal, some concepts may be assigned with a combination of these.

#### Concepts

1. **Solar arrays** are dependent on an external energy source, the Sun. Not only is this a popular concept to sustain long duration space missions, it also comes with a high TRL and due to the abundance of industry application and information also a lower design risk and increased reliability. Disadvantages to solar cells are their low efficiency, expensive and complex production and their need for additional protection in harsh environments such as the Venus

atmosphere. The integration of the solar arrays is an important factor when considering this concept for the mission. Compared to mounted solar arrays, integrated systems will have lower risks, less need for structural reinforcements, lower volume and lower mass. However, integrated systems will leave less room for instruments and thermal coating and paint. Note that mounted systems will introduce different moments and forces on the structure, complicating the stability of the probe if used. Lastly, solar arrays can be flexible or rigid. Flexible ones will have a lower TRL and will save space. On the other hand, a rigid one would introduce lower risks as it has fewer joints and is less complex.

2. **Batteries** are generally selected for their reliability and energy density as they make use of internal energy sources. However, the use of batteries would generally lead to significant weight and volume increase for long duration missions. It is therefore not particularly interesting as a primary power source. In the function of a secondary power source, however, rechargeable batteries could offer a good solution for eclipse times and peak power requirements.
3. **Thermo-electric cells** are another concept making use of an external energy source, implying the aforementioned benefits. Power is provided by converting temperature differences into energy and by recycling wasted heat energy. It is generally reliable and compact, and efficient with respect to the space it takes up in the vehicle. The very low energy conversion rate and low TRL, however, make the concept significantly less attractive.
4. **Fuel cells** are efficient energy sources with high power density characteristics. If chosen right, some of the converted fuel can be reused, thus decreasing the fuel mass. It still stands, however, that this system would need on-board fuel and accompanying infrastructure. Therefore, an increase in mass and volume is unavoidable. Furthermore, fuel cells are mostly used in missions with a shorter duration (Zabihi and Saafi, 2020).

### Components

Based on the information presented above, solar arrays were chosen to be used in combination with batteries as a secondary energy source. Fuel cells were not preferred due to their additional complexity and mission duration constraints. A part of the dynastat structure will inflate and deflate as temperature changes happen in the atmosphere. Therefore, flexible arrays are needed. As to avoid additional drag and structural mass, the solar arrays will be integrated rather than wing mounted.

As the power subsystem is expected to be a main driver for the total mass of the dynastat, high specific properties are desired for both the battery and the solar cells. Therefore, the battery selected is a lithium ion battery, manufactured by Eagle-Pitcher. Lithium ion has good specific properties and a sufficiently good operating temperature range. Next to that, it is often considered for aerospace applications, therefore displaying proof of concept. The solar arrays will be build around the triple junction flexible GaAs cells, provided by SpectroLab. This is considered the best option as it displays high efficiency and specific power, thus implying limited solar array area and mass. Note that use will be made of maximum power point trackers and bypass diodes to maximise the extraction of power under all conditions the solar arrays are subjected to and to bypass defective solar cells as to not jeopardise the effectiveness and power output of the over coupling modules.

A Power Control Unit (PCU) and a Power Distribution Unit (PDU) will be put in place to guarantee a secure power flow between the solar array and the receiving systems and to control charge and discharge of the battery as well as to distribute power over the probe systems and arrange communication with the OBS (on-board computer).

Finally, the individual solar cells will be covered with oxidised cover glass, CMX 100 AR, to protect the cells from the environment and will be supported by a 1050 Aluminium substrate (Li et al., 2021), chosen for its good thermal properties and high tensile strength. This will be important since the array will be divided in separated modules on the inflatable part of the probe that will need to limit the deformation of the solar cells.

**Table 3.14:** Lithium ion battery specifications<sup>20</sup>

Characteristic	Value	Unit
Operating temperature range, $T_{op}$	0 – 85	°C
Depth of discharge, $DOD$	0.9	-
Energy transfer efficiency, $\eta_{BAT}$	0.82	-
Specific energy, $E_{sp, BAT}$	113.1	Wh l <sup>-1</sup>
Energy density, $E_{\delta, BAT}$	343	Wh kg <sup>-1</sup>

**Table 3.15:** Triple junction GaAs solar cell specifications<sup>21</sup>

Characteristic	Value	Unit
Average angle of incidence, $i$	30	°
Solar cell efficiency, $\mu$	0.3	-
Inherent degradation, $I_d$ (Wertz et al., 2011)	0.77	-
Yearly degradation, $C_d$	0.1	-
Area density, $\rho_{sp}$	1.18	kg m <sup>-2</sup>

### Sizing

First, the sizing of the battery will be considered. As the battery is selected as a secondary power source, its main function will be to provide power during eclipse time, with the secondary function being to support peak power impulses. As propulsion is the driving source of power consumption, however, power usage is expected to be quite uniform. Therefore, the requirement for peak power is considered to be the same as average daytime power at the design altitude of 65 km. Another assumption is that only GNC components and the on-board computer (OBC) will operate at nighttime. The energy

<sup>20</sup><https://www.eaglepitcher.com/sites/default/files/LP33333.pdf>, retrieved on 4-06-2021

<sup>21</sup>[https://www.spectrolab.com/photovoltaics/UTJ-CIC\\_Data\\_Sheet.pdf](https://www.spectrolab.com/photovoltaics/UTJ-CIC_Data_Sheet.pdf), retrieved on 8-06-2021

required at night is thus given by Eq. (3.1). Finally, using the battery characteristics stated in Table 3.14, the weight volume of the battery are thus provided by Eq. (3.2) and 3.3:

$$E_{req} = \sum_i \frac{P_{i,e} t_{i,e}}{\eta_{BAT} DOD} \quad (3.1)$$

$$W_{BAT} = \frac{E_{req}}{E_{\delta,BAT}} \quad (3.2)$$

$$V_{BAT} = \frac{E_{req}}{E_{sp,BAT}} \quad (3.3)$$

where  $E_{req}$  is the required energy,  $P_{i,e}$  the power consumed by a certain subsystem component in eclipse,  $t_{i,e}$  the duration of the consumption per rotation in eclipse. Note that the depth of discharge is relatively high due to the low number of cycles the battery will have to perform. Note that due to the long time spend in eclipse, it is impossible to size the battery such that it can provide the high power required for propulsion without driving up the mass to an unfeasible extent. For similar reasons, no telecommunications or scientific payload operations will be performed at nighttime, meaning that the battery mass comes solely from the power needed to sustain GNC instruments and the on-board computer. As the battery is rechargeable, the solar array will have to provide to support operations in day time as well as the necessary power to charge the battery in accordance with the energy that it requires. This relation is given by:

$$P_{req,BOL} = \frac{\sum_i P_{i,d} t_{i,d} + \sum_i P_{i,e} t_{i,e}}{t_d \cos i} \quad (3.4)$$

where  $P_{i,d}$  the power consumed by a certain subsystem component in daytime,  $t_{i,d}$  the duration of the consumption per rotation in daytime. This, however, only leads to the power required at BOL (begin of life). To find the power needed at EOL (end of life), yearly degradation factors have to be taken into account, the power needed at EOL is then found accordingly:

$$L_d = (1 - C_d)^{t_{mission}} \quad (3.5)$$

$$P_{req,EOL} = \frac{P_{req,BOL}}{L_d} \quad (3.6)$$

where  $C_d$  is the yearly degradation coefficient, given in Table 3.15.

Although the AM0 (exoatmospheric solar spectrum) at Venus can be assumed identical to the AM0 in Earth orbit, the same can not be said for the solar spectrum in the Venusian atmosphere. It can be observed that the spectral intensity, which offers a relation between atmospheric and exoatmospheric conditions, differs between different wavelengths of the solar spectrum and decreases with altitude. This is an important given, as for a triple junction solar cell, each layer covers a different part of the solar spectrum. This means that one of these layers will pose a limiting condition to the cell, thus decreasing the overall efficiency of the cell. Taking into account this effect on the triple junction GaAs solar cell, as well as temperature and altitude effects on voltage and current flow, an overview can be provided for the power output of these cells per unit of area (G. Landis and Haag, 2013). These values are stated in Table 3.15. Note that this is not to be interpreted as solar flux, but rather as the resulting power per unit area when taking into account solar flux, inherent degradation and the effective cell efficiencies in the Venusian atmosphere. Finally, by relating EOL power to this power per unit area relation for the condition of 65 km altitude, as prescribed by the mission planning, and plugging in the value for the area density of the assembly, the final area and weight of the solar array are found:

$$S_{SA} = \frac{P_{req,EOL}}{S_{i,Venus,65}} \quad (3.7)$$

$$W_{SA} = S_{SA} \rho_{sp} \quad (3.8)$$

where  $S_{i,Venus,65}$  is the power flux in the Venusian atmosphere at 65 km altitude and  $\rho_{sp}$  mass of the solar cell assembly per unit of area. A summary of the final power subsystem design for the atmospheric probe is given in Table 3.16, where it can be found that the requirements set in Section 3.4.5 were fulfilled. Values on mass, volume, efficiency and product specific characteristics are stated, as well as recommended suppliers.

### Design overview

The final characteristics for the probe's power subsystem are given in Table 3.16. From this, it can be derived that the total mass, found by combining all components that make up the subsystem, comes down to 225.8 kg.

**Table 3.16:** Power system summary: constituents

Item	Brand	Specifications	Efficiency
Solar arrays	TJ GaAs by Spectrolab	Mass: 123.2 kg; Area: 104.4 m <sup>2</sup>	0.3
Batteries	Lithium ion by Eagle Pitcher	Mass: 40 kg; Volume: 0.0132 m <sup>3</sup> ; Energy density: 343 J kg <sup>-1</sup> ; Specific energy: 113.1 J l <sup>-1</sup>	0.85
Substrate layer	1050 Aluminium	Mass: 26.1 kg	-
PCDU	Thales	Mass: 36.5 kg	0.97

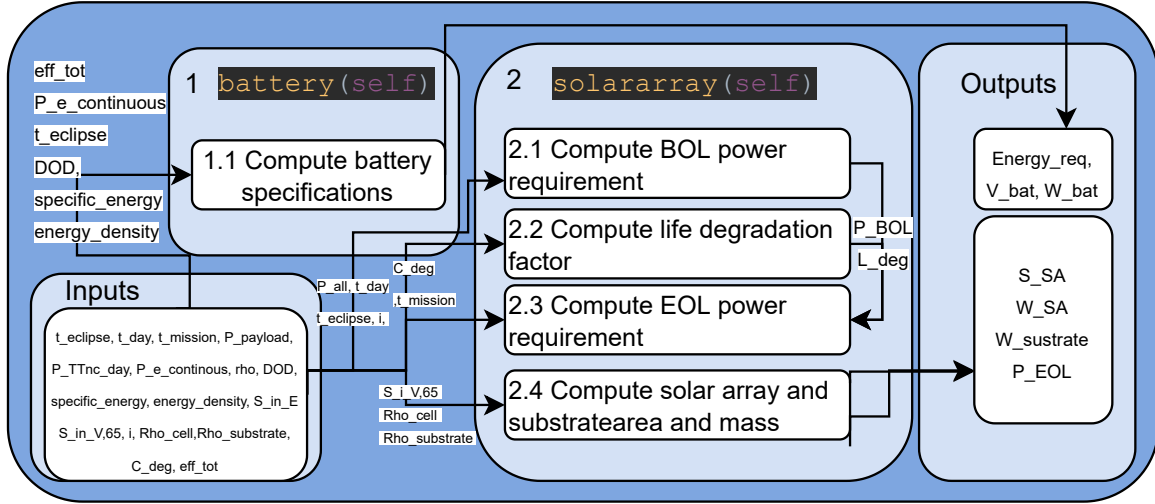


**Figure 3.9:** Flowchart of the power code

**Table 3.17:** Unit verification of power for the probe

Test	Variables	Expected outcome	Verified
VER-POW-U111	<b>Input:</b> $DOD, \eta_{BAT}$ <b>Outputs:</b> $E_{req}, V_{BAT}, W_{BAT}$	Multiplying either of the inputs by a factor of 5 should lead to a decrease of the output values by the same factor of 5. Setting either of the inputs to zero should lead to a division by zero error and thus divergence of the output values.	✓
VER-POW-U112	<b>Inputs:</b> $t_e$ <b>Outputs:</b> $E_{req}, V_{BAT}, W_{BAT}$	$5 * t_e$ , should lead to an increase of the output values by the same factor of 5. $t_e = 0$ , should lead to the output values also taking on the same value of zero	✓
VER-POW-U113	<b>Inputs:</b> $E_{\delta, BAT}$ <b>Outputs:</b> $W_{BAT}$	$5 * E_{\delta, BAT}$ , should lead to a decrease of the output value by the same factor of 5. $E_{\delta, BAT} = 0$ , should lead to a division by zero error and thus divergence of the output value.	✓
VER-POW-U114	<b>Inputs:</b> $E_{sp, BAT}$ <b>Outputs:</b> $V_{BAT}$	$5 * E_{sp, BAT}$ , should lead to a decrease of the output value by the same factor of 5. $E_{sp, BAT} = 0$ , should lead to a division by zero error and thus divergence of the output value.	✓
VER-POW-S21	<b>Input:</b> Incidence angle $i$ <b>Outputs:</b> $P_{req, BOL}, P_{req, EOL}, W_{SA}, S_{SA}$	$i / 5$ , should lead to an increase of the output values. $i = 90^\circ$ , should lead to a division by zero error and thus divergence of the output values.	✓
VER-POW-U241	<b>Input:</b> $S_{I, Venus}$ <b>Outputs:</b> $W_{SA}, S_{SA}$	$5 * S_{I, Venus}$ , should lead to a decrease of the output values by the same factor of 5. $S_{I, Venus} = 0$ , should lead to a division by zero error and thus divergence of the output values.	✓
VER-POW-U242	<b>Input:</b> $\rho_{sp}$ <b>Outputs:</b> $W_{SA}$	$5 * \rho_{sp}$ , should lead to an increase of the output value by the same factor of 5. $S_{I, Venus} = 0$ , should lead to the output taking on the same value of zero.	✓
VER-POW-S22	<b>Input:</b> $C_d, t_{mission}$ <b>Outputs:</b> $P_{req, BOL}, P_{req, EOL}, W_{SA}, S_{SA}$	Multiplying either of the inputs by a factor of 5 should lead to an increase of the output values.	✓

**Table 3.18:** Additional propulsion subsystem requirements

Identifier	Requirement	Check
KUMO-PROP-01	The propulsion system shall have an overall efficiency of 0.45.	✓
KUMO-PROP-02	The propulsion system shall comply with the launcher dimensional constraints.	✓
KUMO-PROP-03	The propulsion system shall be able to operate at a thrust level of 770N.	✓
KUMO-PROP-04	The propulsion system shall rely on electrical energy.	✓
KUMO-PROP-05	The propulsion system shall be able to provide differential thrusts when necessary.	✓

### 3.4.4. Verification of power codes

The power computations were verified by testing the units as well as systems presented in Fig. 3.9. S refers to system tests while U is unit tests. A test ID of VER-POW-U111 means that the test is the first unit test which is performed on block indexed 1.1. The unit tests are listed in Table 3.17.

Finally, the assumptions stated in Section 3.4.2 were verified. They were verified either by code, or by using literature sources.

- **PW.A.1:** This assumption was justified by performing a sensitivity analysis. Interchanging the peak power values with the nominal power values required for the operations of the probe led to an effective difference of 0.2% for the total solar array area.
- **PW.A.2:** This assumption was set because the PDU at the time of design was not yet selected and its efficiency deemed negligible. For given PDU, efficiencies of 99% are recorded. Performing a sensitivity analysis on the design with inclusion of the PDU efficiency led to an effective difference of 1.2% for the total solar array area.
- **PW.A.3:** Reviewing literature on the fluctuation of solar flux, no large fluctuations were reported (G. Landis and Haag, 2013). On top of that, the composition and density of the cloud layers in the Venusian atmosphere were reported to be fairly uniform, thus reducing the probability of considerable fluctuations in solar flux (Titov et al., 2012).

### 3.4.5. Propulsion requirements

Throughout the course of the design, the subsystem requirements for propulsion subsystem were revisited. The design was tailored in a way that the results clarify the unknowns in the requirements as well as demonstrating that the final design is in line with the performance and safety requirements. In Table 3.18, the revised propulsion subsystem requirements can be found. Note that, due to the uncertainties on the probe design and mission scope, in the beginning of the project, the team came up with propulsion requirements for the orbiter only. Therefore, additional requirements have been added to guide the design of Tori.

### 3.4.6. Propulsion design process

The propulsion subsystem is the main mass-driving subsystem with the highest power consumption overall. It is composed of propellers, a gearbox and a lightweight electrical motor. Making sure that the probe can propel with the lowest possible power is of utmost importance as it will decrease the amount of solar arrays needed and will decrease the total mass. The power required to propel is determined from the equations of motion and the cruise velocity of the probe. The subsystem was designed to ensure that the power required is minimised, propulsive efficiency is the highest and the propellers are fitting the launcher dimensional constraints. This section will elaborate upon the subsystem trade-offs that were done to ensure the above-mentioned attributes were achieved.

#### Propeller sizing and placement

The propellers were sized to deliver the power required to fly. The power requirement was computed using:

$$P_r = (P_{r,sustain} + P_{r,climb})SF = \frac{1}{2}\rho V^3 S^2 C_D + mg_V(1 - BR)ROC \quad (3.9)$$

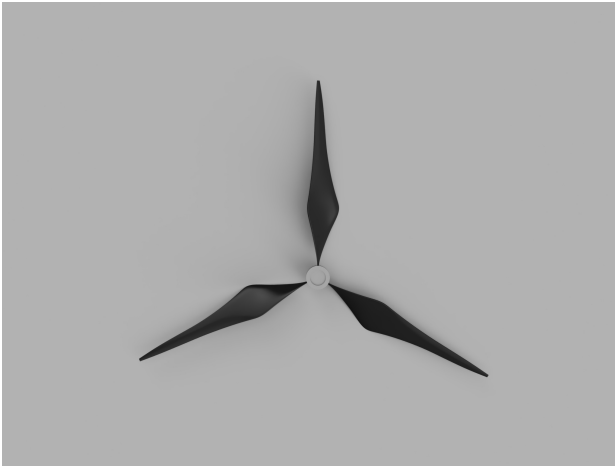
The condition at which power required is calculated was at 65 km altitude, right after the climb ends, with an rate of climb (ROC) of  $4 \text{ m s}^{-1}$ . This point in the flight trajectory was set as the limiting condition for the design, as the power required is maximised. A safety factor of 1.1 was used to account for any unpredicted inefficiencies in the system that could lead to an increase in required power. In the end, the power that the propellers need to provide was calculated to be 35.5 kW.

Once the required power is known, an iterative process was run to find the optimal rotations per minute (RPM) and diameter combination that is able to provide the required amount of power. The optimal RPM was found to be 1600 while the diameter is 2 m. The higher the diameter the better it is for the efficiency. However, due to launcher dimensional constraints 2 m was set to be the maximum. Then, the propellers were sized in detail using a propeller design tool called Javaprop<sup>22</sup>, which is a straightforward tool for designing and analysing propellers and wind turbines. It can be used in

<sup>22</sup><https://www.mh-aerotoools.de/airfoils/javaprop.htm>, retrieved on 22-06-2021

**Table 3.19:** Javaprop assumptions

Item	Effect
Mach number at the tip of the propellers are optimised to be lower than 0.85. <sup>24</sup>	The propeller tips can reach supersonic speeds at greater speeds, resulting in a shock wave and limited propulsive efficiency as the flow around the propeller blade is split.
The tool works best for propellers with low number of blades (<15) as is the case for Tori <sup>25</sup> .	There is no significant interaction between the blades due to overlap.
The underlying blade-element-momentum theory is only valid when compressible flow effects are minimal and largely two-dimensional. <sup>26</sup>	The optimised design will have no winglets or sharply curved blades. In reality, this may be needed.

**Figure 3.10:** Top view of the propeller in CATIA**Figure 3.11:** Propeller placement

both aviation and maritime applications within its limits. The traditional blade element design and analysis methodologies that have been adopted are based on a combination of two-dimensional airfoil properties and momentum considerations. Detailed information on the underlying theory of the software can be found in the References section of the Manual.<sup>23</sup> The design considerations of Javaprop are presented in Table 3.19. Initially, this consideration led to the decision that KUMO-PROP-01 has been set to 45% efficiency. In the end, the propellers have a maximum propulsive efficiency of 0.56 for an advance ratio of 0.487 which satisfies the requirement. Furthermore, each four of them produces 192.1 N of thrust which satisfies KUMO-PROP-03. Note that the low propulsive efficiency was expected due to the low cruise velocity of Tori and atmospheric conditions of Venus.

The number of blades was chosen to be three to minimise propeller-caused vibrations and have higher thrust levels. More blades were not utilised, since they introduce additional mass to the structure and decrease the efficiency. Additionally, carbon-fibre composite material will be used to minimise the mass of the propellers as it is strong enough to withstand the bending stresses. The rigid section of the probe was decided to be equipped with four propellers. This means that there will be four propellers and four electrical motors powering them in total. The propellers will be placed into the four corners using an extension to ensure that the air leaving the propeller does not interfere a lot with the rigid structure, hence, propulsive efficiency is improved. This is done to ensure that both KUMO-PROP-01 and KUMO-PROP-05 are fulfilled. To fit the propellers into the launcher the blades and the extensions will be folded inwards. Furthermore, four propellers allow for sustained flight under certain failure modes such as losing a motor. If one of the propellers stops working, the probe can still be stabilised with the help of other propellers and control surfaces. The position of propellers with respect to the rigid structure is visualised in Fig. 3.11. Furthermore, as the motors are not operating at maximum power, when differential thrust is needed, some of the motors can be operated at a higher power input and hence control the probe.

### Motor selection and operation

Next to the propellers and the electrical motors, gearboxes will be utilised in order to transfer the optimal RPM and torque combination to the propellers. For maximised motor efficiency, electric motors run at higher RPMs than the propellers can handle. Thus a gearbox is unavoidable. Due to the high power requirement, a high torque was needed. Hence, a high torque motor from Alva Industries, HT250 was picked. This motor can provide a maximum continuous torque of 35.4 Nm. Assuming a gearbox efficiency of 0.9, each propeller needs to provide 9.9 kW of power. Using  $P = RPM \cdot \frac{2\pi}{60} \cdot T$ , (T stands for torque), the motor should operate at an RPM of 2668. This value is below the maximum permissible speed

<sup>23</sup><https://www.mh-aerotoools.de/airfoils/javaprop.htm>, retrieved on 22-06-2021

<sup>26</sup><https://www.mh-aerotoools.de/airfoils/java/JavaProp20Users20Guide.pdf>, retrieved 22-06-2021

**Table 3.20:** Propulsion system summary: constituents

Item	Brand	Specifications	Efficiency
Four electrical motors	Alva HT250	RPM: 2668, T: 35.4Nm , Mass=17.9kg	0.90
Propellers	Self-made	Material: Carbon-fiber composite RPM: 1600, T: 52.93Nm, thrust: 192.1N, blade count: 3, Mass: 52kg, $c_p = 0.0701$ , $c_t = 0.0809$ , pitch: 1.49m	0.56
Gearbox	Off-the-shelf	Mass is expected to be lower than 10-12 kilograms. Transmission ratio of around 0.6 ( $\frac{1600}{2668}$ ) is ideal	0.90

of the motor, which is 3500 rpm, meaning that the motor will not wear out easily. For this configuration a motor efficiency of 90% was assumed. The summary of the propulsion subsystem components can be found in Table 3.20, which includes the proposed manufacturers, components specifications and efficiencies.

**Figure 3.12:** Alva HT250 motor

### 3.4.7. Verification and validation of propulsion

Verification of Javaprop was done by running code verification, as well as calculation verification tests. This was done as there was limited information on the verification of the software and algorithm. To summarise the design, first, an embedded Javaprop algorithm as provided by Dr Hepperle<sup>27</sup>, has been developed further to detect the most efficient thrust (highest eta), RPM and diameter combination. Following that, Javaprop software was run using these values to create an optimal propeller geometry that complies with the assumptions presented in Table 3.20. A calculation verification process was executed to check the reliability of the computations, using the maximum theoretical efficiency of a propeller. Due to lack of time, a full scale analytical model was not developed. However, literature was utilised to come up with an expression for the maximum theoretical propulsive efficiency which is shown in Eq. (3.10). This relationship was used to predict the outcome of some verification tests as well as to compare the final efficiency value that Javaprop calculated to theory. The verification tests are listed in Table 3.21.

$$\eta = \frac{2}{1 + \sqrt{1 + \frac{Th}{\frac{1}{8}\rho\pi D^2 V^2}}} \quad (3.10)$$

The computational processes of propeller design have been illustrated in Fig. 3.13.

#### Validation of Javaprop and power computations

Javaprop has been validated<sup>28</sup>. The software has been documented to correspond well to tests. However, due to time constraints, the validation of power subsystem computations was not possible. As a future suggestion, solar flux measurements from future missions can be monitored to compare them to the solar flux simulation used in Kumo's power computations. Furthermore, small-scale testing will be done in the latter stages of the mission to validate the design further.

### 3.4.8. Risk assessment

The technical risks for the probe power and propulsion subsections are given in Table 3.22 and 3.23, respectively. This includes the ratings given to each risk, as well as a mitigation strategy to each. From this it was concluded that the most critical risks for the atmospheric probe mission segment are risk 8f-1, related to electrical failures lead to inoperative electrical systems, for the power subsystem and risk 9a-1, related to an insufficient amount of power for propulsion operations, for the propulsion subsystem post mitigation.

<sup>27</sup><https://www.mh-aerotoools.de/airfoils/javaprop.htm>, retrieved on 22-06-2021

<sup>28</sup><https://www.mh-aerotoools.de/airfoils/javaprop.htm>, retrieved on 22-06-2021

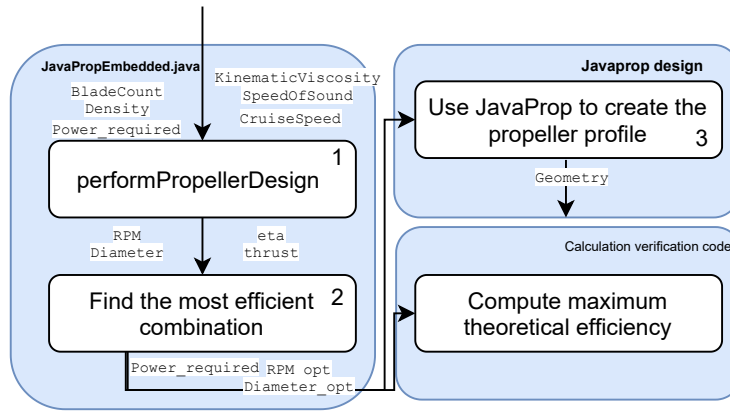


Figure 3.13: Flowchart showing propulsion subsystem computations

Table 3.21: Unit verification of the probe propulsion code

Test	Variables	Expected outcome	Verified
VER-PROP-011	<b>Input:</b> <i>Diameter</i> <b>Outputs:</b> <i>eta</i>	Diameter will be doubled. This should cause a increase in the efficiency as Eq. (3.10) suggests.	✓
VER-PROP-012	<b>Input:</b> <i>Density</i> <b>Outputs:</b> <i>eta</i>	Setting density to 0 should give undefined efficiency as the power required will be 0 and the division will diverge to infinity. This is further backed by Eq. (3.10).	✓
VER-PROP-021	<b>Input:</b> <i>RPM</i> <b>Outputs:</b> <i>eta</i>	Overwriting RPM to a higher value should increase the efficiency of the propeller as there will be amplified blade interference effects.	✓
VER-PROP-022	<b>Inputs:</b> <i>CruiseSpeed</i> <b>Output:</b> <i>M</i>	The tip Mach number of the optimum combination should be lower than 0.8. For the computation speed of sound at Venus is used.	✓
VER-PROP-024	<b>Inputs:</b> <i>RPM, Torque</i> <b>Output:</b> <i>P<sub>a</sub></i>	RPM times torque should give the power that the propeller is providing.	✓
VER-PROP-025	<b>Inputs:</b> <i>P<sub>r</sub>, P<sub>a</sub></i> <b>Output:</b> <i>eta</i>	Power required divided by power available (= <i>RPM · Torque</i> ) should give the efficiency.	✓
VER-PROP-CV-1	<b>Inputs:</b> <i>P<sub>r</sub></i> <b>Output:</b> <i>eta</i>	The theoretical maximum should be higher than the efficiency that Javaprop calculates but should be within ±20% of the calculated value.	✓

Table 3.22: Table showing possible risks for the power subsystem, their severity and likelihood

**8a-1 Partial failure of the solar arrays.**

**Assessment L2S3 :** Partial loss of the primary power, the solar arrays, source due to either mechanical or electrical failure would reduce the available peak and average power and thus have a noticeable impact on the operations of the probe. The likelihood is considered low as use is made of systems that have proven successful in the past.

**Mitigation L1S2 :** (1) A five percent margin in the design as a contingency would reduce the impact of partial power loss. (2) Choice of a reliable system, cells that are typically used in aerospace applications. (3) MPPT and bypass diodes limit the power loss in case of partial failure of the solar array. (4) In case of power shortage, priority is given to payload and a lower altitude is chosen to save power.

**8b-1 Full failure of the solar arrays.**

**Assessment L1S4 :** Complete loss of the primary power source due to either mechanical or electrical failure would reduce the available power to the extent that it could significantly impact the mission as only the secondary power source, the battery, is left. The likelihood is considered very low, as use is made of systems that have proven successful in the past.

**Mitigation L1S3 :** (1) Choice of a reliable system, cells that are typically used in aerospace applications. (2) The mission plan will be altered and only measurements will be taken at 55 km, where there is full dependency on buoyancy. (3) Subsystems e.g., thermal control have limited active applications.

**8c-1 Failure of the rechargeable battery.**

**Assessment L2S4 :** Complete loss of the secondary power source due to either mechanical or electrical failure would reduce the power available at night and peak power at all times, which could jeopardise some of the mission operations. The likelihood is considered low, as use is made of systems that have proven successful in the past.

**Mitigation L1S2 :** (1) The average cycle life of the chosen battery is well above the required amount of cycles. (2) The on-board computer will contain a low power mode with reduced functionality to save power at nighttime.

**Table 3.23:** Table showing possible risks for the propulsion subsystem, their severity and likelihood

<p><b>8d-1</b> <i>Inability to provide the necessary EOL power.</i></p> <p><b>Assessment L3S3 :</b> Unexpected component degradation or wrong estimations of either the available power or the required power could lead to insufficient power at EOL conditions. Despite having a lot of literature, some uncertainties can not be considered, thus increasing the likelihood.</p> <p><b>Mitigation L2S3 :</b> (1) A five percent margin in the design as a contingency would reduce the impact of partial power loss. (2) At EOL, power usage by the payload and linked subsystems is reduced as only repeat measurements are taken. (3) In case of power shortage, priority is given to payload and a lower altitude is chosen to save power.</p>
<p><b>8e-1</b> <i>Degradation of the electric components in the atmosphere.</i></p> <p><b>Assessment L3S4 :</b> Due to the hostile atmosphere of Venus, external systems could experience forms of degradation, e.g., corrosion. This could jeopardise mission operations. Although design should prevent this, there is still a probability that this will occur as it is a long-duration mission.</p> <p><b>Mitigation L2S4 :</b> (1) The internal systems are shielded from the environment by the material. (2) Exposed components are treated with chemicals or protected with cover glass.</p>
<p><b>8f-1</b> <i>Electrical failures lead to inoperative electrical systems.</i></p> <p><b>Assessment L2S5 :</b> The failure of electrical systems due to, e.g., short circuits can lead to loss of mission equipment or essential systems and therefore failure of the mission. An efficient platform should decrease the probability of occurrence.</p> <p><b>Mitigation L1S5 :</b> (1) A protective insulation layer should help to avoid unwanted contact between cables, electrical losses and mechanical stresses. (2) A PCDU will help regulate the electric flow between systems.</p>
<p><b>9a-1</b> <i>Insufficient amount of power for propulsion operations.</i></p> <p><b>Assessment L2S4 :</b> Unforeseen manoeuvres or wrong estimations of power usage could lead to there not being enough power available to perform all operations. Despite having a lot of literature, some uncertainties cannot be considered, thus increasing the likelihood.</p> <p><b>Mitigation L2S3 :</b> (1) A five percent margin in the design as a contingency would reduce the impact of partial power loss. (2) In case of power shortage, priority is given to payload and a lower altitude is chosen to save power.</p>
<p><b>9b-1</b> <i>Failure of a propeller or motor.</i></p> <p><b>Assessment L2S4 :</b> A propeller and motor could break down and therefore reduce the propulsion and stabilisation capabilities of the probe. This could lead to an alteration of the mission capabilities and would thus be a critical failure. Due to the choice and analysis of proven components, the probability is deemed low.</p> <p><b>Mitigation L1S2 :</b> (1) In case of power shortage, priority is given to payload and a lower altitude is chosen to save power. (2) Four propellers/motors are used at below their maximum capabilities as a means of hot redundancy.</p>
<p><b>9c-1</b> <i>Leakage of lighter-than-air gas tanks.</i></p> <p><b>Assessment L2S4 :</b> Leakage of the lighter than air gas could interfere with the measurement of these gases in the atmosphere and to a decrease in lift capabilities, which could have a critical impact to the mission. The fuel tanks are, however, specifically designed to hold these gases, thus implying a low likelihood.</p> <p><b>Mitigation L1S2 :</b> (1) Splitting the probe in compartments reduces the effect of a leakage.</p>

### 3.4.9. Sustainability

This subsection briefly explains the sustainability of power and propulsion subsystems for Tori. The propulsion subsystem is the most power-consuming as it has to deliver sufficient power to make Tori propel in the atmosphere. The propulsion system should be optimised so that the total mass of the probe decreases. This way, fuel reliance to deploy Tori to the atmosphere will diminish, making a power-efficient and sustainable propulsion subsystem of utmost importance to the mission. Furthermore, the power subsystem, whose design is highly dependent on the propulsive power requirement, should also be designed to execute the power conversions with maximum efficiency and minimum reliance on toxic chemicals. Hence, power and propulsion subsystems were given a weight of four, meaning that it has a noticeable contribution to sustainability among other subsystems.

The Earth phase, which comprises the manufacturing process, waste processing, and transportation to the launch site, is the first sustainability evaluation process of power and propulsion. The selected components of the subsystems will be examined for this purpose. The interplanetary phase includes the transfer to Venus. Finally, the Venus phase includes the scientific mission that takes place in the orbit and atmosphere of Venus. Ideally, all three phases will be addressed and scored for relevant subsystem components in order to come up with a final mark for sustainability. If the component is not relevant for a mission phase, then the average score will be calculated for the existing phases.

- **Triple junction flexible GaAs cells:** Gallium arsenide is a compound that includes both gallium and arsenic. Gallium has been linked to health complications in the past. Arsenic, a deadly chemical and a carcinogen, has been discovered to be stable in this combination, meaning that it does not break down. This indicates that it does not put people who are exposed to it in danger. While safety is not a serious concern, the manufacturing of these solar cells has environmental downsides linked to the usage of caustic chemicals. The manufacturing of other power options

also involves chemicals; hence, it is hard to replace solar cells with more sustainable alternatives. Therefore, the solar cells were scored to be low in the sustainability of the Earth phase, receiving a score of (2).

- **Lithium ion batteries:** The lithium ion batteries that Tori will use can be manufactured using recycled battery components. Therefore, a score of (2) will be given for the Earth phase. Furthermore, lithium ion batteries were preferred over fuel cells which require the storage of on-board fuel storage. Fuel cells are not only less efficient in terms of the mass budget but also pose serious threats to the atmospheric composition of Venus. A potential overheating of the fuel can end up causing explosions which can damage the valuable traces in the atmosphere. Therefore, the usage of batteries is considered highly sustainable for the Venus phase, receiving a score of (3).
- **Carbon fibre composite propellers:** Carbon fibres are energy-intensive to produce, meaning that they can significantly release greenhouse gasses if produced in mass scales. Regardless, it is hard to compare the total emissions to substitute materials since the mass reduction also decreases the carbon footprint of its transportation. Since it is difficult to replace it with more sustainable alternatives, a total score of (1) is given for the Earth phase. For Tori, carbon fibre usage allows a considerable reduction in the total mass, which means less structural mass and less fuel used during the interplanetary phase. As the mission is mass constrained, no alternative is suitable to the mission and more sustainable at the same time. Hence, the interplanetary phase receives a “high” score of (3).
- **Electrical motor:** The motors that will be used are reasonably small and easy to produce. They do not have high transportation costs nor energy-intensive production techniques. Hence a score of (3) is given for the Earth phase. For the Venus phase, the motors will rely on the energy extracted via the solar arrays. The reliance on solar power means that the motor will not release any toxic gases into the atmosphere. Therefore, a score of (3) is given for the Venus phase.

All subsystems will have to be protected to the harsh thermal conditions in the Venusian atmosphere. This will be performed by the thermal control subsystem, which will be discussed below.

## 3.5. Thermal control

Being an atmospheric probe, Tori will be subjected to different conditions of solar, albedo, and planetary flux, along with the heat from the ambient temperature conditions. There are some components on board, e.g. the payload, batteries, and sensors, which are sensitive to ambient temperature values and have specific operating temperature ranges, beyond which they are no longer functional. Furthermore, large temperature differences in the structure may induce thermal stresses, making Tori susceptible to structural failure. These may also give rise to calibration errors in the measurements by payload instruments and cause distortion of sensor alignment. To avoid these risks, an effective thermal control subsystem for Tori is explained in the following section.

To start with, the design drivers will be explained in Section 3.5.1. Thereafter, the assumptions used for design are stated in Section 3.5.2, which will be followed by the summary of requirements for Tori’s thermal control subsystem. This is followed by showing the steps of the actual design process in Section 3.5.3. After this, an overview of the design strategy is presented in Section 3.5.4, followed by carrying out model verification and listing product verification tests in paragraph 3.5.4. Finally, the section is concluded by assessing the possible risks and discussing their mitigation strategies in Section 3.5.5, as well as an analysis of sustainability of the subsystem components in Section 3.5.6.

### 3.5.1. Requirements and design drivers

The initial step to design the thermal control subsystem, is to have an overview of three aspects. First, the ambient temperatures of the Venusian atmosphere; second, the working temperature ranges of the on-board components; and third, the incoming and outgoing heat fluxes for Tori. This subsection will highlight these three primary design drivers, which influence the selection of thermal control methods. There are also other design drivers such as the material thermal resistance to temperature gradients, however, this aspect was considered secondary in the initial phase. After achieving a design target from the primary design drivers, it was then checked for the secondary drivers.

#### Ambient temperatures

According to Tori’s planned flight, it will spend 0.6 day at an altitude of 65 km, and 1.8 days at an altitude of 55 km during the day. During the night, Tori will fly at an altitude of 55 km. As stated in Section 1.3, the Venus International Reference Atmosphere (VIRA) model was used to return the temperatures and pressures of the Venusian atmosphere at each altitude level. From this model, the ambient temperatures for 55 km and 65 km altitude were found to be 302.3 K and 244.2 K, respectively. Based on the target operational temperature for the components, in combination with the ambient temperatures specified earlier, excess heat would have to be dissipated from the probe at a lower altitude, while additional heat would have to be retained or absorbed into the probe at a higher altitude.

#### Operational temperature range study for on-board components

The next step, was to have an overview of the operational temperature ranges of the on-board components. Tori carries its payload and instrumentation to perform scientific measurements in the atmospheric cloud layers. It also carried batteries on board as a secondary power source and to facilitate electric propulsion. Furthermore, there are sensors needed for GNC,

**Table 3.24:** Operating temperature ranges of the instruments on Tori

Instrument	Minimum temperature [K]	Maximum temperature [K]
MASPEX <sup>29</sup>	233	323
UVI (Torr et al., 1992)	263	313
IMU	243	323
Sun Sensor	223	358
Lidar	243	323
Batteries	273	358
Solar arrays	168	383
On board computer	263	323
<b>Target range</b>	<b>273</b>	<b>313</b>

and there is a computer on-board, which forms the primary building block of command and data-handling for the probe. All these instruments have their own temperature ranges, which are listed in Table 3.24. These values of temperature ranges, were obtained from the respective component departments.

From Table 3.24, the optimum temperature range for all components was found to be between 273 K and 313 K. This means that the internal target equilibrium temperature of Tori would have to be in this range.

### Analysis of thermal fluxes and modes of heat transfer

It is also important to identify the incoming and outgoing thermal fluxes acting on Tori. A numerical model was created to return equilibrium internal temperature of the probe. For this, the following seven heat fluxes were modelled:

- **Solar radiation flux:** This is a measure of the solar intensity flux, that is incident on Tori. It is modelled as in Eq. (3.11).

$$J_{sVenus} = \frac{J_{sEarth}}{d^2} \quad (3.11)$$

Using this relation, a constant solar flux value of  $2798 \text{ W m}^{-2}$  was obtained. This is the true value of incoming solar flux. However, the cloud layers filter some of the incoming sunlight, as seen also in the power subsystem sizing in Section 3.4. It must be noted, that if the standard equation for finding the solar flux from the power emitted by the Sun, and the distance if Venus from the Sun is used, it returns the same values. It was found that for an altitude of 65 km, the effective incoming solar flux on Tori is equal to  $2507 \text{ W m}^{-2}$ , while for a 55 km altitude it is equal to  $1307 \text{ W m}^{-2}$ .

- **Albedo flux:** Next, albedo flux was considered, which measures how strongly the Venusian surface reflects solar radiation. The visibility factor  $F_a$  was computed using Eq. (3.12) for flight on the day side and set to 0 for flight on the night side. Note that  $R_v$  here stands for the radius of Venus.

$$F_a = \left( \frac{R_v}{R_v + h_{probe}} \right)^2 \quad (3.12)$$

Using the albedo factor  $a_F$  and the visibility factor  $F$ , the albedo flux intensity  $J_a$  is modelled as seen in Eq. (3.13).

$$J_a = a_F F_a J_{sVenus} \quad (3.13)$$

- **Planetary flux:** The planetary radiation flux is the energy radiated by Venus itself. Its intensity  $J_{IR}$  can be calculated using the black body effective radiation temperature of Venus  $T_{IR}$  in Eq. (3.14).

$$J_{IR} = \sigma T_{IR}^4 \quad (3.14)$$

- **Conduction:** The first mode of standard heat transfer identified was conduction. The wall separating the payload bay from the inflatable gas containing part, would act as a medium of conductive heat transfer. This can be modelled using Eq. (3.15), where  $k$  is the thermal conductivity of the combination of materials (Vectran, Mylar, PTFE and aramid) taken equal to 0.25,  $t_{wall}$  being the thickness of the insulating wall between the two compartments equal to 0.37 mm (this value was also calculated while carrying out structural analysis for Tori),  $A_{cond}$  is the area through which conduction takes place, and  $\Delta T$  is the temperature change due to conduction.

$$Q_{cond} = \frac{k A_{cond} \Delta T}{t_{wall}} \quad (3.15)$$

<sup>29</sup><https://analyticalsciencejournals.onlinelibrary.wiley.com/doi/10.1002/jms.4454>, retrieved 15-21-2021

**Table 3.25:** Requirements for thermal control

Identifier	Requirement	Check
KUMO-TORI-TC-01	The overall internal temperature of Tori shall be constrained between 273 K and 313 K.	✓
KUMO-TORI-TC-04	The thermal control subsystem of Tori, shall be equipped to cope with any temperature change during the mission for other subsystems.	✓
KUMO-TORI-TC-06	The thermal control subsystem shall be atleast 90% reliable.	✓
KUMO-TORI-TC-07	The temperature gradient of the outer and inner structure of the spacecraft or probe must not exceed 15 K.	✓
KUMO-TORI-TC-08	The thermal control subsystem shall be effective during all active mission phases.	✓
KUMO-SUS-TC-01	The use of toxic surface finish paints for temperature control shall be avoided.	✓

- **Convection:** The next mode to be considered was convective heat transfer. This is due to the velocity of the moving probe, that convective heat transfer can occur from and into Tori. This can be modelled using Eq. (3.16), where  $h_c$  is the convective heat transfer coefficient of surrounding air. This value was taken to be equal to the free convective heat transfer coefficient of carbon dioxide equal to  $1.5^{30}$ , as the Venusian atmosphere consists primarily of carbon dioxide. Further,  $A_{conv}$  is the area through which convection takes place, and  $\Delta T$  is the temperature change due to convection.

$$Q_{conv} = h_c A_{conv} \Delta T \quad (3.16)$$

- **Radiation:** The last mode of heat transfer would be radiation. Due to the type of material, and the surface finished applied, heat is radiated throughout the surface of Tori. This can be modelled using Eq. (3.17), where  $\epsilon$  is the emissivity of the material,  $A_{rad}$  is the area through which radiation takes place,  $T_{in}$  is the internal temperature of the probe and  $T_{out}$  is the outer temperature .

$$Q_{rad} = \sigma \epsilon A_{rad} (T_{in}^4 - T_{out}^4) \quad (3.17)$$

- **Internal heat:** This is the internal heat within the gas. Assuming it to be homogeneously distributed, the gas internal heat temperature depends on the amount of heat generated by the working payload components and the batteries. This heat is distributed internally, by means of the gas which ensures uniform heating of the probe. To model it in Python, the average power consumed during the day and the night was multiplied by the electrical efficiency.

### Summary of requirements

This subsection will give an overview of the requirements for the thermal control subsystem. They are also reviewed and checked whether the design actually fulfils the requirements, as seen in Table 3.25.

Requirement KUMO-TORI-TC-01 originates from the design driver requirement for on board components. KUMO-TORI-TC-04 originates from the mission need statement, which requires proper functional thermal subsystem at all times, to carry out the mission objective. Since, an overall mission reliability requirement of 95% is needed, it means that the thermal subsystem shall atleast be 90% reliable, as per KUMO-TORI-TC-06, which in combination with the other subsystem reliability scores, shall comply with the overall mission reliability requirement. KUMO-TORI-TC-07 originates from the structural thermal gradient limits. This is stated in (Zandbergen, 2017), which defines the allowable temperature gradients across a structural component to be  $8 \text{ K m}^{-1}$ , while the same across an optical instrument to be  $12 \text{ K m}^{-1}$ . A contingency or safety factor of 0.25 was applied to the theoretical limits, which specified the limit in KUMO-TORI-TC-07 to be 15 K across any point.

### 3.5.2. Assumptions

Having identified the main design drivers and heat fluxes, the design can start. However, before that, there are some simplifying assumptions that are made to finish the design. They will be verified and validated in paragraph 3.5.4.

**TC.A.1** The internal temperature of the probe for both chambers, is assumed equal to be equal to the ambient altitude temperature, without any thermal control measures.

**TC.A.2** The helium gas is assumed to be an ideal gas, which has homogeneous internal heat distribution.

**TC.A.3** Venus is assumed to be a black-body, which radiates all of the incoming energy back to space without absorbing any heat into the surface.

**TC.A.4** Apart from the 7 heat fluxes identified earlier, there is no other fundamental mode of heat transfer for Tori.

<sup>30</sup>[https://www.engineeringtoolbox.com/convective-heat-transfer-d\\_430.html](https://www.engineeringtoolbox.com/convective-heat-transfer-d_430.html), retrieved on 20-06-2021

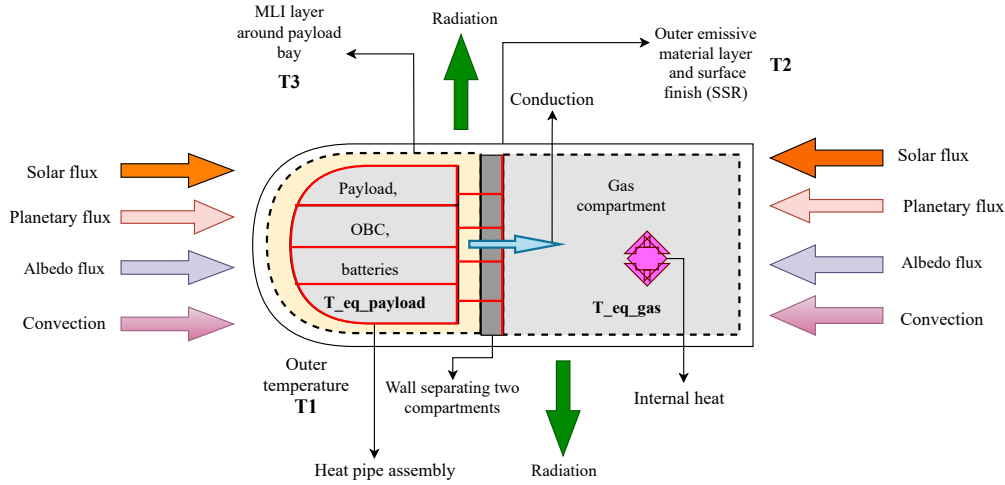


Figure 3.14: Thermal model of Tori

### 3.5.3. Design process

As seen earlier, an optimum target range was set to ensure efficient functioning of the on-board components. It was obvious, that there was a needed amount of temperature change needed from the body of the probe. The net heat flux flow needed through the probe, for the desired temperature change could be calculated with Eq. (3.18).

$$Q_{net} = \frac{m_{probe} c_{probe} \Delta T}{\Delta t} \quad (3.18)$$

Here,  $m_{probe}$  is the overall probe mass,  $c_{probe}$  is the specific heat capacity of the probe (this was found to be equal to  $1000 \text{ J kg}^{-1} \text{ K}^{-1}$  for the materials),  $\Delta t$  is the time throughout which the temperature change of  $\Delta T$  takes place.

The design process was carried out for three flight modes : flight during day time at 65 km, during day time at 55 km and at night time at 55 km. This would imply getting six different equilibrium temperature values, for each of the two chambers. At first, passive thermal control methods were investigated starting with very simple surface finishes. A code in Python was written which followed the principle of heat equilibrium, for different combinations of absorptivity ( $\alpha$ ) and emissivity ( $\epsilon$ ) factors. To be able to follow the acting fluxes on the probe, a thermal model is provided in Fig. 3.14.

#### Step 1: Surface finishes

The first venture was to dissipate the heat from the probe into the surrounding atmosphere, using passive methods. The basic principle used while applying surface finishes was that of the heat balance equation, which simply means that  $\dot{Q}_{absorbed} + \sum P_d = \dot{Q}_{emitted}$ . The values of  $\dot{Q}_{absorbed}$  and  $\dot{Q}_{emitted}$  could be found using Eq. (3.19) and Eq. (3.20). The dissipated power or  $P_d$  comes from the internal heat produced by the batteries and payload.

$$\dot{Q}_{absorbed} = \alpha_s J_{sVenus} A_{solar} + \alpha_s J_a A_{albedo} + \alpha_{IR} J_{IR} A_{IR} \quad (3.19)$$

$$\dot{Q}_{emitted} = \sigma \epsilon A_{emitted} T_2^4 \quad (3.20)$$

The areas  $A_{solar}$ ,  $A_{albedo}$  and  $A_{IR}$ , refer to the areas of Tori absorbing the solar, albedo and planetary fluxes respectively.  $\alpha_s$  and  $\epsilon$ , are variable values representing the absorptivity and emissivity factors for chosen surface finishes.

Initially, the values for white paint were used. Although, this provided good results for the surface temperature, it would need at least three coatings of usual Z-93 paint, along with a corrosion protecting coating. This was causing a significant hike in the subsystem mass by 32 kg. Moreover, white paint of Type Z-93 is toxic in nature. As an alternative, the combination of materials was reviewed. For the triple material layer of Vectran, PTFE and Mylar, very good absorptivity and emissivity properties were found. The material combination had a low absorptivity factor of 0.075, and a high emissivity factor of 0.85. Using these values in the Python code, did reduce the temperatures, close to target temperatures. However, it was not enough for all the flight modes. During the day at 65 km, the internal temperature for both the sections rose up to 298 K. Although, this was within the limit, it was still on the higher side, which meant it would increase further when iterated. Hence, optical solar reflectors were considered. 8 mil quartz mirrors were selected, due to their high performance characteristics and reliability. These mirrors had a value of 0.006 for absorptivity, and 0.86 for emissivity. They were decided to be placed equally distributed on the top surface of Tori, infused along with the solar panel cells. These reflectors were quite effective in reflecting most of the heat absorbed by the solar cells, in the process of generating power. The selected reflectors were quite compatible with the solar cells, and were flexible enough to be integrated on the inflatable part of Tori. The temperature with this combination came down to 282.9 K during the day at

65 km altitude, 279.2 K during the day at 55 km, and to 276.4 K during the night. One can see these numbers for the gas part, in Table 3.26.

After some trial and error, the area on which the optical solar reflectors would be installed was calculated to be 6 m<sup>2</sup>. A total of 3884 pieces of 8 cm X 8 cm individual solar reflectors would have to be integrated on top of the probe. Also, compared to the 32 kg of white paint, the mass of solar reflectors was only 6 kg, which was a considerable mass reduction.

Hence, following Fig. 3.14, the temperature change from ambient temperature  $T_1$  to the outer surface temperature of the probe  $T_2$  was obtained by means of the material combination properties and placement of optical solar reflectors.

### Step 2: Insulation

The inflatable part of the probe is less critical than the rigid part. This is because the rigid part of Tori contains the sensitive components, which must be protected from adverse temperature gradients. To ensure the same, the payload bay was decided to be insulated. After conducting a lot of research in the properties of insulating materials, Multi-Layer Insulation (MLI) was chosen. This was chosen for three reasons: first, it has been used on almost all space missions and is reliable; second, it is cheap yet has good performance characteristics; third, using MLI provides an efficient passive thermal control technique, thus reducing the power required for the thermal subsystem

The MLI modelling was done in a way, to reduce heat transfer by conduction, convection and minimising thermal radiation exchange. The internal temperature was set to a target value of 280 K. The combined emissivity of an MLI blanket with  $n_{MLI}$  layers, is given by Eq. (3.21).

$$\epsilon^* = \frac{1}{\frac{1}{\epsilon_{in}} + \frac{1}{\epsilon_{out}} - 1} \left( \frac{1}{n_{MLI} + 1} \right) \quad (3.21)$$

Here,  $\epsilon_{in}$  is the emissivity of the internal face, while  $\epsilon_{out}$  is the same for the outer surface. The heat transfer rate  $\dot{Q}_{MLI}$ , to be blocked through an overall area of  $A_{MLI}$ , can be found through Eq. (3.22) (Ley, Wittmann, and Hallmann, n.d.).

$$\dot{Q}_{MLI} = \epsilon^* \sigma A_{MLI} (T_{target}^4 - T_2^4) \quad (3.22)$$

After the heat flow rate for a desired temperature gradient was found using Eq. (3.22), Eq. (3.23) was then applied. Here,  $t_{MLI}$  is the thickness of the MLI foils, and  $k^*$  is the heat conductivity value for a chosen set of MLI.

$$T_3 = T_2 + \frac{\dot{Q}_{MLI} t_{MLI}}{k^* A_{MLI}} \quad (3.23)$$

After some iterations, it was decided that ten layers of Kapton foils of individual thickness of 40  $\mu\text{m}$  would be wrapped on the interior of the rigid part. These individual layers were coated with aluminium on both sides, to minimise the radiative heat transfer. For ten layers, the effective emissivity value used was  $3.6 \cdot 10^{-3}$ , while the conductivity value was found to be  $2.1 \times 10^{-2} \text{ W m}^{-2} \text{ K}^{-1}$  (Ley et al., n.d.). Using these above equations, the internal temperature for the payload rigid bay  $T_3$ , was obtained. This was done for all three flight conditions, iterating to be in similar ranges of temperature values. The values obtained for all three conditions was in the range of 280 K. These values can be found in Table 3.26.

Hence, following Fig. 3.14, the internal temperature  $T_3$  was obtained by using multi-layer insulation, isolating the insulated rigid payload bay from the outer surface temperature  $T_2$ .

### Step 3: Heat pipes and sensors

Although, the temperatures for rigid and inflatable part were controlled by means of surface finishes and MLI, the heat flow still had to be uniformly distributed. This is mainly to ensure minimal thermal structural gradient. After an initial iteration, it was seen that some heat generated by the payload instruments and batteries could be used to regulate the temperature in the inflatable part of Tori.

To efficiently transport the heat throughout the probe, two phase cooling loops or passive heat pipes are used. They consist of hermetically sealed, cylindrical tube with a capillary wick in the middle. After evacuating the interior of the pipe, it is filled with a fluid heat carrier. When heat is conducted into an evaporator section, the fluid carrier transports the heat from this section, and condenses at the cold condenser section. Heat pipes are fully passive in nature, working without any energy supply from the external environment. In principle, since evaporation and condensation takes place at the same temperature, heat can be transported with very small temperature differences. This can be visualised in Fig. 3.15.

One of the criteria for selecting the heat pipe, is analysing the thermo-hydraulic properties of the selected flowing liquid. It must be chosen such that it does not is compatible with the wall material of the pipe structure. To study this, a  $G$  value representing the figure of merit, is found using Eq. (3.24).

$$G = \frac{\kappa \rho \tau}{\eta} \quad (3.24)$$

Here, it is observed that liquids with high heat of vaporisation  $\kappa$ , density  $\rho$  and surface tension  $\tau$  and a low value of dynamic viscosity  $\eta$  are most suitable. After some study into this, it was seen ammonia was a good choice, with a  $G$  value close to  $10 \text{ W m}^{-2}$ , for the temperature ranges Tori is exposed to. For the outer material, aluminium was chosen. The

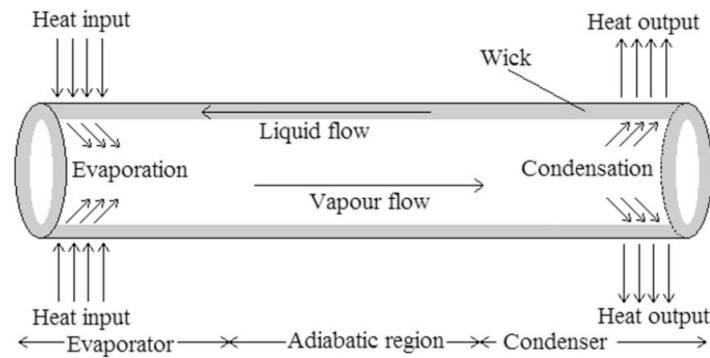


Figure 3.15: Working principle of a passive heat pipe (Ley et al., n.d.)

Table 3.26: Thermal control overview

Flight mode	Rigid chamber (payload) temperature [K]	Inflatable chamber (gas) temperature [K]	Temperature gradient [K]
Day time flight at 65 km	280.0	282.9	2.9
Day time flight at 55 km	280.0	279.2	0.8
Night time flight at 55 km	280.2	276.4	3.8

combination of aluminium and ammonia was deemed quite efficient and reliable, since they operate for a wide range of temperatures between 193 K and 353 K (Ley et al., n.d.).

Hence, aluminium pipes of diameter 1.3 cm, filled with ammonia were integrated into the internal wall structure of the rigid part. These pipes take one turn around the wall perimeter for each of the four compartments, and end on the other side of the wall separating the chambers. The side view of the integration of the heat pipes can be visualised in Fig. 3.14, where the heat pipes are denoted by the red lines. The total length of the heat pipes was estimated to be around 14.8 m. This efficiently helps in regulating the uniform heat flow even in the gas section.

After heat pipes, for temperature control, sensors were used. A total of ten platinum sensors of 150 °C series from Innovative Sensor technology was used<sup>31</sup>. These sensors have an internal resistance of 100 Ω, and support a current flow of 1 mA. Hence, the power required for each of these sensors is 0.1 mW. Tori will use ten sensors: two for each payload instrument, two for the battery system, and two for the on-board computer; all sensors are placed in pairs for cold redundancy. There is an assembly of cables connecting the sensors to the instruments and the computer. Measurements are taken every 10 seconds, and data is sampled every 16 bits. This results in an overall data rate of the thermal subsystem to be 16 bps. The total power required by the sensors is 1 mW, which is very small.

### 3.5.4. Thermal control overview

This section summarises the design of the thermal control subsystem, by providing an overview of the strategy that was used to come up with an effective design, discussed in Section 3.5.3. The design process was started for an initial target temperature of 280 K. Thereafter, the target temperature was updated with each iteration to the new equilibrium temperature found. This was repeated for each of the flight phases. After several iterations, the converged values were obtained. They can be seen in Table 3.26.

The total mass from the thermal subsystem components is 23.27 kg. The subsystem uses passive components, and the only power needed is from the sensors needing 1 mW. The data rate for the subsystem is 16 bps.

**Verification and validation** This subsection deals with the process of verification and validation for the subsystems. First, a verification process of the numerical model made will be explained. This will be followed by product verification. The assumptions will also be verified.

#### Model verification

After the code for thermal control was written, the next step would be to verify the correctness of the same. To do so, unit tests were conducted. Some of the parameters were set to 0, to test the output for the linked variable. Some parameters were doubled, to see how that scaled a linear variable output. The unit tests can be found in Table 3.27.

<sup>31</sup><https://www.thermocoax-space.com/electrical-heating-system/>, retrieved on 20-06-2021

**Table 3.27:** Unit tests to verify thermal code

Test	Variables	Expected outcome	Verified
VER-TC-01	<b>Input:</b> $k$ <b>Outputs:</b> $Q_{conduction}$	Setting the thermal conductivity of material to 0, results in 0 conductive heat flux. Also, doubling input, doubles the output.	✓
VER-TC-02	<b>Input:</b> $t_{wall}$ <b>Outputs:</b> $\Delta T_{cond}$	Setting the thickness of the wall to 0, would give the value of $\Delta T$ change due to conduction to be 0. Also, doubling input, doubles the output.	✓
VER-TC-03	<b>Input:</b> $h_c$ <b>Outputs:</b> $Q_{convection}$	Setting the thermal convective coefficient to 0, results in 0 convective heat flux. Also, doubling input, doubles the output.	✓
VER-TC-04	<b>Input:</b> $c_{probe}$ <b>Outputs:</b> $Q_{net}$	Setting the value of specific heat capacity of the material to 0, would result in 0 net heat flux. Also, doubling input, doubles the output.	✓
VER-TC-05	<b>Inputs:</b> $\alpha_s, \alpha_{IR}$ <b>Output:</b> $Q_{absorbed}$	Setting the surface finish coefficients to 0, results in no heat absorbed.	✓
VER-TC-06	<b>Inputs:</b> $\alpha_s, \alpha_{IR}, \epsilon$ <b>Output:</b> $T_2$	Setting the coefficients to 1, would lead to the ambient temperature value at that altitude (no thermal control condition).	✓
VER-TC-07	<b>Input:</b> $n_{MLI}$ <b>Output:</b> $\epsilon^*$	Setting the number of MLI layers to 0, gives the value of effective emissivity equal to that of one foil only (instead of a blanket).	✓
VER-TC-08	<b>Input:</b> $t_{MLI}$ <b>Output:</b> $T_3$	Setting the thickness of the MLI blankets to 0, gives effective MLI temperature equal to the surface temperature $T_2$ (as if ignoring the presence of MLI)	✓
VER-TC-08	<b>Input:</b> $t_{MLI}$ <b>Outputs:</b> $T_2, T_3$	Increasing the thickness of the MLI wall, increased the temperature gradient ( $T_3 - T_2$ ) of the two chambers.	✓

## Validation

To conduct validation, the NASA Flagship mission model paper was studied. A second analytical model was not explicitly made, however the assumptions and results obtained were studied and compared to Tori's design. The major difference in the design was that the flagship model made the use of phase-change materials for thermal control (Gilmore, Lynch, and Amato, 2020). They used foam insulation, instead of kapton foil MLI blankets. Moreover, they do not use solar optic reflectors, which do not dissipate the excess heat. Hence, the expected internal temperature from NASA Flagship model should be higher than the same for Tori. Indeed, it was seen from the paper, that the internal temperature of Flagship model was somewhat close to 308 K. This difference in Flagship and Tori temperatures is mainly due to the design choices. The four assumptions that were used to model Tori's thermal control model, are similar to the ones for the Flagship thermal model. Rather, the latter has some more assumptions, which is speculated to be the cause in the difference in design choices, as well as internal temperature values. Although, there is a difference, the values from both the models are definitely in the same order of magnitude. The relative error in the values is also 8%, which is neglected, owing to the extra design assumptions in the Flagship model. This validates Tori's thermal model, which produces similar results to an actual NASA model.

**Assumption verification** There were four assumptions before the design process even started. They were verified either by code, or by using literature sources.

- **TC.A.1:** The assumption of having the initial internal and external temperatures to be equal, is verified by carrying out unit test VER-TC-06. By setting the coefficients of surface finishes to 1, i.e. assuming that no fraction of the solar, albedo and planetary fluxes acting on Tori are radiated into the atmosphere, the equilibrium temperature output is equal to the ambient atmospheric temperatures. The same assumption is a valid assumption, since it was also used to design the NASA Flagship thermal model (Gilmore et al., 2020). This justifies the assumption of having same internal and ambient temperatures for the probe.
- **TC.A.2:** For the assumption considering helium to be an ideal gas, the kinetic theory of ideal gases was reviewed. Helium is an inert gas with a low molecular mass. The particle behaviour can thus be compared to an ideal gas, where collisions are perfectly elastic. It implies, that the average kinetic energy of the particles is proportional to the temperature in kelvins. The same assumption is a valid assumption, since it was also used to design the NASA Flagship thermal model (Gilmore et al., 2020). Hence, the assumption of uniform heat distribution is justified.

- **TC.A.3:** For the assumption considering Venus a completely reflecting black body, the Stefan-Boltzmann Law was reviewed. This law states, “radiated power density of a black body is proportional to its absolute temperature  $T$  raised to the fourth power”. Assuming this law holds true, Venus was assumed to be a black body, radiating planetary flux into the atmosphere. The same assumption is a valid assumption, since it was also used to design the NASA Flagship thermal model (Gilmore et al., 2020). Hence, this assumption was also justified.
- **TC.A.4:** The assumption of not having more than 7 heat fluxes, was justified from literature. The heat fluxes that were modelled were conduction, convection, radiation, solar flux, albedo flux and planetary flux (Ley et al., n.d.). Also, the remaining power needed was assumed to be generated from internal heat of the gas, battery and payload instruments (Wertz et al., 2011). The same assumption is a valid assumption, since it was also used to design the NASA Flagship thermal model (Gilmore et al., 2020).

**Product verification and validation** After the model and assumptions are verified, a number of different tests can be carried out on the actual product to verify and validate the thermal model employed. These tests should preferably be space-environment simulation tests, to simulate and thus verify the response of the probe to the Venusian atmospheric environment that it will be exposed to, a number of which are listed in the following:

- **Thermal balance tests** verify the response of the spacecraft to thermal load cases with specified sources of radiation.
- **Bakeout tests** verify the outgassing that is required before the spacecraft is launched. The spacecraft is heated to a higher than operational temperature and left in a vacuum chamber for a day. This stimulates the release of the trapped or dissolved gas from the surface and thus reduces the risk of contamination.
- **Thermal cycling tests** measure the response of the spacecraft to temperature changes outside of a vacuum environment. These are much cheaper and thus will be performed more times for individual components.
- **Thermal micro vibration tests** are used to choose multi-layer insulation foils. Foil specimens up to 1 m<sup>2</sup> in size are attached to a plate with known eigenfrequencies. This fixture is suspended at low frequency in a thermal vacuum chamber and exposed to space conditions. By means of infrared lamps, the foils are exposed to the relevant thermal conditions. Their behaviour is then registered optically as well as with very sensitive accelerometers mounted on the plate. The thermally induced movements of the multi-layer insulation foil excite eigenfrequencies in the plate, giving an insight into the activity of the material.

**Requirement verification** There were five main requirements for the probe thermal control. They are verified as well.

- **KUMO-TORI-TC-01** From Table 3.26, the equilibrium temperatures can be seen. They are well within the ranges specified in the requirements.
- **KUMO-TORI-TC-04** The thermal control subsystem has 10 sensors on board of Tori, which monitor the internal temperature every 10 seconds. The design is based on the temperature ranges of the components from other subsystems. Any major change in temperature will be communicated with the the orbiter instantly.
- **KUMO-TORI-TC-06** Since, the components are all passive, they are less prone to failure. Apart from that, there have been risk mitigation strategies identified, for any kind of possible threat to the working of the subsystem. Furthermore, the components will undergo product verification, as discussed earlier, and hence are estimated to be at least 90% reliable.
- **KUMO-TORI-TC-07** From Table 3.26, the temperature gradients at each flight phase can be seen. It thus fulfils the requirement of being under 15 K.
- **KUMO-TORI-TC-08** Since, the thermal control methods are passive, they do not need external power to be able to operate at all times. The design has been done such that, the subsystem is active for all three flight modes, and communicates the instantaneous equilibrium temperature every 10 seconds.
- **KUMO-SUS-TC-01** The use of white paint was initially considered, but it was discarded owing to high mass and toxicity levels. Hence, this requirement on sustainability was also fulfilled.

### 3.5.5. Risk assessment

The risks for the thermal subsystem, as well as their mitigation strategies are presented in Table 3.28. From the table follows that the most prominent risks related to the thermal control subsystem are risks 7f-1 and 7g-1, which both cover the temperature of the lifting gas.

### 3.5.6. Sustainability

This subsection briefly entails the aspect of sustainability of thermal control subsystem for Tori. Usually, in most space missions, the thermal control subsystem employs the usage of different surface chemical finishes. Often, the aspect of sustainability is somewhat undermined. For instance, to enable the spacecraft to radiate excess heat, white paint is used. However, the same paint could prove to be a potential threat due to its toxic nature to workers, as well as be a part of space

**Table 3.28:** Table showing possible risks for the thermal control subsystem, their severity and likelihood

<p><b>7a-1: Overheating of atmospheric platform.</b></p> <p><b>Assessment L3S4:</b> Absorbing too much solar heat or not being able to eject enough waste heat could cause the temperature to increase beyond the operational range of subsystems and instruments, this being a range from 273 K to 313 K, as set by the requirements, thus impacting the mission and its objectives. This is moderately likely to happen, if only briefly for some period of the mission. Depending on the duration of the malfunction, the severity can range from very low to critical.</p> <p><b>Mitigation L2S3:</b> The means of reflecting solar radiation and shedding heat are passive, to reduce the likelihood of malfunction. To reduce the severity, the payload has extra thermal control measures, like heat pipes, to transfer heat away.</p>
<p><b>7b-1: Failure of thermal active and semi-active control.</b></p> <p><b>Assessment L2S4:</b> Failure of active thermal control would happen due to a power surge or power depletion, leading to loss of thermal control on the craft. This is not very likely, but would result in critical failure.</p> <p><b>Mitigation L2S2:</b> The thermal control system contains only passive means for thermal control, to reduce the risk of loss of thermal control due to the power system malfunctioning. The severity of active control failing is also limited to marginal, as the probe would only lose its heating elements, thus undercooling to ambient night temperatures which are outside of the operating range, but not harmful to the materials and systems. In case of a temporary loss of primary power, the power system does contain a battery that can supply power to bridge the temporary loss.</p>
<p><b>7c-1: Degradation of thermal control materials.</b></p> <p><b>Assessment L3S2:</b> Degradation of the insulation, covers and coatings over the mission duration is moderately likely as the materials will have to survive a multitude of conditions and harsh environments. A partial reduction in insulation performance poses a marginal severity.</p> <p><b>Mitigation L2S1:</b> No thermal control materials are applied to the inflatable hull, so only the insulation on the rigid part is exposed to the outside, reducing both the severity and likelihood. The rest of the systems are contained in the controlled environment of the probe.</p>
<p><b>7d-1: Corrosion of heat pipes and or other metallic components.</b></p> <p><b>Assessment L3S2:</b> The cooling system could involve metal pipes to cool and heat the spacecraft. However, after a while, corrosion might occur. This could lead to critical damage and eventually failure. This is a moderately likely risk.</p> <p><b>Mitigation L2S2:</b> Metallic components are contained inside the atmospheric craft, where the environment is benign compared to the outside. This reduces the likelihood of corrosion to low.</p>
<p><b>7e-1: Undercooled lifting gas.</b></p> <p><b>Assessment L2S5:</b> Changes of the lifting gas temperature cause the internal pressure to vary accordingly. Large pressure drops can cause the hull to lose rigidity, leading to a collapse. Hence the severity is catastrophic and likelihood low.</p> <p><b>Mitigation L1S5:</b> The severity of a collapse cannot be reduced, as it is a process that is hard to recover from. However, to reduce the likelihood of a collapse from low to very low, the equilibrium temperature of the gas compartment must not drop too far, and the ambient pressure may not become larger than the internal pressure. To do so, the heat pipes leading excess heat into the gas compartment help prevent a collapse during night at the low altitude, and if the overpressure reduces too far, power can be applied to fly to a higher altitude where lower ambient pressures stabilise the hull.</p>
<p><b>7f-1: Too high lifting gas temperature.</b></p> <p><b>Assessment L2S5:</b> If the temperature of the lifting gas compartment increases too far, this will increase the internal pressure, imposing more stresses on the hull. If the hull material were to fail, the lifting gas would escape and thus the severity is catastrophic. A low likelihood is assigned because the conditions do not appear without warning signs and thus provide time for mitigation.</p> <p><b>Mitigation L1S5:</b> Bursting remains a catastrophic effect of a too high lifting gas temperature. However, to reduce the chance of bursting from low to very low, the temperature and pressure of the gas compartment are constantly monitored, especially close to the extremes of the flight envelope. If an excess temperature or pressure is detected, a dive to higher ambient pressures and lower solar flux shall be initiated to reduce the pressure differential and solar heat flux.</p>

debris due to it chipping off. Hence, owing to the risk it could potentially pose, the thermal control subsystem was given a weight of 3, meaning that among other subsystems, it has a noticeable contribution to sustainability.

The first aspect to be taken is the manufacturing process, waste handling and transportation to the launch site. For this, the individual components would have to be reviewed.

- **Optical solar reflectors:** The solar arrays are not 100% efficient, and hence, the incoming solar flux would also generate heat which would affect the temperature of the probe. To mitigate this, optical solar reflectors were used on *Tori*. To be precise, they are 8 cm by 8 cm off-the-shelf optical mirrors from the company Excelitas Technologies<sup>32</sup>, from Singapore. They are a company, which have previously supplied solar reflectors in most major satellite programs for both civilian and military applications in Europe, USA and Japan. They are a highly specialised member responsible for using dedicated glass melting technology in the most sustainable way possible, with minimal waste production. A “high” (3) score was given for the optical solar reflectors on *Tori*.

<sup>32</sup><https://www.excelitas.com/product/optical-solar-reflectors>, retrieved on 17-06-2021

- **Multi-layer insulation:** The inside of Tori's payload bay will be covered in ten layers of Kapton MLI, coated with aluminium on both sides. The layers will be developed by the DUNMORE Corporation, a company which has also provided the same product to the Rosetta mission, sustaining it for more than 10 years<sup>33</sup>. However, it must be noted that both Kapton and aluminium must be handled with caution, since they may be toxic if exposed for a long time. Kumo will ensure DUNMORE Corporation pay heed to the health of the workers in manufacturing and testing of the MLI. A "reasonable" (2) score was given for the MLI blanket on Tori.
- **Heat pipes:** To ensure, uniform heat circulation between the two chambers of Tori, aluminium heat pipes with ammonia in them will be used. These will also be off-the-shelf heat pipes from the company Boyd Corporation<sup>34</sup>. They distribute their resources from India, to clients worldwide at cheap prices. They also take the aspect of safety of workers and waste management into account. For instance, they get health checks every week for the workers who work with aluminium dust and ammonia, which may cause health issues if exposed for prolonged times. Additionally, they recycle the scrap aluminium from production processes. Hence, a "reasonable" (2) score was given for the heat pipes of Tori.
- **Temperature sensors:** There will be ten temperature sensors on-board Tori. Each component has one sensor extra for redundancy, thus mitigating the risk of failure. These sensors are also off-the-shelf sensors from the company Innovative Sensor Technology (IST)<sup>35</sup>. This company has many years of experience with the platinum sensors used on Tori. They efficiently handle energy usage and also repair dysfunctional sensors to re-use them instead of making new ones. This way, they sell sensors at a cheaper price and also consider the aspect of recycling and reusing. Hence, the sensors were given a "high" (3) score.

Moreover, all the components on board are passive control techniques which do not require power to operate. Their masses are also optimised to be the lowest as possible, leading to a total mass of 23.27 kg for the subsystem. This means it constitutes 4.5% of the total probe mass which is comparable to most space mission thermal mass budgets.

Summing up the scores per component, it was seen that a total score of 10 was obtained out of a possible total score of 12. This meant that the thermal subsystem for Tori is 83% sustainable in terms of components and concepts. The thermal subsystem uses the same components during all three phases of Earth operations ( $SP_1$ ), interplanetary travel ( $SP_2$ ) and Venus operations phase ( $SP_3$ ). Hence, for all the phases for Tori, a "high" (3) score was given from the mission perspective, to aid in calculating the final sustainability score for Tori.

The subsystems will need support and protection from the environment, which will be delivered by the structures. Here, the structures as well as the materials chosen to withstand the environment in the Venusian atmosphere will be explained.

## 3.6. Materials and structures

This section elaborates on the materials and structural elements of the probe. First, the materials of the probe will be analysed in Section 3.6.1 for the inflatable body of the probe, followed by the rigid body. Extra materials used for other elements, such as the windows for the payload will also be explained. Second, the structures of the probe will be explored in Section 3.6. Here, the structural layout will be described, followed by a structural analysis of the stress' of Tori.

### 3.6.1. Materials

In this section the requirements and their relevant assumptions for materials are evaluated. The inflatable body material layers are explained as well as the material choices for the rigid structure of Tori. This is followed by verification and validation of the material choices as well as risk assessment and sustainability analysis.

The materials of the probe need to be able to withstand the harsh environment of Venus as well as the operational loads during flight, entry and launch, where the extremes are felt. The maximum design values are shown in Table 3.29 and are used for material selection.

The maximum temperature felt by the body is based on the temperature of the Venus' atmosphere. In the worst case scenario, at 55 km, Tori will experience the highest temperature of 302 K. There will also be a margin of error applied of 10% based on an estimation of temperature fluctuation considering maximum solar flux. The maximum pressure differences was taken from what Tori will feel during flight, this being between 55 and 65km. The value is roughly 35,000 Pa, however a margin of error of 15% was applied and a design value of 40,000 Pa was chosen. The maximum acidity level is derived from the acidity of the cloud layer at 75-99%. Therefore a material with a good acidity resistance should be chosen. Finally, the number of thermal and pressure loading cycles the body will have to endure during the altitude changes is given as 20 and was determined by the flight plan. The body of Tori should remain rigid during flight to maintain the airfoil shape and also have a high fatigue strength to combat the pressures felt at different altitudes. All of these considered, the materials shall be able to tolerate the extreme conditions for the 63 day nominal duration of the mission.

<sup>33</sup><https://www.prweb.com/releases/mli-film/esa-rosetta/prweb12316545.htm>, retrieved on 17-06-2021

<sup>34</sup><https://www.boydcorp.com/resources/temperature-control/heat-pipe-technology.html>, retrieved on 17-06-2021

<sup>35</sup><https://www.ist-ag.com/en/products-services/temperature-sensors>, retrieved on 17-06-2021

**Table 3.29:** Maximum design values<sup>36</sup>

Max temperature [K]	Pressure difference [Pa]	Acidity at 55 km [%]	Maximum loading cycles [-]
332	40000	70-99	20

### Requirements for materials

Table 3.30 gives the requirements considered for the material design of Tori. These were another useful tool to narrow the search for materials which best suit the function of the mission. Some requirements are missing here as they are more relevant to the orbiter design and have been discussed in Chapter 4

**Table 3.30:** Requirements relevant to Tori materials

Identifier	Requirement	Check
KUMO-MAT-02	The materials of the platform shall be able to withstand pressures between 10,000 Pa and 50,000 Pa.	✓
KUMO-MAT-03	The materials shall at least survive exposure to the Venus atmosphere for 60 days.	✓
KUMO-MAT-05-a	The materials shall be able to survive at least 20 pressure loading cycles.	✓
KUMO-MAT-05-b	The materials shall be able to survive at least 20 thermal loading cycles.	✓
KUMO-MAT-06	The materials shall be able to withstand a temperature range of 245K to 307K	✓
KUMO-MAT-07	The materials shall be able to be made into parts with existing production methods.	✓

### Assumptions for design

In addition to the requirements, assumptions were made to help with material selection for the probe. These assumptions will be evaluated at the end of this chapter.

- **M.A.1** The temperature and pressure felt during the mission will not exceed the ranges indicated in the requirements.
- **M.A.2** Material properties taken from Granta Edupack 2020 program provided by TU Delft are accurate.

**Material selection.** The materials for the probe are considered for both sections of Tori. First, inflatable body will be analysed followed by the rigid section of the probe. When researching materials, the role of each component must be considered. Regardless of the functionality, a light weight material is desirable. Furthermore, if the component is exposed to the environment not only is the acid resistance and temperature resistance important but also UV resistance. In Fig. 3.6.1, all of these properties of the chosen materials will be given.

**Material configuration of the inflatable body.** Due to the nature of the design and the harshness of the Venusian atmosphere, a method of layering materials was considered. It was chosen by looking at previous and promising mission designs to Venus. Additionally researching materials with promising characteristics was also done. The requirements were reflected upon and the production and functional feasibility was considered. With this, a layering configuration was found which consisted of three layers.

The first layer is gas tight seal which will need to withstand a 40,000 Pa pressure difference as indicated in **KUMO-MAT-02**. This layer must also be able to withstand the temperature range as given in **KUMO-MAT-06** and must be resistant to a large number of fatigue cycles. As this is an internal layer, the sulphuric acid resistance does not need to be high. This will be accounted for in the outer layers.

A fluorinated polymer was deemed the best choice for this layer. Specifically, a PET, Mylar film was chosen. Not only was this material used in previous balloon probe missions to Mars and Venus such as the VEGA mission (Kerzhanovich et al., 2003) and future missions such as the Venus Multiprobe (Yavrouian et al., 1999) but it is also used in components such as foil balloon and airships. Looking at Fig. 3.16, it can be seen that PET has a high temperature range as well as a high fatigue strength justifying the material choice of the gas sealant layer. The figures shown were created using Granta software and the gradient of blue represents the pureness of the polymer.

The second layer properties are mainly driven by the mechanical strength. It shall be able to withstand flight loads and have a high fatigue strength. The material should not be too flexible to allow for Tori to keep its shape during flight. Therefore a material with a high yield strength should be picked. This layer should also be able to withstand a large temperature differences.

The graph for the maximum service temperature against yield strength (Pa) used, shown in Fig. 3.17. The different colours represent the material classes. Pink are the nano materials and black are composites. Blue, as shown in the Fig. 3.16, are polymers. It can be extracted that graphene has the highest yield strength and a high service temperature but upon further investigation, the density was deemed too high. Vectran (LCP) on the other hand, is also in an acceptable range and has a high yield strength as well as a high fatigue strength and lower density. Therefore, it was chosen as the mechanical layer of the inflatable structure.

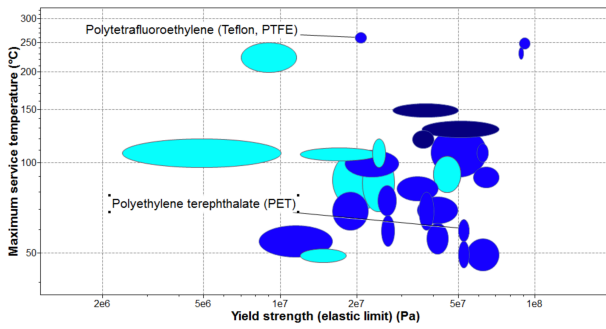


Figure 3.16: Maximum service temperature vs fatigue strength at  $10^7$  cycles

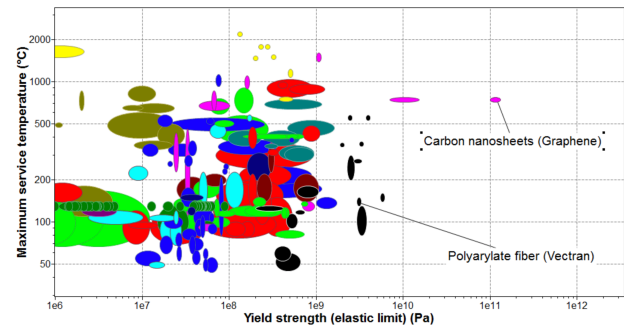


Figure 3.17: Maximum service temperature (K) vs yield strength (Pa)

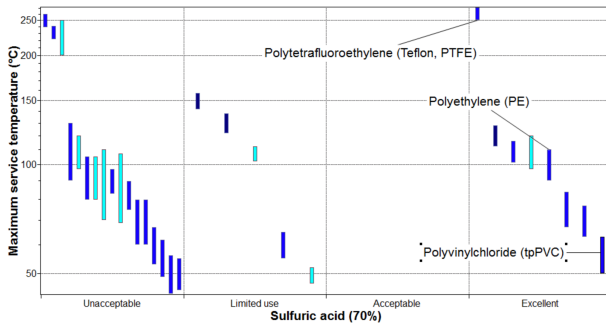


Figure 3.18: Sulphuric acid vs maximum service temperature

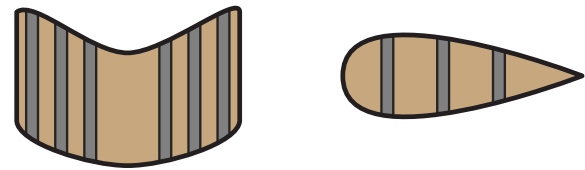


Figure 3.19: Illustration of aramid fibres

The final layer must protect the other two layers against the outside environment. At the altitudes that Tori will operate in, sulphuric acid at ranges between 70-99% and a max pH of -1.2 can be found due to the thick cloud layer. Therefore, a resistance to high acid concentrations is vital.

A polyimide was chosen to be on the outer most layer of the balloon. Fluoropolymers are known for having good chemical resistance and have been used in many previous mission (Yavrouian et al., 1999). Therefore, it would be a good choice for the corrosion resistance layer. Considering Fig. 3.18, Teflon (PTFE) was chosen. The other materials considered were PE and PVC. PE has both the temperature range and acidic resistance and thus was equally considered. However, PTFE was chosen as the protective coating because it was also used in previous Venus missions such as the Vega mission<sup>37</sup>.

Finally, a layer of structural support will be placed on the inside of the material layers to help support the shape and reduce the thickness of the materials. This will be done with the help of webbing inside the structure. The webbing will be made from aramid fibres. It will be installed as illustrated in Fig. 3.19. Each wing will have four webbed sections in both longitudinal and vertical directions. This will allow for stresses in both top and bottom faces to be distributed throughout the whole body and will reduce the stress concentrations at joints.

### Rigid body materials

This rigid body will have two faces exposed to the atmosphere, whereas the other four faces will be shielded by the inflatable body. The rigid body must be able to hold the payload securely whilst also withstanding operational flight loads. The mass of the total carried payload in the probe is 178 kg, placed on three shelves. Aluminium 7050<sup>38</sup> was chosen as the material of the rigid section, however it will also be coated in Teflon (PTFE) to prevent corrosion as Aluminium 7050 does not have enough resistive properties to withstand the environment. Teflon (PTFE) will also be sprayed on to all components of the probe exposed to the environment. This includes antenna, propellers and the exposed rigid structure. The Teflon will not interfere with the function of these components.

The rigid structure will also have multiple windows for the instrumentation to take measurements from. The dimensions will be elaborated on in structures however the material of the window have been chosen as Sapphire<sup>39</sup>. This is because, it has a spectral range of 150 nm to 4.5  $\mu\text{m}$  which is enough to not effect the measurements of the instrumentation.

Other than the probe structure, the solar cell structure for the solar panels will have to be created. The structure of the solar cells will be made from Aluminium 1050 as the solar arrays are flexible and Aluminium 1050 will allow for small displacements without damage.

<sup>37</sup><https://nssdc.gsfc.nasa.gov/nmc/spacecraft/display.action?id=1984-128F> Retrieved 18/06/2021

<sup>38</sup><https://www.azom.com/article.aspx?ArticleID=6650> retrieved on 18/06/2021

<sup>39</sup><https://www.azom.com/article.aspx?ArticleID=4767>, retrieved 18/06/2021

**Table 3.32:** Verification of Granta source compared to other websites

	Granta	Other source	Error [%]
Yield stress of Vectran [MPa]	2900	2840 (matweb.com)	+2%
Yield stress of Aluminium 7050 [MPa]	455	455 (Azom)	0%
Density of Mylar film [kg m <sup>3</sup> ]	1300	1390 (matweb.com)	7%

### Conclusion of materials

In conclusion, the inflatable structure will be made three layered materials. The first layer is a Mylar film, a gas sealant layer followed by Vectran, a layer to carry mechanical loads and Teflon (PTFE), to protect against corrosion. The Teflon will also be applied to all exposed surfaces of the probe including the rigid section. The rigid section will be made of out Aluminium 7050 and will contain 3 shelves with a number of windows made out of Sapphire for the payload. Finally, the solar panel structure will be made out of Aluminium 1050. The materials used and their most important properties are given in Table 3.31.

**Table 3.31:** Probe materials

Parameter	Mylar film (PET)	Vectran (LCP)	Teflon (PTFE)	Al 7050	Sapphire	Al 1050
Density [kg m <sup>-3</sup> ]	1300	1400	2410	2700	3980	2710
Yield strength [MPa]	50	2900	21	455	480	103
Maximum service temp [K]	328	403	523	353	2070	623
Acid resistance	Limited use	Excellent	Excellent	Fair	Excellent	Excellent
UV resistance	Fair	Good	Good	Excellent	Excellent	Excellent
Fatigue strength [MPa]	19.3	52.8	7.00	240	52.0	57

### Verification and validation

The material properties were taken from Granta CES database and were deemed reliable. The values were compared to other sources<sup>40</sup>, which produced a small error deemed negligible and so assumption **M.A.2** is verified. Some of the values from both sources have been given in Table 3.32 The materials chosen can all withstand the requirement pressures and temperatures plus a small margin of error, therefore able to withstand a unexpected increase if it occurs. **M.A.1** is also verified.

**Requirement verification** Here, the requirements of the materials are verified based on what was complete during this section.

- **KUMO-MAT-02** The materials have been chosen to hold pressure, specifically the gas sealant layer and the mechanical loading layer.
- **KUMO-MAT-03** was checked by looking into research papers which clarified if it was possible for the materials chosen to withstand 60 days in Venus.
- **KUMO-MAT-05** a and b were both fulfilled by using high fatigue strength materials and materials with high service temperatures.
- **KUMO-MAT-06** was checked by looking at materials which are able to withstand such temperatures, which they were.
- **UMO-MAT-07** is checked as it is addressed in the production plan in Chapter 7. is checked as it is addressed in the production plan in Chapter 7.

### Risk assessment

This subsection introduces the risks for materials as presented in Table 3.33. The risks from materials are largely based on the mission duration. As the Kumo mission has a mission duration of 60 days, the likelihood of material degradation is high. Most previous mission have only lasted a numbers of hours to a number of days. Therefore, resistance to the environment for a long period of time is a large area of concern for the mission success. Due to this, a number of risks aside in the performance of the materials.

<sup>40</sup><https://www.azom.com/article.aspx?ArticleID=6650>,retrieved on 23/06/2021

**Table 3.33:** Table showing possible risks, their severity and likelihood for materials

<p><b>6a-1:</b> <i>Materials eroding due to acidic atmosphere of Venus.</i></p> <p><b>Assessment L4S4:</b> The Venus atmosphere is very acidic, and the materials will be exposed to it for a prolonged period of time. Also it will be first time a probe will be flying for this long (60 days) in the Venus atmosphere so acid degradation is a risk</p> <p><b>Mitigation L2S2:</b> (1) A non-erosive material should be considered for areas that will be exposed. (2) Acid tests can be done to check which material is the least reactive. (3) Additional coatings should be considered for additional protection.</p>
<p><b>6b-1:</b> <i>Materials piercing due to high pressures.</i></p> <p><b>Assessment L3S5:</b> The pressure generated due to the buoyancy components of the platform, as well as the altitude differences, could cause failure in the structure. This is moderately likely to happen but would be catastrophic if it does.</p> <p><b>Mitigation L2S2:</b> (1) Materials chosen should have a high yield stress. (2) Inflation and pressure tests should be performed on the inflatable structure.</p>
<p><b>6c-1:</b> <i>Delamination of materials when exposed to atmosphere for prolonged periods.</i></p> <p><b>Assessment L3S4:</b> The platform will have multiple layers of materials. If the layers are not well attached, this could cause a structural failure such as gas leaks, corrosion and bursting. However, the likelihood of this is moderate, but would cause critical damage.</p> <p><b>Mitigation L2S4:</b> (1) Complete material layering should be well applied and tested before installation. (2) Allow for a margin of error with thickness of complete material layering.</p>
<p><b>6d-1</b> <i>Leakage of the lighter-than-air gas through the inflatable material.</i></p> <p><b>Assessment L3S3 :</b> Due to the relative small size of lighter-than-air molecules, there is a moderate likelihood that they could diffuse through the balloon material. This could interfere with the measurement of these gases in the atmosphere and to a decrease in lift capabilities and given the expect size of the leakage the impact is expected to be noticeable.</p> <p><b>Mitigation L3S3 :</b> 1) Apply gas-tight material with extra caution at joints. (2) Test for leaks through inflation tests</p>

### Sustainability analysis

The sustainability rating of the materials subsystem primarily depends on the life-cycle assessment of the materials selected. As such, a total of four materials have been selected for probe design: Mylar, Vectran, PTFE and Aluminium.

The environmental impact of the primary production and processing phases have been summarised in Table 3.34. The total material impact in terms of  $CO_2$  footprint as well as the total embodied energy is lower than that for a typical production of a car, which emits 17 t of  $CO_{2eq}$ <sup>41</sup> and entails 58,520 MJ of embodied energy (Sato and Nakata, 2020).

Furthermore, none of the used materials are toxic or dangerous for humans. Of the ten largest producers of the metal, only four are located in China and India with the remaining six stationed in countries with higher spots in the ITUT Global Rights Index, which measures the number of violations of internationally recognised collective labour rights<sup>42, 43</sup>.

Mylar is a common plastic produced around the world, thus minimising emissions resulting from transportation. Mylar is a bi-axially layered PET material, which is typically considered unsustainable around the world. However, considering the frequency of deep space missions, the cumulative environmental impact is incomparable to the volumes used on the daily basis on Earth.

Vectran is a Japanese trademark for a type of liquid-crystal polymer (LCP), primarily produced in Japan<sup>44</sup>. As such the social sustainability mark is high because of Japan's high placement in the ITUT Global Rights Index. However, the transportation distance to the US is large, adding up to the transportation emissions of greenhouse gases.

Aramid is a heat resistant and strong synthetic fibre. It is commonly used in aerospace and military application for reinforcing structures. It is expensive to make as it involves a chemical process to make the polymer into a thread. Therefore, a lot of water is needed in the production process.

Lastly, the water requirement for the production and initial processing of the materials for the probe is 52.2001. It is significant and thus shall be replenished using water offset programs for a negligible cost in comparison with the mission budget (Hoekstra, 2008).

To conclude, the sustainability of the structures and materials subsystem is quite high. Although, on their own the materials may not be considered sustainable with respect to every-day use, the quantity of the materials used is incomparable to any industrial standards. Using 14.7 kg of PET with the frequency of space launches, for example, can be labelled negligible. Additionally, the materials used are relatively easy to produce. Unlike high-performance reinforced polymers, which require heavy machinery and durable temperature control for manufacturing, materials that are used for Tori are either common and mass-produced or required in very little quantities. Finally, participating in the water offset program will reduce the mission's environmental impact even further. For the above mentioned reasons, a "reasonable" score of (2) is given for the Earth operations phase ( $SP_1$ ), a "high" score of (3) for the interplanetary phase ( $SP_2$ ) and again a "high" score of (3) for the Venus operations phase ( $SP_3$ ).

<sup>41</sup><https://www.theguardian.com/environment/green-living-blog/2010/sep/23/carbon-footprint-new-car>, retrieved on 18-06-21

<sup>42</sup><https://www.thoughtco.com/the-10-biggest-aluminum-producers-2339724>, retrieved on 18-06-21

<sup>43</sup><https://www.ituc-csi.org/IMG/pdf/ituc-global-rights-index-2018-en-final-2.pdf>, retrieved on 18-06-21

<sup>44</sup><https://www.kuraray.com/news/2007/070122>, retrieved on 18-06-2021

**Table 3.34:** Environmental impact of materials

Material	Mass [kg]	Embodied energy [MJ]	CO <sub>2</sub> [kg]	Water [l]
Mylar	10.30	1,052	50.11	-
Vectran	41.01	10,450	737.8	-
PTFE	32.20	10,780	606.4	15,460
Aluminium 7050	49.10	17,110	1015	36,770
Aramid	15.62	1,200	101	-
<b>Total</b>	<b>148.2</b>	<b>70,592</b>	<b>2510</b>	<b>52,200</b>

**Table 3.35:** Requirements for structures

Identifier	Requirement	Check
KUMO-STR-01	The complete structure with subsystems shall not exceed a mass of 180 kg.	✓
KUMO-STR-02	The structure as placed in entry vehicle shall have maximum dimensions of 3 m x 3 m x 3 m	✓
KUMO-STR-03	The structure shall resist temperatures within the range of 245 K and 307 K.	✓
KUMO-STR-04	The structure shall withstand internal stresses of 40.000 Pa.	✓
KUMO-STR-05	The structure shall be able to withstand launch frequencies of 35 Hz.	✓
KUMO-STR-07	The structure shall be able to withstand launch loads.	✓
KUMO-STR-08	The structure shall be able to withstand entry loads of 92g.	✓
KUMO-STR-09	The structure shall contain the payload.	✓
KUMO-STR-10	The structure shall be produced using current production methods.	✓
KUMO-STR-11	The structure shall not compromise safety of personnel during production.	✓
KUMO-STR-12	The structure shall be tested with non-destructive testing methods.	✓

### 3.6.2. Structures

In this section the structures are described. The requirements are first given, followed by an explanation of the configuration inside the probe and a structural analysis. The structural analysis consists of shear stress analysis and frequency analysis to check that the requirements are met. The thickness of the materials are also determined here and a number of different characteristics such as the moments of inertia and centre of mass are also found. Python was used to find such values, therefore a verification and a validation is also mentioned within this section. Finally, to conclude this section of structures, the sustainability and risks are assessed.

In Table 3.35, the requirements for the structure of the probe is given. The structure will hold the payload of the mission as well resisting the loads felt during launch, entry and flight. KUMO-STR-01 and KUMO-STR-02 are a result of minimising the mass and size of the structures for the sake of being able to fit inside of the entry vehicle and the launch vehicle. Falcon 9, the launch vehicle can carry a mass of 5.5 tonnes and the entry vehicle can hold a structure of 3 x 3 x 3 m. KUMO-STR-04 is similar to the requirement written in Section 3.6.1 and KUMO-STR-05 was based on the maximum felt frequency inside of the launch vehicle so Tori should be able to withstand this without any damage.<sup>45</sup> KUMO-STR-08 was found by looking at the loads the entry vehicle will feel.

#### Assumptions

In combination to using the requirements, as given in Table 3.35, a number of assumptions were also used to aid the design process. These have been listed below and will be evaluated in the verification and validation section.

**S.A.1** The probes inflatable body will be considered as 16 smaller sections as separated by the Aramid fibres.

**S.A.2** The pressure that the inflatable body must withstand will be fully felt by the mechanical load layer.

**S.A.3** The material layers can be considered as idealised booms when calculating moments of inertia and shear.

**S.A.4** The structure will be assumed infinite when considering hole stress concentration.

**S.A.5** Mylar and Teflon will be 12.5% of the thickness of Vectran.

#### Thickness of the structure

The design values given in Section 3.6.1 were used to find the thickness of the materials found on inflatable structure. This was done by applying Eq. (3.25) and rearranging it for thickness( $t$ ).  $\Delta p$  is the maximum pressure difference, taken from Table 3.29 and  $\sigma$  is yield stress of the materials used. During flight, the inflatable body should not stretch or deform significantly to minimise flapping and drag. Therefore, the yield stress was chosen for the calculations.  $r$  was taken to be the assumed radius of each section of the wing when inflated. Assumption S.A.1 and S.A.2 were used here to simplify this calculation. As mentioned in Fig. 3.6.1, Vectran was chosen as the layer which holds the mechanical loads during flight. As a result, the yield stress of Vectran was applied and a thickness was found. From this value, the thickness of Mylar, Teflon and Aramid were also done by assuming a thickness ratio. As a result of S.A.1, which assuming small areas along

<sup>45</sup>[https://www.spacex.com/media/falcon\\_users\\_guide\\_042020.pdf](https://www.spacex.com/media/falcon_users_guide_042020.pdf), retrieved on 21/06/2021

**Table 3.36:** Thickness, mass and cost of the materials

Material	Thickness [mm]	Mass [kg]	Cost [€]
Mylar film	0.02	10.3	433
Vectran	0.05	41.00	1234
PTFE	0.02	32.2	433.3
Aramid fibre	0.08	26.0	399.6
Aluminium 7050	0.13	49.1	98.7

**Figure 3.20:** Slice view of rigid structure

the cross section area and span, the Aramid layer was taken to be the same thickness as Vectran. Teflon and Mylar were then sized based on S.A.5 as 12.5% of the thickness of Vectran.

$$\sigma = \frac{\Delta pr}{t} \quad (3.25)$$

To calculate the thickness of the rigid structure, the composition of the structure was first assumed. three shelves, equally spaced are to be placed inside the rigid structure, 525 mm between each shelf. Each shelf must carry the payload of the mission as well be able to withstand flight loads. The payload was assumed to be a point load on each shelf and the width of the section was decided upon based on the space the payload needed to operate in. Therefore, the width of the rigid structure was chosen to be 2m, the depth was chosen to be 10% of the root chord, which was 600 mm, and finally the height was a result of the chosen depth and was given to be 2100 mm. Now the dimensions were determined, the thickness could be chosen based on the forces the rigid structure had to carry. The forces included, the payload mass, wind speed forces and pressure forces. This all considered,  $\sigma = \frac{F}{A}$  was used, where A is the cross sectional area (width by thickness), F being the force applied to the rigid structure and  $\sigma$  being the yield strength of the rigid material. This equation was rearranged for t and the thickness was found. Initially, the thickness was calculated to be quite thick and therefore increasing the mass of the structure, so stiffeners are also added to the shelves to reduce thickness but to maintain stiffness.

Once the thickness of the materials were found, the mass and the cost could be calculated. The mass was found by using the density of the relevant materials and the surface area of Tori. Then, a cost per kg value was used for each material to find the total cost<sup>46</sup>. These values are given in Table 3.36. It should be noted that the stiffeners are added to the thickness of the aluminium in Table 3.36 and so in practice is 0.1 mm with 0.03mm added as stiffeners.

### Structural configuration

Tori is hollow apart from the aramid webs to hold the shape and the rigid structure which contains the payload for the mission. On the outside, the antenna and propellers are the only two components being exposed to the environment. The propeller is attached to an arm to increase the height of the propeller. This way there will be little to no obstruction due to the body and the propeller efficiency is increased. Both the propellers and the antenna will be retractable so to be able to fit inside the entry vehicle.

The layout of the payload can be seen in Fig. 3.20. As mentioned previously, there will be three shelves installed inside of the rigid structure. To maintain stability, the payload is placed in a way that is close to symmetric over all three axis'. The payloads are installed as follows. The middle shelf hold the 3 scientific instruments, shown in red. This being the UVI, the MASPEX and the Nephelometer. In addition to this, the PCU and PDU are also placed here along with the battery shown in black. The top shelf contains the sensors, in blue, this includes the sun sensors and the laser sensors as well as two motors for each propeller, shown in yellow and the IMU in the centre shown in white. Lastly, the bottom shelf contains the second IMU, placed in the centre and another two motors for the bottom two propellers.

<sup>46</sup><https://markets.businessinsider.com/commodities/aluminum-price>, retrieved on 10/06/2021



Figure 3.21: complete structure of Tori

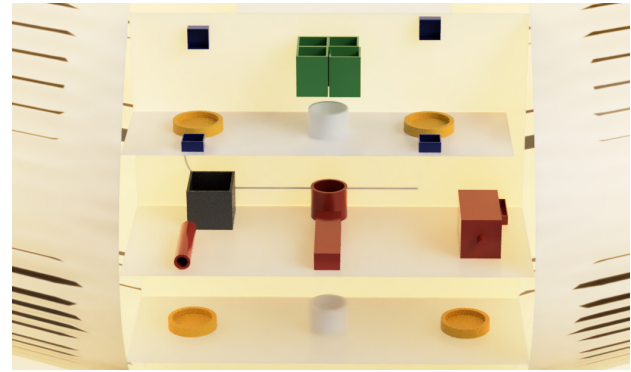


Figure 3.22: Open front view

Table 3.37: Probe components, dimensions, mass, and quantity

Component	Dimensions [mm]	Mass [kg]	Quantity
UVI	99x206x376 220x220x50	4.1	1
Nephelometer	D:88x165 508x89x127	4.4	1
MASPEX	400x40	8	1
Solar panel	3000x3000	95.7	46
Propellers	R:950	52.2	4
PCU	540x520x180	24.4	1
PDU	425x285x160	12.3	1
Battery	360x360	40.0	1
Motor	D:250x51x194	17.9	4
Antenna (HGA)	D:3100x600	3.15	1
Antenna (LGA)	914x100	0.04	1
IMU	198x132	4.1	2
Sun sensors	108x108x52.5	0.38	4
Laser sensors	155x156	3.79	4
Pressure sensors	100x10	0.03	3

The list of the main components is given in Table 3.37 and an open section is shown in Fig. 3.22. In addition to the list, thermal pipes, joints and hinges are also part of the structure. With this configuration, the production plan can be orchestrated. The production plan can be found in Chapter 7.

### Structural analysis

It is important to verify that the requirements of Tori have been met. For that purpose, the structure of Tori has been analysed in a number of ways. The centre of mass was found as well as the mass moment of inertia, which was calculated using an iterative code that took into consideration the airfoil dimensions and thickness of the materials as well as the point loads applied to Tori. A shear stress analysis was also done followed by a cutout analysis of the windows which highlight any stress concentrations and finally, a frequency and displacement analysis was done to better understand the behavior of Tori during flight.

**Centre of mass** To begin, the centre of mass was found by using Eq. (3.26) for  $x$ ,  $y$ , and  $z$ . The structural mass of Tori as well as the payload were all considered to find the values. The axis is placed at the nose of Tori with X-axis going from the leading edge to the tail of the wing, Y-axis going from the root to the tip of the wing and Z-axis going up. The values were found to be  $x = 9972$  mm,  $y = 3$  mm and  $z = 1166$  mm. The X-axis makes sense as most of the mass is concentrated at the nose of Tori. The Y value is nearly zero indicating a close symmetry around this axis. The z axis is high due to the vertical tail and the solar panels placed on the top skin.

$$\bar{x} = \frac{\sum \bar{x} \cdot m}{m} \quad (3.26)$$

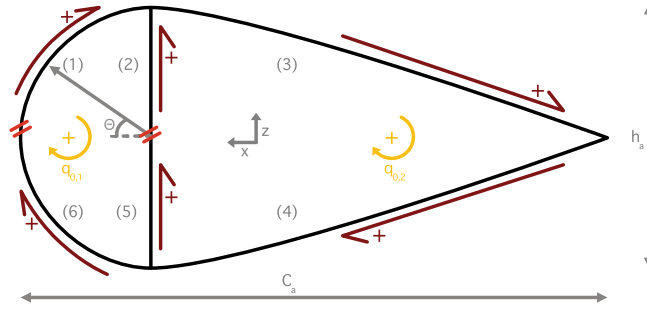


Figure 3.23: airfoil cross section

**Moments of inertia** The values of the centre of mass were used to find the moments of inertia. These were found using a python script as well as being verified on a CAD program which looked at the structure including payloads components. The values are given in Table 3.38. The code took the airfoil type of the wing and applied an idealisation by assuming point masses, or booms, at different points along the circumference of the wing. This was done all across Tori to find the values in Table 3.38.

Table 3.38: Values for mass moments of inertia

Mass moments of inertia	Value [kg mm <sup>2</sup> ]
$I_{xx}$	15570
$I_{yy}$	23420
$I_{zz}$	3513
$I_{xy} = I_{yx}$	54.93
$I_{xz} = I_{zx}$	1226
$I_{yz} = I_{zy}$	3.152

**Shear stress** With the use of the centre of mass and the mass moments of inertia previously calculated, a shear distribution was performed. For this, it was assumed that only the outer skin would carry the shear stress. Webs within the inflatable body were ignored as these webs were assumed to be made out of a relatively thin material. The shelves within the rigid part were also ignored for the shear stress calculations as its only purpose is to support the components located in the rigid structure. Therefore, the structure evaluated is seen in Fig. 3.23. Furthermore, the structure is assumed to be symmetrical. By applying this assumption, only the moments of inertia  $I_{xx}$  and  $I_{zz}$  have to be considered.

To calculate the shear stress, the structure was cut in two different places on its symmetry line, dividing the structures into six parts as seen in Fig. 3.23. For each of the six parts, the shear stress has been calculated in two different ways. First, it was calculated using the analytical approach. Second, it was calculated using the numerical approach, which will be used to verify the procedure. The equations for the analytical<sup>47</sup> as well as the numerical model used, are shown respectively:

$$q_b(s) = \frac{-V_z}{I_{xx}} \int_s tz ds + \frac{-V_x}{I_{zz}} \int_s ty ds + q_{b0} \quad (3.27)$$

Where  $V_y$  and  $V_z$  are unit shear flows, in this case set to -1. The thickness and analysed length are indicated by  $t$ , and  $z$  or  $y$  respectively.  $I_{zz}$  and  $I_{yy}$  indicate the moments of inertia. Finally,  $s$  denotes the to be considered interval.

$$q_b(s) \approx \frac{-V_z}{I_{xx}} \sum_{j=0}^{j_{max}} t(j\Delta s)y(j\Delta s)\Delta s + q_{b0} - \frac{V_x}{I_{zz}} \sum_{j=0}^{j_{max}} t(j\Delta s)z(j\Delta s)\Delta s + q_{b0} \quad (3.28)$$

This equation is also known as the Riemann Sum, where the step size  $\Delta s = 0.01 \cdot h_a$  and the resulting error in each integration step  $\approx O(\Delta s)$ . Also,  $q_b(s) = q_b(j_{max}) \cdot \Delta s$  where  $j_{max} = integer(s/\Delta s)$ . The redundant shear flow,  $q_{s0,i}$ , is calculated with the following equation:

$$q_{s0,i} = \frac{\oint_{cell_i} (q_b(s)/t(s)) ds}{\oint_{cell_i} ds/t} \quad (3.29)$$

By splitting this in a contribution to the previous defined base shear flows along with the to be calculated redundant shear flow, this results in a matrix equation of the following form:

$$[\mathbf{A}] \cdot [\mathbf{q}] = -[\mathbf{b}] \quad (3.30)$$

<sup>47</sup> AE2135-I: Structural Analysis & Design, "Shear of thin-walled sections"

**Table 3.39:** Vertical shear flow

Part	Function	Range	Step	Contribution
$q_{b_1}$	$y = h_a/2\cos(\theta)$	$0 < y < \theta/2$	$\Delta s = h_a/2\Delta\theta$	none
$q_{b_2}$	$y = y$	$0 < y, h_a/2$	$\Delta s = \Delta y$	none
$q_{b_3}$	$y = \frac{h_a/2 - h_a s}{2l_{sk}}$	$0 < s < l_{sk}$	$\Delta s = \Delta s$	$q_{b_1}(\pi/2)$ and $q_{b_2}(h_a/2)$
$q_{b_4}$	$y = \frac{-h_a/2s}{sl_{sk}}$	$0 < s < l_{sk}$	$\Delta s = \Delta s$	$q_{b_3}(l_{sk})$
$q_{b_5}$	$y = y$	$-h_a/2 < y < 0$	$\Delta s = -\Delta y$	none
$q_{b_6}$	$y = h_a/2\cos(\theta)$	$-\pi/2 < \theta < 0$	$\Delta s = h_a/2\Delta\theta$	$q_{b_4}(l_{sk})$ and $q_{b_5}(-h_a/2)$

**Table 3.40:** Horizontal shear flow

Part	Function	Range	Step	Contribution
$q_{b_1}$	$z = -(1 - \cos(\theta)) * h_a/2 - \tilde{z}$	$0 < \theta < \pi/2$	$\Delta s = h_a/2\Delta\theta$	none
$q_{b_2}$	$z = -h_a/2 - \tilde{z}$	$0 < y < h_a/2$	$\Delta s = \Delta y$	none
$q_{b_3}$	$z = (-h_a/2 - z) - (c_a - h_a/2)/l_{sk}s$	$\Delta s = \Delta s$	$q_{b_1}(\pi/2)$ and $q_{b_2}(h_a/2)$	
$q_{b_4}$	$z = (-c_a - z) + (c_a - h_a/2)/l_{sk}s$	$0 < s < l_{sk}$	$\Delta s = \Delta s$	$q_{b_3}(l_{sk})$
$q_{b_5}$	$z = -h_a/2 - \tilde{z}$	$-h_a/2 < y < 0$	$\Delta s = -\Delta y$	none
$q_{b_6}$	$z = -(1 - \cos(\theta)) * h_a/2 - \tilde{z}$	$-\pi/2 < \theta < 0$	$\Delta s = h_a/2\Delta\theta$	$q_{b_4}(l_{sk})$

and  $q_{b_5}(-h_a/2)$

where  $\mathbf{A}$  is a 2x2 matrix that equals the denominator of Eq. (3.29),  $\mathbf{q}$  is a 2x1 matrix, which contains the redundant shear flow of both the rigid and inflatable part of the airfoil cross section and  $\mathbf{b}$  is a 2x1 matrix, which equals the nominator of Eq. (3.29). The  $b$  matrix is solved with the following equation for the numerical method:

$$\int_s q_b(s) \approx \frac{-V_z}{I_{xx}} \sum_{k=0}^{k_{max}} \left( \sum_{j=0}^k t(j\Delta s) \cdot y(j\Delta s) \Delta s \right) \Delta s + q_{b_0} - \frac{V_x}{I_{zz}} \sum_{k=0}^{k_{max}} \left( \sum_{j=0}^k t(j\Delta s) \cdot z(j\Delta s) \Delta s \right) \Delta s + q_{b_0} \quad (3.31)$$

The thickness is constant within the separate six sections, allowing to neglect the contribution of the thickness variations  $t(j\Delta s)$ .

First, the shear flow calculated only in the vertical direction,  $V_y$  where computed using this procedure. Here, the contribution by  $V_z$  were set to zero. Then, the reverse process was done to compute the shear stress distribution in the horizontal direction.

For the numerical analysis, the parameters used in Eq. (3.28) and in Eq. (3.31) for the vertical and horizontal shear flow were defined as seen in Table 3.39 and Table 3.40, respectively.

Here,  $h_a$  is the rigid spar length,  $c_a$  is the chord length,  $l_{sk}$  is the length of the skin, which equal to  $\sqrt{(h_a/2)^2 + (c_a - h_a/2)^2}$  and  $\tilde{z}$  is the distance to the z-coordinate of the centroid of the structure. The angle between the skin and the chord is given by Eq. (3.32).

$$\phi_{sk} = \arctan \left( \frac{h_a/2}{c_a - h_a/2} \right) \quad (3.32)$$

By computing these values, the shear distribution along the cross-section is computed for both the analytical and numerical model as seen in Fig. 3.24 and Fig. 3.25.

**Cutouts** A cut-out analysis was also done in the areas where window will be placed. There will be 4 windows with the diameters 88 mm, 40 mm, 50 mm, and 30 mm. These will be circular holes and will therefore need to be reinforced. S.A.4 will be used to assume there is infinite material as the holes are very small and the aluminium sheet is substantially larger than the holes. The given load case has a stress concentration factor of 3, which will thus be used to size the reinforcing sheets. A diameter of 100 mm around the holes will therefore be 0.15mm in thickness.

**Frequency and displacement analysis** To calculate the frequencies of the structure Eq. (3.35) was used (Thomas et al., 2018). The stiffness,  $k$ , must be found for a inflatable structure. For simplicity of calculations, the structure was assumed to be an inflatable beam. First Eq. (3.33) was used to find the stiffness of the beam where  $\phi_P$  is given in Eq. (3.34).  $E$  is the Youngs modulus of the beam, this was taken as the modulus of Vectran.  $I$  is the moments of inertia in the cross section,  $P$  is the load applied. This will be taken as 400N as a conservative estimate of the force from the propellers.  $S$  is the surface area of the beam,  $l_0$  is the length of the beam,  $G$  is the shear modulus of the beam and  $\rho$  is the density of the material. Finally,  $n$  is the number of supports the beam has. For this analysis a value of 2 was used. Using values which assume Tori is a circular beam, a stiffness of 4554 GPa and a frequency of 3.335 Hz was found. Therefore, it can be concluded that the beam is stiff enough as it is lower than **KUMO-STR-05** which is the value that Tori must be below

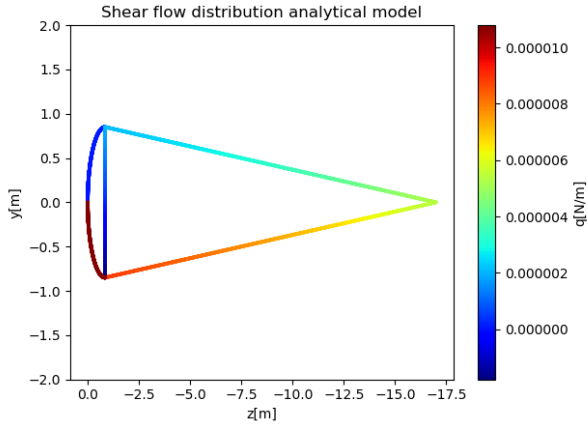


Figure 3.24: Analytical shear distribution

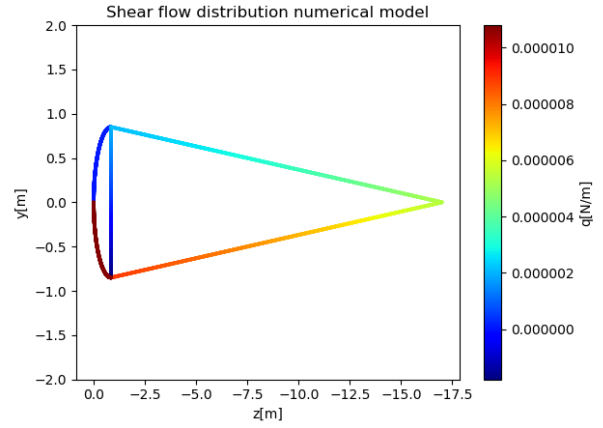


Figure 3.25: Numerical shear stress distribution

to safely be added to the launch vehicle. In the future, it would be useful to do a frequency analysis with the shape of the probe taken into consideration.

$$[K] = \frac{\left(EI_0 + \frac{PI_0}{S_0}\right)}{\ell_0^3 (1 + \phi_p)} \begin{bmatrix} 12 & 6\ell_0 & -12 & 6\ell_0 \\ \ell_0^2 (4 + \phi_p) & -6\ell_0 & \ell_0^2 (2 - \phi_p) & \\ sym & 12 & -6\ell_0 & \\ & & \ell_0^2 (4 + \phi_p) & \end{bmatrix} \quad (3.33)$$

$$\phi_p = \frac{12 \left(EI_0 + \frac{PI_0}{S_0}\right)}{(P + kGS_0) \ell_0^2} \quad (3.34)$$

$$\omega_n = \sqrt{\frac{n^4 \pi^4}{\frac{\rho_0 S_0 l^4}{EI + \frac{PI}{S}} + \frac{\rho_0 S_0 n^2 \pi^2 l^2}{P + kGS}}} \quad (3.35)$$

Fusion 360 was also used to show the areas of largest displacement when a frequency was applied. The purpose of this is to show the areas most prone to movement and therefore in the next round of design should be reinforced. Due to the complexity of the program, a simplified version of the probe was analysed and a frequency of 4 Hz was applied. The natural frequency could not be applied as the program had pre-programmed values, however this was the closest to its natural frequency. As shown in Fig. 3.26, the colours show the amount of displacement of the materials. The dark blue shows little movement while the more red shows a lot of movement. As can be seen, the large panels show the most movement as there is little to no reinforcement there.

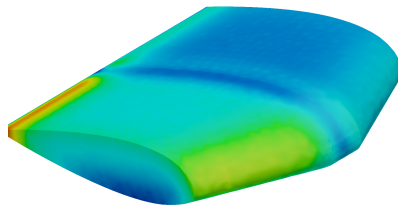


Figure 3.26: Colour mapped wing showing the displacement due to the applied oscillation

### Verification and validation

This section describes the verification and validation procedures performed for the structural components of Tori. First, the numerical model created for the structures is explained followed by requirement verification and product verification validation.

### Model verification

Here, the codes created for structures is verified. A table and a flow chart for each code is added to show the organisation of the code as well as to keep track of unit tests completed.

**Thickness:** The materials thickness code is described in Fig. 3.27. This method of finding the thickness from stress was inspired from one paper which assumed the airfoil was a hoop(Wang and Li, 2017), in combination with another which took hoop stress to find the thickness(Breukels and Ockels, 2008). The model in these papers are similar in purpose to allow for the application here.

**MOI** The values of mass moments of inertia were verified by using Fusion 360. The code structure is given in Fig. 3.28. The values were within the uncertainty margin and were therefore verified. The method of using idealisations were taken from a paper which shows how this method can gives values accurate with less than 8% difference on average(Mutluay, 2015). This error is small enough to verify the use of the method for this purpose. The unit test are described in Table 3.41.

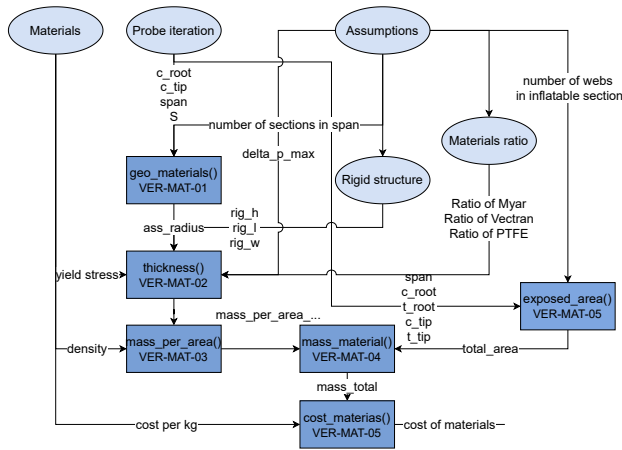


Figure 3.27: Code structure of materials

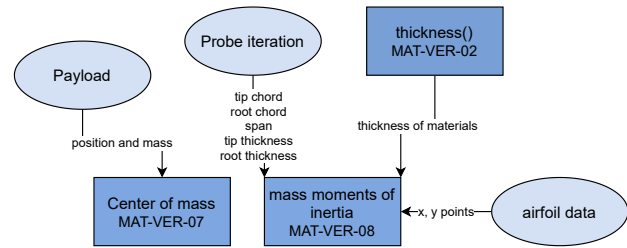


Figure 3.28: code structure to find mass moments of inertia

Table 3.41: Unit tests for structures

Test	Variables	Expected outcome	Verified
VER-MAT-01	<b>Input:</b> n_spansec, c_root,c_tip,span,S <b>Output:</b> ass_radius	Setting inputs to 0 should give a zero error.	✓
VER-MAT-02	<b>Input:</b> ass_radius, rig_h, rig_l, rig_w, y_stress <b>Output:</b> t_materials	By doubling stresses, the output should halve.	✓
VER-MAT-03	<b>Input:</b> t_materials, density_materials <b>Output:</b> materials mass per area	Doubling input should double the output	✓
VER-MAT-04	<b>Input:</b> materials mass per area, total area <b>Output:</b> total material mass	Doubling input should double the output	✓
VER-MAT-05	<b>Input:</b> n_websec, span, c_root, c_tip, t_root, t_tip <b>Output:</b> total_area	Increasing span should increase exposed area	✓
VER-MAT-06	<b>Input:</b> mass_total, cost_per_kg <b>Output:</b> cost_materials	Doubling input should double output	✓
VER-MAT-07	<b>Input:</b> position and mass of payload <b>Output:</b> Centre of mass x and y	Increasing distance from axis should increase centre of mass value	✓
VER-MAT-08	<b>Input:</b> com_x, com_y,t_tip,t_root,c_tip,c_root, span,t_(materials) x and y of airfoil <b>Output:</b> Ixx, Iyy, Izz, Ixy, Izx, Iyx, Iyz, Izx, Izy	Increasing mass by 2 of all masses should double the values	✓

**Shear distribution** For the shear stress, a numerical model as well as an analytical model was made to verify the outcomes. The code contains several functions where the equations for both the numerical and analytical model were constantly placed below each other. The outputs and error margin were then compared. A flow of the code is seen in Fig. 3.29.

Table 3.42: Unit tests for structures

Test	Variables	Expected outcome	Verified
VER-SHE-01	<b>Input:</b> $\theta, y, s$ <b>Output:</b> base shear flows in x-direction $qb1V_x, qb2V_x, qb3V_x, qb4V_x, qb5V_x, qb6V_x$	For all shear flows, both the output computed in the numerical as well as in the analytical model should be equal.	✓
VER-SHE-02	<b>Input:</b> theta, y, s <b>Output:</b> Base shear flows in z-direction. $qb1V_z, qb2V_z, qb3V_z, qb4V_z, qb5V_z, qb6V_z$	By doubling stresses, the output should halve.	✓
VER-SHE-03	<b>Input:</b> base shear flows in z-direction, theta, s, y <b>Output:</b> integrated shear flows in z-direction, redundant shear flow $qs0,1$ and $qs0,2$	For all shear flows, both the output computed in the numerical as well as in the analytical model should be equal.	✓
VER-SHE-04	<b>Input:</b> base shear flows <b>Output:</b> total shear flow in z-direction	For all integrals, both the output computed in the numerical as well as in the analytical model should be equal. Also, the redundant shear flows should be the same.	✓
VER-SHE-05	<b>Input:</b> total shear flow z- and y-direction <b>Output:</b> total shear flows	Total shear flow should be equal for numerical and analytical outputs.	✓
VER-SHE-06	<b>Input:</b> total shear flows <b>Output:</b> shear distribution diagrams	Both diagrams should be equal.	✓

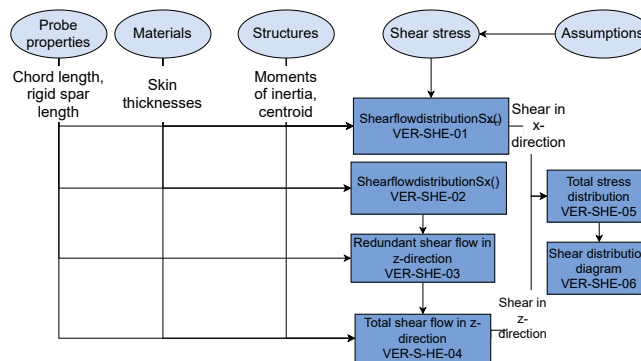


Figure 3.29: Code for the shear distribution

The exact values for the final shear flows in each of the six sections is seen in Table 3.43. Here, the values of the outcomes of both the numerical and numerical model are given as well as the absolute errors between them. As is shown, the absolute error give a significant small difference between the outcomes, which concludes that the total shear flows have been verified.

Since the total shear flow depend on the base shear flow in the x-direction, the base shear flow in the z-direction and the redundant shear flows, it can be assumed that these intermediate steps are correct and verified as well. To be certain that the outputs for the intermediate steps are equal, the values in the program have been printed and compared as well as verified by hand.

Table 3.43: Shear flow results

Components	Analytical	Numerical	Absolute error [%]
$q_1$	1.5128e-07	1.5121e-07	7.8859e-09
$q_2$	1.9691e-06	1.9669e-06	2.1961e-07
$q_3$	5.3517e-06	5.3496e-06	2.1166e-07
$q_4$	8.8815e-06	8.8765e-06	5.1115e-07
$q_5$	-1.7861e-06	-1.7842e-06	1.9425e-07
$q_6$	1.0797e-05	1.0789e-5	7.0686e-07

**Assumption verification S.A.1** This assumption was used in Section 3.6.2. This can be verified by VER-MAT-01 where the number of sections is implemented. The purpose of this assumption was to reduce the thickness by allowing the aramid

to act as reinforcement. When the number of sections is reduced to 1, the thickness increases. The total envelope thickness goes from 0.08mm to 0.24mm which is a 3x increase in thickness.

**S.A.2** This assumption assumes the Vectran will be the only layer to hold the pressure forces of Tori. Vectran makes up 75% of the materials in the outer layers with both Mylar and PTFE making up the other 25%. Therefore it can be concluded Vectran will in fact take up most of the forces.

**S.A.3** The booms assume all the mass is concentrated in the parameter of the probe. The material is nearly constant except for the rigid structure. The volume of the rigid section is only 5% of the total value. Therefore, it is reasonable to assume booms for moments of inertia.

**S.A.4** The holes made in the structure are considerably smaller than the total surface area of the probe, making this assumption valid. The largest hole is 88mm and the shortest dimension of the rigid is 2000mm. This only makes up 4.4% of the panel. This is deemed small enough to verify the assumption.

**S.A.5** The material thickness is relatively thin as it is inflatable on top of this a majority is the Vectran layer. The Mylar which is the gas sealant layer is also very thin and only purpose is to hold the gas so a percentage of 12.5% is reasonable. Same holds for Teflon which will be sprayed on so is assumed to be thin.

### Product verification and validation

Once the whole structure is complete there are a number of tests that can be done physically on the model once it has been constructed.

- **Frequency tests:** Although a numerical frequency test has been complete, a physical vibrations tests can confirm if the structure has been constructed correctly. The probe shall be placed on a rig which is then subject to multiple frequencies expected during the mission as indicated in the requirements.
- **Environment tests:** This test can confirm if the probe can survive in the the atmospheric conditions. Although much thought was put into what the materials must be able to withstand, this will highlight any unknowns. This includes acidity, temperature.
- **Inflation checks:** The probe shall be inflated and deflated to check for gas leaks and pressurisation problems.
- **Wind tunnel testing:** Although mainly used to tests the aerodynamics of the airfoil, it can also act as a check to see the behaviour of the inflatable body in high winds. This will be done by placing the body in a wind tunnel and subjecting it to the wind velocities expected on Venus.

**Requirement verification** In this section, the requirement verification is shown. Each requirement has been met or proven by the choice of materials or a test which has been complete within the previous sections.

- **KUMO-STR-01** was checked as the mass of the structure is 148.1kg which is below the 180kg requirement.
- **KUMO-STR-02** was checked as the dimensions of the probe deflated will be 3 by 1.5 depth and 2.5 height which is below the 3m requirement.
- **KUMO-STR-03** was checked as the materials chosen can all withstand these temperature as described in Table 3.31.
- **KUMO-STR-04** was checked as 40,000Pa was used as the design pressure for the materials to be able to withstand.
- **KUMO-STR-05** was checked as a frequency analysis found the natural resonance at 3.35 Hz.
- **KUMO-STR-07** and **KUMO-STR-08** were used as a design forces for the probe to able to withstand so are checked.
- **KUMO-STR-09** was checked as it carries the payload.
- **KUMO-STR-10**, **KUMO-STR-11** and **KUMO-STR-12** are check as they are all considered in the production plan found in Chapter 7.

### Risk assessment

This subsection introduces the risks for the structures and materials department, as shown in Table 3.44. From the table, it can be concluded that all risks related to materials for the atmospheric probe have successfully been mitigated to a point were the severity of the consequences are no more than marginal.

**Table 3.44:** Table showing possible risks, their severity and likelihood for structures

<p><b>5a-1:</b> <i>Failure of structure due to failure modes - Crippling, buckling and torsion.</i></p> <p><b>Assessment L2S5:</b> The structure could fail due to these failure modes during operation. The failure of the structure in any way would jeopardise the mission itself. Therefore this is a catastrophic failure. The likelihood of this happening is low.</p> <p><b>Mitigation L1S4:</b> (1) Calculate crippling, buckling and torsional loads on the structure and design against it. This could be done by performing a sensitivity analysis. (2) Identify and reinforce areas which are prone to the failure.</p>
<p><b>5b-1 &amp; 5c-1 &amp; 1d-1</b> <i>Failure due to launch or entry loads</i></p> <p><b>Assessment L2S5 :</b> During the launch or entry the payload will be exposed to high loading conditions, damaging the structure and payload. As the entry vehicle protects against most of these conditions, there is still a low possibility for the payload to get damaged.</p> <p><b>Mitigation L2S4 :</b> (1) Calculate launch and entry loads with a 15% safety factor and design for them. (2) Test for entry loads scenarios with a 15% safety factor via simulation testing.</p>
<p><b>5d-1</b> <i>Failure due to deployment of probe</i></p> <p><b>Assessment L3S5 :</b> This could be a structural failure due to unchecked openings of the structure which could lead to failed deployment of the platform.</p> <p><b>Mitigation L2S2 :</b> (1) Test deployment mechanism before launch. (2) Check for loose probe section and make sure they are secure via inspection.</p>
<p><b>5e-1</b> <i>Payload incorrectly attached in the dynastat</i></p> <p><b>Assessment L3S5 :</b> If the payload is wrongly attached to the dynastat, the payload could start moving which will affect the stability of the dynastat and could also damage the inner material of the platform. This would be catastrophic as this could potentially lead to the platform crashing. The attachments are complex components which increases the risk of failing.</p> <p><b>Mitigation L2S5 :</b> The attachments should be tested to see if they survive the critical loads. Also a safety factor should be applied when attaching it to account redundancy. Wrapping the payload could also work to reduce the risk of the damage cause by eventual sharp corners of the payload.</p>

On top of the already mentioned risks, it could also be useful to have the 16 sections of the probe separated into airtight bubbles. That way, if one section of the probe was to burst, there would be the remaining bubbles to hold everything together. However, this is a large design change so would be a recommendation for future projects.

### Sustainability

The structure of the probe will be assembled in an area close to the launch site to reduce carbon emissions as well as sourcing all the materials from local hardware locations, which will further add to lessening of emissions. The structure is designed in a way to reduce the amount of materials which is needed, therefore there is less waste materials and also less work required to create the probe with less complex components. Reduced structure also adds to reduced mass of the probe. As the materials and structure are strongly intertwined, the scores from materials also apply to the structures. These being a “reasonable” score of (2) for the Earth operations phase ( $SP_1$ ), a “high” score of (3) for the interplanetary phase ( $SP_2$ ) and a “high” score of (3) for Venus operations phase ( $SP_3$ ).

The entire structure, including the subsystems within, will have to be stable during flight as crashes are not desired. Therefore, the stability of Tori as well as the aerodynamic aspects will be discussed as final aspect.

## 3.7. Aerodynamics and stability

This section defines the aerodynamics and stability of the probe, beginning by outlining the assumptions made in Section 3.7.1. Following this is an elaboration on the aerodynamic design of the probe in Section 3.7.2, split into sizing for buoyancy and sizing for dynamic lift. This is followed by a stability analysis in Section 3.7.3 and assumption verification in Section 3.7.4. Verification and validation of aerodynamic properties is presented in Section 3.7.4 and a sustainability analysis in Section 3.7.6.

### 3.7.1. Assumptions and definitions

For the ensuing calculations a number of assumptions have been made. Below you can find each assumption with its associated identifier. In Section 3.7.4 the assumptions will be justified.

- **A.A.1** The lifting gas is assumed to be an ideal, monoatomic gas at ambient temperature.
- **A.A.2** The volume of the wing is entirely filled with lifting gas.
- **A.A.3** Gravitational acceleration is assumed constant during atmospheric flight.

### 3.7.2. Aerodynamic design

In the following sections the relations used to size the aerodynamic aspects of the atmospheric probe are laid out. First the lifting gas volume of the probe is sized for full buoyancy at the lower altitude of 55 km. This volume is then shaped into

an aerodynamic flying wing-like blimp, giving the design dimensions and a power required to cruise at partial buoyancy at the upper altitude of 65 km.

### Sizing for buoyancy

The relation for buoyant lift is given by Eq. (3.36), as derived from the difference between the mass of the displaced air  $m_{air}$  and the mass of the lifting gas  $m_{gas}$ . This further relates to the volume of the lifting gas  $v_{gas}$ , the density of the air and lifting gas at 55 km,  $\rho_{air,55}$  and  $\rho_{gas}$ , respectively. By assuming equal temperatures in- and outside and applying the ideal gas law, the final equation is only a function of the ambient density and pressure  $p_{air}$ , the molar masses  $M_{air}$  and  $M_{gas}$  and the overpressure  $\Delta p$  of the inflatable structure.

$$L_{buoy} = m_{air}gV - m_{gas}gV = \rho_{air,55}v_{gas}gV \left(1 - \frac{\rho_{gas}}{\rho_{air,55}}\right) = \rho_{air,55}v_{gas}gV \left(1 - \frac{p_{gas}M_{gas}}{p_{air}M_{air}}\right) \quad (3.36)$$

Designing for neutral buoyancy of the probe at a given altitude implies that lift is equal to weight ( $L = W = m_{probe}gV$ ). Hence the buoyant gas volume necessary is given by:

$$v_{gas} = \frac{m_{probe}}{\rho_{air,55} \left(1 - \frac{p_{gas}M_{gas}}{p_{air}M_{air}}\right)} = 706 \text{ m}^3 \quad (3.37)$$

Where  $m_{probe} = 555 \text{ kg}$ ,  $p_{gas} = p_{air,65} + \Delta p_{max} = 40,000 \text{ Pa}$  from Section 3.6.1 and the VIRA model (Kliore et al., 1986). Finally  $M_{gas} = 4.00 \text{ g mol}^{-1}$  is the molecular weight of helium (Meija et al., 2016) and  $M_{air} = 43.45 \text{ g mol}^{-1}$  is the mean molecular weight of Venus' atmosphere<sup>48</sup>.

### Sizing for dynamic lifting flight

From the previously found lifting gas volume required to have neutral buoyancy at 55 km, the dimensions of the probe can be computed given the airfoil, aspect ratio, taper ratio, and leading edge sweep angle determined in Section 3.7.3 to ensure the stability of the probe during forward flight.

The gas volume contained within a trapezoidal wing can be obtained by integration of the airfoil's enclosed area over the span of the wing. From this integration, Eq. (3.38) is found, where  $\left(\frac{S_{encl}}{tc}\right)$  is the geometric property of the airfoil that relates the area enclosed to its bounding box,  $\left(\frac{t}{c}\right)$  is the maximum thickness to chord ratio (another geometric property of the airfoil),  $A$  is the aspect ratio of the wing and  $\lambda$  is the taper ratio. These geometric ratios allow expressing the volume inside the wing with ratios and only one physical dimension, in this case the root chord  $c_r$ . Inverting this relation for  $c_r$  allows finding the root chord dimension from a volume and shape and then derive the rest of the wing dimensions from the root chord through the geometrical shape parameters.

$$v_{gas} = \left(\frac{S_{encl}}{tc}\right) \left(\frac{t}{c}\right) A \left(\frac{1}{3} + \frac{2}{3}\lambda\right) c_r^3 \Rightarrow c_r = 17.1 \text{ m} \quad (3.38)$$

The next step was to find the most critical physical parameters. First of all, since the structural mass was expected to be significant for a large dynastat body, it was important to make sure that the surface area to enclosed volume ratio is minimised. Low surface area to volume ratio not only minimises the structural mass directly by having a lower area for the volume required for the lifting gas, but also minimises stress concentrations inside a pressurised vessel. For these reasons, the ideal aspect ratio might seem to be 1, as a square has the lowest surface area to volume ratio of all rectangles. However, because the thickness of the airfoil depends directly on the chord length, increasing chord length turned out to be more important than span. Over iterations, the ideal aspect ratio converged to 0.9.

Using the aspect ratio, other non-trivial parameters have been found. An estimation for the Oswald's efficiency factor was found from literature to only depend on the wing aspect ratio as a first order estimation (Obert and Slingerland, 2009):

$$e = \frac{1}{1.05 + 0.007\pi A} = 0.9348 \quad (3.39)$$

Aspect ratio can also be used together with the computed Oswald's efficiency factor  $e$  to compute the zero-lift drag coefficient  $C_{D,0}$  using the relations below<sup>49</sup>. The same source provides a range of values for equivalent skin-friction drag coefficient  $c_f$  of 0.003 to 0.007 for a twin-engine propeller aircraft. Identical values are given for a single-engine aircraft, thus for a wing with four propellers, the value is expected to stay approximately the same. A value of 0.003 was used for calculations, justified by the absence of the fuselage. Furthermore, the source provides the ratio of  $\frac{S_{wet}}{S}$  for flying wings of 2.2. The value was later then replaced with the exact ratio for the designed wing, which was 2.8.

$$k_E = \frac{1}{2} \sqrt{\frac{\pi e}{c_f}} = 15.64 \quad (3.40)$$

<sup>48</sup><https://nssdc.gsfc.nasa.gov/planetary/factsheet/venusfact.html>, retrieved on 28-06-2021

<sup>49</sup><https://www.fzt.haw-hamburg.de/pers/Scholz/materialFM1/DragEstimation.pdf>, retrieved on 22-06-21

$$E_{\max} = k_E \sqrt{\frac{A}{S_{wet}/S}} = 8.87 \quad (3.41)$$

$$C_{D,0} = \frac{\pi \cdot A \cdot e}{4 \cdot E_{\max}^2} = 0.0084 \quad (3.42)$$

At a latter stage of the design, it was argued that the zero lift drag estimation returned a value that is too optimistic. The value is comparable to some of the most drag-efficient fighter jets and thus could be based on erroneous assumptions. One source of error could result from the fact that the drag estimation method used exploits empirical relationships for seemingly commercial aircraft, which has a fuselage. On the other hand, it is merely a speculation as it is not reflected in the limitations of the source. Furthermore, the use of wetted surface area for the calculation of the maximum glide ratio  $E_{\max}$ , suggests some accountability for designs without a fuselage. Overall, a significant safety margin of 1 should be applied in the next design phase to account for the uncertainties in the limitations of the model as well as the interference of propellers.

Once the physical dimensions of the wing are known, the power required to fly at 65 km can be computed from the wing surface area  $S$ , wing performance parameters like the zero-lift drag coefficient  $C_{D,0}$ , Oswald efficiency factor  $e$  and aspect ratio  $A$  as calculated above, as well as the buoyancy ratio  $BR$  at 65 km. The latter can be calculated from the wing gas volume  $v_{gas}$ , total probe mass  $m_{probe}$ , lifting gas density  $\rho_{gas}$  and ambient density  $\rho_{air,65}$  at 65 km using Eq. (3.43), assuming that the wing envelope does not stretch significantly from the increased overpressure at higher altitude.

$$BR_{65} = \frac{v_{gas}(\rho_{air,65} - \rho_{gas})}{m_{probe}} = 0.0946 \quad (3.43)$$

For the most efficient flight, power is minimised when  $C_L = \sqrt{3C_{d,0}\pi Ae}$ , and thus  $C_D = 4C_{D,0}$  according to (Anderson, 2016). Flying at this  $C_L$  means that the probe will need to fly at a true airspeed for cruise given by Eq. (3.44). Accordingly, the power required for sustaining flight is given by Eq. (3.45).

$$V_{cruise} = \sqrt{\frac{2(1 - BR_{65})m_{probe}gV}{\rho_{air,65}SC_D}} = 25.9 \text{ m s}^{-1} \quad (3.44)$$

$$P_{r,sustain} = \frac{\rho_{air,65}}{2} V_{cruise}^3 SC_D = 14.4 \text{ kW} \quad (3.45)$$

On top of sustaining flight at the upper altitude, a power margin for a chosen rate of climb of  $4 \text{ m s}^{-1}$  is computed using Eq. (3.46) where  $ROC$  is the required rate of climb at 65 km. The choice of climb rate and its use as a performance margin, will be motivated in Section 3.8.5.

$$P_{r,climb} = m_{probe}(1 - BR_{65})gV ROC = 17.8 \text{ kW} \quad (3.46)$$

The output of these relations will serve as input for the sizing of the various subsystems during the iteration as will be described in Section 3.8.3. The final performance parameters will be computed and presented in Section 3.8.5 given the final probe sizing.

### 3.7.3. Stability

Determining stability of the probe is a complex process, which requires an iterative approach. First, a design is proposed with a set of design characteristics as defined by system engineers. The stability is then assessed for a given design. Changes to geometric parameters are then made if the design cannot be made stable. The iterations converged to the following stability-related properties: sweep angle -  $30^\circ$  and dihedral angle-  $9^\circ$ . Furthermore a vertical tail will be present at 80% of the chord with a taper ratio of 0.7 and a NACA0010 airfoil. Explanation of the entire iteration used to arrive at the mentioned values will be avoided, rather adherence to stability requirements of the final design will be proven. Note that any aspiration for traditional control surfaces have been abandoned, because of the flexibility of the structure.

Therefore, this section will describe the method used to ensure a stable system. Generally, determining the degree of stability of the dynamic probe system was approached in four phases. First, a fitting airfoil was selected. Next, Athena Vortex Lattice (AVL) software was utilised to compute the stability and body-axis derivatives, using the selected airfoil as input. Afterwards, missing or incorrect derivatives were re-calculated using relations from Mulder et. al. Finally, the same source was used to determine the eigenvalues of the symmetric and asymmetric cases and thus to prove the passive stability of the system.

### Airfoil selection

All airfoils have positive lift curve slopes in the operational range. This means that if the angle of attack is increased, the airfoil will generate more lift. This additional lift will act on the aerodynamic centre (a.c.) some distance away from the centre of gravity, thus generating a pitching moment. In order to achieve passive stability around the y-axis, the pitching moment must counteract the initial disturbance - the increase of the angle of attack. Therefore, the c.g. must always be located in front of the a.c., such that any disturbance of the angle of attack is counteracted, and not amplified by the changed lift.

This, however, means that to ensure longitudinal equilibrium with the absence of a horizontal tail, an airfoil with a positive moment coefficient at the aerodynamic centre shall be chosen. These airfoils are commonly known as reflex airfoils and five options were discovered in an airfoil database search<sup>50</sup>.

Furthermore, there are two additional objectives to airfoil selection. First, the ratio of the enclosed area to maximum thickness shall be maximised because it optimises the surface area to volume ratio for carrying the lifting gas. The thickness to chord ratio of airfoils may be altered to a degree without the loss of reflex property (W.A. Timmer, personal communication, June 3, 2021), which is why the most optimal shape is not the thickest one, but rather the most circle-resembling one. Secondly, because the c.g. had to be shifted as much forward as possible at the preliminary stage of the design, the airfoil with aft-most centre of area was selected to make sure the centre of buoyancy is as far aft as possible. Guided by the two objectives, NACA 22112 airfoil was selected.

The maximum thickness to chord ratio of the nominal airfoil is 12%. The value produced an unsatisfactory enclosed volume to surface area ration, required for efficient storage of lifting gas. As such, the airfoil was stretched in the thickness direction as much as possible without significant depreciation of aerodynamic properties, most importantly the reflexivity. Using Xfoil, the maximum thickness to chord ratio was found to be 24%.

### Computing stability derivatives

One of the most powerful tools to compute stability and body-axis derivatives for a body is the AVL software developed by MIT. Using a numerical Vortex Lattice Method, the software models the flow over a flying body with a specified number of span- and chord-wise horseshoe vortexes. Thin-airfoil theory is utilised by default. The flow around the body is assumed inviscid and incompressible.

While the inviscid and incompressible flow closely resembles the operating conditions for the probe, the thin airfoil theory was not particularly applicable to the selected airfoil. As such, the  $CLaf$  factor was applied as per software documentation, see equations below.

$$C_{L_\alpha} = \frac{\partial C_L}{\partial \alpha} = 2\pi(CLaf) \quad (3.47)$$

$$CLaf = 1 + 0.77 \frac{t}{c} \quad (3.48)$$

Upon modelling the dynastat, the stability coefficients required to construct the A matrix for state space representation were found. A few body-axis derivatives as well as all derivatives with respect to accelerations were missing. These were then found using the following equations (Mulder et al., 2013):

$$C_{Z_\alpha} = -C_{L_\alpha} \quad (3.49) \quad C_{Z_0} = -C_L \quad (3.50)$$

$$C_{X_u} = -2C_D \quad (3.51) \quad C_{Z_u} = -2C_L \quad (3.52)$$

$$K_X = \sqrt{\frac{I_{xx}}{mb^2}} \quad (3.53) \quad K_Y = \sqrt{\frac{I_{yy}}{mb^2}} \quad (3.54)$$

$$K_Z = \sqrt{\frac{I_{zz}}{mb^2}} \quad (3.55) \quad K_{XZ} = \frac{I_{xz}}{mb^2} \quad (3.56)$$

<sup>50</sup><http://airfoiltools.com/>, retrieved on 11-06-21

**Table 3.45:** Eigenvalues and eigenvectors for symmetric modes

Eigenvalue	Eigenvector
-38.727	$\begin{bmatrix} 0.012 & 0.977 & -1. & -0.999 \end{bmatrix}^T$
-1.205	$\begin{bmatrix} -0.027 & -0.192 & 0.017 & 0.012 \end{bmatrix}^T$
-0.29	$\begin{bmatrix} 0.026 & -0.061 & -0.006 & 0.034 \end{bmatrix}^T$
0.113	$\begin{bmatrix} -0.999 & 0.073 & 0.002 & 0.004 \end{bmatrix}^T$

**Table 3.46:** Eigenvalues and eigenvectors for asymmetric modes

Eigenvalue	Eigenvector
-27.5 + 0j	$\begin{bmatrix} 0.02 & 0.33 + 0.17j & 0.33 - 0.17j & 0.3 \end{bmatrix}^T$
-2.04 + 1.09j	$\begin{bmatrix} 0.03 & 0 + 0.12j & 0 - 0.12j & 0.083 \end{bmatrix}^T$
-2.04 - 1.09j	$\begin{bmatrix} -0.82 & -0.12 - 0.25j & -0.12 + 0.25j & -0.028 \end{bmatrix}^T$
-0.34 + 0j	$\begin{bmatrix} -0.57 & 0.88 & 0.88 & 0.38 \end{bmatrix}^T$

$$C_{X_\alpha} = C_L \frac{2C_{L_\alpha}}{\pi A e} \quad (3.57)$$

$$C_{X_0} = C_D - T'_c = 0 \quad (3.58)$$

where the moments of inertia were extracted from Table 3.38. Furthermore,  $C_{X_0}$  is the difference between the thrust and drag coefficients and is 0 during steady flight. Using the aforementioned relations, Table 3.45 provides the overview of the computed eigenvalues for the symmetric and asymmetric cases.

Perhaps the most important stability mode is that of longitudinal stability. Having selected a reflex airfoil, the location of the c.g. shall be within the stability margin ahead of the aerodynamic centre. As a rule of thumb, a static margin of  $5/\zeta$  has been implemented, which drove the positioning of individual components inside of the probe.

### Eigenmode analysis

Having computed all required coefficients, dynamic stability shall be analysed. The state vectors for the symmetric and asymmetric cases are as follows:

$$x_s = \begin{pmatrix} \hat{u} \\ \alpha \\ \theta \\ \frac{q\bar{c}}{V} \end{pmatrix} \quad (3.59)$$

$$x_a = \begin{pmatrix} \beta \\ \varphi \\ \frac{pb}{2V} \\ \frac{rb}{2V} \end{pmatrix} \quad (3.60)$$

The generated eigenvalues and respective eigenvectors can be found in Table 3.45 and 3.46. The asymmetric mode is totally stable, whereas one of the symmetric eigenvalues is positive, suggesting instability. At least one eigenvalue remained positive even after a diligent modification of parameters. This configuration was agreed on due to the low magnitude of the eigenvalue and lack of oscillatory motion, which should make it easy for the on-board automatic control system to supervise the problematic eigenmode using differential thrust from the top and bottom propellers.

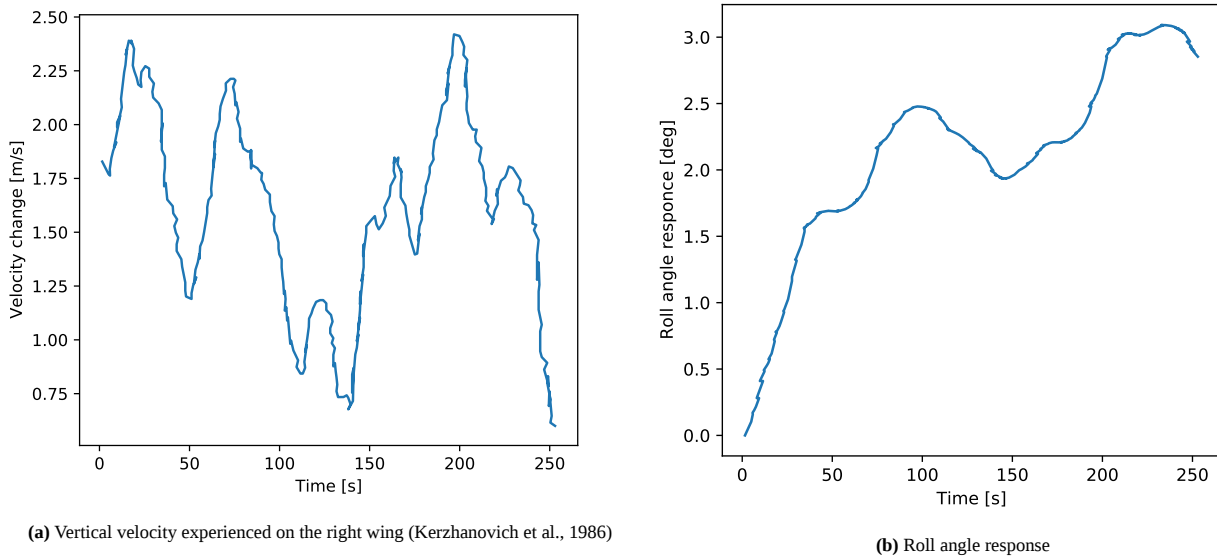


Figure 3.30: Roll response simulation

### Critical disturbances

The primary source of disturbance expected in the Venusian atmosphere are the winds. Therefore, it is important to make sure that disturbances can be easily damped using the presented geometry. The disturbances to the longitudinal moment equilibrium are the only ones, unable to be damped by differential thrust. Thus longitudinal stability analysis will be performed.

When the disturbances have high frequency, they are expected to be damped using the inherent stability of the wing. Using the disturbances of the vertical velocity identified as 'worst case' during the Vega 2 mission, the response as a function of the roll angle with time is computed, assuming that the disturbance acts on the right wing only. Two important conclusions can be drawn. First of all, the roll angle after 240 s of the worst-case disturbance is only  $2.7^\circ$ , allowing for sufficient time for the differential thrust to stabilise the system. Secondly, the maximum roll rate experienced is only  $0.038^\circ \text{ s}^{-1}$ , allowing for adaptation of the scientific instrumentation. Similar tests have been performed for pitch and yaw angles, which were found to be even lower.

### 3.7.4. Verification of assumptions

Firstly, the assumptions made for the aerodynamic sizing have to be justified. Starting with **A.A.1**, helium is a monoatomic and inert gas so the ideal gas assumption is close to reality. Additionally, the thermal subsystem calculations in Section 3.5 show that the lifting gas will be at a higher temperature than ambient during travel at the higher measurement altitude, and lower during travel at the lower measurement altitude. The effect of a deviating temperature on the sizing is only present indirectly, in that the full buoyancy at low altitude would require a bit less. A more detailed sizing of the probe would have to account for the change in buoyancy of the probe due to this temperature difference.

Next, **A.A.2** assumes that the entire wing is filled with gas and that any components stored inside the wing, like batteries or computers, take up negligible volume compared to the lifting gas. This assumption holds true, as the subsystem sizes in the front of the wing have linear dimensions in the order of 1 m, rendering the volume they take up (order of  $1 \text{ m}^3$ ) negligible compared to the lifting gas volume of around  $700 \text{ m}^3$ .

Lastly, **A.A.3** assumed the gravitational acceleration by Venus to be constant at the value at the surface  $g_V = 8.87 \text{ m s}^{-2}$ , as given in Section 1.3, as the altitudes and variations are orders of magnitude smaller than Venus' radius. To check this assumption, the squared radius ratio from Eq. (1.1) is recomputed for 55 km and 65 km altitude, giving a 1.8% and 2.1% deviation from the surface level gravity, respectively. For the preliminary design of the atmospheric platform these deviations can be disregarded and the constant surface level value is used. Note that this assumption is not used for the atmospheric entry computations, as that phase covers a much larger range of altitudes.

### 3.7.5. Verification and validation of aerodynamic properties

The calculations done for aerodynamic sizing are mostly rearranged algebraic relations. However, the derivation of the volume contained in a trapezoidal wing can be verified by setting shape parameters like the taper ratio to 1, thereby reducing the trapezoidal wing to a straight wing for which the volume is given by Eq. (3.61). As can be seen from inspecting Eq. (3.38), setting  $\lambda = 0$  indeed reduces the equation to the straight wing volume below.

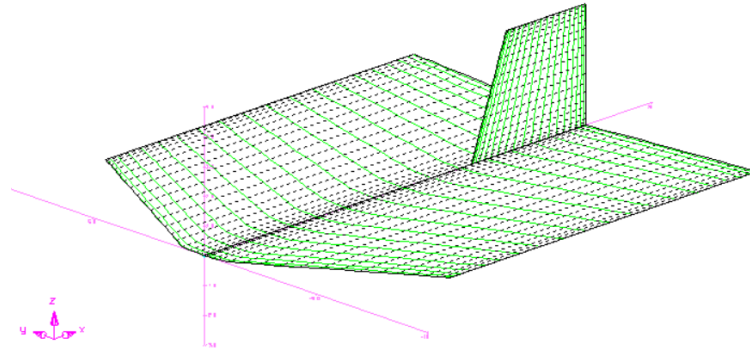


Figure 3.31: AVL input geometry

Table 3.47: Verification of the AVL model through changing coefficients

	Increased sweep	Increased vertical tail size	Increased dihedral
$C_{Y\beta}$	-	↑	-
$C_{l\beta}$	↑	-	↑
$C_{n\beta}$	↑	↑	-
$C_{Yp}$	-	↑	-
$C_{lp}$	↓	↑	-
$C_{np}$		↓	-
$C_{Yr}$		↑	-
$C_{lr}$		↑	-
$C_{nr}$		↑	-

Table 3.48: Comparison of stability derivatives with common aircraft (Cessna Citation CE172 and CE500) for symmetric and asymmetric motion (Mulder et al., 2013)

Symmetric			Asymmetric		
Coefficient	Tori	CE172	Coefficient	Tori	CE500
$C_{X_0}^*$	0	0	$C_{Y_b}$	-0.106	-1
$C_{X_u}$	-0.068	-0.093	$C_{Y_p}$	-0.022	-0.087
$C_{X_q}^*$	0	0	$C_{Y_r}$	0.238	0.43
$C_{Z_0}$	-0.268	-0.310	$C_{l_b}$	-0.081	-0.077
$C_{Z_u}$	-0.538	-0.620	$C_{l_p}$	-0.094	-0.344
$C_{Z_a}$	-1.35	-4.6	$C_{l_r}$	0.165	0.28
$C_{Z_q}$	-2.39	-2	$C_{n_b}$	1.22	0.164
$C_{m_u}$	-0.140	0	$C_{n_p}$	-0.047	-0.0108
$C_{m_a}$	-0.249	-0.89	$C_{n_r}$	-0.197	-0.193

$$v_{gas} = \left( \frac{S_{encl}}{t \cdot c} \right) tcb = \left( \frac{S_{encl}}{t \cdot c} \right) \left( \frac{t}{c} \right) Ac^3 \quad (3.61)$$

Verification and validation of the stability subsystem of the probe was performed in four stages. As a first verification step, the geometry of the input file generated for the use in AVL software has been confirmed. To do so, it was reworked in the digital format and displayed on screen, see Fig. 3.31. Please note that only the chord-lines are depicted with no thickness for the sake of clarity. Analysis was performed on a 3D shape. The coordinate system was also verified this way.

Secondly, in order to verify the AVL software itself, different inputs were fed for three variables: sweep, dihedral and the size of the vertical tail. The resulting coefficients were compared to those known from theory and expected behaviour was confirmed, see Table 3.47.

Having performed the perturbations outlined in Table 3.47 and recorded expected behaviour of the most influential coefficients, the model must now be validated. The values of the coefficients were compared to those of common aircraft. Note that the starred coefficients have been assumed. The fact that the values in Table 3.48 differ is unsurprising, given the vast differences between the two designs. Attention should be paid, however, to the order of magnitude and more importantly the sign of each coefficient as it gives insight into whether the design is stable rather than how stable it is.

Finally, as the last verification procedure of the code used to find and comment on stability of present eigenmotions, the code was fed with coefficients of the two Cessna aircraft instead. It was shown that of the five common eigenmodes

four are stable – all except the spiral mode, just as expected.

### 3.7.6. Sustainability

The sustainability of the aerodynamics and stability of the probe was scored “low” (1) for the Earth segment, since the selected lifting gas is helium, which is a rare Earth material that is generally extracted from the Earth’s crust<sup>51</sup>. The lifting gas choice is thus not very sustainable, but other alternatives would either result in a heavier probe (using nitrogen, for instance) or reduce its reliability (for instance using hydrogen, which is highly flammable).

The aerodynamics and stability of the probe does not contribute to the sustainability of the interplanetary trajectory segment and hence was not factored into the score.

For the Venus segment, the sustainability of the aerodynamics and stability was scored “high” (3), since the hybrid aerodynamic and buoyant design allows for the probe to float un-propelled at its lowest measurement altitude and be passively stable.

The aerodynamics and stability department was given a weight of 3, since it was relevant to the success of the probe operations. Failure of the probe due to stability issues, could lead to a negative impact on social sustainability.

## 3.8. Design overview

The final design overview includes the hardware diagram of *Tori*, which depicts the interrelations between subsystems. The iterative integration process will be elaborated on in this section. Also, the final cost, mass and data rate budgets will be presented. Finally, a sensitivity analysis on the iteration is performed to portray the susceptibility of the algorithm to changes in the inputs.

### 3.8.1. Interfaces

To give an overview of the components of each subsystem and the interfaces between the subsystems, a hardware diagram is shown in Fig. 3.32. The interfaces between the subsystem help facilitate the iteration process of the *Tori*, by portraying the inter-dependencies of subsystems which have been divided into four types: power flow, data flow, command flow, and mechanical flow. The flow justification for each subsystem is summarised in the upcoming paragraphs.

1. The TT&C and C&DH are the subsystems that have direct contact with the orbiter. Therefore, all data measured by other subsystems is first sent to this subsystem and then sent to the orbiter. This is shown by the data flow arrows that flow from each subsystem to TT&C and C&DH. Furthermore, this subsystem will forward the commands to the other subsystems given by the CDMU on board or directly from the orbiter. Therefore, a command flow arrow from the TT&C and C&DH to all other subsystems is depicted. Finally, TT&C and C&DH will require power. Thus, a power flow arrow goes from the power subsystem to this subsystem. Also, a deployment mechanism is needed to deploy and move the antenna. This is indicated by a mechanical flow arrow going from structures to TT&C and CD&H.
2. The GNC includes the sensors and actuators needed for ADCS along with the control surfaces to keep *Tori* stable. The measured data is sent to TT&C and CD&H, but also propulsion and power as data regarding the attitude are needed to control the propellers and power required to manoeuvre. Furthermore, the GNC will receive commands from TT&C and CD&H, which is shown by the command flow arrow. Also, the components of GNC will use power to function, which comes from the power subsystem depicted by the power flow arrow going from the power subsystem to GNC. Finally, a mechanical flow arrow is drawn from structures to GNC to indicate the structural support that GNC needs.
3. The thermal control will send data about the temperatures *Tori* will experience to TT&C and C&DH, denoted with a data flow arrow.
4. The payload will measure data which will be sent to TT&C and C&DH given by the data flow arrow. Subsequently, it will also receive commands from TT&C and C&DH. Therefore, a command flow arrow is going from TT&C and C&DH to the payload. Additionally, the instruments will use the power, which is the power flow arrow from power to payload. Furthermore, the mechanical flow arrow indicates the structures support a deployment mechanism for NEP.
5. The structures subsystem provides support and the deployment mechanisms to deploy components from other subsystems. Therefore, mechanical flow arrows go from structures to all other subsystems. Additionally, the deployment mechanisms might move according to commands given by TT&C and C&DH to perform certain manoeuvres. This is shown with the command flow arrow from TT&C and C&DH to structures. Also, to move the mechanisms, power will be required, denoted by the power flow arrow.
6. The power subsystems provide power for all subsystem’s active components. Therefore, power flow arrows are drawn from power to all other subsystems except thermal control, since that one only includes passive components. Just as the other subsystems, power will also send internal data shown with the data flow arrow that subsequently might lead to necessary commands from TT&C and C&DH shown with the command flow arrow.

<sup>51</sup><https://www.nationalgeographic.com/science/article/news-helium-mri-superconducting-markets-reserve-technology>, retrieved 21-06-2021

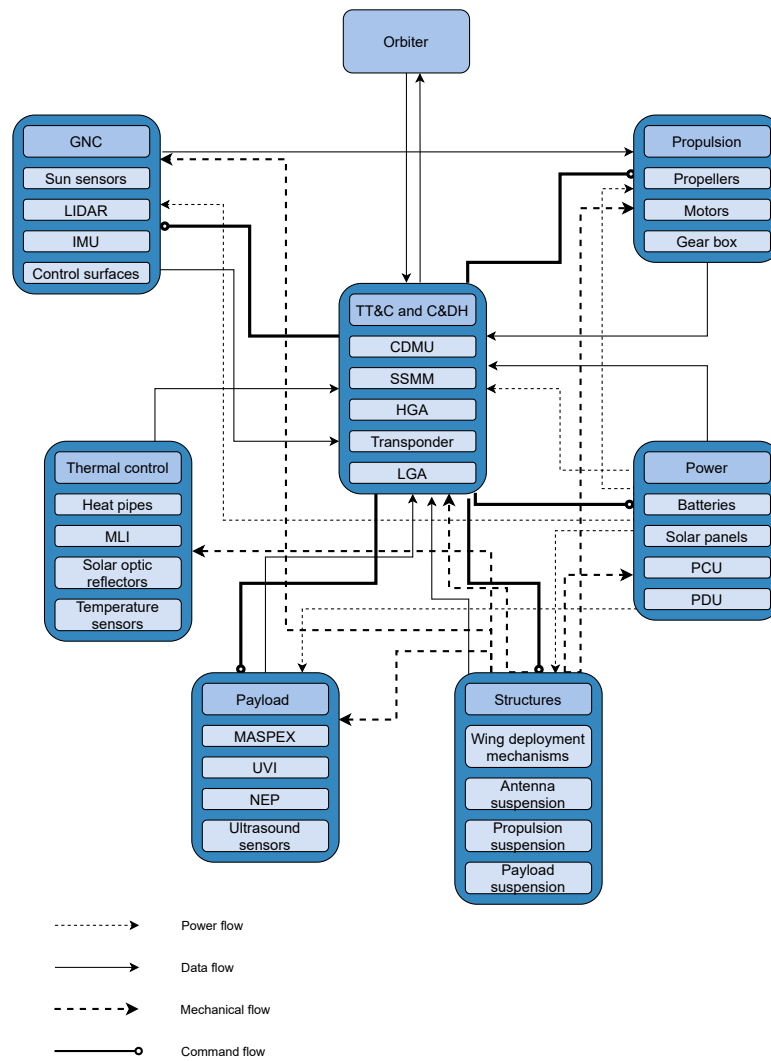


Figure 3.32: Hardware diagram probe

7. First, the propulsion subsystem requires power for the propellers. This is included as the power flow arrow from power to propulsion. Second, it will need structural support for the motors and mechanisms to point the propellers for certain manoeuvres, which is denoted by the mechanical flow arrow. Third, it will send data to and receive commands from TT&C and C&DH, shown as data flow arrow and command flow arrow, respectively. Finally, it will also receive data from GNC to position the propellers for specific manoeuvres.

### 3.8.2. Electrical block diagram

The electrical block diagram shows the electrical equipment within the probe and the interaction between the different power components and the so-called loads, which are the systems that require power. For the probe, this overview is provided in Fig. 3.33.

Here, the maximum power point tracker (MPPT) regulates the power flow between the solar arrays and the batteries. This way, the batteries are protected from overcharge, while the solar arrays are used to their maximum capability as the MPPT keeps track of the maximum power configuration and directs the bypass diodes to skip defective or ill-positioned solar cells. Next to the MPPT, the battery charge regulator (BCR) and battery discharge regulator (BDR) are put in place to provide controlled charge and discharge of the battery. These components together form the power conditioning unit (PCU). Finally, upon communication with the on-board computer, the power distribution unit (PDU) distributes power over the loads, which are in this case the relevant subsystems. This power flow is again regulated to avoid overcharge or overloading of the systems. The known voltages corresponding to the loads are given in the figure.

### 3.8.3. Probe integration algorithm

This section will explain the working principle of the probe iteration algorithm which combines the masses of each subsystem and iterates over to find the total mass of Tori. The steps and inputs inside the algorithm are summarised in Fig. 3.34.

The probe integration algorithm is composed of several subsystem codes. These are the subsystems whose computa-

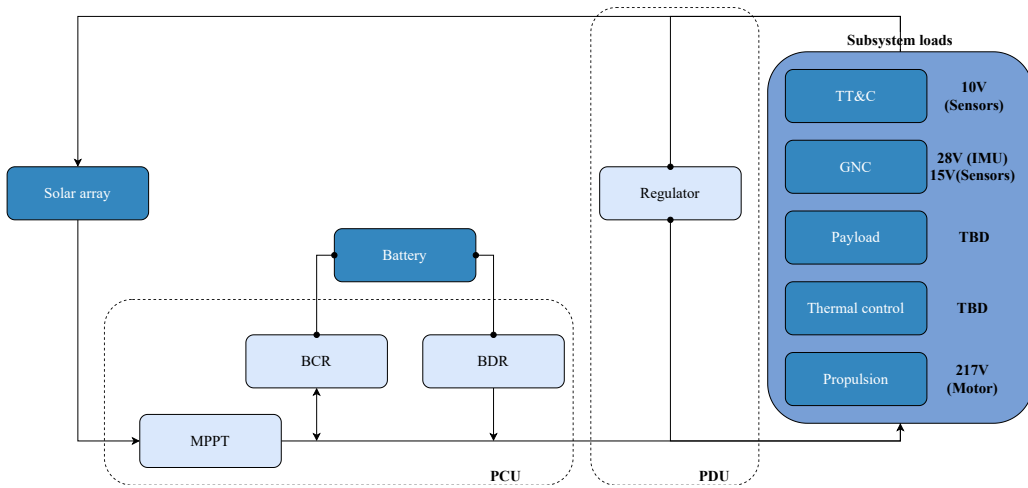


Figure 3.33: Electrical block diagram diagram probe

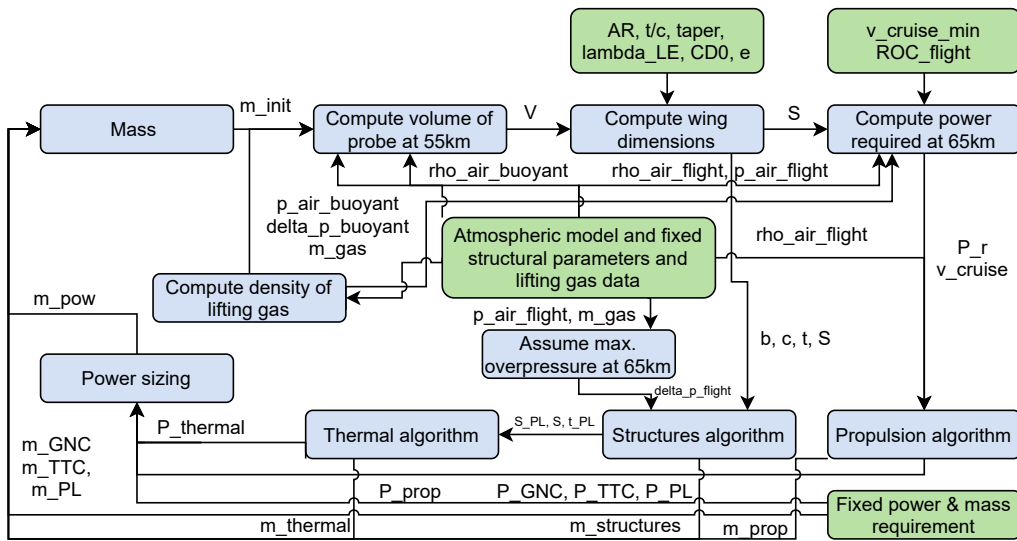


Figure 3.34: Flowchart of the iteration

tions depend on the size, mass and power requirement of the probe. Next to that, there are also subsystems which have fixed masses. The code is initiated with an initial total mass which is equal to the sum of the fixed masses and variable masses. The variable masses are set equal to the preliminary sizing estimations of the team and converges at each iteration to a fixed final value. The trend that the mass computations follow can be observed in Fig. 3.35.

Table 3.49: Iterated probe sizing results

Parameter	Value
$m_{probe}$	555 kg
$v_{gas}$	$706 \text{ m}^3$
$S$	$236 \text{ m}^2$
$b$	15.4 m
$c_r$	17.1 m
$v_{cruise,65}$	$25.9 \text{ m s}^{-1}$
$P_r$	32.3 kW
$S_{SA}$	$104 \text{ m}^2$

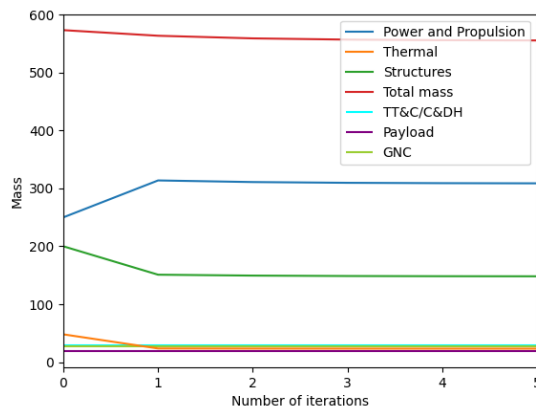


Figure 3.35: Mass breakdown total during iteration

The top level end result of the sizing iteration is presented in Table 3.49. A budget breakdown is given in Section 3.8.4,

and the end results of the sizing will be further analysed in the near future.

The iteration code is composed of the power, thermal, structures and propulsion algorithms which are verified in their respective sections in this report. This means that only the operations that take place in the probe iteration code shall be verified in this section. These include the computations of volume at 55 km, wing dimensions, power required at 65km, density of lifting gas and summation of total mass. To test these computations, code verification unit (U) and system (S) tests will be performed in a way that at least one input for each of the above-mentioned operations has been altered. The tests are listed in Table 3.50.

**Table 3.50:** Verification tests on the integration algorithm

Test	Variables	Expected outcome	Verified
VER-INT-U1	<b>Input:</b> $m_{init}$ <b>Outputs:</b> $V$	Overwriting initial mass to 0 should give a volume of 0. Increasing the mass by 20% should increase the volume by 20%.	✓
VER-INT-U2	<b>Input:</b> $\rho_{airbuoyant}$ <b>Outputs:</b> $V$	Increasing the density to infinity should make the volume converge to zero as it is the denominator $\frac{m_{tot}}{(\rho_{airbuoyant} - \rho_{liftbuoyant})}$ .	✓
VER-INT-U4	<b>Input:</b> $V$ <b>Outputs:</b> $cr$	Overwriting the volume of the probe to double should cause the root chord to increase by $(2)^{\frac{1}{3}}$ . Setting it to zero should make the chord length zero.	✓
VER-INT-U5	<b>Input:</b> $V$ <b>Outputs:</b> $cr$	Overwriting the volume of the probe to double should cause the root chord to increase by $(2)^{\frac{1}{3}}$ . Setting it to zero should make the chord length zero.	✓
VER-INT-U6	<b>Input:</b> $ct\ ct$ <b>Outputs:</b> $taper$	The ratio of tip chord length to root chord length should be equal to the taper ratio.	✓
VER-INT-U7	<b>Input:</b> $b$ <b>Outputs:</b> $S$	Overwriting span to 0 should give a surface area of 0.	✓
VER-INT-S1	<b>Input:</b> $m_{thermal}$ , $m_{prop}$ , $m_{structures}$ , $m_{prop}$ <b>Outputs:</b> $m_{tot}$	The variable masses shall be overwritten to zero in the iteration. This shall give a final iterated mass which is equal to the initial mass estimate.	✓
VER-INT-S2	<b>Input:</b> $m_{init}$ <b>Outputs:</b> $m_{tot}$	Increasing the initial estimate for variable masses such as the mass of propulsion subsystem shall not make a difference on the final value that the mass converges to.	✓
VER-INT-S3	<b>Input:</b> $m_{init}$ <b>Outputs:</b> $m_{tot}$	Increasing the initial estimate for fixed masses such as the mass of GNC shall cause the total iterated mass to increase more than the increase in GNC mass.	✓

### 3.8.4. Budgets

The mass, power, data rate and cost budget of Tori can be seen in Table 3.51. Note that, the total power required for propulsion subsystem is found by dividing the power required to propel by the inefficiencies ( $\frac{35.5}{0.9 \cdot 0.9 \cdot 0.56}$ ). The mass breakdown is visualised in Fig. 3.36. The other budgets were not visualised in a pie-chart as the contributions were dominated by one of the categories.

**Table 3.51:** Tori budget

Components	Mass [kg]	Power [W]	Data rate [kbps]	Costs [M\$]
Payload	18.5	51.7	107	120
TT&C/C&DH	29	127	-	45
GNC	27.6	51.3	0.06	15
Thermal	23.3	-	0.00105	1.5
Structures	148.1	-	-	12.5
Propulsion	82.6	78260	0.0038	4
Power	225.9	-	0.0011	25
<b>Total</b>	<b>555</b>	<b>78490</b>	<b>107</b>	<b>223</b>

On top of the 555kg structural mass, 69 kg of buoyant gas is stored inside the structure. However, this gas lifts the structure, decreasing its effective weight, so it is treated as a force rather than a mass. Note that the mass of the gas is included in the entry calculations while it is still inside its tank, as it does need to be taken into account for calculating accelerations.

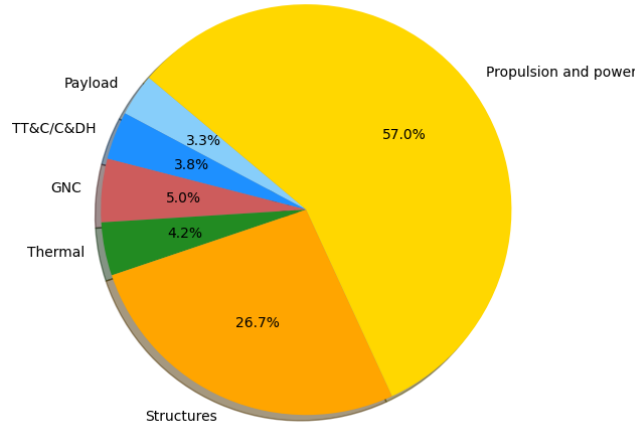


Figure 3.36: Pie chart visualising the structural mass breakdown

### 3.8.5. Performance analysis

To conclude the design overview of the hybrid airship for Venusian atmosphere exploration, the point performance calculations are summarised for the final iterated mass. Afterwards, the probe's overall flight performance will be analysed and presented.

The critical design condition for the sizing iteration was the powered flight at 65 km altitude, 30° latitude and straight below the Sun in terms of local time/longitude. Next to the power for sustaining flight, a power margin for a climb rate of  $4 \text{ m s}^{-1}$  was designed for, to incorporate sufficient margin to sustain flight in non-optimal conditions as well (the choice drove/was driven by the maximum local time of sustained flight, which will be explained later on). Using Eqs. (3.44), (3.45) and (3.46) yields a cruise velocity of  $25.9 \text{ m s}^{-1}$  and a power required of 32.3 kW, as listed in Table 3.49.

Principally, the operational envelope of the dynastat is based on the neutrally buoyant altitude. The lighter-than-air aspect of the design was sized such that the probe would be able to float purely on static lift at 55 km. Below that, the higher ambient pressure can lead to the collapse of the envelope if the overpressure is reduced to or beyond zero. On the other hand, climbing in altitude has the risk of bursting the hull from too high pressure differentials. The structure has been sized for the hull to withstand the pressure difference between lifting gas (internal) pressure and the lower ambient pressure at 65 km with some margin, but the limit for safe operation is the design point.

As the craft is solar powered, the performance under power depends on the power available, which varies with solar power generated. The relation between solar cell specific power generated  $P_{sol,sp}$  [ $\text{W m}^{-2}$ ] and altitude  $h$  [km], given by Eq. (3.62), is obtained via the method described in Section 1.3.

$$P_{sol,sp}(h) = 0.6625h^2 - 44.078h + 818.11 \quad (3.62)$$

Combining this with the solar array area  $A_{sol}$ , the power consumed by other subsystems  $P_{fix}$  and the efficiency of the propulsion system  $\eta = \eta_{motor}\eta_{propeller}\eta_{gearbox} = 0.9 \cdot 0.56 \cdot 0.9$  from Table 3.20, the power available as a function of altitude  $h$  and local time angle  $\theta$  (angle between Sun-Venus and probe-Venus vector in the invariant plane) is presented in Eq. (3.63). This is a worst case estimate as flight at the extreme latitude of 30° is assumed, introducing an additional  $\cos(30)$  factor.

$$P_a(h, \theta) = (P_{sol,sp}(h)S_{SA} - P_{fix})\eta \cos(30) \cos(\theta) \quad (3.63)$$

Sustaining flight at altitudes away from the neutrally buoyant altitude requires dynamic lift from propelled forward motion. This limits the off-buoyant flight envelope to the day-side of the planet, and there the power generated by the solar cells again imposes a constraint on how far away from the subsolar point flight at the 65 km upper altitude can be sustained. From equating the power available, given by Eq. (3.63), with the constant power required to fly at the upper altitude in Eq. (3.64), it is found that the probe can fly to local times of up to 16:14 solar time, or  $\theta = 63.4^\circ$  away from the Sun (at 30° latitude).

$$P_r = \frac{\rho_{air,65}}{2} V_{cruise}^3 SC_D \quad (3.64)$$

Beyond this point the Sun is too low above the horizon for the solar panels to generate enough power for sustained flight at 65 km, forcing the probe to descend in gliding flight. As a simplification, it is assumed that no power is used during the descent, which at the same time provides the flight planning with a conservative estimate of the time that the probe can stay up with less incoming power than required for level flight. From the drag polar an optimum  $C_L$  and  $C_D$  can be found for minimum sink rate, using Eq. (3.65) from (Anderson, 2016). The climb rate (negative because sinking) itself is given by Eq. (3.66) as a function of altitude because  $BR$  and the ambient density are a function of altitude themselves.

$$C_{L,opt} = \sqrt{3\pi AeC_{D,0}} = 0.269, \quad C_{D,opt} = C_{D,0} + \frac{C_{L,opt}^2}{\pi Ae} = 0.0336 \quad (3.65)$$

$$ROC(h) = -\sqrt{\frac{2m_{probe}(1 - BR(h))g_V}{\rho_{air}(h)SC_{L,opt}}} \frac{C_{D,opt}}{C_{L,opt}} \quad (3.66)$$

At low altitudes the sink rate is asymptotically small because of the close to neutral buoyancy, while the maximum sink rate at 65 km is  $3.2 \text{ m s}^{-1}$ . The total descent time then is found by numerically integrating the descent rate over time until the altitude has decreased from 65 km to within 0.5 % of the lower 55 km altitude<sup>52</sup>. The final probe design thus has a descent time of 122.4 min.

Conversely, the climb performance is evaluated in a similar way as the glide, only that in this case there is a third dependence on altitude via the power available. As the optimum lift and drag coefficients for minimum sink rate are the same as for minimum power required, or also maximum rate of climb, the airspeed for best climb rate is given by Eq. (3.67). The theoretical rate of climb as a function of altitude is given by Eq. (3.68).

$$V_{opt}(h) = \sqrt{\frac{2m_{probe}(1 - BR(h))g_V}{\rho_{air}(h)SC_{L,opt}}} \quad (3.67)$$

$$ROC(h) = \frac{P_a(h) - 0.5\rho_{air}(h)V_{opt}^3SC_{D,opt}}{m_{probe}(1 - BR(h))g_V} \quad (3.68)$$

It can be seen from the buoyancy ratio in the denominator of Eq. (3.68) that the theoretical rate of climb would be infinite at  $BR = 1$ , but for practical considerations the rate of climb is capped at  $6 \text{ m s}^{-1}$  which is slightly higher than the top value for fully buoyant aircraft like the Coastal class airship<sup>53</sup>, as the dynastat is designed for powered climb. At the top of the climb the climb rate slows down to the  $4 \text{ m s}^{-1}$  that the propulsion system was designed for, which is a good cross-check to verify that the calculations are consistent. Integrating this climb rate from the low to the high altitude gives a total time of climb of 32 min.

Lastly, the performance in terms of airspeeds is assessed. At 65 km the speed to fly is the optimum  $v_{cruise} = 25.9 \text{ m s}^{-1}$  from Table 3.49. During the climb and descent manoeuvres the probe flies at the altitude-dependent optimum speed for minimum power required. At the lower altitude of 55 km the probe does not propel at all during night, and during daytime it can use all propulsive power to fly at zero lift. Then, the power required only depends on the zero-lift drag coefficient, so the maximum possible airspeed at a given local time  $\theta$  is given by:

$$V_{max,55}(\theta) = \left( \frac{2P_{a,55}(\theta)}{\rho_{air,55}SC_{D,0}} \right)^{\frac{1}{3}} = 26.1 \text{ m s}^{-1} \quad (3.69)$$

The theoretical maximum speed at 65 km can be obtained by equating the available power from Eq. (3.63) with the power required for lifting flight:

$$P_r = \frac{\rho_{air,65}}{2} V^3 S \left( C_{D,0} + \frac{C_L}{\pi Ae} \right) \quad (3.70)$$

As the lift coefficient  $C_L$  depends on the airspeed too, there is no analytical solution for  $V$ . Instead a numerical solver was used to find that the maximum possible speed at 65 km is  $48.5 \text{ m s}^{-1}$ .

These performance parameters serve as input to the flight planning in Section 2.8.2, showing that the probe can comply with the performance requirements on coverage, as it is able to reach up to  $30^\circ$  northern latitude and it can climb all the way between 55 km and 65 km.

<sup>52</sup>This avoids the asymptotically low sink rates close to the low altitude at which the probe is neutrally buoyant.

<sup>53</sup>[https://www.airshipsonline.com/airships/coastal/Coastal\\_Specifications.htm](https://www.airshipsonline.com/airships/coastal/Coastal_Specifications.htm), retrieved on 28-06-2021

# 4. Tsubuyaki design

Since design is an iterative process, design of the orbiter, Tsubuyaki, took place simultaneously with the design of Tori. Since, direct communication between Tori and Earth was proven unfeasible in the preceding reports, a relay orbiter must be designed to facilitate a communication link between Tori and Earth. The same design order of the subsystem will be followed as explained in the introduction of Chapter 3.

This chapter will conclude by giving an overview of Tsubuyaki's budget as well as the hardware diagram and its performance.

## 4.1. Payload

Tsubuyaki will carry instruments to fulfil its own requirements. In Section 4.1.1, the payload requirements will be stated to relate the chosen instruments to the requirements similar to Section 3.1. Afterwards, an overview of the final chosen instruments will be given in Section 4.1.2. Next, the verification and validation will be discussed in Section 4.1.3. Finally, the risks and sustainability strategy will be defined in Section 4.1.4 and Section 4.1.5.

### 4.1.1. Payload requirements

The requirements related to Tsubuyaki obtained from the mission objectives and the market analysis are given in Table 4.1. Again, KUMO-STH-SCI indicate a stakeholder requirement and are of primary importance whereas requirements with the identity KUMO-MA-SCI are derived from the market analysis.

Table 4.1: User requirements

Identifier	Requirement	Checked
KUMO-STH-SCI-07	The mission shall investigate the structure of UV-absorbers in the atmosphere.	✓
KUMO-MA-SCI-MO2-2	Tsubuyaki shall measure the cloud structure, composition and scattering properties with a spectral resolution of 3 nm.	✓
KUMO-MA-SCI-MO4	Tsubuyaki shall measure the temperatures in the upper atmospheric layer.	✓
KUMO-MA-SCI-MO6	Tsubuyaki shall measure airglow with an spectral resolution of 5 nm.	✓
KUMO-MA-SCI-MO7	Tsubuyaki shall measure hot spots with a spectral resolution of 5 nm.	✓

### 4.1.2. Payload overview

To measure UV-absorbers from outside of the atmosphere, the Visual Monitoring Camera (VMC) <sup>1</sup> (Markiewicz et al., 2005) has been chosen. This instrument measures the UV-spectrum within the range of 300-400 nm. This spectrum overlaps the spectrum measured by the UVI previously chosen for Tori in Section 3.1. Therefore, measurements from within as well as outside of the atmosphere can be compared. The VMC will fulfill requirement KUMO-STH-SCI-07.

Furthermore, the Visible and Infrared Thermal Imaging Spectrometer (VIRTIS) <sup>2</sup> (Drossart et al., 2004; Coradini, 1999; Piccioni et al., 2004; Barstow et al., 2010; Markiewicz et al., 2005) will be added on Tsubuyaki for additional value. As seen in Table 4.2, VIRTIS is made up of three different components, with each their specific dimensions. It exists of 2 different channels which form the VIRTIS-M and VIRTIS-H. The VIRTIS-M is the imaging channel and exists of two categories which are the UV-visible (250 nm to 1000 nm) and infrared spectra (950 nm to 5000 nm <sup>3</sup>, forming two out of the three components. Then, the VIRTIS-H is the high resolution channel which measures in the IR-range (2000 nm to 5000 nm) (Coradini, 1999), forming the third and final component. This instrument will be used to accomplish the requirements KUMO-MA-MO2-2, KUMO-MA-SCI-MO4, KUMO-MA-SCI-MO6 and KUMO-MA-SCI-MO7.

Both instruments have previously been used for the Venus Express mission. Since Tsubuyaki will fly in the same orbit as Venus Express, the resolution will be sufficiently accurate.

A final overview of the orbiter instruments and the corresponding characteristics is seen in Table 4.2. Here, a total mass of 33.43 kg as well as a total power consumption of 41.2 W and a data rate of 50 kbps have been concluded.

### 4.1.3. Verification and Validation

Both instruments have previously been used on the Venus Express mission. Furthermore, Tsubuyaki will orbit in the same orbit that Venus Express did, meaning that the accuracy with which VIRTIS and VMC will measure will be as accurate as

<sup>1</sup><https://blogs.esa.int/vmc/faq/>, retrieved on 31-05-2021

<sup>2</sup>[https://www.leonardocompany.com/documents/20142/3150278/Copia\\_di\\_VIRTIS\\_LQ\\_mm08061\\_.pdf?t=1538987592073](https://www.leonardocompany.com/documents/20142/3150278/Copia_di_VIRTIS_LQ_mm08061_.pdf?t=1538987592073), retrieved on 31-05-2021

<sup>3</sup>[https://www.leonardocompany.com/documents/20142/3150278/Copia\\_di\\_VIRTIS\\_LQ\\_mm08061\\_.pdf](https://www.leonardocompany.com/documents/20142/3150278/Copia_di_VIRTIS_LQ_mm08061_.pdf), retrieved on 09-05-2021

**Table 4.2:** Orbiter instruments

Parameter	VIRTIS	VMC	Total
Mass [kg]	33	0.43	33.43
Power [W]	36	5.2	41.2
Size [mm]	590x650x380 220x250x100 200x250x190	65x60x108	$161.15 \times 10^6 \text{ mm}^3$
Data rate [kbps]	40	10	50
Cost [\$]	32	2.5	34.5
Spectral range [nm]	250-5000	300-1000	-
Resolution	3-15 nm	3 nm	-
Sensitivity [ $\mu\text{m}$ ]	1.5 to 2.6	0.3 to 1.0	-

when used for Venus Express.

Nevertheless, testing needs to be done to confirm its functionalities. For this, the testing facilities at ESA/ESTEC can be utilised<sup>4</sup>. The instruments can be exposed to UV-radiation as well as IR-radiation. The results can then be compared with the results obtained from the same instruments obtained when flying around Venus for other missions.

#### 4.1.4. Risk assessment

Several risks are incorporated when placing the payload. Most of the risks are similar to the ones mentioned in Section 3.1.4. Some risks can be replaced by risks applying to Tsubuyaki in particular. The changes are seen in Table 4.3. The most prominent risk for this payload would be 1a-2, where the payload could be damaged due to radiation.

**Table 4.3:** Table showing possible risks, their severity and likelihood

<b>1a-2 Instrument damaged due to radiation</b>
<b>Assessment L1S4 :</b> Due to the radiation exposed to space, instruments could get damaged to a serious extent, with critical consequences.
<b>Mitigation L1S3 :</b> Instruments will be protected by box like structures, which are radiation hardened to prevent any possible damage caused by radiation.
<b>1b-2 Instrument damaged during launch</b>
<b>Assessment L2S5 :</b> During the launch from Earth, the payload will be exposed to high pressures and loading conditions, which can damage the payload.
<b>Mitigation L1S4 :</b> The instruments will be insulated properly to avoid damage caused by launch conditions.

#### 4.1.5. Sustainability

The payload on board of Tsubuyaki, is a significant contributor to the social sustainability aspect of Kumo. Similar to Tori, the instruments on board the orbiter also contribute to the success of the mission, promoting sustainability socially. However, sustainability also considers the environmental, political and economical aspects of the mission. Hence, being considered, a noticeable contributor to sustainability, mission payload and instrumentation was given a weight of 3. In this subsection, a brief outline of the contribution of payload components, management and transportation to sustainability will be presented.

First, the individual components on board are reviewed:

- **VIRTIS** is an off-the-shelf instrument developed by INAF-ISAF Milano (Istituto di Astrofisica Spaziale e Fisica cosmica Milano)<sup>5</sup>. This instrument, as explained earlier, is added on Tsubuyaki for additional market value experiments. This instrument has been previously used on the Venus Express mission and hence, is quite reliable working in similar environmental conditions. During production and testing of the instrument, utilisation of resources will be checked. Also, the safety of personnel at ESA ESTEC during the radiation tests will be actively monitored<sup>6</sup>. Hence, a “high” score of (3) was given to VIRTIS.
- **VMC** is also an off-the-shelf instrument from ESA. It was previously used in the Rosetta, Venus Express, Mars Express missions successfully<sup>7</sup>. The transportation from the Netherlands to the US after testing and verification would have a smaller costs, since they can be tested at the same location. Transportation emissions would need to be monitored. The costs for UV-radiation tests for VMC are a bit higher than other tests due to the importance of

<sup>4</sup>[http://www.esa.int/Enabling\\_Support/Space\\_Engineering\\_Technology/Materials\\_Electrical\\_Components\\_Laboratory](http://www.esa.int/Enabling_Support/Space_Engineering_Technology/Materials_Electrical_Components_Laboratory), retrieved on 14-06-2021

<sup>5</sup><https://www.iasf-milano.inaf.it/>, retrieved on 28-06-2021

<sup>6</sup>[https://www.esa.int/Science\\_Exploration/Space\\_Science/Rosetta/VIRTIS](https://www.esa.int/Science_Exploration/Space_Science/Rosetta/VIRTIS), retrieved on 21-06-2021

<sup>7</sup>[https://www.esa.int/Enabling\\_Support/Operations/About\\_the\\_Visual\\_Monitoring\\_Camera\\_VMC](https://www.esa.int/Enabling_Support/Operations/About_the_Visual_Monitoring_Camera_VMC), retrieved on 21-06-2021

the component to the success of the mission. Similarly for the test, special attention must be paid to the safety of the workers. Hence, a “reasonable” score of (2) was given to VMC.

Moreover, a major point to be considered while transportation is the cost that is associated with customs for transporting instruments between the United States and the European Union. Getting the time slot and relevant permission to relocate the instruments can be costly and time consuming. This is kept into account and hence, the plan is to get the instruments deported and stored in advance.

Out of a possible score of 6, the payload instruments on board were scored to have a total of 5. This means that the subsystem sustainability score for the payload components is 83%. However, for the overall sustainability towards mission operations, the three phases; Earth operations ( $SP_1$ ), interplanetary travel ( $SP_2$ ) and Venus operations ( $SP_3$ ), have to be separately scored.

A “reasonable” score of (2) for the Earth phase is given for payload. This is considering manufacturing costs and transport emissions from production and testing locations to the launch site. For the interplanetary phase, payload on board Tsubuyaki will not be used and will not contribute to any space debris and will also not use power. Hence, it is given a “high” score of (3). Finally, for the Venus operations phase, payload on Tsubuyaki actually starts consuming power, communicating with both Tori and the ground station at Earth. The instruments are already tested for optimised operations on Earth, and are made sure to be non-destructive to the Venusian orbit. The payload selection also reviewed the contaminating properties of the concerned instruments. For EOL, the payload on board would just burn up while crashing near the surface, due to high atmospheric temperatures. Hence, a “high” score of (3) was given for this phase.

These scores will be used to further calculate the overall mission sustainability score later.

Now, once Tsubuyaki gathered all data received from Tori as well as its own scientific data, the data must be sent to the ground stations. This is done by the TT&C and C&DH subsystem explained in the following section.

## 4.2. Telecommunications and command

All data collected by Tsubuyaki and Tori has to be send to Earth. In this section the telecommunications regarding the orbiter will be discussed. However, to establish the link budgets in Section 3.2.5 the antennas of the orbiter and the ground station had to be established already. This section should not be read on its own but rather seen as an expansion on Section 3.2.

In Section 4.2.1 the requirements are listed. The orbiter operational modes are discussed in Section 4.2.2. The communication instruments and the link budgets are listed in Sections 4.2.3 and 4.2.4. The CD&H of the orbiter is discussed in Section 4.2.5. The subsystem is finalised with verification and validation, risk assessment and sustainability in Sections 4.2.7, 4.2.8 and 4.2.9 respectively.

### 4.2.1. Requirements

The requirements of the telecommunication and command subsystem can be found in Table 4.4. As explained in Section 3.2.1, requirement KUMO-GNC-02 changed from 261 million km to 158 million km as this will be the most design driving distance. Based on Fig. 4.1, the orbiter shall be able to receive messages from the ground station at a time interval of 12.6 hours (KUMO-TD-09) as this is the shortest time between uplinks from the ground station to the orbiter. This time could be prolonged by the design if needed. To shorten this time would mean to have a shorter interval between rotations which is possible if necessary for command purposes. Since the DSN is used for the mission this is definitely doable.

**Table 4.4:** Requirements for telecommunications and command subsystem for Tsubuyaki

Identifier	Requirement	Check
KUMO-TD-01-2	Tsubuyaki shall use a frequency range of between 8.40-8.45 GHz (X-band) and 2.29–2.30 (S-band) GHz for sending messages as downlink.	✓
KUMO-TD-02-2	Tsubuyaki shall use a frequency range of between 7.145–7.19 GHz (X-band) and 2.11–2.12 GHz (S-band) for for receiving messages as uplink.	✓
KUMO-TD-03-2	Tsubuyaki shall use a data rate of 60 kbps for sending messages as downlink.	✓
KUMO-TD-04-2	The Tsubuyaki shall use a data rate of 2 kbps for receiving messages as uplink.	✓
KUMO-TD-05	The system shall be able to detect a communications error with a probability of 0.85 <TBC>.	✓
KUMO-TD-06-2	Tsubuyaki shall have a storage capability of 440 GB of data.	✓
KUMO-TD-07	The system shall be able to encode messages to a QPSK Coded Rate 0.8 format.	✓
KUMO-TD-08	The system shall be able to decode messages of a QPSK Coded Rate 0.8 format.	✓
KUMO-TD-09	The system shall be able to receive messages from the ground segment at a time interval of 12.6 hours.	✓
KUMO-GNC-02-2	On-board antenna gain shall be sufficient to communicate at the bandwidth of 60 kbps at distances of up to 158 million km.	✓
KUMO-GNC-03	Ground segment shall allow for a 60 kbps bandwidth.	✓

**Table 4.5:** Mission link budgets Tsubuyaki to the groundstation and emergency downlink

Parameter	Unit	Downlink Phase 1	Downlink Phase 2	Emergency Phase 2
Antenna gain	dBi	41.4	41.4	0.1
Satellite TX power	dBW	17.8	17.8	10.0
Line loss	dB	-1.2	-1.2	-0.65
EIRP	dBW	57.9	57.9	9.5
Propagation range	AU	0.99	1.06	1.06
Space loss	dB	-274.4	-274.9	-263.7
Atmospheric losses	dB	-0.17	-0.17	-0.04
Gain	dBi	68.3	68.3	57.0
Line loss	dB	-0.5	-0.5	-0.5
C	dB	-148.9	-149.4	-197.7
System noise temperature	dB-K	26.6	26.6	26.6
G/T	dB/K	41.7	41.7	30.4
Receiver C/N <sub>0</sub>	dB-Hz	53.1	52.6	4.27
Data rate per user	dB-Hz	47.8	47.8	0.0
Available Eb/No	dB	5.4	4.8	4.3

### 4.2.2. Operational modes

Using the description of the telecommunications overview in Section 3.2.2, the operational modes of the orbiter can be defined. The orbiter will, just like the probe, have a general operations mode and a safety mode. However, the orbiter will also have an antenna-turning mode. These modes are defined so that they can be automated and do not require uplink data from the orbiter.

#### General operations mode

The general operational mode for the orbiter will be split into two different phases. In the general operational mode for phase one, the orbiter will only act as a relay for sending the data. In the general operational mode for phase two, the orbiter will switch on its instruments and start measuring science data, as well as sending the probe data to Earth.

#### Antenna turning mode

The orbiter uses one HGA to send all its data to Earth. The reason only one HGA is chosen and not two, is because of the additional weight, mass and power needs for the satellite. Since the location of Earth relative to Venus changes during the mission, the antenna must be turned anyway to establish a communication link. The turning time will be 0.3 hour. This time was estimated as turning faster would mean that more mass is needed, while going slower would yield a unnecessary slow turn. If required the turning rate could be sped up or slowed down.

The  $\delta V$  of the rotation was determined by using Eq. (4.1). The radius was determined by the size of the orbiter as described in Section 4.6. This radius was thus determined to be 0.75 m. The  $\omega$  was determined by the rotation of 180° at a speed of 0.3 hour to be 0.006 rad/s. Thus the  $\Delta V$  is 0.007 m/s.

As described in Section 3.2.2 there will be 5 rotations per orbit in the first phase and less in the second phase. This means that the total amount of  $\Delta V$  will be very low. Thus the fuel mass added by the rotations is not a point of concern.

$$\Delta V = \frac{\omega}{R} \quad (4.1)$$

### 4.2.3. Telecommunication instruments

The antennas for Tsubuyaki were selected in a similar fashion as the antennas for Tori (See Section 3.2.4 and Section 3.2.4 for a more detailed explanation behind the choices of the antennas).

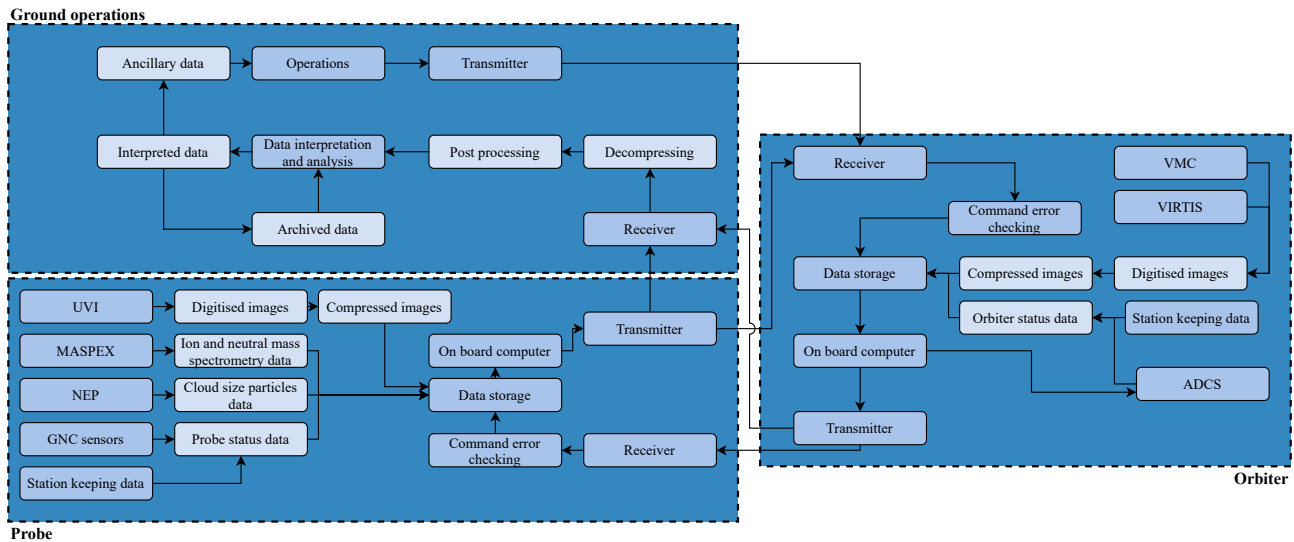
The specific antennas selected for Tsubuyaki include an omni-directional LGA and a HGA. The LGA is the same as for Tori and can be found in Section 3.2.4. This section also includes the HGA selected for the orbiter and the ground station selection.

### 4.2.4. Link budgets

The values for the link budgets have been completely written out in Section 3.2.5. In this section the link budgets with respect to the probe are discussed. The link budgets included in Table 4.5 are the design driving budgets for the orbiter. As shown in the table, the links close the budgets.

**Table 4.6:** Mass and power budget of the telecommunication and command subsystem of the orbiter

Component	Mass [kg]	Power [W]
HGA	6	60
LGA	0.04	10
Transponder	5.4	38
Cables	3	-
Gimbal	7.5	30
C&DH unit	10	34
<b>Total</b>	<b>31.73</b>	<b>172</b>

**Figure 4.1:** Communication diagram

#### 4.2.5. CD&H

The CD&H architecture of Tori will be the same as the orbiter. This is done as the orbiter will have to perform the similar tasks as the probe. It can be found in Section 3.2.7.

#### 4.2.6. Subsystem overview

In this section the mass and power budget of the subsystem is given. The mass of the HGA was estimated using similar missions to be 6 kg. The power of the HGA was taken from NASA<sup>8</sup>. The mass and the power of the LGA, Transponders and cables can be found in (Sivac and Schirmann, 2007; Wertz et al., 2011). The gimbal mass and power is provided on its website<sup>9</sup>. To estimate the C&DH unit a similar unit from the Magellan mission was used<sup>10</sup>.

An overview of the communications with the probe and ground station is given in Fig. 4.1. This diagram has been used in the design of the telecommunications system and outlines the information discussed in Section 3.2.2.

#### 4.2.7. Verification and validation

The orbiter uses the same model to verify the link budgets. The verification of this model can be found in Section 3.2.9. The same can be said for the overall verification and validation of the subsystem which is described in Section 3.2.9.

#### 4.2.8. Risk assessment

This section is the final risk assessment of Tsubuyaki's TT&C subsystem, which is needed after a detailed design has been performed. Table 4.7, includes all the main risks of the subsystem including updated risks from previous assessments and new risks that consider the designed architecture and operation of the subsystem.

#### 4.2.9. Sustainability

The sustainability scores of the orbiter are based on similar rhetoric as used for the probe. The justification of these scores can be found in Section 3.2.11.

<sup>8</sup>[https://pds.nasa.gov/ds-view/pds/viewInstrumentProfile.jsp?INSTRUMENT\\_ID=MRS&INSTRUMENT\\_HOST\\_ID=MEX](https://pds.nasa.gov/ds-view/pds/viewInstrumentProfile.jsp?INSTRUMENT_ID=MRS&INSTRUMENT_HOST_ID=MEX), retrieved on 22-6-2021

<sup>9</sup>[https://www.moog.com/content/dam/moog/literature/Space\\_Defense/spaceliterature/spacespacecraft\\_mechanisms/moog-type-22-apm-datasheet.pdf](https://www.moog.com/content/dam/moog/literature/Space_Defense/spaceliterature/spacespacecraft_mechanisms/moog-type-22-apm-datasheet.pdf), retrieved on 22-6-2021

<sup>10</sup><https://magellan.aero/wp-content/uploads/C&DH.pdf>, retrieved on 22-6-2021

**Table 4.7:** Risk assessment and mitigation

<b>3a-2:</b> <i>Loss in communication between Tsubuyaki and GS due to equipment failure.</i>
<b>Assessment L4S4:</b> With an antenna failure, Tsubuyaki would not be able to return the science data to Earth.
<b>Mitigation L3S3:</b> Tsubuyaki contains a HGA and a LGA. That means that if one antenna fails, the other can be used for communication with Earth. Similar to risk 3a-1, science data would only be partially retrieved if the HGA fails.
<b>3b-2:</b> <i>Loss in communication between Tsubuyaki and GS due to software failure.</i>
<b>Assessment L4S4:</b> The telecommunication software could wrongly handle the received and sent data. This type of failure, even though critical, is not very common.
<b>Mitigation L3S3:</b> The likelihood of software failure is low. Therefore, no additional effort is needed to mitigate the risk besides extensively testing the system on Earth.

The Tsubuyaki TT&C subsystem scores are similar to the probe's with one difference. The score for the interplanetary segment is a "reasonable" (2) rather than a "high" (3) as the C&DH unit and the antenna will be turned on and using a lot of power and propellant.

Since Tsubuyaki only carries one antenna on board, the orbiter must rotate towards once receiving the data from Tori in Venus. Once the time is known to rotate the orbiter, adequate reaction wheels should be sized, which is done in GNC explained in the following section.

### 4.3. Guidance, navigation and control

GNC is in charge of the control and navigation of Tsubuyaki. The orbiter must resist all disturbances from its environments and orient itself to communicate with both Tori and Earth. In Section 4.3.1, the design requirements are presented. In Section 4.3.2, the disturbance environment is quantified. The design of the sensors and actuators used in the subsystem is shown in Section 4.3.3. The script used to design the subsystem is verified and validated in Section 4.3.4. Last, the risks and sustainability aspects of the subsystem are discussed in Table 4.12 and Section 4.3.6, respectively.

#### 4.3.1. Requirements

The design of the GNC subsystem of Tsubuyaki was led by requirements set during the design of the Kumo mission. Those requirements have been updated since the architecture and more details of the mission have been defined. For example, in the initial design stage, requirements were created for a single-vehicle mission. However, at this stage, it is known that Kumo contains a probe and an orbiter. Therefore, some requirements have been specified for both vehicles. Those requirements received the "-b" suffix to indicate that they are a Tsubuyaki requirement that has been derived from a similar requirement formulated to Tori. The final list of Tsubuyaki's GNC requirements and their status is shown in Table 4.8

**Table 4.8:** Requirements for Guidance, Navigation and Control

Identifier	Requirement	Check
KUMO-AD-01-b	The attitude determination system shall determine the vehicle orientation with a minimum of 5° accuracy.	✓
KUMO-AD-02-b	The attitude control system shall be able to orientate the vehicle with 0.25° accuracy.	✓
KUMO-AD-03	The attitude control system shall be able to achieve the commanded orientation with a maximum 0.33 ° s <sup>-1</sup> slew rate.	✓
KUMO-AD-05-b	The attitude control system shall be able to operate with a maximum of 1 actuator failure.	✓
KUMO-GNC-01	The guidance subsystem shall translate received ground commands into measures, to be taken by the control subsystem.	✓
KUMO-GNC-06	Guidance communications shall be prioritised in the downlink and uplink.	✓
KUMO-GNC-11	The control subsystem shall maintain a stable orbit autonomously for 24 <TBC> hours.	✗
KUMO-GNC-14-b	Functional redundancy shall be implemented for the control subsystem.	✓

#### 4.3.2. Disturbances environment

The disturbances experienced by the vehicle and the requirements drive the sizing and selection of sensors and actuators. For that, the disturbance environment that Tsubuyaki will experience was quantified. From past missions to Venus, it is known that the planet lacks a magnetic field. Therefore, no disturbances due to the magnetic field were considered. Furthermore, Tsubuyaki will have a minimum altitude of 250 km, which is high enough to make the disturbances due to atmospheric drag negligible. This section, therefore, displays the measured disturbances due to gravity gradient and solar radiation only. The results and formulas used to quantify the disturbances are given in Table 4.9

For the gravity gradient equation shown in Table 4.9,  $\mu$  is Venus' gravitational constant,  $R$  the distance of the vehicle to the centre of the planet,  $I$  the mass moment of inertia,  $\theta$  the angle between vertical and principal axis. In the same table,

**Table 4.9:** Quantification of disturbances experienced in Tsubuyaki's orbit (Wertz et al., 2011)

Disturbance	Equation	Torque value [Nm]
Gravity gradient	$T_g = \frac{3\mu}{2R^3}  I_z - I_y  \sin(2\theta)$	0.20
Solar radiation	$T_s = \frac{\Phi}{c_s} A_s (1 + q) (cp_s - cm) \cos\phi$	0.06

for the solar radiation equation  $\Phi$  is the solar constant,  $A_s$  the sunlit surface area,  $q$  the reflectance factor,  $cp_s$  the centre of solar radiation pressure,  $cm$  the centre of solar radiation mass and  $\phi$  the angle of incidence of the sun.

### 4.3.3. Sensors and actuators

Tsubuyaki's attitude determination system includes two sensors. First, a star tracker, which will be used to determine the absolute attitude of the vehicle. An extra star tracker is included to guarantee redundancy. Second, with the same reason given for the probe design, the orbiter will contain two IMUs.

Four reaction wheels will perform the vehicle's attitude control in a pyramid configuration. This selection is inspired by the most recent orbiter on the planet, Venus Express. To size the reaction wheels, Eq. (4.2) was used. This equation, which is a preliminary estimation provided by (Zandbergen, 2017), determines the mass of the wheels based on the maximum momentum it needs to store. The maximum momentum occurs at the maximum wheel torque, which can be determined by Eq. (4.3). This equation takes the critical angle and time to slew as input. For Tsubuyaki, the extreme slew manoeuvre is defined by requirement KUMO-AD-03. With the wheel torque calculated, the maximum momentum was determined by:

$$M_{rw} = 1.7881 \cdot h_{max}^{0.422} \quad (4.2)$$

$$T_D = \frac{4I \cdot \theta}{t^2} \quad (4.3) \quad h_{max} = \frac{\sqrt{2}}{2} T_D \frac{P}{4} \quad (4.4)$$

In Eq. (4.2),  $M_{rw}$  is the estimated mass of the reaction wheels and  $h_{max}$  the maximum momentum the reaction wheels need to provide. For Eq. (4.3),  $T_D$  is the maximum torque,  $I$  the mass moment of inertia,  $\theta$  the slew angle and  $t$  the slew time. In Eq. (4.4),  $h_{max}$  is the maximum momentum,  $T_D$  the maximum torque and  $P$  the orbital period.

In addition to reaction wheels, the vehicle needs a way to correct the momentum bias introduced by the environment. This correction, for Tsubuyaki, will be performed by thrusters. Eq. (4.5), was used to determine the minimum force the thrusters should provide. It was found that each thruster needs at least 10 N force to provide the required momentum bias correction in the worst case of the mission. Six thrusters will be used to allow the correction in all three axes. However, six extra thrusters will be presented in the orbiter's body to comply with the redundancy requirement KUMO-AD-05-b. A complete budget of sensors and actuators can be seen in Table 4.10.

$$F = \frac{h}{L \cdot t} \quad (4.5)$$

**Table 4.10:** Tsubuyaki's attitude determination sensors and actuators

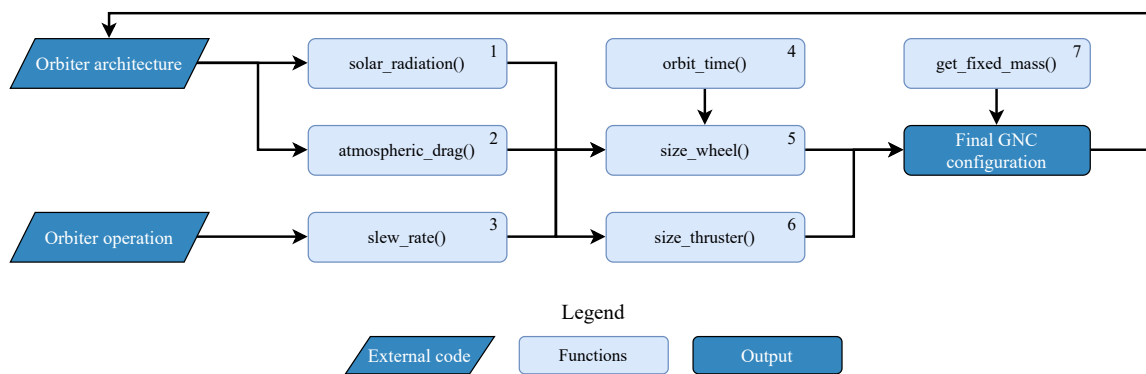
Component	Quantity [-]	Mass [kg]	Power [W]
IMU	2	4.08	34
Star tracker	2	3.55	8.9
Sun sensor	3	0.375	0.25
Reaction wheel	4	3.60	4.5
Thruster	12	4.08	-

### 4.3.4. Verification and Validation

In this section, a code was created to quantify the disturbances due to the environment, size the reaction wheels and thrusters, and integrate the GNC subsystem to the spacecraft. Verification and validation tests were needed to certify that those scripts result in a trustworthy design. A diagram showing the scripts functions and interactions is shown in Fig. 4.2. In this image, the numbers given to each function are used for reference in the verification and validation tests. The elements presented in the diagram were used to determine the critical parts of the code that needed verification. The verification tests and their results can be found in Table 4.11.

**Table 4.11:** GNC verification tests and results

Test	Expected outcome	Verified
<b>VER-GNC-1:</b> This test comprises a compilation of individual test for each function on Fig. 4.2. For each test, the input is multiplied by a factor $n$ . Then, the output is compared to the expected outcome.	For each function, the effect of each input in the outcome is known. Therefore, the outcome of a function multiplied by a factor $n$ should be equal to the expected value.	✓
<b>VER-GNC-2:</b> Functions 2, 5, and 6 contains at least one input in the denominator. The test involves bringing those inputs to a value near zero and examining the output.	For each input in the denominator, it is confirmed if the function diverges to infinity when the input gets closer to zero.	✓
<b>VER-GNC-3:</b> Function 4 is the only one that contains an input inside a root. This test analyses the function output to negative input.	For a negative input inside the root, the function should raise an error	✓

**Figure 4.2:** GNC sizing code structure

Data from the SMAD book was used to validate the code that sized the Tsubuyaki's GNC subsystem (Wertz et al., 2011). The data included input and output for two spacecraft: FireSat II and SCS. Because the equations used in the book are the same as used in the GNC code, it was expected that using the input for the two spacecraft would result in the same output encountered in the book. Those tests were successful, which indicate the code is validated for preliminary sizing of Tsubuyaki's GNC subsystem. However, it is recommended to validate the code using data from additional sources in future design stages. This way, the sizing method can be compared with vehicles that were sized using different methods. This second type of validation will allow determining the accuracy of the method used in this report.

#### 4.3.5. Risk assessment

The final risks have been set up in a similar way to the risks related to the atmospheric probe in Section 3.3.4. The risk assessment of the subsystem for the orbiter can be seen in Table 4.12. Both risks were mitigated to a level of low likelihood and noticeable effects.

**Table 4.12:** Table showing possible risks for the GNC subsystem, their severity and likelihood

##### 2a-2: Failure of attitude determination sensors.

**Assessment L4S4:** For this type of failure, the vehicle would not be able to determine its orientation. That means the required attitude pointing would not be provided. This is a high severity risk with a low chance of occurring.

**Mitigation L2S3:** All attitude sensors have been designed to be single-failure tolerant. That means a failure of a single component would not result at the end of the mission. Therefore, this makes the likelihood and severity of the risk to be reduced to noticeable and low, respectively.

##### 2b-2: Failure in actuators.

**Assessment L4S4:** Tsubuyaki needs to send data to both Earth and Tori. This architecture uses Tsubuyaki's rotation to point its antennas to each of the receivers. With a failure in the actuators, the vehicle cannot perform this manoeuvre, which is vital to the mission's return of science data to Earth.

**Mitigation L2S3:** Both types of actuators, reaction wheels and thrusters, have been designed to allow single-component failure. This, similar to the case of the sensor, reduced the likelihood and severity of failure to noticeable and low.

### 4.3.6. Sustainability

The sustainability of Tsubuyaki's GNC subsystem is very similar to Tori's GNC subsystem, as described in Section 3.3. The orbiter needs the GNC to determine its position during the mission meaning that it will be on for most of the mission duration.

In contrast to the probe, the orbiter GNC will be turned on during both the interplanetary phase and the mission phase to determine its position at all time. At this time, however, the solar panels will be deployed and thus it will work mostly on solar energy. Redundancy of the thrusters ensures that the satellite is able to turn. This, however, takes extra mass. Since the thrusters use hydrazine they will not be very sustainable. The orbiter uses mostly off-the-shelve products and thus the design and development time of this subsystem will be shorter. The GNC subsystem of Tsubuyaki received a score of "high" (3) for the first segment of the mission while the second and third segments receive a "low" (1). This is justified by the orbiter using hydrazine in its design. The weight of the subsystem is 2, as it has some influence on the sustainability but not a very significant one.

To perform the manoeuvres the GNC communicated to the orbiter, a propulsion system is needed that can steer the orbiter. Subsequently, power will be required for the GNC to function. These aspects are explained in the next section.

## 4.4. Power and propulsion

As will become evident in this section, the designs of the power and propulsion subsystems for the orbiter are vastly different from the design for the atmospheric probe. Therefore, the emphasis of this section will be on the sizing of the two independent subsystems, rather than looking at the subsystems as a coupled system. Requirements for both subsystems will be discussed in Section 4.4.1 and 4.4.4. Afterwards, the design for the power subsystem and later the design for the propulsion system will be laid out in Section 4.4.2 and Section 4.4.5. Finally, a risk assessment and a sustainability analysis for both power and propulsion will be performed in Section 4.4.7 and 4.4.8.

### 4.4.1. Power requirements

Table 4.13: Power subsystem requirements

Identifier	Requirement	Check
KUMO-PW-01	The power system shall be operational for the duration of the mission.	✓
KUMO-PW-02	The primary power source shall generate a nominal power of 413 W at EOL conditions.	✓
KUMO-PW-03	The power system shall be able to provide a peak power of 628 W at EOL conditions.	✓
KUMO-PW-04	The power storage unit shall have a capacity of 2.46 kJ at EOL conditions.	✓
KUMO-PW-05	The power storage unit shall have a specific energy of 25 Wh/kg at EOL conditions.	✓
KUMO-PW-06	The power storage unit shall have an energy density of 2000 Wh/m <sup>3</sup> at EOL conditions.	✓
KUMO-PW-07	The power storage unit shall have a cycle life of at least 66 cycles.	✓
KUMO-PW-08	The power distribution system shall provide continuous power distribution.	✓
KUMO-PW-09	The power distribution cables shall be shielded from temperature differences and the corresponding stresses.	✓
KUMO-PW-10	The power distribution system shall be able to supply power with an efficiency of 90 %.	✓

- KUMO-PW-02 - This value was found based on what the subsystems need in terms of power and with an assumed yearly degradation coefficient of 0.1, not taking into account cell efficiencies and the inherent degradation factor.
- KUMO-PW-03 - This value was found based on what the subsystems need in terms of power, with telecommunications providing most of the deviation with nominal power, and with an assumed yearly degradation coefficient of 0.1, not taking into account cell efficiencies and the inherent degradation factor.
- KUMO-PW-04 - This value was found based on the total amount of energy needed to provide the selected subsystems with power at night time.
- KUMO-PW-05 - This value is needed to keep the overall orbiter mass within a reasonable range of 1500 kg.
- KUMO-PW-06 - This value was found from the energy capacity needed and the constraining dimensions of the orbiter/launcher.
- KUMO-PW-07 - This value was found based on the times the battery will have to be charged/discharged, with a margin of 50%. These cycles are directly related to number of orbits over the duration of the mission.
- KUMO-PW-09 - This value was argued based on need to maximise efficiency to avoid divergence of solar array mass upon iteration as well as to minimise heat generated by energy losses.

### 4.4.2. Power design process

As mentioned before, a simple approach is followed for the design of the power subsystem for the Tsubuyaki orbiter. Similar to the probe, the concepts that were considered for the power source were the solar arrays, fuel cells, batteries and thermoelectric cells. Here, the solar arrays were selected as for this concept, the Sun is used as the external energy

**Table 4.14:** Preliminary power budget for the orbiter (\*Corrections only apply for systems for which the actual power usage is known)

Subsystem	Power fraction	Power estimate [W]	Power estimate with contingency [W]	Corrected power usage* [W]
Payload	0.22	41.2	41.2	41.2
Structures	0.01	1.87	3.67	3.67
Thermal control	0.15	28.09	55.04	28
Power	0.1	18.73	36.7	36.7
Telecommunications	0.18	33.71	66.05	127
Processing	0.11	20.6	40.36	40.36
GNC	0.12	22.47	44.03	34
Propulsion	0.11	20.6	40.36	40.36
<b>Total orbiter power</b>	<b>1</b>	<b>187.27</b>	<b>347.19</b>	<b>371.47</b>

source. Since Venus is closer to the Sun than Earth, the incoming solar flux for an object in orbit around this planet is considerably higher, reaching  $2622 \text{ W m}^{-2}$ . Next to that, Tsubuyaki will be receiving sunlight continuously due to the choice of its orbits. Therefore, the solar arrays could be selected as the only power source. The solar array will be rigid and be attached to the orbiter in a wing-mounted setting as to ease the application of thermal control. It also provides the option to always have a zero incidence angle with incoming solar radiation as use will be made of sun sensors and solar wing rotation mechanisms. As to have some sort of redundancy in place, a battery will also be selected in case of temporary or partial solar array failure and support at peak power conditions. Again, use will be made of a triple junction (rigid) GaAs solar cell and a lithium-ion rechargeable battery.

The most important factor for the sizing of the power subsystem is the power usage of the orbiter. For this, the preliminary power budget was used, which is presented in Table 4.14. This was done using average power fractions based on previous missions (Wertz et al., 2011, p.424). As to provide a level of contingency to the design, total power usage data was collected from previous recent Venus missions, these being Akatsuki, Magellan, Venus Express, IKAROS, Messenger, and BepiColombo. The standard deviation in this data was found and applied as a contingency factor to the power usages determined for the subsystems, which are now set within a 95% confidence interval. The level of contingency added to this budget reduces the risk of the power subsystem delivering insufficient power, despite the uncertainties regarding the actual power usage of the orbiter. In addition to this, corrections were made for the subsystems for which the actual power usage is known, these being payload, telecommunications and thermal control.

First the battery was sized, where it was decided to size for 10% of the total orbital period as to provide a power margin for the aforementioned reasons. Both the battery and the solar array were designed for the orbit in the first phase, as this comes with the longest orbital period and is thus considered the critical case. For the battery, the same characteristics and sizing method were used as stated before for the atmospheric probe.

The solar arrays are sized in a slightly different way compared to the atmospheric probe. In this case, the cells are not influenced by the planetary atmosphere, which means that calculation can simply be performed based on the specific power and cell efficiency that are listed in Table 3.15. First, the power required is found using:

$$P_{req,BOL} = \frac{\sum P_{i,d}t_{i,d} + \sum P_{i,e}t_{i,e}}{t_d} \frac{1}{\mu I_d \cos i} \quad (4.6)$$

where  $P_{i,d}$  and  $P_{i,e}$  are the power consumed by a certain subsystem component in regular orbit and in case the battery is used and  $t_{i,d}$  and  $t_{i,e}$  are the orbital period and the duration for which the battery would be turned on, in this case 10% of the orbital period. This, however, only leads to the power required at BOL. To find the power needed at EOL, yearly degradation factors have to be taken into account using Eq. (4.7). Finally, by relating EOL power to the solar flux experienced in space at a distance of 0.7 AU and plugging in the value for the area density of the assembly, the final area  $S_{SA}$  and weight of the solar array  $W_{SA}$  are found. This is given by Eq. (4.8) and 4.9 for the area and weight, respectively.

$$P_{req,EOL} = \frac{P_{req,BOL}}{(1 - C_d)^{t_{mission}}} \quad (4.7)$$

$$S_{SA} = \frac{P_{req,EOL}}{S_{i,Venus}} \quad (4.8)$$

$$W_{SA} = S_{SA} \rho_{sp} \quad (4.9)$$

Finally, a PCDU was again selected fitting to the given needs for power distribution.<sup>11</sup> The finally weights and dimensions for the power subsystem are listed in Table 4.15.

<sup>11</sup><https://www.airbus.com/space/spacecraft-equipment/power.html>, Retrieved on 15-06-2021

**Table 4.15:** Final weights and dimensions of the orbiter power subsystem

Component	Value	Unit	Component	Value	Unit
Solar arrays	1.22	kg	Batteries	21.7	kg
Solar arrays	1.04	m <sup>2</sup>	Batteries	7.16	L
PCDU	22.5	kg			

### 4.4.3. Verification of the orbiter power codes

Verification was performed for the orbiter power code. A flowchart of the code can be found in Fig. 4.3. Unit tests can be found in Table 4.16

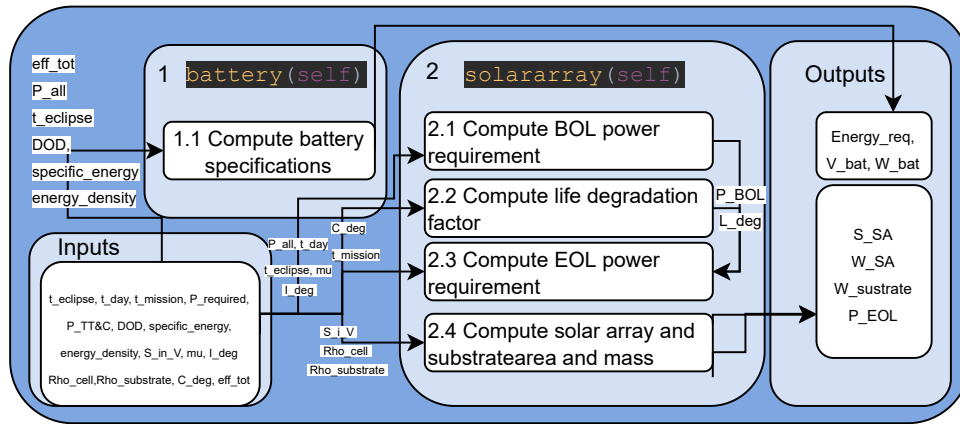


**Figure 4.3:** Flowchart showing propulsion subsystem computations

**Table 4.16:** Power verification tests and results

Test	Variables	Expected outcome	Verified
VER-POW-111	<b>Input:</b> $DOD, \eta_{BAT}$ <b>Outputs:</b> $E_{req}, V_{BAT}, W_{BAT}$	Multiplying either of the inputs by a factor of 5 should lead to a decrease of the output values by the same factor of 5. Setting either of the inputs to zero should lead to a division by zero error and thus divergence of the output values.	✓
VER-POW-121	<b>Inputs:</b> $t_e$ <b>Outputs:</b> $E_{req}, V_{BAT}, W_{BAT}$	$5 * t_e$ , should lead to an increase of the output values by the same factor of 5. $t_e = 0$ , should lead to the output values also taking on the same value of zero	✓
VER-POW-131	<b>Inputs:</b> $E_{\delta, BAT}$ <b>Outputs:</b> $W_{BAT}$	$5 * E_{\delta, BAT}$ , should lead to a decrease of the output value by the same factor of 5. $E_{\delta, BAT} = 0$ , should lead to a division by zero error and thus divergence of the output value.	✓
VER-POW-141	<b>Inputs:</b> $E_{sp, BAT}$ <b>Outputs:</b> $V_{BAT}$	$5 * E_{sp, BAT}$ , should lead to a decrease of the output value by the same factor of 5. $E_{sp, BAT} = 0$ , should lead to a division by zero error and thus divergence of the output value.	✓
VER-POW-211	<b>Input:</b> $\mu, I_d$ <b>Outputs:</b> $P_{req, BOL}, P_{req, EOL}, W_{SA}, S_{SA}$	Multiplying either of the inputs by a factor of 5 should lead to a decrease of the output values by the same factor of 5.	✓
VER-POW-212	<b>Input:</b> $\mu, I_d$ <b>Outputs:</b> $P_{req, BOL}, P_{req, EOL}, W_{SA}, S_{SA}$	Setting either of the inputs to zero should lead to a division by zero error and thus divergence of the output values.	✓
VER-POW-221	<b>Input:</b> $S_{I, Venus}$ <b>Outputs:</b> $W_{SA}, S_{SA}$	$5 * S_{I, Venus}$ , should lead to a decrease of the output values by the same factor of 5. $S_{I, Venus} = 0$ , should lead to a division by zero error and thus divergence of the output values.	✓
VER-POW-231	<b>Input:</b> $\rho_{sp}$ <b>Outputs:</b> $W_{SA}$	$5 * \rho_{sp}$ , should lead to an increase of the output value by the same factor of 5. $S_{I, Venus} = 0$ , should lead to the output taking on the same value of zero.	✓
VER-POW-241	<b>Input:</b> $C_d, t_{mission}$ <b>Outputs:</b> $P_{req, BOL}, P_{req, EOL}, W_{SA}, S_{SA}$	Multiplying either of the inputs by a factor of 5 should lead to an increase of the output values.	✓

**Table 4.17:** Propulsion subsystem requirements, main thruster only

Identifier	Requirement	Check
KUMO-PROP-01	The propulsion system shall have restart capabilities	✓
KUMO-PROP-02	The propulsion system shall have a specific impulse of 317 s at vacuum conditions.	✓
KUMO-PROP-03	The propulsion system shall provide a minimum thrust of 236 N.	✓
KUMO-PROP-04	The propulsion system shall provide a maximum thrust of 58,860 N.	✓
KUMO-PROP-05	The propulsion system shall provide a $\Delta V$ of $3.20 \text{ km s}^{-1}$ .	✓
KUMO-PROP-06	The propulsion system shall survive a minimum of 180 ignition cycles.	✓
KUMO-PROP-07	The propulsion system shall be able to provide orbit maintenance manoeuvres after failure of a thruster.	✓
KUMO-PROP-08	The propulsion system shall have a fuel consumption of $0.074 \text{ kg s}^{-1}$ .	✓

#### 4.4.4. Propulsion requirements

The requirements for the orbiter propulsion system are given in Table 4.17. At the end, it was checked whether all requirements were satisfied.

- KUMO-PROP-02 - This value was found for the reference mission Venus Express. Lower values would lead to unreasonably large propellant tanks.
- KUMO-PROP-03 - Based on the given orbits and required manoeuvres, this value is needed to treat the manoeuvres as impulsive shots, with the burn time being less than 2% of the orbital period, similar to reference mission Venus Express.
- KUMO-PROP-04 - This value is selected such that non of the extended components e.g., solar arrays would be damaged in case of maximum acceleration.
- KUMO-PROP-05 - Calculations are provided by mission planning.
- KUMO-PROP-06 - Value based on the orbital period and the assumption that primary orbit maintenance manoeuvres should be performed four times per orbit.
- KUMO-PROP-08 - Derived from specific impulse and minimum thrust.

#### 4.4.5. Propulsion design sizing

Firstly, a propellant is to be selected that possesses the characteristics necessary to fulfil the mission as described in the mission planning. Several concepts, including solar sailing and electromagnetic propulsion, are discarded without performing an in-depth analysis due to either low TRL, unfitting characteristics for the given mission or complexity of the design. Another option, nuclear power, is discarded as a result of user and sustainability requirements. Instead, more traditional chemical propulsion methods will be considered. A first division is made between solid propellants and liquid propellants. The former is considered to be more reliable, less expensive and less complex, while providing a sufficient amount of thrust. This does, however, come at the cost of no or limited restart capabilities. Given the mission planning, which describes the need for multiple manoeuvres, and the desire to use the same propellant source for both GNC manoeuvres and main orbit manoeuvres, solid propellant is thus not considered a viable option to the design. Liquid propellant, the other form of chemical propulsion considered here, does offer very good performance and generally leads to more controllable systems with restart capabilities, making it a fitting choice for the mission. Another division is made here, as both monopropellants and bipropellants are categorised as liquid propellants. Monopropellants see the oxidiser and fuel combined, making for more straightforward, less heavy and more reliable designs. Its performance is, however, not as good as for bipropellants. These generally display higher thrust and specific impulse, and tend to be more chemically stable as the oxidiser and fuel are divided over separate tanks. This is reflected by the choice of bipropellants for similar mission, including Venus express.

For the specific choice of propellant, the incentive to achieve a high sustainability for the mission led to the consideration of propellants other than harmful options that are often selected for space missions due to their high performance and high development in the past decades and thus their high reliability. An example of a green propellant with potentially high performance is hydrogen peroxide ( $H_2O_2$ ) in combination with either isooctane or ethanol. In the end, it was decided that green propellants are, in their current stage of development, not developed enough to be used for this mission. Next to that, cryogenic, less harmful alternatives were also discarded as they are deemed unfit for missions of longer duration and therefore too much of a risk. Therefore, it was opted to select nitrogen tetroxide (NTO) in combination with monomethyl hydrazine (MMH) as the propellant for this mission. As the date of launch is currently still far off, it might still be possible to select a green alternative in case TRL raising is sped up to a point where the use of these propellants can be considered reliable enough to replace the currently selected propellant. (Pasini et al., 2013) (DeSantis, 2014)

Based on the selected propellant, a thruster is to be chosen that meets the requirements set in Table 4.17. As most thrusters are designed to work with the selected propellant, there is a wide variety of options left. In the end, it was opted

<sup>11</sup><http://adsabs.harvard.edu/fu11/2004ESASP.555E...88H>, retrieved on 11-06-2021

to go with a supplier that has a good reputation and much experience in the aerospace industry, as well as a connection with the client, this being ArianeGroup. The characteristics for this thruster are given in Table 4.18.

**Table 4.18:** Propulsion main thruster summary

Brand	Specifications
ArianeGroup	$I_{sp}$ : 325 s; Mass: 4.3 kg; Thrust: 425 N; Mass flow: $0.133 \text{ kg s}^{-1}$ ; Oxidiser/fuel ratio: 1.65

With the thruster and propellant selected, the propellant tanks can be sized based on an estimate of the total propellant mass. This propellant mass is based on the total  $\Delta V$  needed for manoeuvres as described in Section 2.6.1 and found using Tsiolkovsky's rocket equation, as stated in Eq. (4.10) and the relation between the initial and final mass, given in.

$$M_0 = M_f e^{\frac{\Delta V}{I_{sp} g_0}} \quad (4.10)$$

$$M_{propellant} = M_0 - M_f \quad (4.11)$$

where  $I_{sp}$  is the specific impulse of the main thruster,  $M_0$  the initial mass before performing the manoeuvres and  $M_f$  the mass left after performing the manoeuvres. The final value for the propellant mass will be found using an iterative process, taking into account the variation of masses from other subsystems and their effect on the orbiter dry mass.

With the propellant mass known, the propellant tanks can now be sized. Firstly, The oxidiser to fuel ratio, defined by the thruster, is taken into account. The oxidiser and fuel mass respectively are found using:

$$M_{fuel} = \frac{M_{propellant}}{1 + O/F} \quad (4.12)$$

$$M_{ox} = M_{propellant} - M_{fuel} \quad (4.13)$$

Secondly, the required oxidiser and fuel volumes are found using their respective densities. Here, a margin of five percent is taken as a form of contingency. Next, the required amount of helium, which will act as pressurant gas, is found for both the oxidiser tank and the fuel tank using Eq. (4.14). Note that this gas will be contained within the propellant tanks, as use is made of a blowdown system.

$$V_{He} = \frac{\frac{P_f}{P_i} V_i}{1 - \frac{P_f}{P_i}} \quad (4.14)$$

where  $P_f$  is the final pressure required in the tank at EOL and  $P_i$  the initial pressure required in the tank at BOL. For a nominal chamber pressure of 1 Pa, these values are set to 3 Pa and 0.9 Pa, respectively (Muhaim et al., 2010).  $V_i$  is defined here as the volume of either the oxidiser or the fuel. Finally, by summing up the results, the required propellant tank volumes are obtained, leading to the selection of a propellant tank. Here, it was chosen to go with a titanium tank from a reliable supplier, ArianeGroup.

The final values for the orbiter propulsion subsystem can be found in Table 4.19. A total propellant mass of just above 700 kilograms will thus be needed to perform all propulsive manoeuvres, amounting to the propellant tanks having a combined volume of almost 1000 dm<sup>3</sup>.

#### 4.4.6. Verification and validation for the orbiter propulsion code

Verification and validation is performed for the propulsion code. It mainly concerns unit tests and validation through an example paper. (Muhaim et al., 2010)

##### Verification

Unit tests for propulsion are seen in Table 4.20.

<sup>11</sup><https://www.space-propulsion.com/brochures/propellant-tanks/700-11081t-mon-mmh-tank-ost-22-x.pdf>, retrieved on 11-06-2021

**Table 4.19:** Final weights and dimensions of the orbiter propulsion subsystem

Component	Value	Unit	Component	Value	Unit
Fuel mass	267	kg	Fuel tank volume	458	dm <sup>3</sup>
Oxidiser mass	440	kg	Fuel tank mass	28.3	kg
Oxidiser tank volume	461	dm <sup>3</sup>	Pressurant gas mass	0.50	kg
Oxidiser tank mass	28.4	kg			

**Table 4.20:** Orbiter propellant code verification

Test	Variables	Expected outcome	Verified
VER-PROP-011	<b>Input:</b> $\Delta V$ <b>Outputs:</b> $M_{propellant}$	$5 * \Delta V$ , should lead to an increase of the output value. $\Delta V = 0$ , should lead to the output taking on the same value of zero.	✓
VER-PROP-012	<b>Input:</b> $I_{sp}$ <b>Outputs:</b> $M_{propellant}$	$5 * I_{sp}$ , should lead to a decrease of the output value. $I_{sp} = 0$ , should lead to a division by zero error and thus divergence of the output value.	✓
VER-PROP-013	<b>Input:</b> $M_f$ <b>Outputs:</b> $M_{propellant}$	$5 * M_f$ , should lead to an increase of the output value.	✓
VER-PROP-014	<b>Input:</b> $O/F$ <b>Outputs:</b> $M_{fuel}, M_{ox}$	$5 * O/F$ , should lead to an increase for $M_{ox}$ and a decrease of the same factor for $M_{fuel}$ . $O/F = 0$ , should lead to $M_{ox}$ taking the value of zero and $M_{fuel}$ taking the value of $M_{propellant}$ .	✓
VER-PROP-015	<b>Input:</b> $M_{fuel}, M_{ox}$ <b>Outputs:</b> $V_{fuel,tank}, V_{ox,tank}$	Increasing either of the input values should lead to an increase of their corresponding output values with the same factor. Setting either of the input values to zero should lead to their corresponding output values taking the same values of zero.	✓
VER-PROP-016	<b>Input:</b> $\rho_{fuel}, \rho_{oxidiser}$ <b>Outputs:</b> $V_{fuel,tank}, V_{ox,tank}$	Increasing either of the input values should lead to a decrease of their corresponding output values with the same factor. Setting either of the input values to zero should lead to a division error and divergence of their corresponding output values.	✓
VER-PROP-017	<b>Input:</b> $\frac{P_f}{P_i}$ <b>Outputs:</b> $\dot{V}_{He}$	A decrease in the input value should lead to a decrease in the output value. $\frac{P_f}{P_i} = 1$ , should lead to a division by zero error and thus divergence of the output value.	✓

**Table 4.21:** Validation values for propellant tank sizing

Component	Unit	Code value	Validation value	Error (%)
Fuel tank volume	m <sup>3</sup>	0.324	0.323	0.3
Oxidiser tank volume	m <sup>3</sup>	0.335	0.333	0.6

### Validation

As means of validation, the tank sizing method was tested using an sizing example from a research paper (Muhallim et al., 2010). Table 4.21 shows the comparison between final values resulting from the code written by the team and final values from the research paper for the volume of the propellant tanks. Finally, the relative error is indicated and deemed small enough to consider the code accurate and fit for use.

### 4.4.7. Risk assessment

The technical risks for the orbiter power and propulsion subsections are given in Table 3.22 and Table 4.23, respectively. This includes the ratings given to each risk, as well as a mitigation strategy to each. In the end, it can be concluded that the most prominent risks for the power subsystem, post mitigation, are related to the failure of electrical systems or the primary power source. For the propulsion subsystem, leakage of the propellant tanks is found to be the most prominent risk for the orbiter mission segment.

**Table 4.22:** Risk assessment and mitigation for power of the orbiter

<p><b>8a-2 Partial failure of the solar arrays.</b></p> <p><b>Assessment L2S3 :</b> Partial loss of the primary power, the solar arrays, source due to either mechanical or electrical failure would reduce the available peak and average power and thus have a noticeable impact on the spacecraft's operations. The likelihood is considered low as use is made of systems that have proven successful in the past.</p> <p><b>Mitigation L1S2 :</b> (1) The preliminary power budget used to size the solar arrays was setup using contingencies. (2) MPPT and bypass diodes limit the power loss in case of partial failure of the solar array. (3) The secondary power source provides hot redundancy to the system.</p>
<p><b>8b-2 Full failure of the solar arrays.</b></p> <p><b>Assessment L1S5 :</b> Complete loss of the primary power source due to either mechanical or electrical failure would reduce the available power to the extent that it could significantly impact the mission as only the secondary power, the batteries, source is left. The likelihood is considered very low, as use is made of systems that have proven successful in the past.</p> <p><b>Mitigation L1S5 :</b> (1) Solar arrays are divided over two wing panels, placed on different sides of the spacecraft, to reduce the probability of full failure.</p>
<p><b>8c-2 Failure of the secondary battery.</b></p> <p><b>Assessment L2S4 :</b> Complete loss of the secondary power source due to either mechanical or electrical failure would reduce the power available at night (in case of an external primary power source) and peak power at all times, which could jeopardise some of the mission operations. The likelihood is considered low, as use is made of systems that have proven successful in the past.</p> <p><b>Mitigation L1S2 :</b> The orbit is chosen such that the eclipse time is limited.</p>
<p><b>8d-2 Health risks to people implementing the system.</b></p> <p><b>Assessment L3S4 :</b> The choice of a safe combination of solar arrays and a lithium ion battery decreases probability of personnel being harmed in the process of manufacturing, testing or installation. Personnel being harmed in the process would be a setback to the mission.</p> <p><b>Mitigation L2S4 :</b> (1) Extra budget is foreseen to hire specialised technicians to handle the propellant. (2) Extra time is given to the pre-launch operations phase to provide for safe handling of the propellants.</p>
<p><b>8e-2 Inability to provide the necessary EOL power.</b></p> <p><b>Assessment L3S3 :</b> Unexpected component degradation or wrong estimations of either the available power or the required power could lead to insufficient power at EOL conditions. Despite having a lot of literature, some uncertainties can not be considered, thus increasing the likelihood.</p> <p><b>Mitigation L2S2 :</b> (1) The preliminary power budget used to size the solar arrays was setup using contingencies. (2) Systems that were previously used at the same time e.g., telecommunications and payload, can be used in turns to reduce peak power.</p>
<p><b>8f-2 Degradation of the electric components in the space environment.</b></p> <p><b>Assessment L3S4 :</b> Due to the hostile space environment, electrical components could be affected by radiation. This could jeopardise mission operations. Although design should prevent this, there is still a probability that this will occur as it is a long-duration mission.</p> <p><b>Mitigation L2S4 :</b> Radiation hardening is used in materials to protect internal components.</p>
<p><b>8g-2 Electrical failures lead to inoperative electrical systems.</b></p> <p><b>Assessment L2S5 :</b> The failure of electrical systems due to, e.g., short circuits can lead to loss of mission equipment or essential systems and therefore failure of the mission. An efficient platform should decrease the probability of occurrence.</p> <p><b>Mitigation L1S5 :</b> (1) A protective insulation layer should help to avoid unwanted contact between cables, electrical losses and mechanical stresses. (2) A PCDU will help regulate the electric flow between systems.</p>
<p><b>8h-2 Extended eclipse time or obstruction of the solar arrays could lead to less available power.</b></p> <p><b>Assessment L2S3 :</b> If eclipse times are miscalculated or altered due to uncertainties, the solar arrays might not be able to generate the required power, which could jeopardise the mission. Atmospheric uncertainties add to the low likelihood.</p> <p><b>Mitigation L2S2 :</b> (1) The preliminary power budget used to size the solar arrays was setup using contingencies. (2) The orbit is chosen such that the eclipse time is limited. (3) The secondary power source is designed with a 2% margin as it also serves as a backup in case of partial loss of the primary power source</p>

#### 4.4.8. Sustainability of power and propulsion subsystem

This subsection briefly explains the sustainability of power and propulsion subsystems for Tsubuyaki. Ideally, all three phases will be addressed and scored for relevant subsystem components in order to come up with a final mark for sustainability. If the component is not relevant for a mission phase, then the average score will be calculated for the existing phases.

Hydrazine will be used in the orbiter as the propellant. This is not the most sustainable option available. Therefore, a score of 1 was given to all three phases. It is important to note that, the team had to prioritise the performance and TRL of the propellant over its sustainability. Other more sustainable options such as ethanol and kerosene were discarded due to low performance and TRL. The team is strongly advised to redirect any additional resources to the TRL raising programs of ethanol. Furthermore, new kerosene thrusters in the market must be monitored.

**Table 4.23:** Risk assessment and mitigation for propulsion of the orbiter

<b>8i-2</b> <i>Failure of the solar array deployment mechanism.</i>
<b>Assessment L1S5 :</b> Failure of the mechanism to properly deploy the solar arrays could leave the spacecraft dependent on only partial power generation of the primary power source or even full dependence on the secondary power source and would thus imply catastrophic consequences to the mission. Due to the use of proven systems and elaborate testing, although not in the environment of Venus, the likelihood of occurrence is low.
<b>Mitigation L1S4 :</b> The ADCS side thrusters could turn the spacecraft to provide sunlight for the undeployed arrays and still operate at half power.
<b>9a-2</b> <i>Insufficient amount of propellant for operations.</i>
<b>Assessment L2S4 :</b> Unforeseen manoeuvres or wrong estimations of fuel usage could lead to there not being enough fuel to perform all operations. Despite having a lot of literature, some uncertainties cannot be considered, thus increasing the likelihood.
<b>Mitigation L1S4 :</b> A five percent margin was introduced in the propellant mass.
<b>9b-2</b> <i>Small leakage of the propellant tanks due to structural imperfections or degradation.</i>
<b>Assessment L5S1 :</b> Valves and seals are connection points that could lead to small fuel leakages over time as a consequence of imperfections and degradation. This is, however, a negligible amount that does not affect the mission.
<b>Mitigation L4S1 :</b> (1) Choice of a reliable system, propellant tanks provided by ArianeGroup. (2) A five percent margin was introduced in the propellant mass.
<b>9c-2</b> <i>Significant leakage of the propellant tanks.</i>
<b>Assessment L2S5 :</b> Imperfections in the material, unexpectedly high loads and cycles could lead to leaks in the fuel tank. Here, it is already assumed that a leak before break approach is used. If large enough, this leak could mean mission failure. The likelihood is considered to be low as use is made of systems that have proven successful in the past.
<b>Mitigation L1S4 :</b> (1) Choice of a reliable system, propellant tanks provided by ArianeGroup. (2) A five percent margin was introduced in the propellant mass.
<b>9d-2</b> <i>Insufficient amount of propellant at EOL.</i>
<b>Assessment L3S2 :</b> Unforeseen manoeuvres or wrong estimations of fuel usage could lead to there not being enough fuel at EOL conditions. Despite having a lot of literature, some uncertainties cannot be considered, thus increasing the likelihood. There are no regulations regarding EOL for satellites in orbit around Venus, thus the severity is only deemed marginal.
<b>Mitigation L1S2 :</b> A five percent margin was introduced in the propellant mass.

## 4.5. Thermal control

To prevent the subsystems from overheating or damage affected by heat in general, a thermal control subsystem should be added to keep all other subsystems within the corresponding operational temperatures. This section briefly shows the thermal control design for the orbiter Tsubuyaki. First, the environmental conditions to which Tsubuyaki is subjected to, is mentioned in Section 4.5.1. This is followed by Section 4.5.2, which lists the requirements formulated to fulfill by the design. The design considerations taken and the ones used are described in Section 4.5.3, followed by a budget estimation in Section 4.5.4. Verification of requirements, risks and sustainability for the orbiter, are covered in Section 4.5.5, Section 4.5.6 and Section 4.5.7 respectively.

### 4.5.1. Environmental conditions

Venus is 0.723 AU away from the Sun, and hence the incoming solar radiation flux is 1.9 times that on Earth. This has an influence on the radiative heat balance both in orbit and during the flight to Venus, as well as on specific subsystem design decisions like the choice of solar cells (Sivac and Schirmann, 2007), see Section 4.4.5.

Furthermore, the albedo factor on Venus is equal to 0.65, i.e. 65% of the incoming sunlight on the planet is reflected back into space. This makes Venus a very bright planet, with 4.8 times higher reflection of albedo radiation than what is experienced on Earth (Wertz et al., 2011).

If combined with the orbit design, this leads to a large range of albedo radiation being received. The smallest amount would occur during crossing of the night side in the distant, circular relay orbit, while the largest incoming flux would occur at the pericentre of 250 km in the highly elliptic science orbit. To handle this large incoming radiative flux, more reflective material can be used to keep out the majority of the heat, also helping to reduce temperature variations overall by making the heat balance less dependent on the variable radiative flux.

Lastly, during the launch and transfer phase the spacecraft experiences less solar flux than during nominal conditions. To avoid one-sided heating, a “barbecue roll” can be used, as will be described in Section 4.5.3.

### 4.5.2. Requirements

The instruments and subsystems on board require a certain operational temperature range. Table 4.24 lists the ranges for the instruments and a number of subsystems. The temperature ranges are taken from Spacecraft System Engineering (2011).

**Table 4.24:** Operating temperature ranges of Tsubuyaki subsystems and instruments (“Spacecraft Systems Engineering”, 2011)

Element	Minimum temperature [K]	Maximum temperature [K]
VMC <sup>12</sup>	223	338
VIRTIS-M Visible <sup>13</sup> (Piccioni et al., 2004)	150	190
VIRTIS-M Infrared, VIRTIS-H <sup>14</sup> (Piccioni et al., 2004)	65	90
Propellant (NTO/MMH) <sup>15</sup>	284	294
Batteries	273	353
Solar arrays	168	383
Sensors	243	323
Thrusters	280	338
Mechanisms	273	323
On board computer	263	323
Transponder/transmitters/receivers	253	333
<b>Target range</b>	284	323

**Table 4.25:** Requirements for thermal control

Identifier	Requirement	Check
KUMO-TSU-TC-01	The overall temperature of the orbiter shall be constrained between 284 K and 323 K.	✓
KUMO-TSU-TC-02	The VIRTIS payload cold boxes in the orbiter shall be able to maintain temperatures between 65 K and 190 K.	✓
KUMO-TSU-TC-04	The orbiter thermal control subsystem shall be equipped to cope with any temperature change during the mission for other subsystems.	✓
KUMO-TSU-TC-05	The orbiter thermal control subsystem shall be able to regulate the temperature of the propellant carried on board.	✓
KUMO-TSU-TC-06	The thermal control subsystem of the orbiter shall be at least 95 % reliable.	✓
KUMO-TSU-TC-07	The temperature gradient of the outer and inner structure of the orbiter must not exceed 15 K.	✓
KUMO-TSU-TC-08	The thermal control subsystem shall be effective during all active mission phases.	✓

Combining these subsystem temperature ranges, the target range can be used as the design target for the thermal control subsystem requirements listed in Table 4.25, together with more specific payload requirements to accommodate the cryocooling of VIRTIS for example. The subsystem requirements relevant to the space segment thermal control were selected and adapted from the generic thermal control subsystem requirements (Bronstring et al., 2021a).

### 4.5.3. Design considerations

To design Tsubuyaki’s thermal control subsystem, inspiration can be drawn from the Venus Express orbiter system design (Sivac and Schirmann, 2007). Since Tsubuyaki also carries both the VMC and VIRTIS instruments, the thermal control methods for the payload can be derived similarly.

First, the passive control methods were investigated. This included looking into surface finishes and insulation. Since, Tsubuyaki will be operating in different space conditions like cold temperatures during interplanetary travel and hot temperatures while approaching Venus, just passive techniques would not be enough. Hence, it was also decided to investigate into active thermal control techniques for Tsubuyaki.

- **Multi-layer insulation:** These are generally used to prevent excess heat loss from a critical component on board the spacecraft. They consist of multiple layers with low emissivity and low conductivity values. For Tsubuyaki, similar to the Venus Express mission, 23 layers of Kapton foil will be used. This will be wrapped on the outside of the spacecraft.
- **Passive louvre assembly:** Next, passive louvre systems were also investigated, by studying the Rosetta mission by ESA<sup>16</sup>. Tsubuyaki will integrate a passive thermal louvre, that uses bimetallic springs to control the position of the flaps. They will be placed on the radiators on its back and sides of the orbiter. When the temperature of Tsubuyaki rises, the bimetallic properties of the springs create expansion, opening the louvres. This helps in modifying the average emissivity of the exterior surface and let the excess heat radiate. Similarly, when Tsubuyaki is in cold conditions, the flaps close, thus, previous retaining the surface emissivity and keeping the heat to itself. This way the need for active control is reduced, saving power.

<sup>13</sup><https://blogs.esa.int/vmc/faq/>, retrieved on 11-06-2021

<sup>14</sup>The operational temperature ranges of the VIRTIS instruments refer to their cold box elements. These cold boxes have their own cryocoolers that dissipate the heat they extract through radiators into space.

<sup>15</sup><http://propulsion-skishnan.com/pdf/N204-MMH%20Upper%20Stage%20Thruster.pdf>, retrieved on 11-06-2021

<sup>16</sup>[http://www.esa.int/ESA\\_Multimedia/Images/2015/08/Rosetta\\_thermal\\_louvres](http://www.esa.int/ESA_Multimedia/Images/2015/08/Rosetta_thermal_louvres), retrieved on 14-06-2021

- **Heaters:** Some active control is needed for keeping the propellant and thrusters in their rather narrow temperature range. For this, patch heaters are used to keep these elements warm during eclipse conditions. The batteries also function better when not too cold, so patch heaters can be used to keep the batteries at operating temperatures as well. Similar to the Venus Express orbiter, Tsubuyaki will have 6 heating distribution units. Each patch heater unit requires 7.16 W of power, to heat up the critical components on board. At a time, 3 heaters are switched on, and 3 are redundant. The temperature sensors for the instruments on board will be sending the measured temperatures to the on board computer, which is pre-programmed for a set of target temperature ranges. When the input temperature falls outside that range, the command to switch on the redundant heaters is initiated.
- **Cryogenic coolers:** As seen in Table 4.24, the VIRTIS-M Infrared and VIRTIS-H have an operating temperature between 65 K and 190 K. This brings in the need of having a cold box for this instrument. Since, the overall orbiter temperature is targeted to be in the range of 279 K and 297 K, individual cold boxes with cryogenic coolers are needed. Furthermore, the cold boxes of the VIRTIS instrument have their own active thermal control system, but need provisions to get rid of the heat they extract from the instrument need to be considered when designing the bus. Therefore, a heat conducting connection to the back-side radiator will be included, covered with louvres as described before.
- **“Barbecue roll”:** After the kick stage has propelled the orbiter and probe onto the transfer trajectory, a “barbecue roll” will be initiated around the pro-grade axis. This helps distribute the sideways incoming solar radiation evenly across the sideways exposed area, while keeping the antenna pointed retrograde for communication with Earth.

Following these temperature control techniques, a constant internal temperature of 286K was found for Tsubuyaki.

#### 4.5.4. Budget estimation

Due to the special thermal control conditions for the VIRTIS instrument and the high solar flux, the estimate of the mass budget for the thermal control subsystem of the orbiter will be on the high side of the values for the mass fractions that are available from (Wertz et al., 2011): combining the 6% thermal control dry mass fraction with the payload mass of 33.43 kg, which typically makes up 15% of the total dry mass, a thermal control system mass of 13.4 kg is found. Adding a contingency of 50% brings the thermal control mass to 20 kg, to account for both the uncertainty at the current design stage, as well as for the more critical thermal conditions that the system has to manage compared to the typical interplanetary missions used as a reference.

For the power budget, the subsystem power fractions from (Wertz et al., 2011) were found not representative of the driving role of the TT&C subsystem in the orbiter. Its power of 172 W is larger than the payload power (41.2 W), so instead it was estimated that the telecommunication power would account for approximately 40% of the total power consumption. With the upper bound thermal control power fraction being 5% of the total power budget, an estimate of 21.5 W is obtained for the thermal control system. Again to allow for contingencies, uncertainties and miscellaneous power draws from small elements like control unit or thermocouple sensors, 30% were added on top, yielding a final thermal control power estimate of 28 W.

To transfer the temperature data of the orbiter to the ground station, a number of temperature sensors are included on key systems to collect household data for monitoring the spacecraft condition. Space grade temperature sensors like the TMP461-SP from Texas Instruments<sup>17</sup> weigh very little compared to the 20 kg of thermal control system mass, so it is accounted for in the contingency, and the same holds for the power draw. The sensors are supposed to provide a new reading every 30 s during normal operations as the time scale of temperature changes is rather slow. Of course during manoeuvres and other critical operations the acquisition rate can be temporarily increased for closer monitoring. The TMP461-SP provides readings as a 12 bit number. Sets of two sensors are added near the fuel and oxidiser tanks each, near the batteries, on-board computers and payload instruments. The rest of the sensors are also added to these components to serve for redundancy. Together, these 22 sensors recording 12 bit numbers every 30 s thus producing data at a rate of 8.8 bps.

#### 4.5.5. Verification of requirements

The design of Tsubuyaki was not done in as much detail, as for Tori. The design choices were mainly motivated by past missions to Venus, which guaranteed reliability of the instruments and heaters. Thus, this section does not do model verification, since a model was not developed in detail for Tsubuyaki. Estimations were based on the Space engineering handbook (Wertz et al., 2011), which were already verified in terms of product for the components.

The following list justifies how for each requirement, verification was done.

- KUMO-TSU-TC-01 : All elements of thermal control contribute to achieving this requirement to be in the operating temperature range. This was validated from previous mission temperature values. It can only be verified either by analysis/simulation or by a physical all-up test in a vacuum chamber.
- KUMO-TSU-TC-02 : To ensure that this payload-specific requirement is met, the radiator with louvres at the back is considered. Its function can be verified during the same all-up thermal vacuum chamber test as proposed earlier, or via analysis/simulation.

<sup>17</sup><https://www.ti.com/product/TMP461-SP>, retrieved on 21-06-2021

**Table 4.26:** Tsubuyaki thermal control risk table

---

**7a-2:** Failure of thermal active and semi-active control.  
**Assessment L2S4:** Failure of active thermal control would happen due to a power surge or power depletion, leading to loss of thermal control on the craft. This is not very likely but would result in critical failure as the propellant on board might freeze.  
**Mitigation L1S4:** The severity of active control failing is remains critical, as the propellant remains unchanged. To reduce the likelihood, the active patch heating system is designed for cold redundancy to replace a failed primary heater patch, but can also be used in case the first set is not strong enough to recover from an unplanned condition of extreme cold. To reduce the likelihood of a temporary loss of power, the power system does contain a battery that can bridge the temporary loss of primary power from the solar panels.

---

**7b-2:** Undercooling during transfer to Venus.  
**Assessment L3S3:** During the transfer, the spacecraft will receive less solar radiation than in the target environment close to Venus. Thus it runs a moderately likely risk of undercooling, with critical consequences like frozen propellant.  
**Mitigation L1S2:** Patch heaters are applied to the propellant tank to keep it from freezing during the transfer, reducing the likelihood of the propellant actually freezing to low. Furthermore, the same patch heaters help mitigate the severity of the frozen propellant risk, as they can also be used to thaw the propellant in case it has frozen, thus reducing the severity to marginal.

---

**7c-2:** Thermal stresses from temperature gradient during transfer.  
**Assessment L4S3:** During the transfer the spacecraft would likely be facing towards Earth for communication purposes, with the Sun heating one side of the spacecraft. This will cause the Sun-facing side to heat up, while the space-facing side cools down. This thermal gradient can have noticeable impact on the structure, and would occur with a high likelihood if no preventive measures are taken.  
**Mitigation L1S3:** Performing a “barbecue roll” along the antennas axis of symmetry during the transfer phase will evenly distribute the incoming solar flux all around the spacecraft, while still allowing the antenna to point towards Earth for communication. This reduces the likelihood of thermal stresses to low.

---

- KUMO-TSU-TC-04 : By including temperature sensors on other subsystems, the status of the satellite can be monitored. These reading can feed back both into the active thermal control loop as well as be sent to the ground station. Hence this requirement is also fulfilled.
- KUMO-TSU-TC-05 : To keep the propellant from freezing, the patch heaters are added. Their function can be tested in a smaller scale test with just the propellant tank, next to the usual analysis and simulation, thus fulfilling this requirement.
- KUMO-TSU-TC-06 : Once all components have been selected, the reliability figures can be combined to obtain the total thermal control system reliability through analysis. The system is designed for maximum reliability by opting for passive control wherever possible. Hence, this requirement is verified.
- KUMO-TSU-TC-07 : This temperature gradient has to be measured or simulated to be verified. To comply with the requirement, the design proposes to constraint the thermal gradient to a maximum of 15K. Since, Tsubuyaki does not have separate compartments like Tori, with different internal temperatures, the risk of having a larger temperature gradient is mitigated. Also, it uses a “barbecue roll”, linked to GNC. This ensures uniform heating, thus fulfilling the requirement of constraining the thermal gradient value.
- KUMO-TSU-TC-08 : The passive thermal control elements do not rely on electric power, hence functioning regardless. For the active elements like patch heaters, they can be powered as long as the system receives sunlight, or alternatively operate on battery power. To verify, an analysis on power available for heating throughout the planned mission can be done. Moreover, the power needed for the 3 heaters to operate is close to 22.8 W, which is already accounted for, in the power budget, meaning that the thermal control subsystem of Tsubuyaki, does not require any additional power than the limits constrained by the power budget. Hence, this requirement is also fulfilled.

#### 4.5.6. Risk assessment

The risks that could affect the mission success, originating from this subsystem is described in the following section. Table 4.26 explains the thermal control risks along with their mitigation strategies.

#### 4.5.7. Sustainability

This subsection briefly entails the aspect of sustainability of thermal control subsystem for Tsubuyaki. Hence, owing to the risk it could potentially pose, thermal control subsystem was given a weight of 3, meaning that among other subsystems, it has a noticeable contribution to sustainability.

The first aspect to be taken is the manufacturing process, waste handling and transportation to the launch site and testing. For this, the individual components would have to be reviewed.

- **Multi-layer insulation** : The external surface of Tsubuyaki, will be covered in 23 layers of Kapton MLI, coated with aluminium on both sides. The layers will be developed by the DUNMORE Corporation, a company which has also provided the same product to the Rosetta mission, sustaining it for more than 10 years<sup>18</sup>. However, it must

<sup>18</sup><https://www.prweb.com/releases/mli-film/esa-rosetta/prweb12316545.htm>, retrieved on 17-06-2021

be noted that both kapton and aluminium must be handled with caution, since they may be toxic if exposed for a long time. Kumo will ensure DUNMORE Corporation pay heed to the health of the workers in manufacturing and testing of the MLI. A “reasonable” score of (2) was given for the MLI blanket on Tsubuyaki.

- **Louvre assembly** : The louvre assembly will be attached onto the two sides and back side of Tsubuyaki. They will be passive in nature, thus being more reliable. They will be Designed by Spain’s Sener company, and will be extensively tested by ESA’s Mechanical Systems Laboratory in advance of Tsubuyaki’s component performance review testing<sup>19</sup>. The manufacture, testing and transportation will be carried out with the aim of optimising resources, and producing minimal emissions. A “high” score of (3) was given for the louvre assembly on Tsubuyaki.
- **Heaters** : This is an active control technique, which needs power from external sources to function. These patch heaters will be manufactured from ESA, similar to the Venus Express orbiter. This implies, extensive product verification will be carried out. Additionally, some wiring and circuits for the heaters can be repaired and reused. Hence, a “high” score of (3) was given for the heaters on Tsubuyaki.
- **Cryogenic coolers**: This is an off-the shelf instrument, needed for cooling one component of the payload specifically. However, there are some hazards while dealing with manufacturing cryogenic coolers. Due to its high pressures and low temperatures, it is prone to flammability. It may cause chemical toxicity, asphyxiation among workers if not handled with care<sup>20</sup>. However, this is only during the Earth phase while manufacturing. Once it is in orbit, these risks do not hold true anymore. However, a “low” score of (1) was given to these coolers on Tsubuyaki.
- **Temperature sensors** : There will be 10 temperature sensors on board Tori. Each component has one sensor extra for redundancy, thus mitigating the risk of failure. These sensors are also off-the-shelf sensors from the company Innovative Sensor Technology (IST)<sup>21</sup>. This company has many years of experience with the platinum sensors used on Tori. They efficiently handle energy usage and also repair dysfunctional sensors to re-use them instead of making new ones. This way, they sell sensors at a cheaper price and also consider the aspect of recycling and reusing. Hence, the sensors were given a “high” score of (3).

Moreover, all the components on board, except the heaters and cryogenic coolers, are passive control techniques which do not require power to operate. Their masses are also optimised to be the lowest as possible, leading to a total mass of 20 kg for the subsystem. This means it constitutes only about 2.2% of the total orbiter mass which is comparable to most space mission thermal mass budgets.

Summing up the scores per component, it was seen that a total score of 12 was obtained out of a possible total score of 15. This meant that the thermal subsystem for Tori is 80% sustainable in terms of components and concepts. The thermal subsystem does not use all components in all three phases of Earth operations, interplanetary travel and Venus operations phase. For Earth operations ( $SP_1$ ), a “reasonable” score of (2) was given. For the interplanetary phase ( $SP_2$ ), a “high” score of (3) was given. For the Venus operations phase ( $SP_3$ ), again a “high” score of (3) was given.

All systems must be supported by a solid structure, which subsequently protects the subsystem from the external environment. This is the final part, which will be discussed below.

## 4.6. Materials and structures

This section covers the materials and structures subsystem for Tsubuyaki, covering the material selection and structural design in Section 4.6.1, followed by the verification and validation in Section 4.6.2, the risk assessment in Section 4.6.3, and the sustainability evaluation in Section 4.6.4.

### 4.6.1. Material selection and structural design

The structures of the materials were first chosen looking at the maximum conditions, the orbiter would feel during the mission. This includes, temperature, pressure and other forms, such as radiation the orbiter might feel. The requirements are listed in Table 4.27. The values given in the requirements are then explained in Table 4.6.1. It is then followed by the sizing method and structural analysis done on Tsubuyaki. This section concludes with a verification and validation analysis, followed by sustainability and risk assessment.

- **KUMO-MAT-01** - the value of 4.5 kPa/sec was taken from the Falcon 9 user manual<sup>22</sup> as this will be the maximum pressure the orbiter will feel during operations.
- **KUMO-MAT-06** - The values of 2.7K to 358K are taken from the average values of space and the maximum temperatures felt in falcon 9 during launch.
- **KUMO-STR-02** - The dimensions of 3m<sup>3</sup> were chosen for the structure to be able to fit into the chosen launch vehicle.
- **KUMO-STR-05** - The frequency of 35Hz was also taken from the Falcon 9 user manual.

<sup>19</sup>[https://www.esa.int/ESA\\_Multimedia/Images/2015/08/Rosetta\\_thermal\\_louvres](https://www.esa.int/ESA_Multimedia/Images/2015/08/Rosetta_thermal_louvres), retrieved on 21-06-2021

<sup>20</sup><https://ehs.cornell.edu/book/export/html/1459>, retrieved on 21-06-2021

<sup>21</sup><https://www.ist-ag.com/en/products-services/temperature-sensors>, retrieved on 17-06-2021

<sup>22</sup>[https://www.spacex.com/media/falcon\\_users\\_guide\\_042020.pdf](https://www.spacex.com/media/falcon_users_guide_042020.pdf)

**Table 4.27:** Requirements relevant for Tsubuyaki materials

Identifier	Requirement	Checked
KUMO-MAT-01	The materials of the bus shall be able to withstand maximum pressure of $4.5 \frac{\text{kPa}}{\text{sec}}$ .	✓
KUMO-MAT-06	The materials shall be able to withstand a temperature range of 2.7 K to 358 K.	✓
KUMO-STR-02	The structure shall have maximum dimensions of $3 \text{ m}^3$ .	✓
KUMO-STR-05	The structure shall be able to withstand launch frequencies of 35 Hz.	✓
KUMO-STR-09	The structure shall contain the payload.	✓

**Material selection** The materials of Tsubuyaki were chosen by looking at previous mission orbiters and their material selection. The preferred properties were identified, such as UV-radiation resistance and allowable frequency from the requirements in Table 4.27, and used to design the orbiter. Active satellites and long term orbiters such as the ISS <sup>23</sup> as well using a NASA materials and manufacturing hand book(Chapline, n.d.) were considered in making design choices. Aluminium 6061 was chosen based on the above reasons.

**Internal configuration** To find the internal layout of the orbiter, the component functions were considered. For example some components need to face the Sun while others must to face Venus. The orbiter must also be balanced in weight over the axis as to add to the stability of the Tsubuyaki. Finally, the surfae area shuld be minimised to conserve mass.

The fuel tank and the oxidiser tanks are the largest internal component with similar mass and dimensions to each other. To keep the orbiter stable, these components were placed diagonal symmetrically with the payload and the other instrumentation placed within the left over space. The scientific payload must be placed on the side facing Venus, as its purpose is to observe the planet. The Sun sensors and solar panels should always be pointing to the Sun while the star sensors should not.

**Orbiter sizing** Considering the payload needed to be housed in the orbiter, the dimensions were taken as 1.5x1.5x1 m in addition to the antenna, thrusters and solar panels attached externally to the orbiter. The internal configuration is given below.

The panel thickness was found using Eq. (4.15) where  $A$  is the width of the panel multiplied by the thickness. The equation was rearranged to Eq. (4.16) to find the thickness. The width ( $w$ ) was found from the procedure described in paragraph 4.6.1 and the force ( $F$ ) was found by considering the total mass of the payload as well as the force from the thrusters.

$$\sigma = \frac{F}{A} \quad (4.15) \quad t = \frac{F}{\sigma \cdot w} \quad (4.16)$$

When applying these equation, the thickness was found to be 0.23 mm. The beams were chosen to be I-beams as they are able to withstand larger moments as well as having a reduce cross section. The size of the beams were found by finding the required shape factor with Eq. (4.19) as well as finding the shape factor for the maximum conditions using Eq. (4.17). The shape factor for the maximum should be less than the required value as indicated by Eq. (4.19). The beam dimensions are 50mm by 50mm.  $S_{max}$  is the shape factor at maximum moment and  $S_{exp}$  is the shape factor at experienced moment.

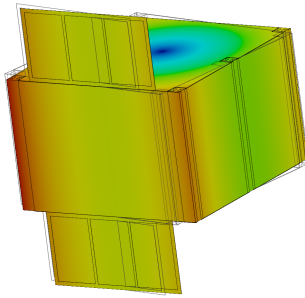
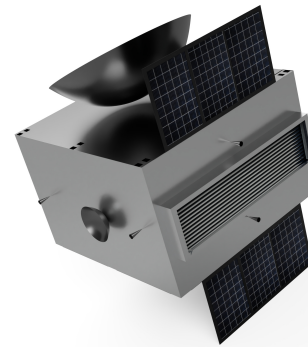
$$S_{max} = \frac{M_{max}}{\sigma_{allowed}} \quad (4.17) \quad S_{exp} = \frac{M_{exp}}{\sigma_{allowed}} \quad (4.18) \quad S_{max} > S_{exp} \quad (4.19)$$

**Frequency analysis** A preliminary frequency analysis was done to the structure of the orbiter. Fig. 4.4 shows a colour map of displacements to an applied frequency of 45Hz. It shows a lot of movement at the edges, symbolised by the red and yellow tones, while the blue and greens show less movement. The frequencies were fixed in Fusions (CAD software) simulation but the results stand useful into showing the most failure prone areas. The map shows the connection points and corners feel the most vibrations and should be reinforced if possible but is not enough to cause failure at this small frequency. A possible solution to minimise the displacement is to consider joints at the edges to help distribute the force felt by the vibrations throughout the whole body and to allow minimise displacement.

<sup>23</sup><https://www.azom.com/article.aspx?ArticleID=12034>,retrieved from 27/06/2021

**Table 4.28:** Components in orbiter

Component	Dimensions [mm]	Mass [kg]	Quantity [-]
Virtis	590x650x380	33.34	1
	220x250x100 200x250x190		
VMC	65x60x108	0.43	1
Oxidiser tank	D:850x808	306	1
Fuel tank	D:850x806	134.9	1
Thrusters	35x100	0.35	12
Star trackers	195x175x290.5	3.55	2
Sun sensors	108x108x52.5	0.38	3
Battery	360x360	21.73	1
Motor	D:250x51x194	17.9	4
Antenna (HGA)	D:3100x600	3.15	1
Antenna (LGA)	914x100	0.04	1
IMU	198x132	4.1	2
Louvre	900x600	10	3
Patch heaters	20x20x2	0.008	6
MLI	1500x1500 x4	-	6
	1500x1000 x2		

**Figure 4.4:** Colour mapping of displacements caused by oscillations**Figure 4.5:** Complete orbiter structure

**Final configuration** The final structure is shown in Fig. 4.5. Fig. 4.6 and Fig. 4.7 show the internal configuration of the orbiter. The structure is 1500 mm x 1500 mm x 1000 mm. There are six I-beams placed for structural support. These are 1000 mm in length and 100 mm x 100 mm cross sectional area. The two large tanks are the oxidiser and the propellant tanks which are shown in red. The boxes on the top right are scientific instrumentation which are shown in green, surrounded by heating pads for thermal protection, shown in blue. The boxes on the bottom left are the on board computers also surrounded by heating pads shown in yellow. The orbiter has two thrusters on each side and radiators on 3 out of the six sides. The antenna is on the opposite side of probe to the payload and the other small boxes represent the sun sensors and star trackers. A list of components is given in Table 4.28 along with their relevant masses and dimensions. The colours of the objects also reflect the weight of all the components. The components marked in red are the heaviest, the ones marked in blue are the lightest.

#### 4.6.2. Verification and validation

In this section, the verification and validation of the orbiter structures and materials has been done. First, the model verification has been complete, where a unit tests and assumption verification is shown. This is followed by a product verification where the suggested physical tests are described for the structure of the orbiter as well as requirement verification is illustrated.

**Model verification** Here, the code used to size the probe will be unit tested and analysed. Fig. 4.8 shows the structure of the code used to find the thickness of the panels and the size of the beams and Table 4.29 shows the unit tests done for the code. Through this analysis, the behaviour of the functions can be determined.

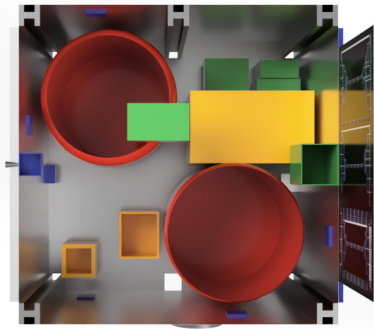


Figure 4.6: Top down view of orbiter



Figure 4.7: Side view of orbiter

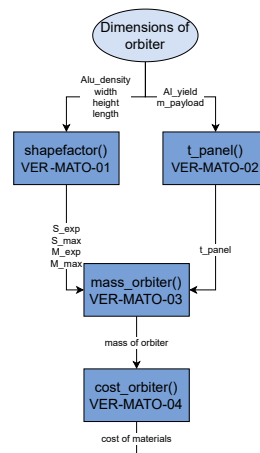


Figure 4.8: Code for orbiter sizing

**Product verification** The complete structure should be tested to prove that the designing stage was successful and built to withstand the requirements assigned. Therefore, the requirements will be verified along with a short list of tests to be performed once the production of the orbiter is complete or to components of the orbiter to assess the quality.

In the list below, the tests are explained as well as what the outcome should be to confirm the quality of the product.

- Frequency tests: This would verify if the orbiter can withstand the launch loads as specified in Table 4.27.
- Environment testing: The orbiter should be placed in a facility to test the durability of the materials in vacuum for a prolonged period of time

**Requirement verification** This section goes through the requirements stated in Table 4.27 and whether they were verified within the design process.

- KUMO-MAT-01 was addressed in the sizing of the thickness as the pressure was considered in the applied loads to consider.
- KUMO-MAT-06 was checked as the material chosen has a maximum service temperature higher and lower than the value stated in this requirement.
- KUMO-STR-02 This requirement was met as the orbiter is less than  $3 \text{ m}^3$ .
- KUMO-STR-09 The structure of the orbiter was designed based on containing the payload.

#### 4.6.3. Risk assessment

In this section the risks of the orbiter will be analysed in Table 4.30. The most prone risks are to the panel areas of the orbiter, specifically that where the tanks and payload are attached to. This is because during launch they will carry the most force and the potential to cause damage is there. Therefore, outlining the mitigation for structural failures help to highlight the most significant and to design against it.

**Table 4.29:** Unit tests for structures

Test	Variables	Expected outcome	Verified
VER-MATO-01	<b>Input:</b> alu_den, width, height, length of panels <b>Output:</b> shape factor and moment of experienced and max	If the width is doubled the moment experienced should double	✓
VER-MATO-02	<b>Input:</b> al_yield, m_payload <b>Output:</b> t_panel	By doubling the stress the thickness should halve	✓
VER-MATO-03	<b>Input:</b> t_panel, shape factor and moment of experienced and max <b>Output:</b> mass of orbiter	Doubling input should double the output	✓
VER-MATO-04	<b>Input:</b> mass of orbiter <b>Output:</b> cost of orbiter	Doubling input should double the output	✓

**Table 4.30:** Table showing possible risks, their severity and likelihood for Structures and materials

<b>5a-2:</b> <i>Failure of structure due to failure modes - Crippling, buckling and torsion.</i>
<b>Assessment L2S5:</b> The structure could fail due to these failure modes during operation. The failure of the structure in any way would jeopardise the mission itself. Therefore this is a catastrophic failure. The likeliness of this happening is low. <b>Mitigation L1S4:</b> (1) Calculate crippling, buckling and torsional loads on the structure and design against it. This could be done by performing a sensitivity analysis. (2) Identify and reinforce areas which are prone to the failure.
<b>5b-2:</b> <i>Failure due to launch loads.</i>
<b>Assessment L3S5:</b> Failure due to launch loads could be caused by the miscalculations or misevaluation of structural response to certain loads. The likelihood of this happening will be moderate because this will be well evaluated and tested as it is a critical part of the mission. <b>Mitigation L2S2:</b> Calculate operational loads and design for them in multiple ways. Test operational load scenarios on virtual programs.
<b>5c-2</b> <i>Failure due to deployment of probe</i>
<b>Assessment L3S5 :</b> This could be a structural failure due to unchecked openings of the structure which could lead to failed deployment of the platform. <b>Mitigation L2S2 :</b> (1) Test deployment mechanism before launch. (2) Check for loose orbiter section and make sure they are secure via inspection
<b>6a-2</b> <i>Materials fail due UV radiation</i>
<b>Assessment L3S3 :</b> Due to the prolonged period of time the materials of the orbiter will be deployed for, the materials could start to decay and lose some vital material properties. <b>Mitigation L3S3 :</b> (1) Apply a UV protective layer on the exposed material (2) Investigate materials with higher resistance to UV radiation

#### 4.6.4. Sustainability of the orbiter structures

The sustainability rating of the orbiter is performed in a similar manner to that of a probe. The primary structure is made out of 158 kg of Aluminium 6061, which has been analysed in Table 3.6.1. In the case of the orbiter, the CO<sub>2</sub> equivalent of the manufacturing and primary processing of the required amount of material is 3678 kg. Furthermore, the embodied energy and water usage required for the same processes are 55,000 MJ and 116,000 l, respectively.

For the orbiter in particular, the sustainability rating of the approach taken with respect to structural design is equally as important as material selection. The objective of minimising mass was set not merely for cost minimisation but also out of sustainable motives. Lower mass of the structural subsystem not only reduces the direct emissions related to the utilisation of a lower quantity of certain materials, but also plays a role in reducing the emissions from other subsystems. For instance, the power subsystem now requires a lower number of solar cells and the propulsion system requires less propellant, the environmental effects of which are much greater than the materials themselves.

Judging from the emissions calculated and the approach taken with respect to structural design, the sustainability rating SP1 can be given a score of 2. Similar to the sustainability rating for the structures of the probe, the remaining phases will be given a score of 3 for the aforementioned reasons.

## 4.7. Design overview

The final design overview includes the hardware diagram of Tsubuyaki, which depicts all interrelations between subsystems. Also, the iteration procedure as well as the final budget is defined. Finally, a sensitivity analysis on the iteration is

performed.

### 4.7.1. Interfaces

To give a concise lay out of all subsystems along with their components and they interrelated interfaces, a hardware diagram shown in Fig. 4.9 is created. This is again used to facilitate the understanding of the interrelations between the components used in the iteration procedure explained in Section 4.7.3.

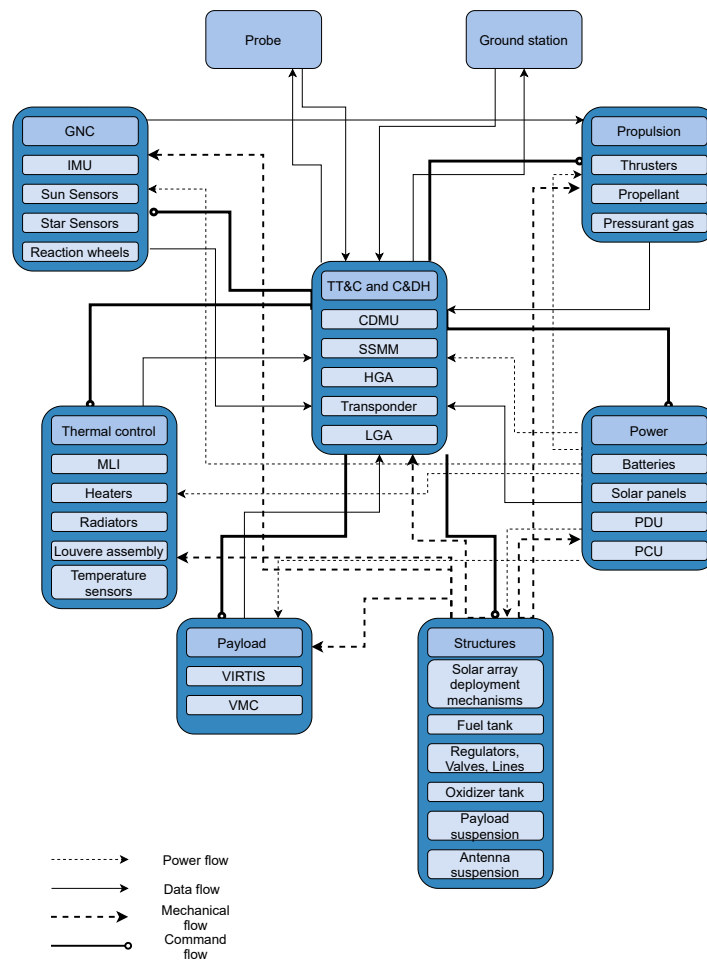


Figure 4.9: Hardware diagram orbiter

Similar explanations for most of the interfaces can be given as explained in Section 3.8.1. The major aspect that changed are the components within the subsystems. However, most of the actual type of interfaces remain equal. The only subsystem that include some differences in interfaces is thermal control.

Thermal control of Tsubuyaki includes active thermal control components this time. This suggests that the components will require power denoted with the power flow arrow. Also, the components will require some deployment mechanism for the radiator as well as structural support indicated with the mechanical flow arrow. Finally, TT&C and C&DH might need to send commands for the optimal radiator positioning which can be done through the command flow arrow.

### 4.7.2. Electrical block diagram

An electrical block diagram is again provided, showing the electrical equipment within the orbiter and the interaction between the different power components and the so-called loads, which are the systems that require power. For the orbiter, this overview is provided in Fig. 4.10.

Due to their similarities, the build up for this interface is virtually the same as that for the probe. Only, the loads and actual power flow through the system is different for the two segments. The known voltages corresponding to the loads are given in the figure.

### 4.7.3. Budgets

After doing the final iteration, the final total mass as well as its subsystems are shown in Fig. 4.11. Note that here, the fixed mass line includes the mass of GNC, payload, thermal, TT&C and C&DH.

The exact values for the mass are stated in the budget seen in Table 4.31. Furthermore, the power per subsystem is stated. A total mass of 1189.78 kg as well as a total power consumption of 340.76 W is concluded from the final iteration

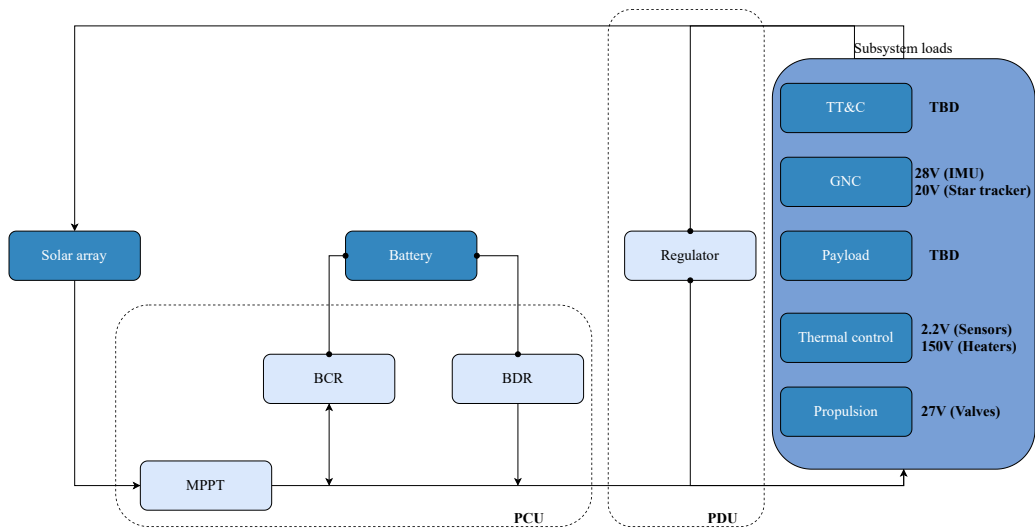


Figure 4.10: Electrical block diagram diagram orbiter

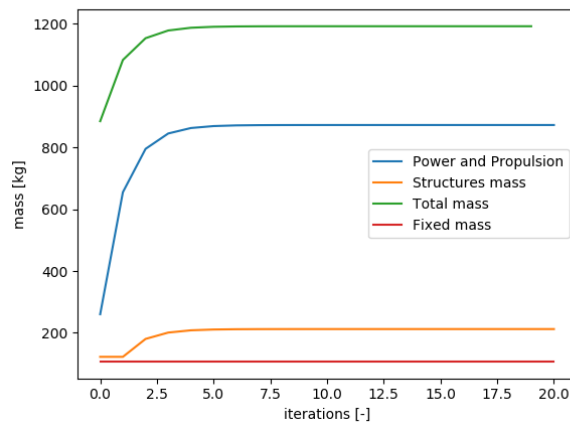


Figure 4.11: Orbiter mass iteration

Table 4.31: Tsubuyaki budget

Components	Mass [kg]	Power [W]	Data rate [kbps]	Costs [\$M]
Payload	33.43	41.2	50	35
TT&C/C&DH	31.43	172.0	-	45
GNC	22.10	22.5	0.001	7
Thermal	20.00	28.0	0.0088	1.5
Structures	212.31	0	0	6
Propulsion	64.70	40.36	0.00375	8
Power	35.62	36.7	0.00124	10
Fuel mass	770.19	0	-	-
<b>Total</b>	<b>1189.78</b>	<b>340.76</b>	<b>50.01479</b>	<b>112.5</b>

for Tsubuyaki. As seen in Table 4.31, the orbiter’s fuel mass covers 65% of the orbiter’s total wet mass. Additionally, it is seen that TT&C and C&DH consume 50% of the total power required. Finally, it is seen that 99% of the data rate is occupied by the scientific instruments, which makes sense as these are responsible for measuring the scientific data required to study the mission objectives. The mass, power and data rate have been mentioned in the sections corresponding to each subsystem. The costs will be further clarified in Section 7.4.1.

**Verification and Validation**

The code for the orbiter iteration has been verified using the code structure seen in Fig. 4.12.

The code included 6 different functions, which were each labelled to facilitate the verification process of all functions. The verification procedure is seen in Table 4.32.

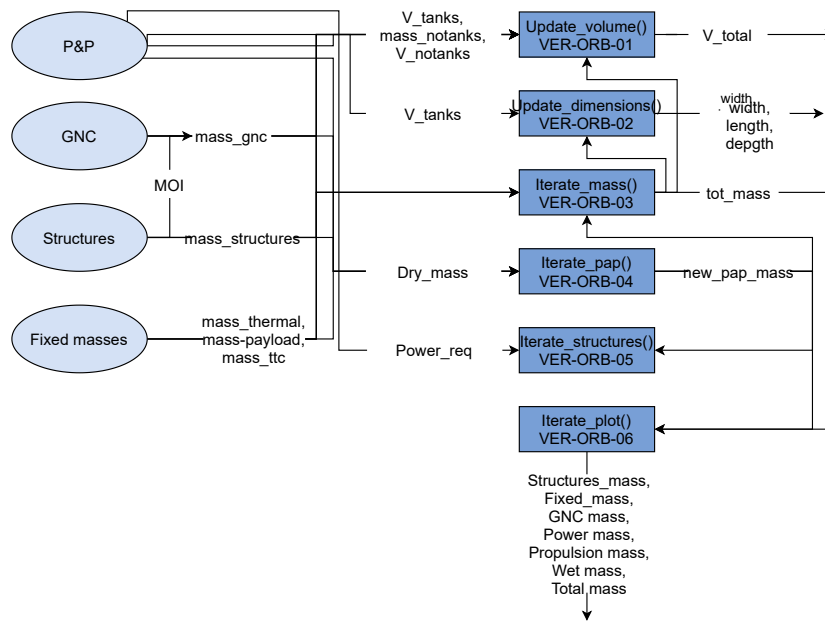


Figure 4.12: Orbiter iteration code structure

Table 4.32: Verification of orbiter iteration code

Test	Variables	Expected outcome	Y/I/N
VER-ORB-01	<b>Input:</b> $V_{tanks}$ , $V_{notanks}$ , $m_{structures}$ , $m_{thermal}$ , $m_{payload}$ , $m_{gnc}$ , $m_{ttc}$ <b>Output:</b> $V_{tot}$	Increasing/decreasing either $V_{notanks}$ or $V_{tanks}$ should increase/decrease $V_{tot}$ by the same amount; doubling $m_{notanks}$ should double $V_{notanks}$	Y
VER-ORB-02	<b>Input:</b> $V_{tanks}$ <b>Output:</b> width, length, depth	Doubling $V_{tanks}$ should increase width by a factor of $2^{1/3}$	Y
VER-ORB-03	<b>Input:</b> $m_{gnc}$ , $m_{payload}$ , $m_{thermal}$ , $m_{ttc}$ , $m_{pap}$ , $m_{structures}$ <b>Output:</b> $total_{mass}$	one of these variables should increase the total mass by the same amount	Y
VER-ORB-04	<b>Input:</b> Dry mass <b>Output:</b> $mass_{pap}$ orbiter	Increasing one of the pap dry masses should increase the mass of pap by the same amount	Y
VER-ORB-05	<b>Input:</b> $mass_{pap}$ , $power_{req}$ <b>Output:</b> $m_{structure}$	Increasing $mass_{pap}$ should increase $force$ by the same amount, increasing $t_p$ , increasing the volume that then increases the mass.	Y
VER-ORB-06	<b>Input:</b> $mass_{tot}$ , $mass_{fixed}$ , $mass_{gnc}$ , $mass_{payload}$ , $mass_{thermal}$ , $mass_{pap}$ <b>Output:</b> Mass diagram	All printed values should correspond to the value in the diagram	Y

# 5. Sensitivity analysis

This chapter elaborates on the sensitivity analyses performed on the atmospheric probe, the entry vehicle, and the orbiter sizing codes, shown in Sections 5.1, 5.2, and 5.3, respectively.

## 5.1. Tori sensitivity analysis

A sensitivity analysis is performed on each subsystem as well as the integrated system. This is done to gain more knowledge on different parameters and their effect on the design outputs. Ideally, a sensitivity analysis should be integrated in the design process and should be used to come up with optimal design procedures that minimise the sensitivity to key system inputs. The main design output parameter that will be analysed is the mass of each system. Power is not analysed as it is used as an input in both the iteration and subsystem codes. Cost is not used as it was not modelled to be variable and the time constraints deemed it not possible to remodel it.

To perform the sensitivity analysis, Monte Carlo Simulation will be used. First, each variable will be modelled using a continuous uniform distribution. A uniform distribution is one in which all values within a range are equally likely and impossible beyond that range. The probability distribution function of a continuous uniform distribution is given in Eq. (5.1).

$$f(x) = \begin{cases} \frac{1}{b-a} & , a \leq x \leq b \end{cases} \quad (5.1)$$

Note that, outside the domain, the function is set to zero. The reason why uniform distribution has been used is because there was insufficient information on the distribution of each variable and the inputs are bounded within a minimum and maximum value. In the analysis, an input variable will be given an uncertainty margin of  $\pm 20\%$ . The analysis will be divided into a singular and global sensitivity analysis. The singular analysis will focus on the variations in one or two inputs at the same time in Section 5.1.1. Global sensitivity analysis, on the other hand, will analyse the possible variations in all the variables introduced in the sections preceding Section 5.1.2. Finally, 300 samples will be drawn for each variable. The more samples are taken, the more representative the data will be of the whole range.

### 5.1.1. Singular analysis

In this subsection, inputs are categorised into four different groups: fixed mass, dimensional parameters, performance parameters and flight conditions. If a group has two inputs, these will be presented together in a three-dimensional cloud graph which maps the final mass values for a combination of the two inputs. For each input, Pearson's correlation coefficient will be used to assess the direction and strength of the association which is expressed as:

$$r = \frac{n \sum xy - \sum x \sum y}{\sqrt{[n \sum x^2 - (\sum x)^2][n \sum y^2 - (\sum y)^2]}} \quad (5.2)$$

The values can range from -1 (indicating perfect negative correlation) to 1, which signifies perfect positive correlation. Anything in between indicates a less than perfect positive or negative correlation, while a value of 0 indicates that no association exists.

**Table 5.1:** Statistical summary of the probe mass with varying fixed masses

Parameter	Value
Maximum value	566.9 kg
Minimum value	552.9 kg
Standard dev.	4.2 kg
Mean	559.9 kg

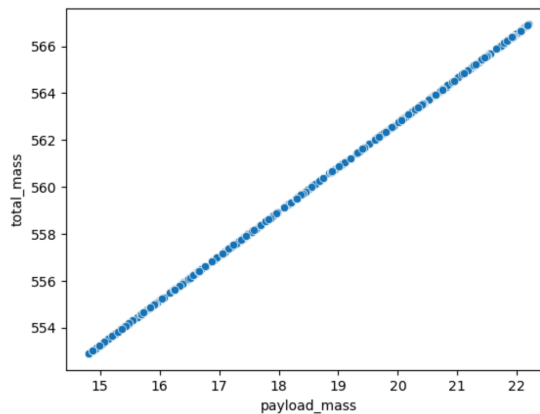


**Figure 5.1:** Probe mass versus payload mass

**Change in fixed mass:** Mass of the payload is a constituent of the fixed mass. This can change if additional payload is introduced. This was set to be 18.5 kg. After taking 300 samples from the interval of 18.5 kg  $\pm 20\%$ , a very high

correlation coefficient of 1 was found. This means that variations in fixed mass show perfectly positive correlation with the total mass. While, the Pearson’s coefficient tells us the strength and direction of the correlation it does not quantify the variation that fixed mass changes can cause. This is illustrated in Fig. 5.1 which shows a slope that is higher than one, hinting that any variation in the fixed mass itself will cause a variation that is higher in the final mass.

**Change in dimensional parameters:** Dimensional parameters include the aspect ratio and thickness-to-chord ratio of the probe. The nominal values for each are 1 [–] and 0.24[–]. The results for mass for each of the above-mentioned inputs’ variation were visually depicted in Fig. 5.2. As can be seen, decreasing aspect ratio causes the total mass of the probe to increase while increasing it makes the mass fall. While it is possible to visually confirm this for the aspect ratio, thickness-to-chord ratio shows a weaker correlation which is not very straightforward to infer visually. The Pearson’s correlation coefficient between the total probe mass and aspect ratio is found to be -0.96. This indicates proximity to perfectly negative association. For the thickness-to-chord ratio, this value is calculated to be 0.22, indicating a weakly positive relationship. The Pearson’s coefficients do verify the visual results and also helps to draw the conclusion that, comparatively speaking, the design is more sensitive to aspect ratio than it is to the thickness-to-chord ratio.

Table 5.2: Statistical analysis of the output mass

Parameter	Value
Maximum value	592.3 kg
Minimum value	530.6 kg
Standard dev.	17.9 kg
Mean	560.5 kg

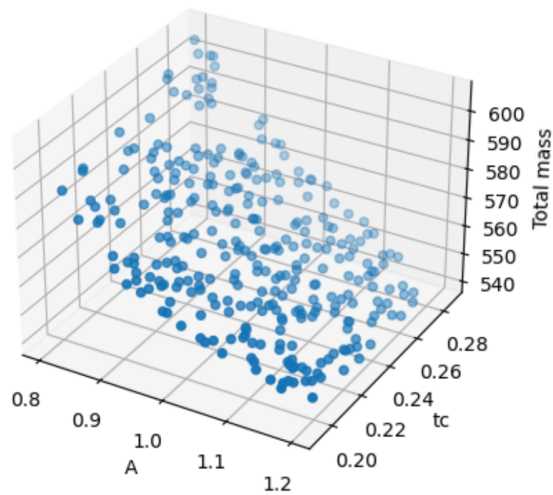


Figure 5.2: Three dimensional plot showing the cloud of mass values for change in dimensional parameters

**Change in performance parameters:** Performance parameters of the design include zero lift drag coefficient,  $C_{D_0}$ , and rate of climb (ROC). The nominal values for each respectively were set at 0.0084 and 4. As can be seen in Fig. 5.3, higher ROC results with a higher probe mass. While not as strong, a similar association exists between  $C_{D_0}$  and mass as well. The Pearson’s correlation coefficient for both respectively are 0.98 and 0.13. From this it can be concluded that ROC has a perfectly positive correlation, while  $C_{D_0}$  has a weakly positive. Hence it can be inferred that the total probe mass is comparatively more sensitive to ROC than it is to  $C_{D_0}$ .

Table 5.3: Statistical analysis of the output mass

Parameter	Value
Maximum value	598.1 kg
Minimum value	525.4 kg
Standard dev.	17.7 kg
Mean	554.5 kg

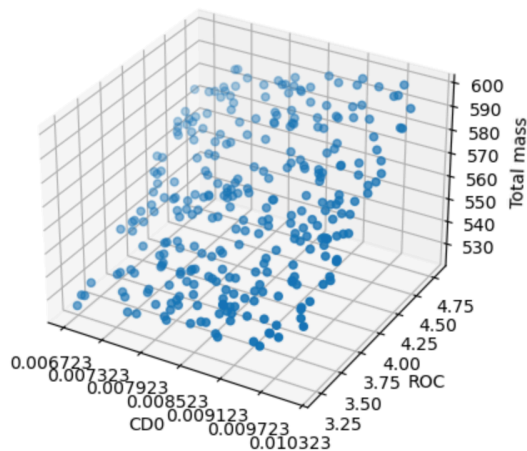


Figure 5.3: Three dimensional plot showing the cloud of mass values for change in performance parameters

**Change in flight conditions:** Flight conditions are defined by the buoyant altitude,  $h_{buoyant}$ , and flight altitude  $h_{flight}$ . The nominal values for each respectively were set at 55km and 65km. As can be seen in Fig. 5.4, higher buoyant altitude results with a higher probe mass. Furthermore, a higher flight altitude leads to an increase in the probe mass. The

Pearson's correlation coefficient for both respectively are 0.21 and 0.98. From this it can be concluded that  $h_{buoyant}$  has a weakly positive correlation, while  $h_{flight}$  has a perfectly positive. Hence it can be inferred that the total probe mass is comparatively more sensitive to  $h_{flight}$  than it is to  $h_{buoyant}$ .

**Table 5.4:** Statistical analysis of the output mass

Parameter	Value
Maximum value	606.3 kg
Minimum value	523.6 kg
Standard dev.	20.4 kg
Mean	559.5 kg

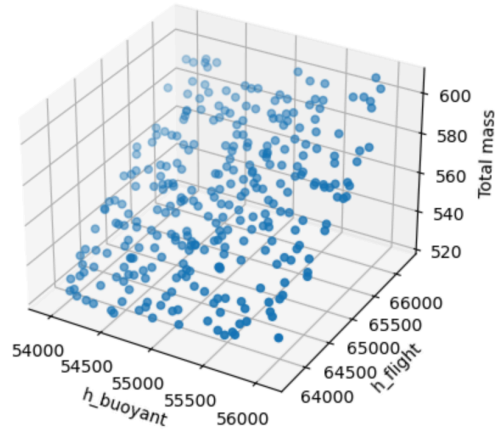


**Figure 5.4:** Three dimensional plot showing the cloud of mass values for change in flight conditions

### 5.1.2. Global analysis

The global analysis will analyse the mass cloud when more than two variables are changed. Note that, as a future suggestion, more inputs can be analysed. While the inputs analysed in this section cover both system and subsystem level inputs, there are still certain constants whose sensitivities may be assessed in the thermal control and structures codes. These include battery power, area of the rigid section and envelope thickness. Due to time constraints this section only analyses the variations in seven inputs which are used in the integration algorithm. These inputs together with their correlation coefficients are given in Table 5.5.

**Table 5.5:** Variables and their Pearson's coefficients

Parameter	r Value
$m_{payload}$	0.197
tc	0.0157
AR	-0.586
$C_{D_0}$	0.042
ROC	0.728
$h_{buoyant}$	-0.024
$h_{flight}$	-0.024

It is expected that the Pearson's coefficients are different this time. This is because the mass cloud is altered since each of the seven variables are drawn randomly from their uniform distributions. It can be concluded that when all these variables are assessed together, the one that has the strongest impact on the design is the rate of climb selection which has a correlation coefficient of 0.728. After that, the aspect ratio follows with a coefficient equal to -0.586.

**Table 5.6:** Statistical analysis of the output mass

Parameter	Value
Maximum value	635.6 kg
Minimum value	514.1 kg
Standard dev.	24.1 kg
Mean	563.6 kg

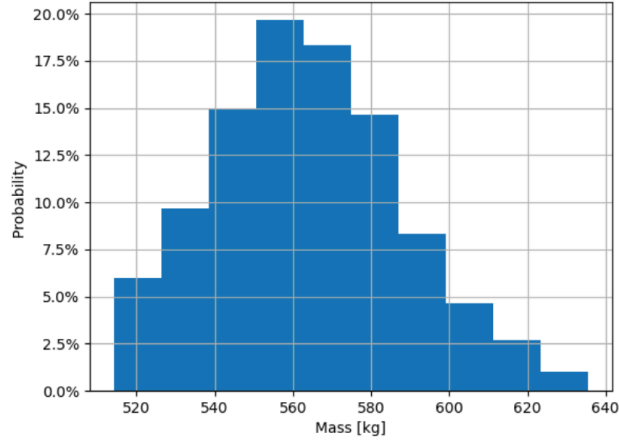


**Figure 5.5:** Histogram showing the distribution of possible outcomes

As can be seen in Fig. 5.5, the mass cloud behaves in the shape of a left skewed distribution. Even with 20% uncertainty in each variable, the mass cloud is expected to be between 516.6-635.6kg. This is a beneficial result as it indicates that even when the variables are allowed to fluctuate within their uncertainty margins, the total probe mass does not go outside  $\pm 14.5\%$  with respect to the nominal mass of 555 kg. Furthermore, the likelihood of having a final mass between 540 and 585 kg is 67.5% based on the distribution of the histogram.

### 5.1.3. Conclusion

The results of the sensitivity analysis can be used to draw important conclusions on the design efforts to the most sensitive parameters for the future design phases. First of all, the analysis confirms that with variations as small as  $\pm 20\%$ , the probe mass can be lowered to as much as 516.6 kg. This would require minor alterations in some of the performance requirements and geometry of the probe. For future iterations, the combination of inputs that yield the lowest mass could be used to reformulate some of the mission requirements to bring the mass and costs budgets down.

Furthermore, performance requirements can be renegotiated. A performance-mass trade off can be performed to determine whether the mission is able to operate at a lower rate of climb. The aspect ratio has a high impact on the probe mass as well. However, this is already minimised to have a nominal value of 1. Therefore, it is not ideal to further investigate the aspect ratio. Lastly, payload mass can be reduced to decrease the total mass. For this, the nephelometer which brings additional value to the mission can be removed. Alternatively, future products in the market can be monitored to see if lighter alternatives are developed.

## 5.2. Tamago sensitivity analysis

Due to time constraints, only a singular parameter sensitivity analysis was performed on the entry vehicle sizing code, analysing the sensitivity of the TPS mass and deployment velocity w.r.t. probe mass, entry descent angle, deployment velocity, and nose radius.

**Change in probe mass:** The probe mass, affecting the fixed mass of the entry vehicle, was sampled 300 times on the interval 555 kg  $\pm 20\%$ . The effect this has on the TPS mass is depicted in Table 5.7 and Fig. 5.6.

**Table 5.7:** Statistical analysis of the TPS mass w.r.t. change in probe mass

Parameter	Value
Maximum value	89.0 kg
Minimum value	80.7 kg
Standard dev.	2.5 kg
Mean	84.9 kg

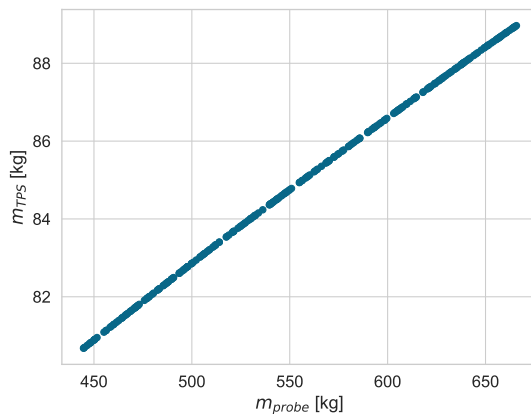


**Figure 5.6:** Plot of TPS mass relationship to probe mass

Furthermore, the change in probe mass also affects the velocity profile. The effect this has on the deployment velocity

is seen in Table 5.8 and Fig. 5.7.

**Table 5.8:** Statistical analysis of the deployment velocity w.r.t. change in probe mass

Parameter	Value
Maximum value	44.0 m s <sup>-1</sup>
Minimum value	39.4 m s <sup>-1</sup>
Standard dev.	1.4 m s <sup>-1</sup>
Mean	41.8 m s <sup>-1</sup>

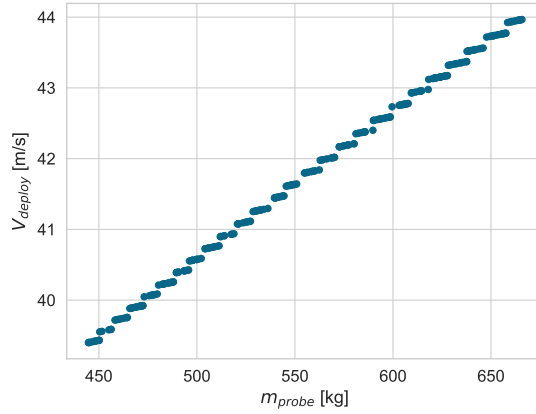


**Figure 5.7:** Plot of deployment velocity relationship with probe mass

**Change in entry descent angle:** The entry descent angle was sampled 300 times on the interval  $-6^\circ \pm 10\%$ . The effect this has on the TPS mass is depicted in Table 5.9 and Fig. 5.6. As can be observed from the value of the standard deviation, the entry angle has a relatively big effect on the TPS mass, and thus on the mass of the entry vehicle as a whole. Choosing a higher entry angle may prove beneficial in terms of reducing the heat shield mass, although it would also result in higher acceleration loads during probe descent.

**Table 5.9:** Statistical analysis of the TPS mass w.r.t. change in entry descent angle

Parameter	Value
Maximum value	127.3 kg
Minimum value	70.1 kg
Standard dev.	15.9 kg
Mean	89.3 kg

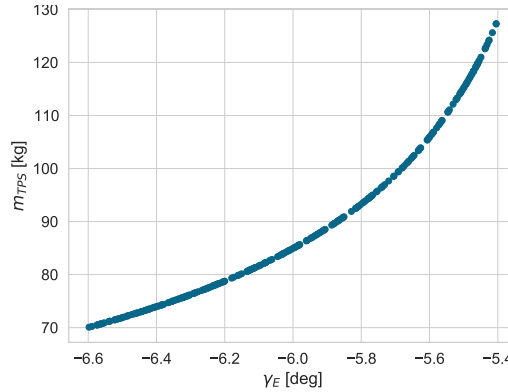
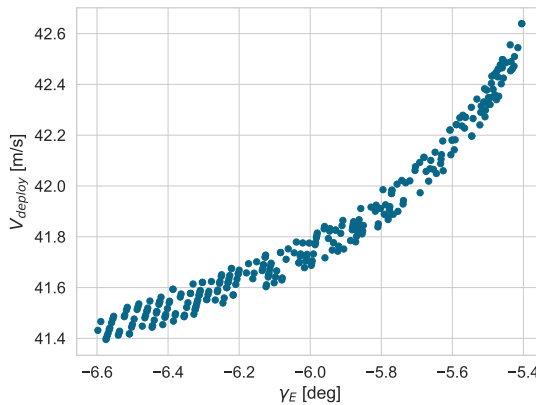


**Figure 5.8:** Plot of TPS mass relationship to entry descent angle

The effect the entry descent angle has on the deployment velocity is seen in Table 5.10 and Fig. 5.9. As can be seen, the change in descent angle only minimally affects the probe deployment velocity.

**Table 5.10:** Statistical analysis of the deployment velocity w.r.t. change in entry descent angle

Parameter	Value
Maximum value	42.6 m s <sup>-1</sup>
Minimum value	41.4 m s <sup>-1</sup>
Standard dev.	0.3 m s <sup>-1</sup>
Mean	41.8 m s <sup>-1</sup>

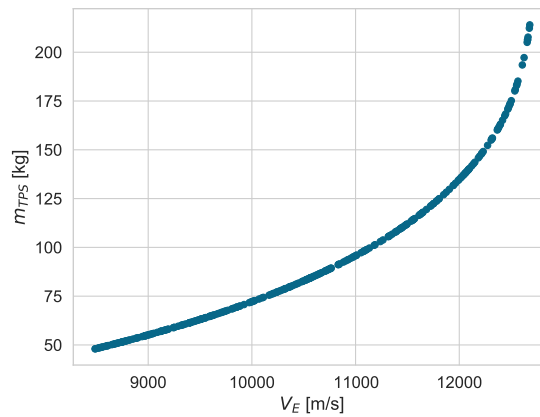


**Figure 5.9:** Plot of deployment velocity relationship to entry descent angle

**Change in entry velocity:** The entry velocity was sampled 300 times on the interval  $10,588 \text{ m s}^{-1} \pm 20\%$ . The effect this has on the TPS mass is depicted in Table 5.11 and Fig. 5.10.

**Table 5.11:** Statistical analysis of the TPS mass w.r.t. change in entry velocity

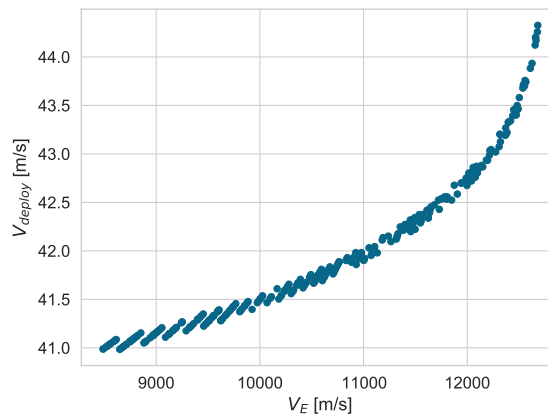
Parameter	Value
Maximum value	214.0 kg
Minimum value	48.0 kg
Standard dev.	39.5 kg
Mean	127.3 kg

**Figure 5.10:** Plot of TPS mass relationship to entry velocity

The effect the entry velocity has on the deployment velocity is seen in Table 5.12 and Fig. 5.11.

**Table 5.12:** Statistical analysis of the deployment velocity w.r.t. change in entry descent angle

Parameter	Value
Maximum value	44.3 m s <sup>-1</sup>
Minimum value	41.0 m s <sup>-1</sup>
Standard dev.	0.8 m s <sup>-1</sup>
Mean	41.9 m s <sup>-1</sup>

**Figure 5.11:** Plot of deployment velocity relationship to entry velocity

**Change in nose radius:** The nose radius was sampled 300 times on the interval  $11 \text{ m s}^{-1} \pm 20\%$ . It was found that the effect this had on TPS mass and deployment velocity was found to be minimal, as found by the fact that the standard deviation has a value of 0.13 for the TPS mass and 0.07 for the deployment velocity.

Observing the results of the sensitivity analysis, the entry vehicle mass is most sensitive to the entry descent angle and entry velocity, while the deployment velocity is most sensitive to the probe mass but overall changes less than the TPS mass.

### 5.3. Tsubuyaki sensitivity analysis

For the orbiter Tsubuyaki, a similar sensitivity study using Monte Carlo Simulation was performed as for the probe (as described in Section 5.1, see there for details on the method) to identify the parameters that the sizing iteration is most sensitive to. First a singular analysis in Section 5.3.1 will look at the isolated effects of two system level parameters, as well as the influence of changing another two subsystem level parameters. Subsequently, the global analysis in Section 5.3.2 will investigate how sensitive the sizing is to varying all four design parameters at the same time. At last, Section 5.3.3 will conclude the sensitivity analysis of the orbiter and provide recommendations for further study.

#### 5.3.1. Singular analysis

The first part of the sensitivity study concerns the variation of orbiter wet mass with a select number of system and subsystem parameters. The parameters are grouped into two approaches: top down, where system performance parameters are varied to see how the system responds to a change of environment or required performance. The bottom up approach, on the other hand, provides insight on how the system mass responds to variations in subsystem design.

**Table 5.13:** Statistical analysis of the orbiter wet mass when changing system performance by 20 %

Parameter	Value
Maximum value	1832 kg
Minimum value	822 kg
Standard dev.	267 kg
Mean	1240 kg

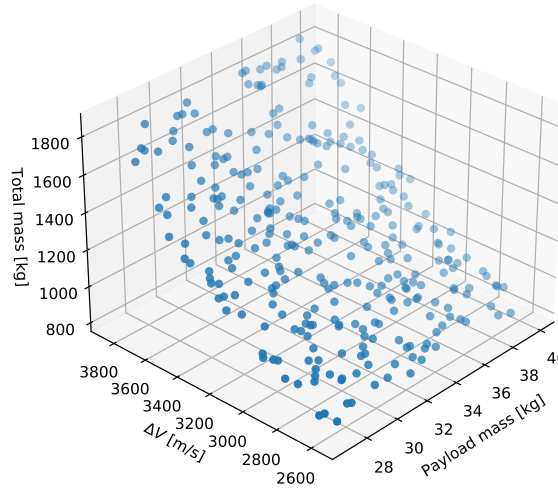


**Figure 5.12:** Three dimensional plot showing the cloud of mass values for change in system performance parameters

**Change in system performance parameters:** The two top down parameters studied were the total  $\Delta V$  requirement on the orbiter’s propulsion system and the payload mass, as those are the main aspects that the orbiter is designed around. The nominal values are  $3212 \text{ m s}^{-1}$  and  $33.43 \text{ kg}$ , respectively. Varying the parameters by 20 % in each direction produced the sensitivity map as shown in Fig. 5.12, with the statistical summary given by Table 5.13. As can be seen, the system sizing is very sensitive to the  $\Delta V$  required, while an increased payload mass only reflects slightly in the total orbiter wet mass. This shows in the Pearson’s correlation coefficient between the orbiter wet mass and  $\Delta V$  of 0.99. For the payload mass, this value is calculated to be 0.064, indicating a very weak positive relationship. Thus an increase in payload mass does increase the final wet mass, but to a much lesser extent than the exponential relationship between  $\Delta V$  and orbiter wet mass.

**Change in subsystem parameters:** For the bottom up approach the main design driver obviously is the propulsion system, as it accounts for most of the mass budget, see Fig. 4.11. Therefore, the  $I_{sp}$ , representing the efficiency of the subsystem, is varied. The next largest system by mass is structures, so there it was decided to vary the structural material density  $\rho_{struct}$  to emulate a structural efficiency change and see how that affects the sizing. From varying these two parameters by up to 20 % away from the nominal value of  $325 \text{ s}$  and  $2700 \text{ kg m}^{-3}$ , respectively, the table and figure below have been obtained.

**Table 5.14:** Statistical analysis of the orbiter wet mass when changing subsystem parameters by 20 %

Parameter	Value
Maximum value	2467 kg
Minimum value	798 kg
Standard dev.	357 kg
Mean	1310 kg

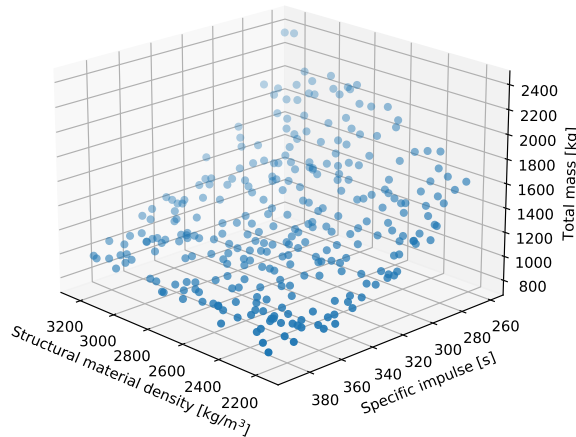


**Figure 5.13:** Three dimensional plot showing the cloud of mass values for a change in subsystem parameters

Again, the propulsion system is found to be the main driver of the orbiter wet mass with a Pearson correlation coefficient of -0.88, indicating that an increased  $I_{sp}$  is very beneficial to the overall weight budget. The structural material density has a slight but significant correlation of 0.30. This makes sense as the structures subsystem is the second largest component in terms of mass, see Fig. 4.11.

### 5.3.2. Global analysis

Next to the singular parameter study, a global analysis is performed to explore the extremes of the iterative sizing computations. Here the worst case estimates of all parameters can occur at the same time, yielding the maximum orbiter wet mass of 4329 kg as shown in Table 5.16.

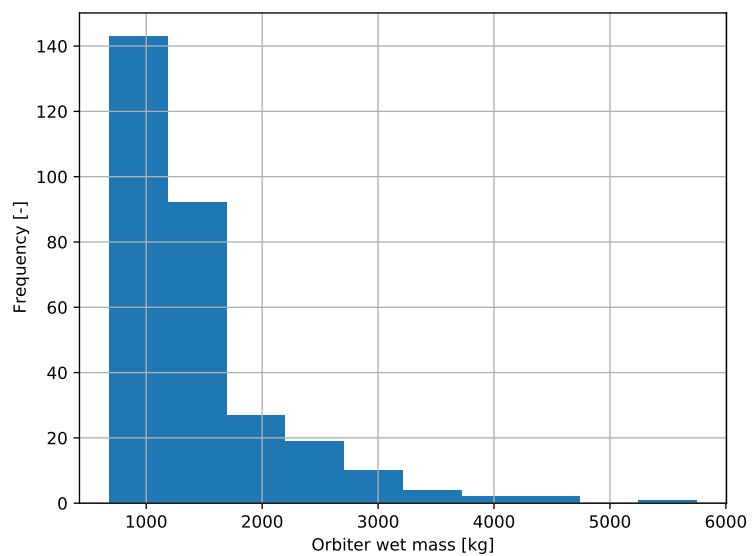
**Table 5.15:** Orbiter sensitivity variables and their Pearson's coefficients w.r.t. wet mass

Parameter	r Value
$m_{payload}$	0.089
$\Delta V$	0.58
$\rho_{struct}$	0.30
$I_{sp}$	-0.57

As mentioned before, the Pearson correlation coefficients listed in the table above are different from before as the samples are different from the singular analysis. The overall trend is still visible though, as it shows that the  $\Delta V$  and  $I_{sp}$  are the main design drivers with an  $r$  of around  $\pm 0.58$ . The equal magnitudes and opposite signs make sense, as in Tsiolkovsky's equation for the fuel mass fraction and  $I_{sp}$  required to achieve a certain  $\Delta V$ , the  $\Delta V$  is directly divided by the  $I_{sp}$ , so the same change in any of the two parameters will have the same effect on the mass of the orbiter. The second most influential factor is the structural material density, as it dictates how fast snowball effect acts on the structural mass, being the second largest subsystem. Lastly the payload mass is rather insignificant, as its mass is small compared to the total orbiter mass to start with.

**Table 5.16:** Statistical analysis of the output mass

Parameter	Value
Maximum value	4329 kg
Minimum value	632 kg
Standard dev.	539 kg
Mean	1357 kg

**Figure 5.14:** Histogram showing the frequency distribution of orbiter wet masses from 20 % variation of system parameters

### 5.3.3. Conclusion

From the sensitivity study on the sizing iteration of the Tsubuyaki orbiter, it can be seen that the propulsion system is the main driving factor. Any improvement in terms of  $I_{sp}$  increase or  $\Delta V$  savings help limit the orbiter mass. Thus, in further studies more efficient thrusters and propellant should be investigated. Furthermore, this steep decrease of orbiter wet mass induced by  $\Delta V$  savings shows that a trade-off between the current propulsive Venus orbit capture/insertion manoeuvre and aerocapture might be worthwhile, as adding a heat shield against atmospheric heating might turn out to be more mass effective than carrying the large amount of fuel currently required for orbit insertion.

# 6. Mission risk and sustainability

After listing all risks and sustainability aspects per subsystem for both Tori and Tsubuyaki, all risks and sustainability aspects were gathered to form the final overview of all risks considered for the mission as well as all sustainability factors. Section 6.1 summarises the risks, while Section 6.2 summarises the mission sustainability.

## 6.1. Mission risk

Below, the risk maps pre- and post mitigation are given. From these maps, the risks that are most prominent to the design can be derived. It also shows the importance of implementing the mitigation strategies in the design. The risks maps for the probe are given in Fig. 6.1 and Fig. 6.2, while the risk maps for the orbiter can be found in Fig. 6.3 and Fig. 6.4.

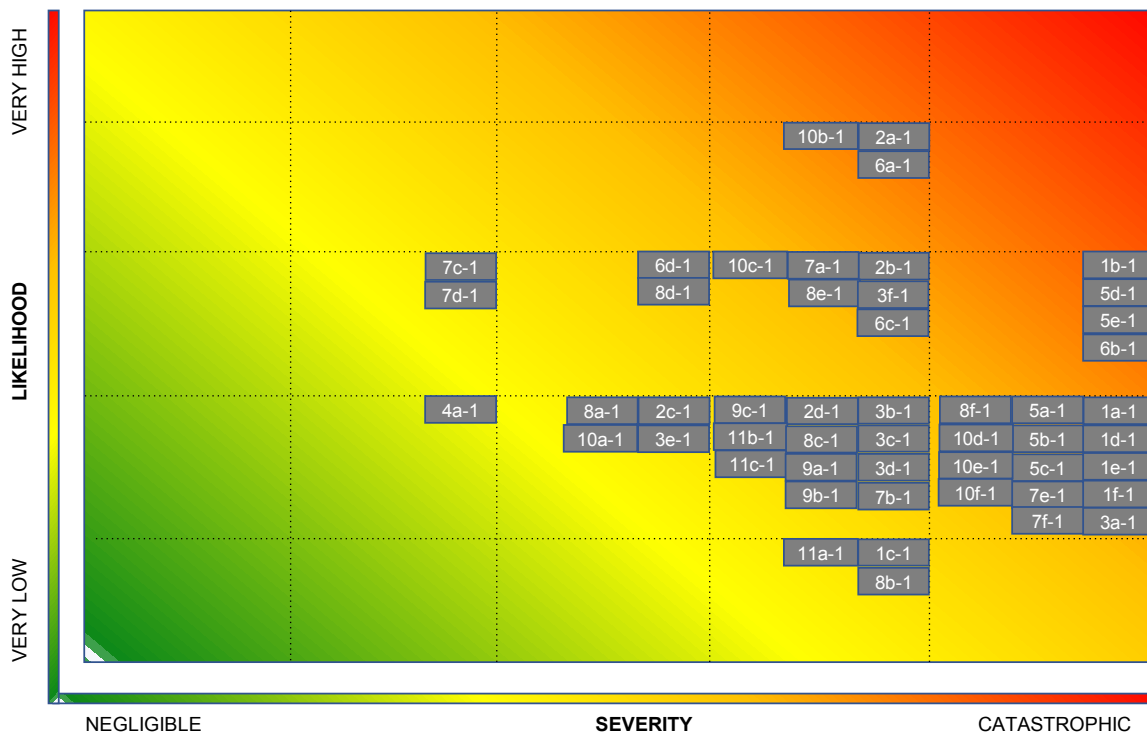


Figure 6.1: Probe risk map pre-mitigation

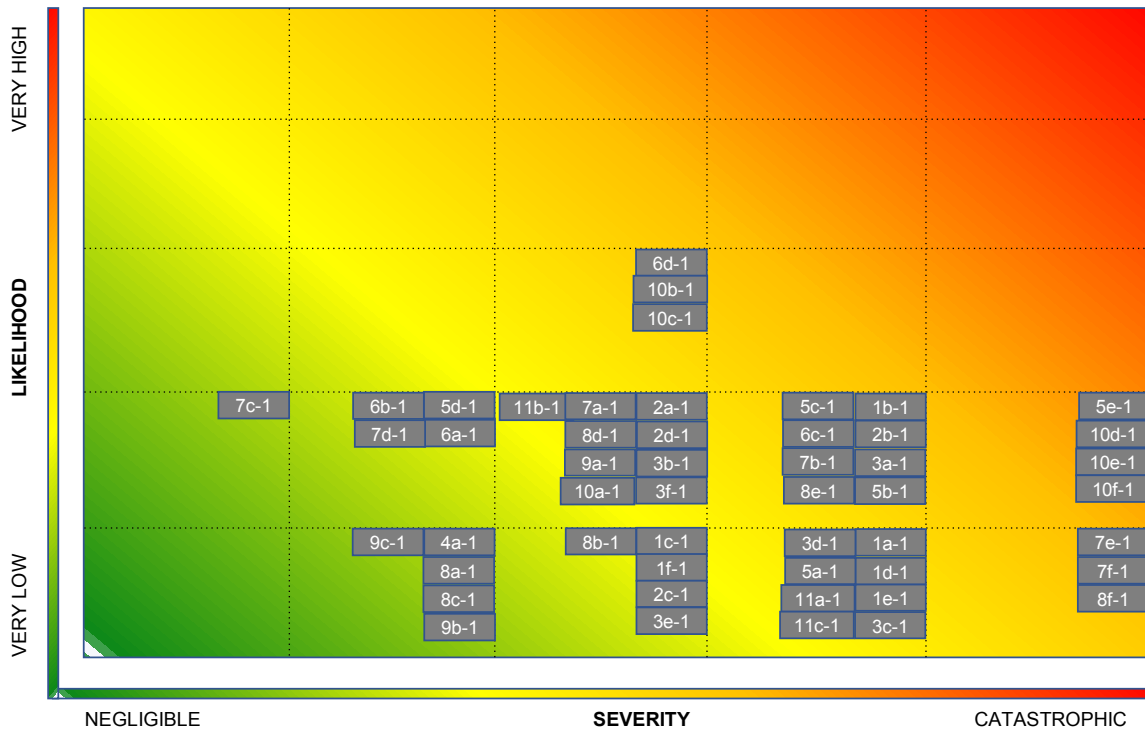


Figure 6.2: Probe risk map post mitigation

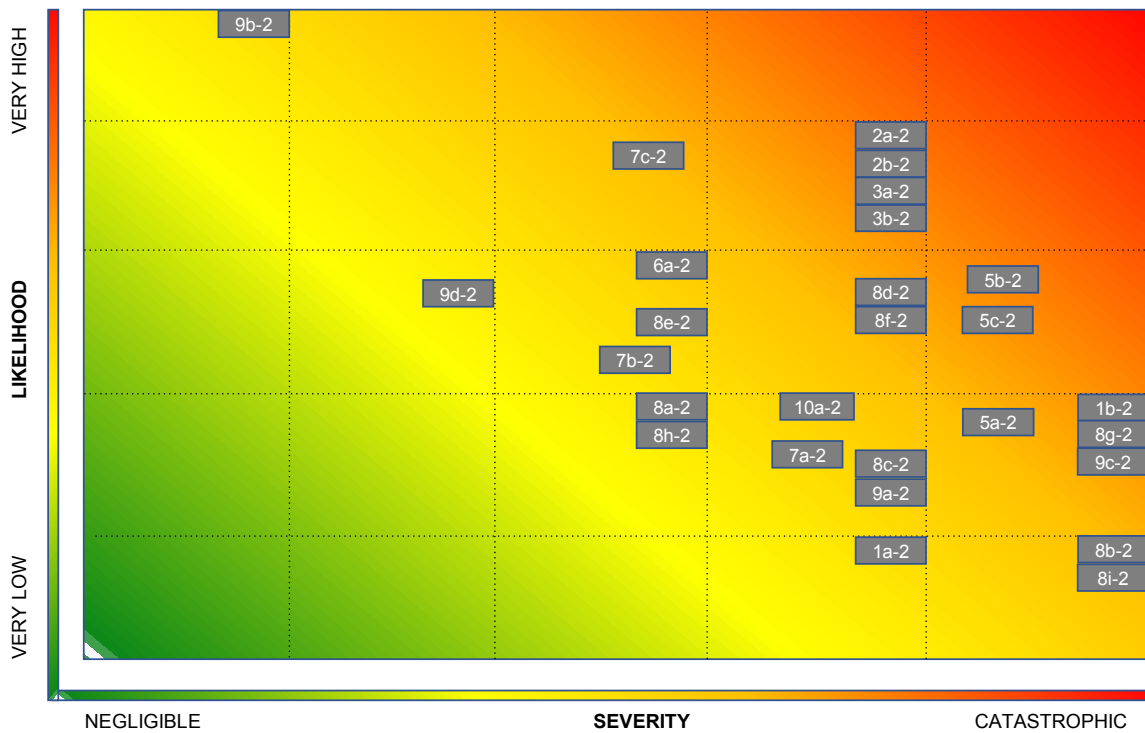


Figure 6.3: Orbiter risk map pre-mitigation

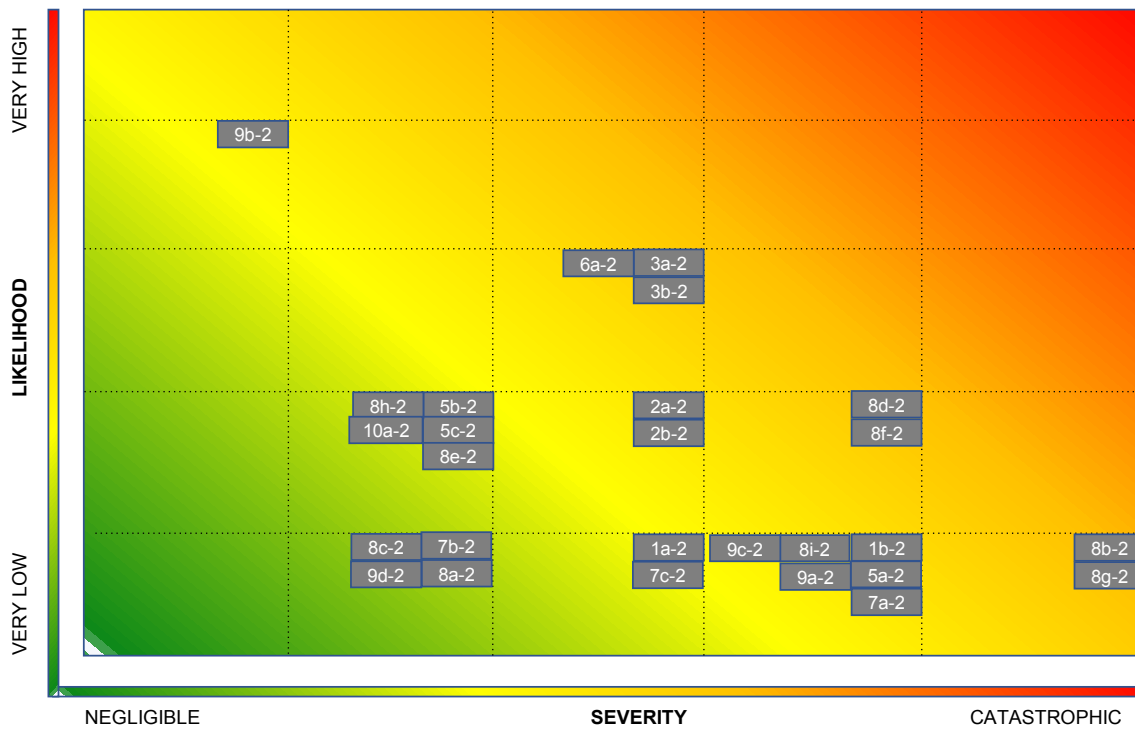


Figure 6.4: Orbiter risk map post mitigation

In conclusion, the most crucial technical risks to the mission were identified and assessed on both a system and a subsystem level for the designs of both the orbiter and the atmospheric probe. For the probe, the prominent risks, pre-mitigation, are related to the subsystems covering materials, payload, thermal control and power. For the orbiter, the subsystems of payload, power and propulsion produced the most prominent risks pre-mitigation. A mitigation strategy analysis led to the reassessment of these risks, after which risks related to power and, to a lesser extent, the telecommunications and propulsion subsystems were found to be most prominent for the orbiter. For the probe, the main concerns are related to the subsystems covering thermal control and power. These departments will thus be given extra attention in the actual development phase of the mission and, where possible, will be further reduced in risk if new mitigation strategies can be found along the way. The implementation of the proposed mitigation strategies in the design is crucial to the success of the mission. Therefore, the recommendations and considerations flowing from the risk assessment should be implemented in the final product. This will include some considerations proposed in the mitigation strategies, as well as the requirements flowing down from the risk assessment. These requirements are given in Table 6.1 and were all satisfied. Finally, the risk assessment should be considered a dynamic tool and will be further updated in the next phases of the mission.

Table 6.1: Risk assessment requirements

Identifier	Requirement	Check
KUMO-RISK-MAT-01	The materials shall be able to withstand an acid concentration of -1.2 pH.	✓
KUMO-RISK-STR-01	The structure shall be able to withstand all operational loads.	✓
KUMO-RISK-TC-01	The heat shield of the probe shall be able to withstand a thermal loading up to $4 \text{ W m}^{-2}$ .	✓
KUMO-RISK-PW-01	The primary power source shall have a reliability of 95%.	✓
KUMO-RISK-PW-02	The secondary power source shall have a reliability of 95%.	✓
KUMO-RISK-PW-03	Nuclear power shall not be used as a power source.	✓
KUMO-RISK-PW-04	The primary power source shall have a degradation factor below 0.8.	✓
KUMO-RISK-PROP-01	The use of lighter-than-air gasses that are considered for measurements shall be avoided.	✗
KUMO-RISK-FLOM-01	The $\Delta V$ budget shall include a contingency of at least 5%.	✓

## 6.2. Mission sustainability

This section integrates the sustainability scores from each technical department, to finalise a sustainability score for the mission. Since, the mission comprises Tsubuyaki and Tori, their sustainability scores will be analysed separately. Section 6.2.1 will briefly go over the political sustainability analysis of Kumo's launch site, followed by Section 6.2.2, which presents an overview of the compliance of the requirements for sustainability. Thereafter, an overview of the scoring per department will be presented in Section 6.2.3 for Tori, and in Section 6.2.4 for Tsubuyaki.

**Table 6.2:** Sustainable development strategy requirements.

Identifier	Requirement	Tori check	Tsubuyaki check
KUMO-SUS-SYS-01	The platform shall favour fewer high-quality components over lower quality sets.	✓	✓
KUMO-SUS-SYS-03	The engineering departments shall account for contingencies, while not exceeding their allotted budgets.	✓	✓
KUMO-SUS-SYS-04	The engineering departments shall aim to minimise the mass of their components.	✓	✓
KUMO-SUS-PROP-01	The use of radioisotope propulsion systems shall be avoided.	✓	✓
KUMO-SUS-PROP-02	Hydrazine shall not be used as the main propellant.	✓	✗
KUMO-SUS-PROP-03	Hydrazine shall not be used as secondary propellant if reaction control thrusters are used.	✓	✗
KUMO-SUS-PW-01	The use of radioisotope thermoelectric generators shall be avoided.	✓	✓
KUMO-SUS-MAT-02	The waste produced by production processes shall be minimised.	✓	✓
KUMO-SUS-TC-01	The use of toxic surface finish paints for temperature control shall be avoided.	✓	✓
KUMO-SUS-PL-01	The measurement techniques employed shall be non-destructive.	✓	✓
KUMO-SUS-PL-02	The likelihood of the payload contaminating the Venusian atmosphere with Earth-originating chemicals and organisms shall be lower than 30%.	✓	✓

### 6.2.1. Launch site sustainability

The selected launch site in Section 2.4.2 is the Kennedy Space Centre (KSC). Since, this launch site is located in Florida, United States, it has a favourable Corruption index (CI) of 67, Human development index (HDI) of 0.926<sup>1</sup>, Gender inequality index (GII) of 0.204<sup>2</sup> and Global Peace index (GPI) of 2.307<sup>3</sup>. The launch site is also 3175 km away from the equator, which is less comparative to other potential launch sites that were studied in the Midterm phase (Bronstring et al., 2021b). Another favourable aspect of the location is its relative proximity to other Aerospace facilities. This could cut the transportation emissions significantly. Hence, the selected launch site is favourable in terms of sustainability.

### 6.2.2. Reviewing sustainability requirements

This subsection lists the primary sustainability requirements. The main subsystems that affect sustainability are mission design and operations, propulsion, power, structures and materials, thermal and payload. Other subsystems less significant to sustainability, include GNC and telecommunications. After having listed the objectives per technical engineering department back in the Baseline report (Bronstring et al., 2021a), sustainability requirements were formulated by the team under the supervision of the sustainability officer in the Midterm report (Bronstring et al., 2021b). They are restated here, with the intention to check their compliance.

The requirements are listed in Table 6.2. There is also a column at the end which indicates whether the sustainability requirement has been complied with or not. As seen in Table 6.2, Kumo's sustainability requirements are listed for each relevant department. These requirements are formulated per department with unique identifiers for both the probe and orbiter. However, the requirement checking is done separately for them.

As seen in the table, all requirements for Tori were fulfilled. For Tsubuyaki, all requirements except KUMO-SUS-PROP-02 and KUMO-SUS-PROP-03 were fulfilled. The ones for Tsubuyaki, that unfortunately could not be complied with, were regarding the use of hydrazine. In a trade off between sustainability and performance of Tsubuyaki, performance was given the priority, which led to non compliance of the above two requirements. Detailed analysis and motivation as to why that choice was made, was seen in Section 4.4.5.

### 6.2.3. Sustainability analysis for Tori

This subsection studies the sustainability analysis for Tori. Based on the score attained, a qualitative analysis of Tori's sustainability is also presented.

The method of classification was already discussed in Section 1.6. Studying Table 6.3, and calculating the weighted average sustainability score using Eq. (1.2), it is seen that Tori is 78 % sustainable. Translating it back to qualitative terms, it means that Tori is "reasonably sustainable" in its manufacturing methods, design and operations.

The scores can be further improved in the future, if some research time is allocated to present more sustainable alternatives to the existing components or concepts.

<sup>1</sup><http://hdr.undp.org/en/countries/profiles/USA>, retrieved on 21-06-2021

<sup>2</sup><http://hdr.undp.org/en/content/gender-inequality-index-gii>, retrieved on 21-06-2021

<sup>3</sup><https://www.visionofhumanity.org/maps/us-peace-index/>, retrieved on 21-06-2021

**Table 6.3:** Sustainability scores for each department and every mission segment for Tori

Index i	Subsystem	SP <sub>1</sub>	SP <sub>2</sub>	SP <sub>3</sub>	S <sub>i</sub>	w <sub>i</sub>	S <sub>i</sub> · w <sub>i</sub>
1	Mission planning and operations	2	2	3	0.77	4	3.06
2	Structures and materials	2	2	2	0.67	4	2.67
3	Payload and instrumentation	2	3	3	0.80	3	2.40
4	Power	2	2	3	0.77	4	3.07
5	Propulsion	2	3	3	0.80	4	1.33
6	GNC	3	3	2	0.90	2	0.90
7	Telecommunications	3	3	2	0.90	2	1.80
8	Thermal control	3	3	3	1	3	3
9	Aerodynamics and stability	1	3	3	0.60	3	1.80
T	Weighted average score						<b>0.78</b>

**Table 6.4:** Sustainability scores for each department and every mission segment for Tsubuyaki

Index i	Subsystem	SP <sub>1</sub>	SP <sub>2</sub>	SP <sub>3</sub>	S <sub>i</sub>	w <sub>i</sub>	S <sub>i</sub> · w <sub>i</sub>
1	Mission planning and operations	2	2	2	0.77	4	2.67
2	Structures and materials	2	2	2	0.67	4	2.67
3	Payload and instrumentation	2	3	3	0.80	3	2.4
4	Power	2	2	3	0.77	4	3.07
5	Propulsion	1	1	1	0.33	4	1.33
6	GNC	3	1	1	0.73	2	1.47
7	Telecommunications	3	2	2	0.87	2	1.73
8	Thermal control	2	3	3	0.80	3	2.67
T	Weighted average score						<b>0.68</b>

#### 6.2.4. Sustainability analysis for Tsubuyaki

This subsection studies the sustainability analysis for Tsubuyaki. Similar to what was done earlier for Tori, based on the score attained, a qualitative analysis of Tsubuyaki's sustainability is also presented.

The method of classification was already discussed in Section 1.6. Studying Table 6.4, and calculating the weighted average sustainability score using Eq. (1.2), it is seen that Tsubuyaki is 68 % sustainable. Translating it back to qualitative terms, it means that Tsubuyaki is also "reasonably sustainable" in its manufacture, design and operations, though ranked lower than Tori.

It must be noted for Tsubuyaki, that there is definitely a lot of scope for improving the scores. The main focus must be to try to comply with requirements KUMO-SUS-PROP-02 and KUMO-SUS-PROP-03. In the future, if some research time is allocated to present more sustainable alternatives to the existing fuel hydrazine, it could increase the propulsion sustainability scores considerable, hence increasing the overall score.

# 7. Future design and development

Designing *Tori* and *Tusbuyaki* does not require only a theoretical explanation of the design, it requires many tasks to be performed after the theoretical design. This chapter elaborates on the future design and development for the probe, orbiter and mission. First, Section 7.1 elaborates on the project design and development logic flowchart and corresponding Gantt chart. This is followed by the testing plan in Section 7.2 and the production plan in Section 7.3. The chapter concludes with the financial breakdown in Section 7.4.

## 7.1. Project design and development logic

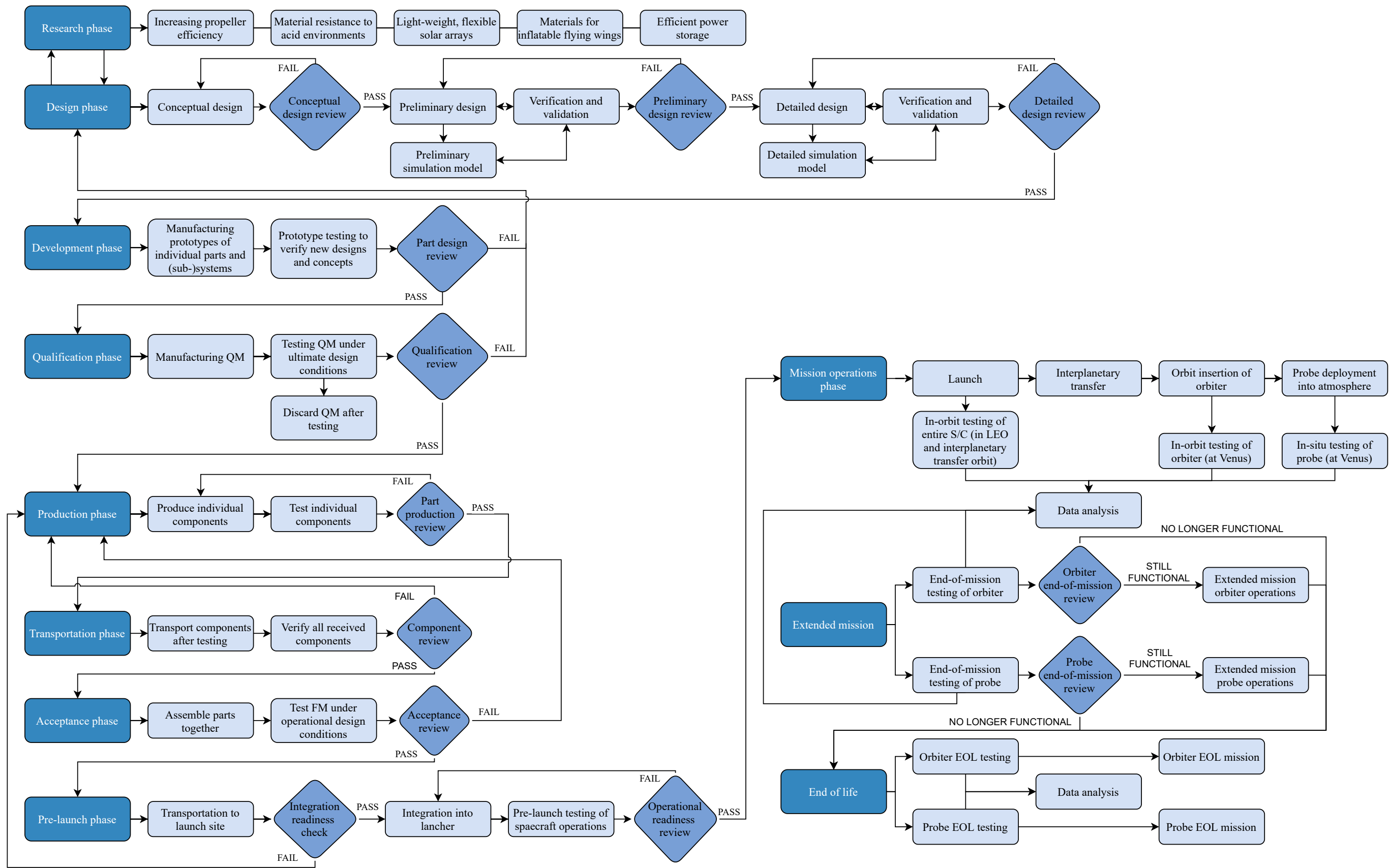
This section elaborates on the Project Design and Development (PD&D) logic, the different phases of which are explained and illustrated in Section 7.1.1. This is then followed by the project Gantt chart in Section 7.1.2 and the Reliability, Availability, Maintenance, and Safety (RAMS) characteristics in Section 7.1.3.

### 7.1.1. Project design and development logic diagram

A flow diagram depicting the PD&D after the completion of the DSE is shown in Fig. 7.1. As seen in the figure, this was split into the following phases:

- **Research phase:** The research phase serves to investigate a number of different areas that can be improved to increase the efficiency and reliability of the mission, as well as reduce its total mass and cost.
- **Design phase:** The design phase, which already started with the DSE, runs parallel to the research phase and is further split into conceptual design, preliminary design, and detailed design. The design is evaluated at each of these stages via a design review. If the design is deemed inadequate, in terms of meeting the requirements during a review, it must be reiterated.
- **Development phase:** During the development phase, the product begins to transition from a theoretical model to a physical one. Individual components and (sub-)systems are manufactured, tested, and reviewed. The development phase runs parallel to the end of the design phase, since any failure of a prototype during the part design review leads back into the design phase, where the component or (sub-)system must be redesigned. This iterative process repeats until all parts pass the part design review.
- **Qualification phase:** During the qualification phase, a Qualification Model (QM) of the final product is manufactured, tested, and reviewed. The QM, which is identical to the final flight model, is tested under ultimate design conditions and discarded after testing. If the QM fails to withstand the ultimate design conditions as expected, the overall design must be reviewed. If the QM passes the qualification review, all phases up to now can be concluded.
- **Production phase:** If the QM is approved, the project enters the production phase, in which all necessary components are manufactured and tested for compliance with the indicated specifications. If a component fails the part production review, it must be corrected or manufactured again.
- **Transportation phase:** All components are transported to the assembly locations and verified to confirm that all necessary parts were received. Should a part have been lost in transit, then it must be produced again.
- **Acceptance phase:** All parts are assembled into the Flight Model (FM), which is tested under operational design conditions. Failure of the acceptance review leads back into the production phase. If the FM passes the acceptance review, it is approved for use in the mission.
- **Pre-launch phase:** The FM is transported to the launch site and checked for integration readiness. Should a part have been irreparably damaged during transit, then it must be produced again. If the integration readiness check is passed, the FM will be integrated into the launcher and reviewed for operational readiness.
- **Mission operations phase:** The health and operations of the entire mission are tracked and tested in GTO, on the interplanetary trajectory, in orbit around Venus, and in the Venusian atmosphere. All data gathered is sent back to Earth and analysed, to evaluate whether any potential adjustments to the mission are necessary and possible.
- **Extended mission:** The operations of the probe and orbiter are both tested at the respective ends of their missions, and the data is sent back to Earth for analysis. Should either of the probe or orbiter, still be functional after the nominal mission ends, then extended mission operations may commence.
- **End of life:** Once the nominal mission and the optional mission operations have been concluded, a final round of post-flight testing data can be sent back to Earth for analysis and the probe and orbiter may proceed to their respective EOL missions.

Figure 7.1: PD&D logic flowchart



### 7.1.2. Project Gantt chart

This section uses the project design and development logic presented in Section 7.1 to create a timeline of events of the end-to-end Kumo mission. The duration of the mission operation has been estimated during the mission planning. For the duration of the design and production phases, (Zandbergen, 2017) has been used. This source presents a representative percentage of the duration of each design phase, which allowed the creation of a preliminary timeline of the complete Kumo mission. The Gantt chart of the mission can be seen in Fig. 7.2

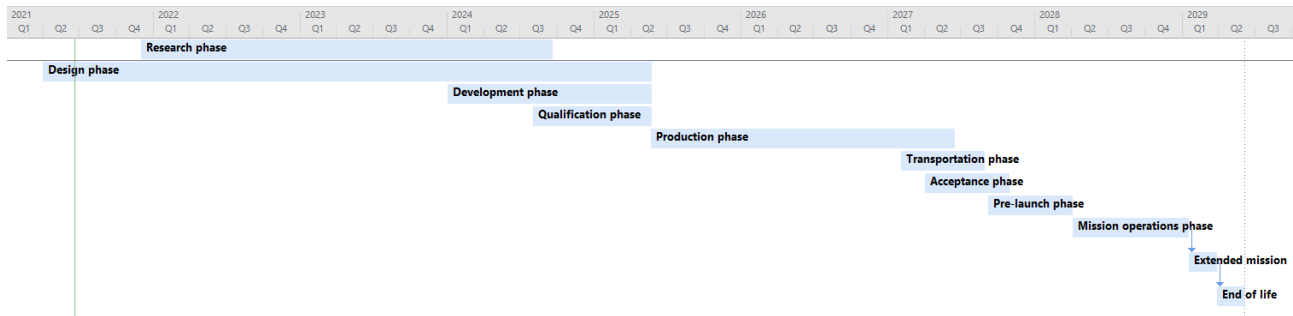


Figure 7.2: Kumo project Gantt chart

### 7.1.3. RAMS

The RAMS analysis covers the reliability, availability, maintainability and safety related to the mission. Reliability covers the reliability of the atmospheric probe and the relay satellite to end up with a combined reliability for the Venusian space segment. Next, the TRL and component readiness is analysed as part of availability. After that, the maintenance related to the mission is discussed. Finally, the safety concerns for the mission are stated.

#### Reliability

Reliability is a means to estimate the probability that a certain component or subsystem will perform its tasks over the duration of the mission without failing. In order to estimate the reliability of the mission, the reliability of both the orbiter and the atmospheric probe were estimated. Table 7.1 gives an overview of the reliability of different subsystems for the orbiter, based on statistical data (Castet and Saleh, 2009). Table 7.2 gives the same overview for the atmospheric probe<sup>1</sup>. Since statistical data is not mission specific, the historic use of the selected subsystem components was analysed to provide a proof of concept and thus a justification for the given reliability scores. Since the statistical data used for the probe is based on UAV's on Earth, an extra factor was applied to account for operations on Venus. Note that all subsystem components will be tested for operations in the Venusian atmosphere, thus justifying this Venus atmospheric factor to be relatively high. Another factor, the dynastat factor, was also added for the probe as a whole as the dynastat concept is not as explored as regular UAV concepts. In the end, the total mission score is found by considering all subsystems and both vehicles to be placed in series, as failure of one subsystem could be catastrophic for the entire mission. This leads to a final reliability of 0.93 and 0.86 for the orbiter and the probe, respectively, and a reliability of 0.81 for the space segment at Venus as a whole by considering the orbiter and the probe segments to be in series.

#### Availability

Not all required components for the mission success are readily available for use. Flush air-data sensing, for example, still needs complete validation to prove the system can operate during the entire mission. Furthermore, to other components, resources might need to be developed, acquired or selected. Those conditions can influence the time at which the mission is ready to proceed. Therefore, this section performs a Technology Readiness Level (TRL) assessment to determine the availability of the mission's components. This way, it can be determined what parts of the mission might restrain the qualification, production and utilisation phases.

In this report, NASA's TRL measurement system will be used to evaluate the maturity level of Kumo's components. The TRL system rates each item from 1 to 9; items with lower TRL indicate more technological development needed. The TRL assessment of Kumo components is shown in Table 7.3

#### Maintenance

In terms of maintenance, the actions that can be undertaken for both the atmospheric probe and the orbiter will be limited. This is because both will be operating at the location of Venus, where no human intervention and therefore no mechanical repairs will be possible. Some form of maintenance can be performed, however, by collecting and analysing housekeeping data sent by the orbiter and probe. This way, software mistakes and mission trajectory can be adjusted and corrected where necessary. Finally, the facilities of the ground segment itself will also have to be maintained to allow communication with the other mission segments and thus collection of the mission data.

<sup>1</sup><https://open.metu.edu.tr/bitstream/handle/11511/27024/index.pdf>, retrieved on 16-06-21

**Table 7.1:** Estimate of Tsubuyaki subsystems reliability with a 95% confidence interval for a two year mission

Subsystem	Reliability	Component history
Payload	0.99	Several of the selected payload instruments were either previously used in other space missions, including Venus, or designed to be used for space missions.
Power	0.98	The solar cells chosen for the mission were developed by AZUR SPACE and used before on space missions, including Venus Express. The selected lithium ion battery was developed and certified for space by Eagle Pitcher, a supplier recommended by NASA.
Propulsion	0.99	The main thruster was developed and certified by ArianeGroup and used in a large number of space missions, including Venus Express. The titanium propellant tanks were also developed and space certified by ArianeGroup and used before in other space missions, including BepiColombo.
Telecommunications	0.99	Both the selected LGA and HGA were used on previous mission, these being Venus Express and Mars Express. Both did not fail. The transponder was developed by NASA, while the gimbals were developed by MOOG. Finally, the CD&H is based on the one used for the Magellan mission, which went without failure. All of this combined shows that the selected telecommunications components are all developed for space applications and likely to be reliable.
GNC	0.99	All sensors and actuators have been used by past orbiters in the planet. Furthermore, all components are single-failure tolerant.
Materials and structures	0.99	The materials and structures used for the orbiter are radiation hardened and all commonly used in space applications.
Thermal control	0.99	All thermal control components selected for this mission, except the louvres, were used before on Venus express, where they went without failing. The louvres were developed by ESA's mechanical systems laboratory and are thus certified for space.
<b>Total</b>	<b>0.93</b>	

### Safety

In terms of safety, a division can be made between three parts of the ground segment; the manufacturing and assembly of components, transportation of components and finally the launch of the orbiter, probe and their supporting systems. Manufacturing and assembly related safety risks are those that are to be mitigated for using standard manufacturing safety procedures. Transportation is mostly concerned with the safety of the assembly and sensitive components. These need slow and specialised transport, for which extra budget is assigned. Finally, standard launch safety procedures will be followed as prescribed by the responsible agency.

## 7.2. Testing plan

Tests will have to be carried out in different phases along the manufacturing process of the platform. First, an explanation of the different testing phases considered will be given in Section 7.2.1. Furthermore, different tests to be performed that can be applied to different components are listed in Section 7.2.1. Finally, testing facilities deemed useful for the testing phase are defined in Section 7.2.2.

### 7.2.1. Testing phases

The testing phases will be divided such that the platform is tested from the bottom up. First, the materials will be tested individually to check their resistance to the exposed environment. Then, separate components will be tested in a number of ways to see their resistance against multiple factors. These subsystems will also be tested individually. Then, the subsystems will be integrated into the main structure, forming it a continuous system, which will then be tested. Finally, the system will be integrated into the launcher. Several tests will then also be done to see if everything is integrated properly.

### 7.2.2. Test types

The product phases will have to be tested rigorously. This can be done by testing several prototypes of the final model until failure to check the requirements. Different tests will be considered, categorised as mechanical tests, thermal tests, and tests conducted under special environmental conditions.

### Philosophies

The verification of different subsystems usually follows one of the two philosophies: the prototype philosophy or the protoflight philosophy (Wertz et al., 2011).

Prototype philosophy involves having multiple prototypes, which are tested for performance along one criterion typically until failure. It is best for mitigation of high-risk areas such as those with complex design or very new concepts. It

**Table 7.2:** Estimate of Tori subsystems reliability based on UAV data

Subsystem	Reliability	Component history
Payload	0.99	Several of the selected payload instruments were either previously used in other space missions, including Venus, or designed to be used for space missions. The instruments are to be tested for the Venusian environment.
Power	0.99	The solar cells chosen for the mission were developed by AZUR SPACE and used before on space missions, including Venus Express. They will be covered with CMX 100 AR oxidised cover glass to account for the Venutian atmosphere. The selected lithium ion battery was developed and certified for space by Eagle Pitcher, a supplier recommended by NASA.
Propulsion	0.99	The motor engine selected for the mission is produced by ALVA, a company specialised in developing high performance, electrical UAV motors. It should, however, be tested for performance in the Venusian atmosphere to increase reliability.
Telecommunications	0.99	The telecommunications used for the probe are the same as those used for the orbiter. Although not certified for the Venation atmosphere, the external instruments will be tested and coated accordingly to increase reliability.
GNC	0.99	Tori's GNC subsystem includes a Laser air-data sensing system that has never been used in a space mission before. The system will be validated through tests in a Venus-like environment. Even though those tests will give insight into the component's reliability, uncertainties during operation might still be present, which is why the subsystem's reliability is considered lower than suggested by the literature.
Materials and structures	0.99	The materials selected for the mission are, amongst others, chosen for their ability to withstand aggressive environments similar to the one found in the Venutian atmosphere. The same materials were also proposed in NASA's Venus Flagship mission study.
Thermal control	0.99	All thermal control components used for the probe are forms of passive control, which is generally more reliable. MLI was tested on previous missions and proposed in NASA's Venus Flagship mission study. OSR was used on Venus Express. Finally, the temperature sensors are from Innovative Sensor Technology, which is a reliable supplier for space missions.
Venus atmospheric factor	0.95	
Dynastat factor	0.95	
<b>Total</b>	<b>0.86</b>	

**Table 7.3:** Failure modes of past missions in Venus

Component	TRL	Rationale
Laser air-data sensing	5	The system has already been tested; However, the tests were performed on Earth. For Venusian flight, the system needs to be tested in a more suitable environment. Furthermore, current tests of the system were performed on conventional aircraft. That means, The system shall also be tested in a prototype of Tori. On top of that, Kumo will be the mission to bring this technology to a TRL 9 when proving its functioning during the actual flight.
MASPEX	6	This is a new instrument designed for the planned Europa Clipper mission. That means it has never been demonstrated in a mission operation. Therefore, the instrument still needs to be tested in a space and a Venus-like environment.
NEP and UVI	7	Those instruments have already been used in space missions, but not on Venus. Therefore, tests in a Venus-like environment are needed.

comes at a price of the increased cost because of the production of multiple prototypes and will therefore be used only for the most critical subsystems, partially based on the established risks from the previous report. These will be the structural subsystem and the flight dynamics, in particular the hybrid lift generation of the dynastat and the entry vehicle separation.

Protoflight philosophy is based on having one model and applying acceptance tests to it. It is not expected to break, so the costs are kept to a minimum. However, the obvious disadvantage is the inability to push the limits of performance and thus receiving less valuable data. The philosophy will be used for testing less important components, those not mentioned under the prototype philosophy.

For the Kumo mission, although expensive, the prototype philosophy is envisioned to be used. This is because of the nature of the mission and how it is to be like no other in the sense that there are a lot of unknowns which must be measured before such a mission can successfully be completed. The prototype philosophy will allow for a number of different iterations to be made and tested and even over tested to see the boundaries of the design.

### Environmental tests

There are tests that shall be performed in a simulated environment expected throughout the testing phases. The tests involved in the verification of the structural integrity of the spacecraft as well as the functionality of the internal subsystems may be encapsulated in the following categories.

### Mechanical tests

Mechanical tests verify the response of the structure to the mechanical loads experienced throughout the flight. These include the launch loads, attitude control manoeuvring loads, separation loads, atmospheric entry loads, and mechanical stresses. Below are the typical tests used in the industry to simulate the dynamic loads experienced in flight (Wertz et al., 2011):

- **Mass property verification:** Mass properties encompass all dynamic properties of the spacecraft such as the mass itself, the centre of mass, the products and moments of inertia around the three principal axis, as well as the axis orientation. These are especially critical for the GNC subsystem and must be computed before other verification tests may be approached. Currently, the mass property verification is conducted using weight and centre of mass scales as well as the torsion pendulum machines. These are more accurate than the direct determination using force and acceleration measurements.
- **Vibration tests:** These are used to simulate transient or quasi-harmonic loads. With the chosen excitation method and the amplitude of the vibration load, it can be proven that the specimen can withstand the specified dynamic loads. Furthermore, the vibration loads may be obtained for individual components during system-level tests.
- **Acoustic noise tests:** These tests are able to simulate the acoustic loads expected during the launch phase. This is similar to a vibration test, albeit in a high-frequency range. Modern equipment is able to simulate noise fields and measure the response of the spacecraft to a specified acoustic spectrum.
- **Shock tests:** These serve to simulate transient, short-term loads, such as those experienced during entry vehicle separation from the orbiter, or the separation of the probe itself from the entry vehicle. The shock response spectrum is specified for the pyrotechnical excitation by shock generating units. Costs are typically high, so only system tests are verified in this way.

### Space simulation tests

To simulate and thus verify the response of the spacecraft to the specific space environment that it will be exposed to, thermal and vacuum tests are used. These tests are able to simulate the right pressure and temperature levels, with a possibility to specify the sources of radiation contributing to the thermal balance. Specific space simulation tests targeting a particular response of interest have been developed (Wertz et al., 2011):

- **Thermal balance tests** verify the response of the spacecraft to thermal load cases with specified sources of radiation.
- **Bakeout tests** verify the outgassing that is required before the spacecraft is launched. The spacecraft is heated to a higher than operational temperature and left in a vacuum chamber for a day. This stimulates the release of the trapped or dissolved gas from the surface and thus reduces the risk of contamination.
- **Thermal vacuum tests** measure the response of the spacecraft to temperature changes. The spacecraft is exposed to frequent temperature cycles under vacuum conditions. The test is also quite expensive for large spacecraft and is only applicable for the entire spacecraft such that the relationship between thermal responses of the components is measured.
- **Thermal cycling tests** measure the response of the spacecraft to temperature changes outside of a vacuum environment. These are much cheaper and thus will be performed more times for individual components.

### Special environmental effects and conditions

Special environmental test might be needed to cover special needs, most importantly including the following (Wertz et al., 2011):

- The **Direct Interface Force Method** consists of clamping the object onto a seismic block equipped with force measurement devices at its interfaces. The generated forces created by the operation of the device in the low-frequency range can be determined directly at the interface. These interface forces can then directly be used to estimate the disturbing (micro-)vibrations for the whole system.
- The **Indirect Interface Force Method** is applied in the case of higher frequencies as the interfaces can no longer be regarded as being stiff. Therefore, the examined devices are suspended under free-free conditions and the spectra of the interface accelerations are measured. To verify the interface forces, the transmitting functions at the interface patches are experimentally determined and converted into force spectra together with the measured acceleration spectra.

- **Thermal micro vibration tests** are used to choose multi-layer insulation foils. Foil specimens up to 1 m<sup>2</sup> in size are attached to a plate with known eigenfrequencies. This fixture is suspended at low frequency in a thermal vacuum chamber and exposed to space conditions. By means of infrared lamps, the foils are exposed to the relevant thermal conditions. Their behaviour is then registered optically as well as with very sensitive accelerometers mounted on the plate. The thermally induced movements of the multi-layer insulation foil excite eigenfrequencies in the plate, giving an insight into the activity of the material.
- Special **optical measurements** of the linear expansion of camera structures are performed during the thermal vacuum tests.
- The **Compact Test Range** is used to conduct performance tests on the antennas of a complete satellite, including the integrated payload. A homogeneous field is created with one or more tilted mirrors at a short distance whose characteristics are identical to those of a far field. Thus, high-frequency characteristics can be determined at short distance.
- **Firing tests** for solid propellant boosters are used to verify the functioning of a booster and the operating parameters. This requires test rigs which can absorb a high amount of propulsive forces and allow the realisation of the mechanical boundary conditions as they occur during flight. Furthermore, vibrational behaviour and interface forces at the connection points to the central stage are investigated.
- **Launch rehearsal** includes testing all functions necessary for the launch.
- The **engine test rig** includes chemical engines that can be operated to verify their functioning, burn duration, and the thrust achieved.
- **Separation tests** consist of initiating the separation phases with pyrotechnics to guarantee high precision and appropriate separation forces.
- **Communication tests** between the satellite and ground stations are carried out by connecting the satellite to the ground station via its actual communications equipment in order to perform various tests.
- **Electronics performance tests** are conducted during the thermal vacuum tests for different temperature ranges.
- **Antenna and boom deployment tests** are performed under high-vacuum and low-temperature conditions in the context of a thermal vacuum test.
- **ADCS performance tests** are conducted by operating ion thrusters and gas thrusters during the thermal vacuum tests to verify their performance under high-vacuum and low-temperature conditions.

### 7.2.3. Testing facilities

To conduct the tests as described above a number of testing facilities were considered. The facilities will vary based on the item or component that needs to be tested. As sustainability plays an important role in this design phase, facilities which are close to the launch site should be considered for manufacturing. However, for testing some of these can be done at other location given that the tests are on smaller prototype components and not the whole product. The tests mentioned above all need a variety of different equipment and testing space, some do not need a testing space at all. Small component or mechanical tests can be done in places like the TU Delft university. The university often works with engineering companies to test out components. The aerospace faculty has access to a number of machines which would be useful including ISO 8, class 100,000 clean room, mechanical testing lab, an instrumentation's lab and a ground station. <sup>2</sup>

Another testing facility in Delft is TNO called the Optomechatronic Lab for aerospace<sup>3</sup>. There are also a number of larger clean rooms which would be useful in assembling and testing out more sensitive equipment and components. They also provide manufacturing equipment used for space grade systems.

On top of this ESA also has the ESTEC Test Centre<sup>4</sup> where there are a number of environment simulation facilities. This would be useful for larger components tests when the reaction to the environment needs to be evaluated. This could be the case for exposed materials or inflated body of the probe as well as instrumentation once assembled in the probe or orbiter and checking if the thermal components are sufficient to stay operational.

However, when systems testing, which involve testing assembled components need to be conducted, the testing facilities should be close to the launch site to minimise emissions. For example, the Blue origins manufacturing facility is based just down the road from KSC which would be an idea, however as Blue origin is a private sector a investigation into leasing a lab would need to be looked into.

## 7.3. Production plan

To manufacture all components of the mission, a production method should be defined. This will allow for all phases of production to be reviewed and a timeline can be made in combination with testing plan for the completion of the mission variable.

The manufacturing, assembly and integration flow diagram is given in Fig. 7.3. It is split into 4 sections. The probe, the orbiter, the aeroshell and the kick stage. Each segment has items which need to be bought, signified by the identifier

<sup>2</sup><https://www.tudelft.nl/en/research/research-facilities>

<sup>3</sup><https://www.labforrent.nl/optomechatronic-lab-for-aerospace/>

<sup>4</sup>[https://www.esa.int/Enabling\\_Support/Space\\_Engineering\\_Technology/Test\\_centre/About\\_ESTEC\\_Test\\_Centre](https://www.esa.int/Enabling_Support/Space_Engineering_Technology/Test_centre/About_ESTEC_Test_Centre)

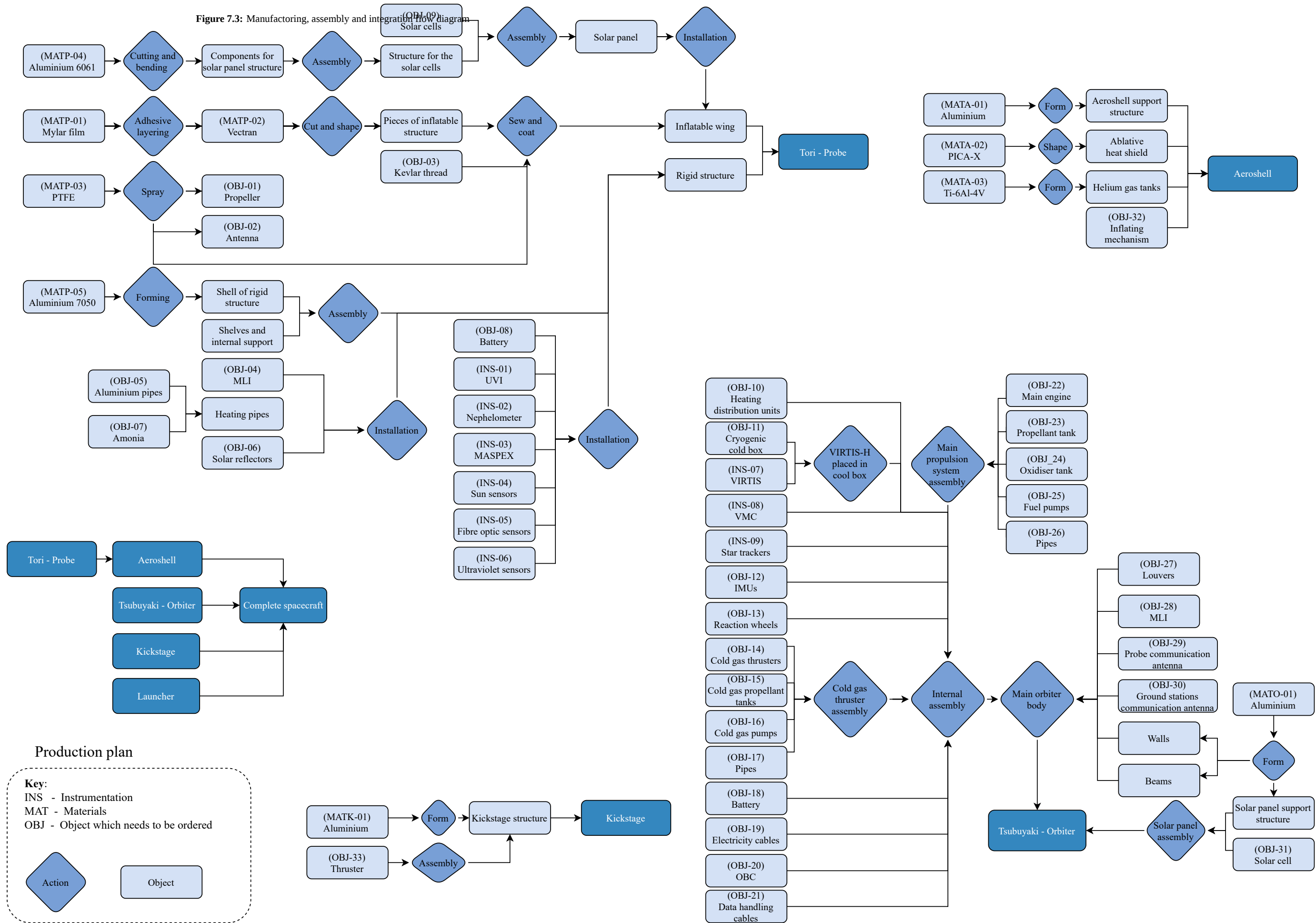
OBJ. Some sections must be manufactured from purchased materials, which are denoted by the identifier MAT. Each mission part has a different key: O for the orbiter, P for the probe, A for the aeroshell, K for the kick stage, and L for the launcher. The boxes with no identifier are parts of the design process which are a product but not a complete part. The diamonds are processes or actions conducted in the production process.

In total there are 32 objects, nine instruments, and ten different materials required to fully assemble the complete Kumo spacecraft. The production method chosen shall minimise energy, waste and cost to reduce the carbon footprint of the mission. All the objects must be bought from a supplier. In order to reduce carbon emissions local suppliers shall be chosen. As the launch site is KSC, all components should be ordered and assembled in the same area. The four different components should be produced close by, if possible, such that transportation costs can also be reduced.

In addition to the production of the mission components, it may also be wise to construct apparatus for testing. This mission is one of a kind and has systems which are unique in shape. Therefore, there will be components needed for testing, which are not available. This includes environment tests for the inflatable body which is rather large and limited in rigidity for a frame to hold the structure. A crane like device would be useful here.

Furthermore, the location for production as well as assembly should also be considered. As the launch site has been chosen for KSC, manufacturing facilities should be chosen close to here to allow for short transportation time and therefore less emissions. The materials will most likely not be able to be sourced from one location so a number of different local distributors will probably be used. The location in which the objects that need to be bought cannot be helped much if only one distributor is available. Therefore, if the choice of a closer distributor is viable, that should be chosen.

Figure 7.3: Manufacturing, assembly and integration flow diagram



## 7.4. Finances

In order to evaluate the financial aspects of the proposed mission, the cost budget was created. Furthermore, the return on investments was computed. It consisted not only of the direct returns in capital, but also the indirect effects on the local financial environment. This way, return of investments (ROI) and operational profits will be disclosed in the latter section.

### 7.4.1. Cost budget breakdown

What follows below is a breakdown of the budget and allocation of resources for the Kumo mission. The mission was divided into three segments, these being the atmospheric probe, the orbiter and the kickstage, and the entry capsule. For each of these segments, a bottom up approach was followed to give an insight on how different aspects and phases of the design will affect the total mission cost. These phases can roughly be divided in design and development, production and ordering of components, acceptance testing and other budget drawers such as pre-launch operations and mission operations. In order to give an estimate for the cost of these phases of the design, a differentiation was made between three main sources of cost, these being components, facilities and labour.

#### Components cost

The raw costs of the components has been collected from each subsystem. The additional extra costs were then added to the raw costs to account for industry-specific overcharges. Especially for relatively cheap components the extra costs could add up five or six times the raw price of the components. The specific values of the additional costs per subsystem are unknown, which is why expected inhibition processes have been identified and individual costs estimated. These primarily stemmed from the amount of paperwork required or availability issues. All component-related testing costs (i.e. certification and component quality assurance) have been included in nominal material cost. The required number of components for the mission was further expanded by the components required for destructive testing, primarily for structures and other relatively cheap subsystems.

#### Facilities cost

To effectively account for the cost of facilities, a division was made based on the function they are to fulfill. The first kind of facilities that are those used for the design phase of the mission segments. Here, prototypes are built and tested. The cost for these facilities could range based on the exact nature of the prototypes, but was estimated to be EUR 10,000 a day on average. Next, the acceptance testing phase was considered. These facilities are expected to be slightly more advanced, depending on the nature of the component to be tested. An average daily cost of EUR 30,000 was accounted for. The main contributors to the total facilities cost are specialised testing facilities. Here, it was estimated that the total cost for the use of such facilities lies between EUR 50,000 and EUR 100,000 a day. Upon scaling with the total duration of a certain research or testing phase, where a five day working week has been assumed, the total facilities cost for a certain phase was found. Note that it was argued that facilities that can be considered outliers in terms of cost would cancel each other out and would not be used as frequently. Therefore, all phases and subsystems were assigned a facilities cost estimate within the aforementioned range.

#### Labour cost

As means to justify the workload and thus the division of labour over the different phases and different aspects of the mission, a system was drawn up in which the assigned number of employees for a task were estimated based on the workload. A balance was sought between the number of employees, expressed in increments of five to maintain consistency and clarity throughout the cost estimation sheet, assigned to a task and the number of weeks set for that task. Note that the number of employees only accounts for employees that rank as senior engineers or specialised technicians. Other personnel, as well as facilities including office space, parking spots and other spendings are all accounted for in the yearly rate of the aforementioned employees, which was set at EUR 200,000 a year. The total labour cost for each phase of the design can be found by taking into account the assigned units and duration for each phase. Finally, the management needed to oversee the progress of each mission segment was assigned a yearly rate of EUR 300,000. The total size of the management staff for each mission segment was found as a balance between the number of employees involved and the number of weeks spend on the design and integration of the segment.

#### Other costs

Although a large part of the total mission budget is outsourced to the main phases of the mission design, there are still several other important aspects that should not be forgotten. The first is transportation. It comes with a high cost, as aerospace components and assemblies often require careful handling and thus slow and specialised transportation. Next, the Kumo mission will take on an insurance for launch, providing the opportunity to recoup part of the mission cost in case of a launch failure. Fees are estimated to be in the order of five percent of the insured value<sup>5</sup>. Also, a sizeable part of the budget goes out to all activities related to launch and active mission operations. Important factors here are the pre-launch checks and the fees for the deep space network, needed for communication. Finally, a margin of 20% was applied on the mission cost as a means of contingency, resulting total mission cost of EUR 995 million.

<sup>5</sup><https://www.spaceintelreport.com/will-insurance-force-russias-proton-rocket-commercial-satellite-business/>, retrieved on 22-06-2021

Table 7.4: Cost breakdown structure

Phase	Probe							Orbiter					Entry vehicle					Total cost - all segments						
	Number of people	Number of weeks	Labour cost [k€]	Component cost [k€]	Facilities cost [k€]	Total probe cost [k€]	Number of people	Number of weeks	Labour cost [k€]	Component cost [k€]	Facilities cost [k€]	Total orbiter cost [k€]	Number of people	Number of weeks	Labour cost [k€]	Component cost [k€]	Facilities cost [k€]					Total EV cost [k€]		
Design - 93 [M€]	Conceptual design	10	26	997	0	0	997	10	26	997	0	0	997	10	26	997	0	0	997	2,992				
	Preliminary design	60	52	11,967	0	0	11,967	30	52	5,984	0	0	5,984	20	52	3,989	0	0	3,989	21,940				
	Detailed design	90	104	35,901	0	0	35,901	50	104	19,945	0	0	19,945	30	104	11,967	0	0	11,967	67,814				
Development - 80 [M€]	Manufacturing prototypes	15	78	4,488	12,000	7,800	24,288	12	78	3,590	7,000	7,800	18,390	10	78	2,992	5,000	7,800	15,792	58,470				
	Prototype testing	15	26	1,496	0	13,000	14,496	12	26	1,197	0	2,600	3,797	10	26	997	0	2,600	3,597	21,890				
Production/ordering of OTS components - 504 [M€]	Payload	5	6	115	120,000	0	120,115	5	6	115	35,000	0	35,115	-	-	-	-	-	-	155,230				
	Power	10	4	153	25,000	0	25,153	5	4	77	10,000	0	10,077	5	4	77	2,000	0	2,077	37,307				
	Structures	10	8	307	12,500	0	12,807	10	6	230	6,000	0	6,230	10	8	307	10,000	0	10,307	29,344				
	Propulsion	5	4	77	4,000	0	4,077	5	4	77	8,000	0	8,077	-	-	-	-	-	-	12,153				
	ADCS	5	4	77	15,000	0	15,077	5	4	77	7,000	0	7,077	5	4	77	3,000	0	3,077	25,230				
	Thermal	5	4	77	1,500	0	1,577	2	6	46	1,500	0	1,546	10	4	153	8,000	0	8,153	11,276				
	TT&C	5	4	77	30,000	0	30,077	5	2	38	30,000	0	30,038	-	-	-	-	-	-	60,115				
	Hardware	10	156	5,984	5,000	7,800	18,784	10	156	5,984	5,000	7,800	18,784	10	156	5,984	5,000	7,800	18,784	56,351				
	Software	20	312	23,934	0	0	23,934	20	156	11,967	0	0	11,967	10	156	5,984	0	0	5,984	41,885				
	CD&H	5	4	77	15,000	0	15,077	5	4	77	15,000	0	15,077	5	4	77	1,500	0	1,577	30,153				
	Kick stage	-	-	-	-	-	-	10	12	460	43,000	0	43,460	-	-	-	-	-	-	43,460				
	Acceptance testing - 24 [M€]	Payload	10	4	153	0	600	753	10	4	153	0	600	753	-	-	-	-	-	-	1,507			
		Power	5	4	77	0	600	677	5	4	77	0	600	677	5	2	38	0	300	338	1,692			
		Structures	10	4	153	0	600	753	10	2	77	0	300	377	10	6	230	0	900	1,130	2,260			
Propulsion		5	4	77	0	600	677	5	4	77	0	600	677	-	-	-	-	-	-	1,353				
ADCS		5	4	77	0	600	677	5	2	38	0	300	338	5	4	77	0	600	677	1,692				
Thermal		5	2	38	0	300	338	5	3	58	0	450	508	5	4	77	0	600	677	1,523				
TT&C		5	2	38	0	300	338	5	2	38	0	300	338	-	-	-	-	-	-	677				
Hardware		5	8	153	0	1,200	1,353	5	8	153	0	1,200	1,353	5	8	153	0	1,200	1,353	4,060				
Software		10	26	997	0	0	997	10	26	997	0	3,900	4,897	2	2	15	0	300	315	6,210				
CD&H		5	2	38	0	0	38	5	2	38	0	300	338	5	2	38	0	300	338	715				
Kick stage		-	-	-	-	-	-	15	12	690	0	1,800	2,490	-	-	-	-	-	-	2,490				
Integration - 29 [M€]	Breadboard test	10	10	384	0	5,000	5,384	10	4	153	0	1,500	1,653	10	4	153	0	1,500	1,653	8,690				
	Assembly	15	12	690	0	1,800	2,490	15	12	690	0	1,800	2,490	10	12	460	0	1,800	2,260	7,241				
	Test FM	10	12	460	0	6,000	6,460	10	8	307	0	3,000	3,307	10	8	307	0	3,000	3,307	13,074				
Other segment costs - 26 [M€]	Management	9	250	1,257	0	0	1,257	6	388	14,283	0	0	14,283	5	370	9,648	0	0	9,648	25,187				
Pre-launch - 7 [M€]	Transport to launch site	10	12	460	0	6,300	6,760																	
	Integrate into launcher	10	3	115	0	0	115																	
	Pre-launch test	15	1	58	0	0	58																	
Mission operations - 65 [M€]	Launch		0	0	51,900	0	51,900																	
	Transfer	15	21	1,200	0	0	1,200																	
	Phase I	10	4	164	0	1,043	1,207																	
	Phase II	10	4.3	164	0	363	528																	
	Extended mission	10	3.6	137	0	313	450																	
	Phase III	5	416	7,978	0	3,000	10,978																	
	End of life	5	1	19	0	0	19																	
Other mission costs	Management (entire duration)	1	365	2,100	0	0	2,100																	

<b>Cost summary</b>		
TOTAL COST [M€]		997
PROBE COST [M€]		377
ORBITER COST [M€]		271
EV COST [M€]		108
INTEGRATED DESIGN COST [M€]		75
<b>Cost assumptions</b>		
	Cost [k,EUR]	Per
Design facility		10 day
Acceptance testing facility		30 day
Assembly testing facility		50-100 day
Senior engineer salary		200 year
Managment personnel salary		300 year

### 7.4.2. ROI and operational profits

Deep space exploration are extremely rare and valuable. Therefore, a regular Return of Investment (ROI) is very hard to make for these particular missions since the market price and market value are different than for regular products. In Section 7.4.2, the market price will be discussed for our mission. Also, the market value will be discussed in Section 7.4.2.

#### Market price

The Kumo mission to Venus is a mission that has never been done before. The concept of using a hybrid airship, also called dynastat, is something hardly used on Earth, let alone for deep space missions. Additionally, Tori will not be able to communicate with Earth from within the Venusian atmosphere to send in-situ data back. Therefore, a special satellite, in this case called Tsubuyaki, will be needed that can communicate with both the probe and Earth.

Since, the dynastat is a complete new concept, the development price and production price will significantly increase. This is not only due to the special materials required to last in the acidic atmosphere, but also the production and development cost that comes along. A significant amount of testing will be needed to verify and validate that the concept will work for the mission.

Looking at these aspects, total cost of approximately EUR 1 billion is estimated for the Kumo mission. This budget will be provided by different countries interested in the mission. Expected is that the funding will mostly come from Germany, which has many space research institutes interested in deep space data such as DLR<sup>6</sup>, OHB<sup>7</sup> and the Max Planck Institute<sup>8</sup>. Another country willing to invest more is the UK, which is very involved in space technology. An example would be the Space campus located in Harwell, which is active in space research. Also, many big companies in the UK such as ClydeSpace and Surrey satellites, as well as research institutions such as Imperial College<sup>9</sup>, Cranfield<sup>10</sup> and Oxford<sup>11</sup> could be interested in this mission. These countries will most likely regain their fundings as intangible assets, including technological insights, experience and knowledge.

As many countries will be involved in the process, the budget will have to be distributed. Testing facilities at ESA ESTEC will be used, which will include a big part of the integration and development cost<sup>12</sup>. Additionally, production facilities are mostly located in France, where the production will be allocated to. Furthermore, the direct operational costs have to be allocated, which will go to ESA ESOC located in Germany and in charge of many scientific operations for previous missions, including the Venus Express<sup>13</sup>.

Finally, the launcher itself will be bought off the shelf. The launcher Falcon 9 has been chosen for this mission due to its large diameter, making it easier to fit the platform. The Falcon 9 will be bought from SpaceX, allocated in USA<sup>14</sup>.

#### Market value

Space exploration programs have various benefits to the society we live in. Investing in the global space business yields multi-fold returns. As indirect it may seem to be, it is estimated that every dollar spent on basic research in space generates USD 40 in economic growth on Earth<sup>15</sup>. The social and scientific reward of such investments lies in the fundamental factor affecting growth is technological developments. Space investment bolsters ongoing research and development and creates grounds for future technological advancements that are implementable to our society. The indirect and slow-moving rate of return of investments sets a challenge to estimate the market value of space missions. Therefore, this section will qualitatively discuss the potential contributions Kumo could bring to the global economy and the scientific community.

Initially, it is crucial to underline that the value brought in by the space economy is heavily dependent on the culture that is developed around space exploration as well as the political pulse of the times. Many people worldwide hold strong opinions against space investment simply because they prefer to have their money redirected into solving other problems that are being faced by the masses daily, such as lack of access to healthcare, shelter, and social security. However, this approach can frequently be misleading as space exploration promotes job creation- which helps to address the problems mentioned above- and is expected to generate revenues up to EUR 1 trillion or more by 2040 according to Morgan Stanley as shown in Fig. 7.4<sup>16</sup>.

The public view on space exploration can heavily influence the political dynamics meaning that the funding is strongly dependent on it. Therefore, it is essential that Kumo makes other missions' way by delivering high value information and contributing the promotion of further investments into the space industry. It is therefore crucial to accentuate the scientific and societal returns of Kumo mission and attract future investment.

Kumo mission will provide Academia with information regarding the atmospheric structure of Venus, which is essential to understand the climate, oceanography and the evolution of the atmosphere. Together with the additional end-of-life

<sup>6</sup>[https://www.dlr.de/EN/Home/home\\_node.html](https://www.dlr.de/EN/Home/home_node.html), retrieved on 17-06-2021

<sup>7</sup><https://www.ohb.de/>, retrieved on 17-06-2021

<sup>8</sup><https://www.mpia.de/en>, retrieved on 17-06-2021

<sup>9</sup><https://www.imperial.ac.uk/space-and-atmospheric-physics/research/areas/>, retrieved on 17-06-2021

<sup>10</sup><https://www.cranfield.ac.uk/research-projects/gclass>, retrieved on 17-06-2021

<sup>11</sup><https://www.ox.ac.uk/news/2019-04-03-university-oxford-and-european-space-agency-sign-new-letter-intent>, retrieved on 17-06-2021

<sup>12</sup>[http://www.esa.int/About\\_Us/ESTEC](http://www.esa.int/About_Us/ESTEC), retrieved on 17-06-2021

<sup>13</sup>[http://www.esa.int/About\\_Us/ESOC](http://www.esa.int/About_Us/ESOC), retrieved on 17-06-2021

<sup>14</sup><https://www.spacex.com/vehicles/falcon-9/>, retrieved on 17-06-2021

<sup>15</sup><https://space.nss.org/settlement/nasa/spaceresvo14/newspace3.html>

<sup>16</sup><https://www.morganstanley.com/ideas/investing-in-space>

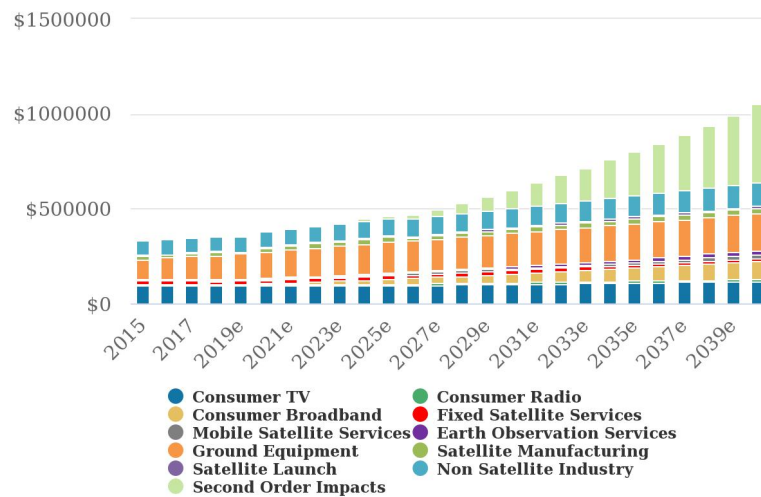


Figure 7.4: The global space economy predictions by Morgan Stanley

mission objectives, scientists will be provided with crucial hints on the possible development of life in Venus, will gain insights on future colonisation in clouds and will be able to use this knowledge to conclude the past, present and future of life on Earth. The increasing pace of climate change makes this information highly valuable. Furthermore, Kumo will provide useful knowledge for future missions. The corrosion of the probe envelope will be tested for 60 days for the first time and will be subject to higher-than-before pressure differentials and cruise speeds. The composition of the layers have been proposed before but have not been used frequently. The corrosion of the material layers will provide future missions with more certainty on the optimal application of acid-resistant material. The returns of this information on Earth could be advancements in air travel, namely on developing efficient and commercialised airships and dynastats.

Finally, the payload used in Kumo can enhance and ease the verification and validation of future missions. Using instruments that have a more extended usage history will raise the overall success rate of the missions. As an example, Kumo will use MASPEX, which has a TRL of 6<sup>17</sup>. This means that the system has not been demonstrated in space environment. Europa Clipper mission is set to launch in October 2024, which will use MASPEX as well. However, there is still a minimal demonstration of the instruments meaning that using them in more missions can raise the TRL levels up to 7-8. This could be beneficial for future missions proposals that use MASPEX as the public confidence in the mission's success will be strengthened, consequently attracting more private investment.

<sup>17</sup><https://ieeexplore.ieee.org/document/7500777>

# 8. Conclusion and recommendations

## Conclusion

The purpose of the final report is to summarise the design outcomes of the Kumo mission. To do so, the project was first introduced with a mission need and objective statements. Constraints to the mission design have been provided in the form of scientific background and system level requirements.

The main goal of the mission is to detect and measure the abundance of UV absorbers, noble gases and biomarkers in the Venusian atmosphere through in-situ observation. The mission, expected to launch in 2028, will consist of an atmospheric probe - dynastat and a relay satellite, equipped with remote sensing scientific payload. The probe will also carry on-board instruments, capable of detecting particles of interest in-situ.

Furthermore, a set of design requirements have been established at the initial design phase. After finalisation of the requirements, the success of the project may be measured by the degree of satisfaction of the requirements. Fortunately, most requirements have been successfully satisfied, especially considering the system-level ones. The proposed design is able to perform the required nominal mission, satisfying the positional excursions around all three axis. The required duration of the mission, of 60 d, will equally be ensured and an end-of-life data collection plan presented. The required scientific measurements will be conducted using a suitable set of payload instruments and data transfer to the ground stations will be ensured.

Nevertheless, some system level requirements could not be met. Most importantly, a sufficient mission success rate of 0.985 could not be ensured. Primarily because of the experimental design of a dynastat as well as the previously unattainable duration of the mission, the maximum mission success rate that could be guaranteed is 0.81, considerably lower than the 0.985 that is required. The inability of meeting the requirement mainly stems from the difficulties of designing an inflatable dynastat in the Venusian atmosphere, rather than any low-level design choices made. Therefore, the client shall be informed about the unattainable requirement, which should then be reconsidered. Further continuation of the mission is thus at discretion of the client.

Most importantly, however, a working design has been proposed. A design that not only meets the scientific requirements, but exceeds many of them. For instance, the proposed design allows for revisiting not only the five locations as required, but hundreds, as long as they are on the same path. Furthermore, steps have been undertaken to maximise the time spent at the 65 km altitude, which is not strictly required. In fact, for almost 10% of the time the probe remains at the high altitude, during which it covers 16.5% of the total length of a revolution. Strictly speaking, spending even 0.1% of the time at the high altitude would suffice to meet the user requirements. Moreover, market analysis has presented a number of additional opportunities, which will be exploited during the nominal mission, such as the creation of atmospheric temperature profile using the temperature sensors on board. Finally, the design presents an extended mission strategy. For the probe, it involves with a descent beyond 55 km, allowing for additional data collection for tremendous scientific benefits.

Furthermore, an extensive sensitivity analysis was able to prove the robustness of the design. The mass of the orbiter was found to only be particularly sensitive to the  $\Delta V$  requirements and the efficiency of the propulsion system. As such, additional scientific constraints on the position of the orbiter will be difficult to accommodate. On the other hand, following the Moore's law describing the rate of advancements in technology, it is safe to assume that more efficient propulsion systems will reach required TRLs by the launch date, significantly lowering the mass. Additionally, the sensitivity analysis has shown that the mass of the probe depends only slightly on the fixed mass carried by the spacecraft. As such, more remote sensing instrumentation may be added at latter stages with little repercussions to the design.

Regarding the probe itself, the mass of the probe was shown to have the strongest correlation with the set rate of climb. The rate of climb at 65 km itself was set at  $4 \text{ m s}^{-1}$ , which significantly overshoots the requirements. Even a  $1 \text{ m s}^{-1}$  rate of climb would be sufficient to meet all requirements, though the time spent at the higher altitude would be reduced. In any case, it creates a large room for potential modifications and thus proves the robustness of the design.

Overall, a functioning probe design that been presented in the final report. The design of each subsystem was sufficiently detailed to allow for a valid conceptual design outcome, shall the failed requirements not be an issue. While there are, undoubtedly, points that have not been taken into account due to the lack of time and resources, the overall coverage of the report is considered sufficient to allow for initiation of the detailed design phase. Furthermore, paramount importance was granted to the issues of risk and sustainability, justifying the relatively high sustainability rating of both the probe and the orbiter as well as relatively low risks with respect to the type of mission planned.

## Recommendations

Even though a working solution has been identified, as demonstrated by this report, ten weeks is in no way sufficient to produce a detailed design of a deep space scientific mission involving an orbiter, an entry capsule and an inflatable probe. As such, the design presented in this report should be considered as the first iteration in the design process, which is commonly

followed by several more iterations. Therefore, this chapter concludes the report with the recommendations for further research and detailed development of the proposed mission. Both system and subsystem level recommendations have been identified. First, the system level recommendations applicable for all subsystems will be described. Furthermore, subsystem-specific recommendations will be briefly repeated.

One of the largest issues with time-limited design is the use of simplifications. The design of all subsystems presented theretofore are based on discrete models with varying accuracy. Shall the mission development not halt, the establishment of integral performance analysis is deemed quintessential to the success of the mission. Indeed, the report presents many approximations, which need to be verified prior to the continuation of the mission. For instance, the flight model shall be modelled as a continuous function of time and altitude in order to confirm the final mission duration and telecommunication window.

Chief engineers of other subsystems identified a strong need for a secondary literature review to use the gained experience as a guide through the abundant information available. It is likely that the dynastat is a sub-optimal (yet totally feasible) concept for the stated mission requirements. Alternative methods of endurance-limited flight shall be revisited. Atypical concepts such as lift generation through dynamic soaring, which generates speed through a vertical speed gradient, could be of use in the Venusian atmosphere. Yet more research is required for conclusive statements.

A number of other system level recommendations have been developed. Firstly, a consistent sustainability framework shall be established across subsystems to allow for objective allocation of sustainability scores. In addition, the risk analysis shall be performed not merely for each subsystem, as it currently is, but also on a broader scale, where the interactions between subsystems are taken into account. Furthermore, the verification of all subsystems shall be additionally performed with analytical models, while for validation, comparison with raw data from similar missions or test data from subsystem tests in a laboratory environment would be required.

Furthermore, the subsystem level recommendations that were brought up in the report will be repeated for the structures, flight dynamics, telecommunications, ADCS, thermal, power, propulsion as well as the entry vehicle and astrodynamical segments. Matching identifiers have been developed and are presented in a list of the identical order:

- REC-STRC1: Perform structural analysis of the internal trusses.
- REC-SRTC2: Perform structural design of propeller arms.
- REC-STRC3: Design retraction mechanisms of the antenna and propellers..
- REC-STRC4: Confirm possibility of inflation of the probe structure. Calculate the size of the folded probe considering malleability of the components.
- REC-STRC5: Design deployment mechanism of solar panels of the orbiter.
- REC-STRC6: Consider cellular structure of the probe interior for structural redundancy.
- REC-FD1: Repeat the probe sizing calculations using a drag coefficient with the applied safety factor of 1.
- REC-FD2: Determine the maximum feasible flow rate during probe expansion and reconfirm inflation feasibility.
- REC-FD3: Confirm sufficient buoyancy lift when accounting for the change in temperature of the lifting gas at both altitudes.
- REC-TT&C1: Maximum degree of automation of the probe shall be researched to limit the uplink requirements.
- REC-TT&C2: Research the effectiveness of the watchdog unit in mistake detection.
- REC-ADCS1: Research the possibility of performing radio frequency experiments using VLBI, besides using it for tracking.
- REC-ADCS2: Separate trade-off between the air-data sensing and laser sensing shall be performed.
- REC-THER1: Study phase change materials and thermal control gels as alternatives for MLI.
- REC-POWR1: Account for increasing propeller efficiencies with increasing velocity when calculating optimal cruise velocity.
- REC-PROP1: Investigate whether the necessary TRL of alternative propulsion systems can be reached before the launch date.
- REC-EV1: Reproduce entry vehicle sizing using altitude-dependant estimates of the drag and lift coefficients.
- REC-EV2: Size the back cover of the entry vehicle. Thickness and mass are the first key parameters to be calculated.
- REC-EV3: Perform stability analysis on the entry vehicle, especially during the inflation of the probe.
- REC-EV4: Alternative methods for the reduction of the maximum speed during entry, such as a parachute or vertical thrusters, shall be run through a trade-off.
- REC-ASTR1: Investigate the optimal separation time by performing a trade off between the  $\Delta V$  and orbiter connectivity.
- REC-ASTR2: Trade off heat shield mass for aerocapture versus propellant mass for propulsive Venus orbit insertion.

Nevertheless, the aforementioned points are not considered detrimental to the success of the mission. For most of them, a workaround could be found if sufficient time is allocated. Therefore, it can be concluded that the Kumo mission is feasible as far as the conceptual phase of the design can be representative. More research, however, is required to take a step back and reconsider some of the lower level design choices made.

## References

- Anderson, J. D. (2016). *Introduction to flight* (8th international ed.). New York, United States: McGraw Hill Education.
- Bains, W., Petkowski, J. J., Seager, S., Ranjan, S., Sousa-Silva, C., Rimmer, P. B., Zhan, Z., Greaves, J. S., and Richards, A. M. S. (2020). *Phosphine on Venus Cannot be Explained by Conventional Processes*. Cornell University.
- Barstow, J., Taylor, F., Tsang, C., Wilson, C., Irwin, P., Drossart, P., and Piccioni, G. (2010). Venus Cloud Properties from Venus Express VIRTIS Observations. *American Astronomical Society, DPS meeting #42*.
- Beningo, J. (2010). A Review of Watchdog Architectures and their Application to Cubesats. *University of Michigan, Department of Aerospace*.
- Beser, N. D. (1994). Space Data Compression Standards. *Johns Hopkins APL Technical Diges*, 15(3).
- Breukels, J., and Ockels, W. (2008). Analysis of complex inflatable structures using a multi-body dynamics approach. *49th AIAA/ASME/ASCE/AHS/ASC Structures, Structural Dynamics, and Materials Conference 16th AIAA/ASME/AHS Adaptive Structures Conference 10t*. doi: 10.2514/6.2008-2284
- Bronstring, A., Dumitrescu, I., Eckstein, P., Maroquin, S., Powis, M. H., Vieira dos Santos, L., Şarlak, E., Sinha, I., Staelens, M., and Voloshyn, S. (2021a). Kumo: Venus Atmosphere Explorer; Baseline Report.
- Bronstring, A., Dumitrescu, I., Eckstein, P., Maroquin, S., Powis, M. H., Vieira dos Santos, L., Şarlak, E., Sinha, I., Staelens, M., and Voloshyn, S. (2021b). Kumo: Venus Atmosphere Explorer; Midterm Report.
- Brown, D., Agle, D., Martinez, M., and Napier, G. (2011). Juno Launch Press Kit. NASA.
- Castet, J.-F., and Saleh, J. H. (2009). Satellite and satellite subsystems reliability: Statistical data analysis and modeling. *Reliability Engineering & System Safety*, 94(11), 1718-1728. doi: <https://doi.org/10.1016/j.res.2009.05.004>
- Chapline, G. (n.d.). Materials and manufacturing. *Engineering Innovations*.
- Clausen, K. C., Hassan, H., Verdant, M., Couzin, P., Huttin, G., Brisson, M., Sollazzo, C., and Lebreton, J.-P. (1999). The Huygens probe system design. ESA.
- Coradini, A. (1999). VIRTIS: The Imaging Spectrometer of the Rosetta Mission. *Advances in Space Research*, 24(9), 1105–1114. doi: 10.1016/s0273-1177(99)00691-2
- Cornish, T., Pham, T. T., and Chang, C. (2014). 34-m and 70-m Command. NASA.
- DeSantis, D. (2014, 04). Satellite Thruster Propulsion: H2O2 Bipropellant Comparison with Existing Alternatives.
- Drossart, P., Piccioni, G., Coradini, A., Reess, J., Semery, A., Suetta, E., Cosi, M., Dami, M., Arnold, G., ... Henry, F. (2004). VIRTIS imaging spectrometer for the ESA/Venus Express mission. *Infrared Spaceborne Remote Sensing XII*. doi: 10.1117/12.557427
- Duev, D. A., Molera Calvés, G., Pogrebenko, S. V., Gurvits, L. I., Cimó, G., and Bocanegra Bahamon, T. (2012). Spacecraft VLBI and Doppler tracking: algorithms and implementation. *A&A*, 541, A43. Retrieved from <https://doi.org/10.1051/0004-6361/201218885> doi: 10.1051/0004-6361/201218885
- Gilmore, M., Lynch, R., and Amato, M. (2020). Venus Flagship Mission Decadal Study. *Planetary and astrobiological decadal survey*.
- Glaze, L. S., Wilson, C. F., Zasova, L. V., Nakamura, M., and Limaye, S. (2018). Future of Venus Research and Exploration. *Space Sci Rev*, 214, 89. doi: 10.1007/s11214-018-0528-z
- Greaves, J. S., Richards, A. M. S., Bains, W., Rimmer, P. B., Sagawa, H., Clements, D. L., Seager, S., Petkowski, J. J., Sousa-Silva, C., ... Hoge, J. (2020). *Phosphine Gas in the Cloud Decks of Venus*.
- Gökçen, T., Chen, Y.-K., Skokova, K. A., and Milos, F. S. (2010). Computational Analysis of Arc-Jet Wedge Tests Including Ablation and Shape Change. NASA.
- Hall, J. L., Bullock, M., Senske, D. A., Cutts, J. A., and Grammier, R. (2009). Venus Flagship Mission Study: Report of the Venus Science and Technology Definition Team. NASA.
- Hirose, C., Ishii, N., Yamamoto, T., Kawakatsu, Y., Ukai, C., Terada, H., and Ebara, M. (2012). The Trajectory Design Strategies for Akatsuki Mission. *Transactions of the Japan Society for Aeronautical and Space Sciences, Aerospace Technology Japan*, 10(ists28). doi: 10.2322/tastj.10.to\_3\_1
- Hoekstra, A. (2008). *Water neutral reducing and offsetting the impacts of water footprints*. Delft, Netherlands: UNESCO-IHE Institute for Water Education.
- Hueso, R., Perez-Hoyos, S., Sánchez-Lavega, A., and Peralta, J. (2008). The atmosphere of Venus: Winds and clouds observed by VIRTIS/Venus Express. *Lecture Notes and Essays in Astrophysics*, 3, 1.
- Häusler, B., Pätzold, M., Tyler, G., Barriot, V.-P., Bird, M., Dehant, V., Hinson, D., Simpson, R., Treumann, R., ... Tellmann, S. (2007). Venus Atmospheric, Ionospheric, Surface and Interplanetary RadioWave Propagation Studies with the VeRA Radio-Science Experiment. *ESA Special Publication, SP 1295*.
- Iess, L., Di Benedetto, M., James, N., Mercolino, M., Simone, L., and Tortora, P. (2014). Astra: Interdisciplinary study on enhancement of the end-to-end accuracy for spacecraft tracking techniques. *Acta Astronautica*, 94(2), 699–707. doi: 10.1016/j.actaastro.2013.06.011
- Imbriale, W. A. (2002). *Large Antennas of the Deep Space Network*. John Wiley & Sons.
- Jones, D. L., Folkner, W. M., Jacobson, R. A., Jacobs, C. S., Dhawan, V., Romney, J., and Fomalont, E. (2014). Astrometry of cassini with the vlba to improve the saturn ephemeris. *The Astronomical Journal*, 149(1), 28. doi: 10.1088/0004-6256/149/1/28

- Justus, C., and Braun, R. (2007). Atmospheric Environments for Entry, Descent and Landing (EDL). NASA Marshall Space Flight Center.
- Kerzhanovich, V., Aleksandrov, Y. N., Andreev, R. A., Armand, N. A., Bakitko, R. V., Blamont, J., Bolgoh, L., Vorontsov, V. A., Vyshlov, A. S., ... Young, R. (1986). Small-scale turbulence in the Venus middle cloud layer. *Pisma v Astronomicheskii Zhurnal*, 12, 46–51.
- Kerzhanovich, V., Cutts, J., and Hall, J. (2003, 07). Low-cost balloon missions to Mars and Venus. , 530, 285-291.
- Kliore, A., Moroz, V. I., Keating, G. M., and COSPAR. (1986). *The Venus international reference atmosphere*. Oxford: Published for the Committee on Space Research by Pergamon.
- Konopliv, A. S., Banerdt, W. B., Sjogren, W. L., and Konopliv, A. (1999). Venus gravity: 180th degree and order model. *Icarus*, 3–18.
- Landis. (2003). Colonization of venus. *Conference on Human Space Exploration, Space Technology & Applications International Forum*. doi: 10.1063/1.1541418
- Landis. (2020). Settling Venus: A City in the Clouds? *AIAA Ascend Conference*. doi: 10.2514/6.2020-4152
- Landis, G., and Haag, E. (2013, 07). Analysis of Solar Cell Efficiency for Venus Atmosphere and Surface Missions.. doi: 10.2514/6.2013-4028
- Lewis, K., Klaasen, K., Susca, S., Oaida, B., Larson, M., Vanelli, T., Murray, A., Jones, L., Thomas, V., ... et al. (2016). Use of model payload for europa mission development ieeee aerospace conference. *2016 IEEE Aerospace Conference*. doi: 10.1109/aero.2016.7500708
- Ley, W., Wittmann, K., and Hallmann, W. (n.d.). *Handbook of Space Technology*. John Wiley & Sons, Ltd.
- Leśniak, A., Danek, T., and Wojdyła, M. (2009). Application of Kalman Filter to Noise Reduction in Multichannel Data. *Schedae Informaticae*, 1718(-1), 63–73. doi: 10.2478/v10149-010-0004-3
- Li, X., Li, P., Wu, Z., Luo, D., Yu, H.-Y., and Lu, Z.-H. (2021). Review and perspective of materials for flexible solar cells. *Materials Reports: Energy*.
- Limaye, S. S., Grassotti, C., and Kuetemeyer, M. J. (1988). Venus: Cloud level circulation during 1982 as determined from pioneer cloud photopolarimeter images: I. Time and zonally averaged circulation. *Icarus*, 73(2), 193-211. doi: [https://doi.org/10.1016/0019-1035\(88\)90093-0](https://doi.org/10.1016/0019-1035(88)90093-0)
- Makovsky, A., Barbieri, A., and Tung, R. (2002). Odyssey Telecommunications. *DESCANSO Design and Performance Summary Series*.
- Margot, J.-L., Campbell, D. B., Giorgini, J. D., Jao, J. S., Snedeker, L. G., Ghigo, F. D., and Bonsall, A. (2021). Spin state and moment of inertia of Venus. *Nature Astronomy*. doi: 10.1038/s41550-021-01339-7
- Markiewicz, W. J., Titov, D., Fiethe, B., Behnke, T., Szemerey, I., and Perplies, H. (2005). Venus Monitoring Camera for Venus Express. *Max-Planck-Institute for Solar System Research*, 1–15.
- Meija, J., Coplen, T. B., Berglund, M., Brand, W. A., Bièvre, P. D., Gröning, M., Holden, N. E., Irrgeher, J., Loss, R. D., ... Prohaska, T. (2016). Atomic weights of the elements 2013 (IUPAC Technical Report). *Pure and Applied Chemistry*, 88(3), 265–291. doi: doi:10.1515/pac-2015-0305
- Meltzer, M. (2007). *Mission to jupiter: a history of the galileo project*. NASA History Division.
- Mogul, R., Limaye, S. S., Way, M. J., and Cordova, J. A. (2021). Venus' Mass Spectra Show Signs of Disequilibria in the Middle Clouds. *Geophysical Research Letters*, 48(7). Retrieved from <http://dx.doi.org/10.1029/2020GL091327> doi: 10.1029/2020gl091327
- Mooij, E. (2019). *AE4870B Re-entry Systems (Lecture series)*.
- Muhalim, N., Muhammad, F. B., and Krishnan, S. (2010). Design of nitrogen-tetroxide/monomethyl-hydrazine thruster for upper stage application.
- Mulder, J., van Staveren, W., van der Vaart, J., de Weerd, E., de Visser, C., in't Veld, A., and Mooij, E. (2013). *AE3202 Flight Dynamics (Lecture Notes)*.
- Mutluay, T. (2015). The development of an inertia estimation method to support handling quality assessment.
- National Research Council. (2012). *Nasa space technology roadmaps and priorities: restoring nasa's technological edge and paving the way for a new era in space*. National Academies Press.
- Obert, E., and Slingerland, R. (2009). *Aerodynamic Design of Transport Aircraft*. Delft, The Netherlands: TU Delft.
- Pasini, A., Torre, L., Pace, G., Valentini, D., and d'Agostino, L. (2013). Pulsed Chemical Rocket with Green High Performance Propellants.. doi: 10.2514/6.2013-3756
- Petropoulos, B. (1988). Physical parameters of the atmosphere of Venus. *Earth, Moon and Planets*, 42, 29-40.
- Piccioni, G., Drossart, P., Suetta, E., Cosi, M., Ammannito, E., Barbis, A., Berlin, R., Bonello, A. B. G., Bouyé, M., ... Soufflot, A. (2004). VIRTIS: The Visible and Infrared Thermal Imaging Spectrometer. *ESA Special Publication*.
- Pogrebenko, S. V., Gurvits, L. I., Campbell, R. M., Avruch, I. M., Lebreton, J. P., and van't Klooster, C. G. M. (2004, February). VLBI tracking of the Huygens probe in the atmosphere of Titan. , 544, 197-204.
- Pérez-Hoyos, S., Sánchez-Lavega, A., García-Muñoz, A., Irwin, P. G. J., Peralta, J., Holsclaw, G., McClintock, W. M., and Sanz-Requena, J. F. (2018). Venus upper clouds and the uv absorber from messenger/mascs observations. *Journal of Geophysical Research: Planets*, 123(1), 145-162.
- Quadrelli, M., Wood, L., Riedel, J., McHenry, M., Aung, M., Cangahuala, L., Volpe, R., Beauchamp, P., and Cutts, J. (2015). Guidance, Navigation, and Control Technology Assessment for Future Planetary Science Missions. *Journal of Guidance, Control, and Dynamics*, 38(7). doi: 10.2514/1.g000525

- Ragent, B., Privette, C. A., Avrin, P., Waring, J. G., Carlston, C. E., and Knight, T. C. D. (1992). Galileo Probe Nephelometer Experiment. *Space Sci Rev*, 60, 179-201. doi: 10.1007/BF00216854
- Sanchez Perez, J., and Canabal, J. (2004). Review of Venus Express Mission Analysis.
- Sato, F. E., and Nakata, T. (2020). Energy Consumption Analysis for Vehicle Production through a Material Flow Approach. *Energies*, 13(9), 2396. doi: 10.3390/en13092396
- Seidelmann, P. K., Archinal, B. A., A'hearn, M. F., Conrad, A., Consolmagno, G. J., Hestroffer, D., Hilton, J. L., Krasinsky, G. A., Neumann, G., ... Williams, I. P. (2007). Report of the IAU/IAG Working Group on cartographic coordinates and rotational elements: 2006. *Celestial Mechanics and Dynamical Astronomy*, 98(3), 155-180. doi: 10.1007/s10569-007-9072-y
- Seiff, A., Juergens, D. W., and Lepetich, J. E. (1980). Atmosphere Structure Instruments on the Four Pioneer Venus Entry Probes. *IEEE Transactions on Geoscience and Remote Sensing*, GE-18(1), 105-111. doi: 10.1109/tgrs.1980.350291
- Shambayati, S., Lee, C. H., Morabito, D. D., Cesarone, R. J., and Abraham, D. S. (2011). Emergency Communications for NASA's Deep Space Missions. NASA.
- Sharpton, V., Esposito, L., and Sotin, C. (2014). Venus Exploration Targets Workshop, Final Report.
- Shin, D. K., Pham, T., and Chang, C. (2014). Frequency and Channel Assignments. NASA.
- Sivac, P., and Schirmann, T. (2007). The Venus Express Spacecraft System Design. *ESA Special Publication*, SP 1295.
- Slanger, T. G. (2001). Discovery of the Atomic Oxygen Green Line in the Venus Night Airglow. *Science*, 291(5503), 463-465. doi: 10.1126/science.291.5503.463
- Spacecraft Systems Engineering. (2011). John Wiley & Sons, Ltd. doi: <https://doi.org/10.1002/9781119971009.index>
- Sánchez-Lavega, A., Hueso, R., Piccioni, G., Drossart, P., Peralta, J., Perez-Hoyos, S., Wilson, C., Taylor, F., Baines, K., ... Lebonnois, S. (2008). Variable winds on Venus mapped in three dimensions. *Geophysical Research Letters*, 35. doi: 10.1029/2008GL033817
- Taylor, J., Sakamoto, L., and Wong, C.-J. (2002). *Cassini Orbiter/Huygens Probe Telecommunications* (Tech. Rep.).
- Thomas, J., Wielgosz, C., and Le Van, A. (2018). Mechanics of Inflatable Fabric Beams. *Thin-Walled Structures*, 225-232. doi: 10.1201/9781351077309-23
- Thornton, C. L., and Border, J. S. (2005a). Range and Doppler Tracking Observables. *Radiometric Tracking Techniques for Deep Space Navigation*, 9-46. doi: 10.1002/0471728454.ch3
- Thornton, C. L., and Border, J. S. (2005b). VLBI Tracking Observables. *Radiometric Tracking Techniques for Deep Space Navigation*, 47-62. doi: 10.1002/0471728454.ch4
- Titov, D. V., Markiewicz, W. J., Ignatiev, N. I., Song, L., Limaye, S. S., Sanchez-Lavega, A., Hesemann, J., Almeida, M., Roatsch, T., and Matz, K.-D. (2012). Morphology of the cloud tops as observed by the venus express monitoring camera. *Icarus*, 217(2), 682-701.
- Topputo, F., Vasile, M., and Bernelli-Zazzera, F. (2004). Interplanetary and lunar transfers using libration points.
- Torr, D., Torr, M., Zukic, M., Spann, J., and Johnson, R. (1992). The ultraviolet imager (UVI) for ISTP. *Proceedings of SPIE - The International Society for Optical Engineering*.
- Verbeek, M. J., and Jentink, H. W. (2012). *Executive summary Optical Air Data System Flight Testing* (Tech. Rep.).
- Villanueva, G., Cordiner, M., Irwin, P., de Pater, I., Butler, B., Gurwell, M., Milam, S., Nixon, C., Luszcz-Cook, S., ... Koppurapu, R. (2020). *No phosphine in the atmosphere of Venus*.
- Wang, H., and Li, Y. (2017). The aerodynamic performance of an inflatable wing in aircraft. *Proceedings of the 7th International Conference on Education, Management, Information and Mechanical Engineering (EMIM 2017)*. doi: 10.2991/emim-17.2017.3
- Wertz, J. R., Everett, D. F., and Puschell, J. J. (2011). *Space mission engineering: The new SMAD* (6th ed.). Hawthorne, CA: Microcosm Press.
- Yamazaki, A., Yamada, M., Lee, Y. J., Watanabe, S., Horinouchi, T., Murakami, S.-y., Kouyama, T., Ogohara, K., Imamura, T., ... et al. (2018). Ultraviolet imager on venus orbiter akatsuki and its initial results. *Earth, Planets and Space*, 70(1). doi: 10.1186/s40623-017-0772-6
- Yavrouian, A., Plett, G., Yen, S., Cutts, J., and Baek, D. (1999). Evaluation of materials for Venus aerobot applications. *International Balloon Technology Conference*. doi: 10.2514/6.1999-3859
- Zabihi, N., and Saafi, M. (2020). Recent developments in the energy harvesting systems from road infrastructures. *Sustainability*, 12(17), 6738.
- Zandbergen, B. T. C. (2017). *AE1222-II Reader: Aerospace Design & Systems Engineering Elements I – Part: Spacecraft (bus) design and sizing*. Netherlands: Delft University of Technology.
- Zurbuchen, T., and Martin, P. (2019). Management of NASA's Europa Mission. NASA, 1-47.